Contribution au pronostic des systèmes complexes. Application aux systèmes énergétiques

Ahmad Al Mohamad

Normandie Université

THÈSE

Pour obtenir le diplôme de doctorat

Spécialité : Automatique, Signal, Productique, Robotique

Préparée au sein de l'Université de Rouen Normandie

En cotutelle internationale avec Universitat Politècnica de Catalunya - Barcelone, Espagne

Contribution to prognostics and health management of complex systems. Application to energy systems

Présentée et soutenue par
Ahmad AL MOHAMAD

Thèse soutenue publiquement le 22/10/2021 devant le jury composé de		
Mme Louise TRAVÉ-MASSUYÈS	Directrice de recherche, LAAS-CNRS, Toulouse, France	Rapporteuse
M. Francesco IANNUZZO	Professeur, Aalborg Universitet, Aalborg, Danemark	Rapporteur
Mme Fatiha NEJJARI AKHI-ELARAB	Professeur, Universitat Politècnica de Catalunya, Terrassa, Espagne	Examinatrice
M. Kamal MEDJAHER	Professeur, École Nationale d'Ingénieurs de Tarbes, Tarbes, France	Examinateur
M. Vicenç PUIG CAYUELA	Professeur, Universitat Politècnica de Catalunya, Barcelone, Espagne	Directeur de thèse
M. Ghaleb HOBLOS	EC-HDR, ESIGELEC, Saint-Étienne-du-Rouvray, France	Directeur de thèse

Thèse dirigée par M. Ghaleb HOBLOS, laboratoire IRSEEM
et M. Vicenç PUIG CAYUELA, laboratoire IRI

UNIVERSITÉ DE ROUEN NORMANDIE

ED 590 MIIS
Mathématiques, Information, Ingénierie des Systèmes

irseem

This page is intentionally left blank

Normandie Université

THÈSE

Pour obtenir le diplôme de doctorat

Spécialité : Automatique, Signal, Productique, Robotique

Préparée au sein de l'Université de Rouen Normandie

En cotutelle internationale avec Universitat Politècnica de Catalunya - Barcelone, Espagne

Contribution au pronostic des systèmes complexes. Application aux systèmes énergétiques

Présentée et soutenue par
Ahmad AL MOHAMAD

Thèse soutenue publiquement le 22/10/2021 devant le jury composé de		
Mme Louise TRAVÉ-MASSUYÈS	Directrice de recherche, LAAS-CNRS, Toulouse, France	Rapporteuse
M. Francesco IANNUZZO	Professeur, Aalborg Universitet, Aalborg, Danemark	Rapporteur
Mme Fatiha NEJJARI AKHI-ELARAB	Professeur, Universitat Politècnica de Catalunya, Terrassa, Espagne	Examinatrice
M. Kamal MEDJAHER	Professeur, École Nationale d'Ingénieurs de Tarbes, Tarbes, France	Examinateur
M. Vicenç PUIG CAYUELA	Professeur, Universitat Politècnica de Catalunya, Barcelone, Espagne	Directeur de thèse
M. Ghaleb HOBLOS	EC-HDR, ESIGELEC, Saint-Étienne-du-Rouvray, France	Directeur de thèse

Thèse dirigée par M. Ghaleb HOBLOS, laboratoire IRSEEM
et M. Vicenç PUIG CAYUELA, laboratoire IRI

UNIVERSITÉ DE ROUEN NORMANDIE

ED 590 MIIS
Mathématiques, Information, Ingénierie des Systèmes

irseem

This page is intentionally left blank

Contents

Acknowledgments

This 3-year research journey has come to an end after a lot peaks and valleys. For this, I would like to express my gratitude to the people from whom I was inspired and received generous support. I would also like to acknowledge the funding entities.

I would like to express my deepest appreciation to my research supervisors, professor Vicenç Puig Cayuela from Universitat Politècnica de Catalunya (UPC) and Institut de Robòtica i Informàtica Industrial (IRI), Spain, and Dr. HDR Ghaleb Hoblos from École D'Ingénieurs-es Généralistes Systèmes Intelligents Et Connectés (ESIGELEC), Institut de Recherche en Systèmes Electroniques Embarqués (IRSEEM), and Université de Rouen Normandie, France for giving me the opportunity to initiate this thesis in the first place, and their continuous scientific guidance as well as the administrative during this journey. Vicenç and Ghaleb never wavered their support by answering my questions and providing valuable advice and practical suggestions. Their dynamism, visions, sincerity, and motivation always inspired me to work harder. I will never forget their extended amount of assistance and time they spent especially during weekends, after-hours, and holidays to read and comment on the publications and my dissertation. I am extremely grateful to them for their profound beliefs in my abilities, and for their feedback and insights into the topic.

Further, I would also like to extend my gratitude to the entities that co-funded this PhD:

• This work is partially funded by the Catalan Agency for Management of University and Research Grants (Agència de Gestió d'Ajust Universitaris i de Recerca (AGAUR)) and the European Social Fund (ESF) of the Government of Catalonia (Generalitat de Catalunya) through the grant FI-SDUR-AGAUR 2020 (ref. 2020-FISDU-307).
• This work is partially funded by European Union and Normandy Region (Région Normandie). Europe is involved in Normandy through the European Funds for Regional Development.
• I would also like to recognize the additional support from UPC.

Special thanks to the members of my Individual Supervision Committee (Comité de Suivi Individuel de thèse), professor Imed Kacem from Université de Lorraine and LCOMS and professor Yacine Amara from Université Le Havre Normandie and GREAH, in addition to the members of the research plan committee, professor Joaquin Blesa Izquierdo, professor Rosa Mari Fernandez Canti, and professor Sebastian Tornil Sin from UPC, for their constructive feedback and propositions. Their insightful suggestions, remarks suggestions, and especially their challenging questions have contributed in improving my research.

I extend a word of thankfulness to all the members of my hosting laboratories IRSEEM and IRI for providing a great working environment and a friendly atmosphere, in Rouen and in Barcelona. I very much appreciate my colleague and friend Dr. Houssam Moumouh for his unlimited support. I would also take the privilege to thank Dr. Riham Ginzarly for her recommendation.

Also, I am grateful to my partner for all her love and support.

Finally, I do believe that I would not have achieved anything in my life without the prayers and the support of my mother.

I dedicate this thesis to the memory of my father who would be proud of me.

Ahmad Al Mohamad
Barcelona, Spain & Rouen, France
September 2021

Abstract in English

This thesis presents contributions to model-based Prognostics and Health Management (PHM) for online Remaining Useful Life (RUL) forecasting of degraded systems. The major issue in such a prognostics approach is that the degradation models are required for prediction purposes. However, this practice is effort- and time-consuming specifically for large systems with mutual degradation and cascading damage effects. Thus, this work aims to overcome the knowledge dependence on the degradation models in addition to the historical data which are accompanied by uncertainties. In consequence, a threefold PHM strategy (system modeling, degradation estimation on the micro level, RUL forecasting) with various prognostics approaches are proposed for degraded systems and can be generalized, with soft tuning, for further applications.

In broad, system-level prognostics are accomplished without a remarkable interest in the root cause of the degradation on the component level. Therefore, the important role of degradation estimation for the critical components in systems is elaborated in this thesis for the sake of improved Condition-Based Maintenance (CBM). Thus, stochastic-based filtering techniques for parameter estimation and degradation prediction of the critical components have been investigated. Whereas, the main challenge lies in the consistency of the RUL forecasting that is subject to modeling and measurement uncertainties on a system level, as concluded based on the examination of various forecasting approaches. Consequently, a fusion between stochastic and deterministic estimation techniques has been investigated in a Zonotopic Extended Kalman filter (ZEKF) framework, which has been upgraded into a Zonotopic Set-Membership (ZSM) observer for degradation estimation and prediction

of multiple-output systems with unknown-but-bounded noises and uncertainties. Furthermore, zonotopes are adopted for their simple computations in addition to their ability to propagate bounded sets that improve the accuracy of RUL forecasting. Additionally, a robustness condition is guaranteed due to the Linear Matrix Inequality (LMI)-based offline optimal tuning of the zonotopic observers.

Moreover, the proposed approaches are applied to a DC-DC converter with three degradation scenarios for the validation of the threefold PHM. Eventually, the nonlinear model of the converter has been linearized online when applied with the stochastic approaches. However, it has been transformed into a polytopic Linear Parameter-Varying (LPV) model that copes with the LMI optimization for reduced online computations in addition to generalization purposes for real-time prognostics.

Keywords: Prognostics and health management, remaining useful life forecasting, deterministic observers, zonotopes, set-membership, stochastic filters, joint estimation of states and parameters, linear matrix inequality, linear parameter-varying.

Résumé en français

Cette thèse est une contribution au pronostic à base des modèles pour la gestion de l'état de santé d'un système (Prognostics and Health Management (PHM)) en estimant en ligne la durée de vie résiduelle (Remaining Useful Life (RUL)). Le problème majeur dans une telle approche de pronostic est que les modèles de dégradation sont nécessaires à des fins d'estimation et de prédiction. Cependant, cette pratique demande beaucoup d'efforts et de temps de calcul, en particulier pour les systèmes à grande échelle avec des effets de dégradation mutuelle et de détérioration en cascade. Ainsi, ce travail vise à dépasser cette contrainte de connaissance vis-à-vis des modèles de dégradation en proposant une stratégie de PHM basée sur plusieurs approches de pronostic par estimation, avec une possibilité d'adaptation et d'extension selon l'application utilisée.

En général, on distingue deux types d'approches de pronostic, global avec une vision macroscopique sur le système ou local allant jusqu'aux composants critiques. Les travaux de cette thèse s'inscrivent dans la 2ème catégorie où l'intérêt final est de suivre la dégradation de quelques composants critiques identifiés et ainsi d'élaborer une stratégie de maintenance conditionnée (Condition-Based Maintenance (CBM)). Pour ce faire, en premier temps, nous avons développé une approche d'estimation par filtre de Kalaman étendu et augmenté (état + paramètres à estimer) pour l'estimation des paramètres et la prédiction de la dégradation des composants critiques. Cela nous a permis d'estimer le RUL pour chaque composant critique sur le système. En deuxième temps, afin d'améliorer la prédiction du RUL, soumis à des incertitudes de modélisation et de mesure au niveau du système, on a opté pour une fusion de deux types de technique, stochastique (par Kalman

étendu augmenté) et ensembliste (par zonotopes), en proposant un filtre de Kalman étendu « zonotopique » ZEKF (Zonotopic Extended Kalman Filter). Cela nous a permis d'améliorer l'estimation des paramètres dégradés dont le système est soumis à des bruits inconnus mais bornés. A noter que les zonotopes sont adoptés pour leurs calculs simples en plus de leur capacité à propager des ensembles bornés qui améliorent la précision du RUL estimé. De plus, une condition de robustesse est garantie en raison de l'ajustement optimal hors ligne basé sur l'inégalité matricielle linéaire (Linear Matrix Inequality (LMI)) des observateurs zonotopiques. En troisième temps, nous avons proposé un pronostic basé directement sur l'estimation par observateurs zonotopiques sans faire recours à un filtre de Kalman étendu. Le calcul du RUL avec ce type d'observateurs donne plus de garanties sur la prédiction de l'état de santé du système en bornant les différentes incertitudes de modélisation et de mesure.

Sur le plan applicatif, les approches proposées ont été appliquées à un convertisseur DC-DC faisant partie d'une chaine de conversion électrique dans un véhicule électrique hybride.

Mots clés : Pronostic et gestion de l'état de santé, prévision de la durée de vie résiduelle, observateurs déterministes, zonotopes, filtres stochastiques, filtre de Kalman, état augmenté, estimation conjointe des états et des paramètres, inégalité matricielle linéaire, Systèmes linéaires à paramètres variants.

Resumen en español

Esta tesis presenta contribuciones al pronóstico basado en modelos y la gestión de la salud (Prognostics and Health Management (PHM)) para la estimación en línea de la vida útil restante (Remaining Useful Life (RUL)) teniendo cuenta la degradación de los sistemas. El problema principal en este enfoque de pronóstico es que los modelos de degradación son necesarios para fines de predicción. Sin embargo, esta práctica requiere mucho tiempo y esfuerzo, específicamente para sistemas grandes con degradación mutua y efectos de daños en cascada. Así, este trabajo tiene como objetivo superar la dependencia del conocimiento de los modelos de degradación además de los datos históricos que van acompañados de incertidumbres. En consecuencia, se propone una estrategia PHM triple con varios enfoques de pronóstico para sistemas electrónicos y se puede generalizar, con ajustes menores, para aplicaciones posteriores.

En este contexto, los pronósticos a nivel de sistema se logran en general sin buscar la causa raíz de la degradación a nivel de componente. Por lo tanto, el papel importante de la estimación de la degradación de los componentes críticos en los sistemas se elabora con el fin de mejorar el mantenimiento basado en las condiciones del sistema (Condition-Based Maintenance (CBM)). Por tanto, existen técnicas estadísticas para la estimación de parámetros y la predicción de la degradación que se han investigado en la literatura. Considerando que la principal dificultad radica en la coherencia de la previsión de RUL que está sujeta a incertidumbres de modelado y medición a nivel de sistema, como se concluyó después del estudio de varios enfoques de previsión. En consecuencia, se ha investigado una fusión entre técnicas de estimación estocásticas y deterministas en un marco ZEKF (Zonotopic

Extended Kalman filter), que se ha actualizado a un observador ZSM (Zonotopic Set-Membership) para la estimación y predicción de la degradación con ruidos e incertidumbres desconocidos pero acotados. Además, los zonotopes se adoptan debido a sus cálculos simples además de su capacidad para propagar conjuntos acotados que mejoran la precisión de la predicción del RUL. Además, se garantiza una condición de robustez debido a la sintonización óptima fuera de línea mediante la técnica LMI (Linear Matrix Inequality) de los observadores zonotópicos.

Finalmente, los enfoques propuestos se aplican a un convertidor DC-DC con tres escenarios de degradación para la validación de los métodos PHM propuestos. Finalmente, el modelo no lineal del convertidor se ha linealizado en línea cuando se aplica con los enfoques estocásticos. Sin embargo, se ha transformado en un modelo de variación de parámetros lineales politópicos (Linear Parameter-Varying (LPV)) que hace utiliza la técnica LMI para reducir los cálculos en línea, además de facilitar el pronóstico en tiempo real.

Palabras clave: Pronósticos y gestión de la salud, pronóstico de vida útil remanente, observadores deterministas, zonotopes, pertenencia a conjuntos, filtros estocásticos, estimación conjunta de estados y parámetros, desigualdad de matrices lineales, variación de parámetros lineales.

Resum en català

Aquesta tesi presenta contribucions en la prognosi basada en models i la gestió de la salut (Prognostics and Health Management (PHM)) per a l'estimació de la vida útil en línia (Remaining Useful Life (RUL)) tenint en compte la degradació dels sistemes. El principal problema d'aquest enfocament per a la prognosi és que els models de degradació són necessaris a efectes de predicció. No obstant això, aquesta pràctica requereix molt d'esforç i temps específicament per a sistemes grans amb degradació mútua i efectes de danys en cascada. Per tant, aquest treball pretén superar la dependència del coneixement dels models de degradació, a més de les dades històriques que van acompanyades d'incerteses. En conseqüència, es proposa una estratègia PHM triple amb diversos enfocaments pronòstics per a sistemes electrònics i es pot generalitzar, amb ajustos menors, per a altres aplicacions.

En aquest context, els pronòstics a nivell de sistema s'aconsegueixen a grans trets sense cercar la causa arrel de la degradació a nivell de component. Per tant, l'important paper de l'estimació de la degradació dels components crítics dels sistemes s'elabora per tal de millorar el manteniment basat en les condicions del sistema (Condition-Based Maintenance (CBM)). Per tant, existeixen tècniques de filtratge basades en estocàstics per a l'estimació de paràmetres i la predicció de la degradació que s'han investigat en la literatura. Mentre que, el principal repte rau en la consistència de la predicció RUL que està subjecta a incerteses de modelització i mesura a nivell de sistema, tal com es conclou després de l'estudi de diversos enfocaments de predicció. En conseqüència, s'ha investigat una fusió entre tècniques d'estimació estocàstica i determinista en un marc ZEKF (Zonotopic Extended Kalman filter), que s'ha actualitzat a un observador ZSM (Zonotopic Set-Membership) per

estimar i predir la degradació amb sorolls i incerteses desconeguts però acotats. A més, s'adopten els zonòtops per als seus càlculs senzills, a més de la seva capacitat de propagar conjunts acotats que milloren la precisió de la predicció RUL. A més, es garanteix una condició de robustesa expressada como una LMI (Linear Matrix Inequality) que permet la sintonització òptima fora de línia dels observadors zonotòpics.

A més, els enfocaments proposats s'apliquen a un convertidor DC-DC amb tres escenaris de degradació per a la validació dels mètodes PHM proposats. Finalment, el model no lineal del convertidor s'ha linealitzat en línia quan s'aplica amb els enfocaments estocàstics. Tanmateix, s'ha transformat en un model lineal politòpic que varia amb paràmetres (Linear Parameter-Varying (LPV)) que fa ús de la tècnica LMI per a reduir els càlculs en línia, a més de facilitat la prognosi en temps real.

Paraules clau: Pronòstic i gestió de la salut, predicció de la vida útil restant, observadors deterministes, zonotop, pertinença a conjunts, filtres estocàstics, estimació conjunta d'estats i paràmetres, desigualtat de matriu lineal, variació lineal de paràmetres.

Nomenclature

Algebra

$\lvert \cdot \rvert$	Absolute value
$\lVert \cdot \rVert_F$	Frobenius norm
$\lVert \cdot \rVert_P$	P-norm
$\lVert \cdot \rVert_\infty$	∞-norm
$\oplus$	Minkowski sum
$\otimes$	Kronecker product
$\in$	It belongs to
$\bigtriangledown f$	Gradient of function f
$\iff$	if and only if
$\forall$	For all
$\approx$	Approximately equal
$\equiv$	Equivalent

Matrices, vectors, scalars

$\mathbf{A}$	General notation for a matrix
$\mathbf{A}^\intercal$	Transpose of matrix $\mathbf{A}$
$\mathbf{A}^{-1}$	Inverse of matrix $\mathbf{A}$
$[\mathbf{A}]$	General notation for an interval matrix
$diag(\mathbf{A})$	Diagonal matrix with appropriate dimensions
$\mathbf{a}$	General notation for a vector
a	General notation for a scalar
$\mathbf{I}_n$	Identity matrix in $\mathbb{R}^{n \times n}$
$\mathbf{0}_n$	Zeros matrix in $\mathbb{R}^{n \times n}$
$\mathbf{A} \succ 0$	General notation for strictly positive definite matrix $\mathbf{A}$
$\mathbf{A} \prec 0$	General notation for strictly negative definite matrix $\mathbf{A}$

$\mathbf{A} \succeq 0$	General notation for positive definite matrix $\mathbf{A}$
$\mathbf{A} \preceq 0$	General notation for negative definite matrix $\mathbf{A}$
$det(\mathbf{A})$	Determinant of matrix $\mathbf{A}$
$tr(\mathbf{A})$	Trace of matrix $\mathbf{A}$
$Im(\mathbf{A})$	Image of matrix $\mathbf{A}$
$\star$	Symmetrical elements in a matrix

Sets

$\mathbb{R}$	Set of real numbers
$\mathbb{R}^n$	Set n-dimensional of real numbers
$\mathbb{R}_+$	Set of strictly positive real numbers
$\cap$	Intersection
$\subset$	Subset
$[\underline{x}, \overline{x}]$	Interval with lower and upper bounds
$mid(\mathcal{I})$	Center of an interval $\mathcal{I}$
$rad(\mathcal{I})$	Radius of an interval $\mathcal{I}$
$\mathcal{S}$	General notation for a set
$\mathcal{Z}\langle \mathbf{c}, \mathbf{G} \rangle$	Zonotope $\mathcal{Z}$ with center $\mathbf{c}$ and generator matrix $\mathbf{G}$
$\mathcal{M}(\mathcal{S})$	Image of set $\mathcal{S}$
$\mathcal{B}^n$	Unitary box in $\mathbb{R}^n$
$\mathcal{B}^1$	Unitary interval
$\blacksquare\mathcal{Z}$	Interval hull of a zonotope $\mathcal{Z}$
$\diamond\mathcal{Z}$	Zonotope inclusion
$\mathcal{V}_\mathcal{Z}$	Notation of the vertex of a zonotope $\mathcal{Z}$
$conv(\mathcal{S})$	Convex hull of $\mathcal{S}$

Variables

t	Continuous-time instant
k	Discrete-time instant
F_s	Sampling frequency
T_s	Sampling period
f_s	Switching frequency
t_s	Switching period
d	Duty cycle
ω	Process noise
υ	Measurement noise
$i = 1, \ldots, n$	variable $i \in \mathbb{N}$ ranging from 1 to n

Acronyms

AGE	Accelerated Aging Experiment.
ANN	Artificial Neural Network.
CALCE	Center for Advanced Life Cycle Engineering.
CBM	Condition-based Maintenance.
CM	Corrective Maintenance.
CRUL	Component Remaining Useful Life.
DEKF	Dual Extended Kalman Filter.
DKF	Dual Kalman Filter.
DoD	Department of Defense.
ECAP	Electrolytic Capacitor.
EKF	Extended Kalman Filter.
EoL	End of Life.
ESR	Equivalent Series Resistance.
FCCF	First Critical Component to Fail.
FDI	Fault Detection and Identification.
HUMS	Health and Usage Monitoring System.
IGBT	Insulated Gate Bipolar Transistor.
ISHM	Integrated Systems Health Management.
IVHM	Integrated Vehicle Health Management.

JESP	Joint Estimation of States and Parameters.
KCL	Kirchhoff's Current Law.
KF	Kalman Filter.
KVL	Kirchhoff's Voltage Law.
LFT	Linear Fractional Transformation.
LMI	Linear Matrix Inequality.
LPV	Linear Parameter-Variant.
LTI	Linear Time-Invariant.
LTV	Linear Time-Variant.
MOSFET	Metal Oxide Semiconductor Field Effect Transistor.
NASA	National Aeronautics and Space Administration.
PCoE	Prognostics Center of Excellence.
PDF	Probability Density Function.
PH	Prognostic Horizon.
PHM	Prognostics and Health Management.
PM	Preventive Maintenance.
PoF	Physics-of-Failure.
RA	Relative Accuracy.
RLS	Recursive Least Squares.
RUL	Remaining Useful Life.
RZSM	Recursive Zonotopic Set-Membership.
SoH	State of Health.
SRUL	System Remaining Useful Life.
TH	Threshold.
UKF	Unscented Kalman Filter.
ZEKF	Zonotopic Extended Kalman Filter.
ZSM	Zonotopic Set-Membership.

List of Figures

This page is intentionally left blank

List of Tables

General Introduction

Context and Motivations

Modern-engineering applications with harsh operating conditions and crucial decision making are interestingly gaining attention in recent years. These critical applications such as electrical and/or autonomous vehicles, aircraft, satellites, outer space vehicles, and huge industrial applications have contributed to emphasizing on the reliability engineering aspect. Thus, apart from the faults with unpredictable behaviors, the degradation is responsible of deviating the optimal desired operation of a system towards a less efficient performance that could lead to a total failure. The degradation in electronic systems is observed through the variation of the internal parameters of active and passive components as well as the soldering, connectors, cables, etc. Moreover, similar deterioration behaviors are resulted in forms of cracks in mechanical systems such as bearings, shafts, etc. Whereas, it is noteworthy to clarify that electronics-rich systems tend to be more complex due to the interdependency of large amount of components with different types, behaviors, duties, and failure rates than most of the mechanical systems (M. G. Pecht 2018). Thus, two major factors that affect the desired operation of those systems can be characterized by thermal and electrical overstresses. In consequence, the resulting cascading damage of the interdependent components in a system could lead to catastrophic events and system failure that require time-consuming and expensive maintenance strategies that affect the system availability and the logistics support.

The fundamental concerns in reliability assessment of the aforementioned

applications are carried out in the practiced maintenance strategies. In other words, the post-failure maintenance strategy is known as the Corrective Maintenance (CM) and practiced after losses in terms in availability, expenses, time, and probably lives. Whereas, the Preventive Maintenance (PM) strategy reduces the life-cycle of the system due to the preventive scheduled maintenance practices that occur before the failure based on historical information. Therefore, the Condition-based Maintenance (CBM) is the only strategy that is applied when needed in order to avoid the catastrophic events from happening in a preventive framework and cost-efficient practice. Consequently, the CBM is elaborated based on current health assessment of systems in addition to failures prediction.

The core of the CBM strategy is consolidated in the Prognostics and Health Management (PHM), since the objectives of the PHM are characterized by online health-monitoring and failure predictions. The online continuous monitoring is employed to assess the State of Health (SoH) of a component or a system that will allow the prediction of the degradation behaviors until reaching known physical thresholds, in order to predict its End of Life (EoL) and forecast its Remaining Useful Life (RUL). The radical outcome of the PHM is interpreted in the life-cycle extension and the indirect cost reduction, in addition to the system availability, and flexible time for precautions and rescheduling of maintenance. On the other hand, some limitations such as uncertainties, on-board monitoring, system-level prognostics, etc., burden the development of PHM.

In broad, there is no single PHM architecture due to the difficulty of its standardizing as a structured practice. The PHM approaches are split into *model-based* and *data-driven* techniques which are diverse and have completely different features and require different specifications depending on the type of each application. Eventually, the aforementioned approaches raise concerns about the selection of the most suitable approach with the proper application. Although the feasibility of system modeling is limited to a certain level of complexity and fidelity, a huge amount of historical data would be required to overcome the modeling phase with the data-driven approach, whereas it is limited due to the fast upgrades of modern systems. Consequently, both approaches face the *uncertainties* whether in *modeling* or in *data acquisition*. By mentioning the latter, there exists various ways to process the data that can be performed online or offline and onboard or offboard the system that will constraint the overall PHM integration. Nevertheless, the RUL forecasting is the main technical objective that leads to the CBM, and as well is split into various practices. The RUL forecasting

methodologies depend on whether it is performed on a *component-level* or a *system-level*. Unlike the component-level, the system-level approaches reflect the real engineering applications that contain multidisciplinary components, subsystems, and devices. Thus, whether Component Remaining Useful Life (CRUL) or System Remaining Useful Life (SRUL), they are both predicted to assess the SoH of a component or a system respectively. Therefore, the SoH assessment methods can be characterized using failure indicators which are known as *failure precursors* that can be adopted by both model-based and data-driven prognostics. The deviation level of the failure precursors indicates the evolving degradation. Whereas, the failure precursors for system-level prognostics are broadly limited to external parameters of the systems such as input/output measurements. On the other hand, the failure precursors of the components are more specific and provide the internal degradation effect. Speaking of component-level prognostics, there exists an accurate yet more effort and time-consuming approach which is based on the modeling of the *failure mechanisms* of the components. The latter requires strong knowledge of the *Physics-of-Failure (PoF)* of each components which increases the modeling fidelity along with the complexity, which could not be practical for components-rich systems.

Technically, the failure is predicted by regressing known PoF-based degradation or empirical failure precursors models, if the models are known. Otherwise, the training-data are then used to fit the degradation trends with data-driven prognostics, for unknown degradation models. Furthermore, the empirical and PoF-based models of the degraded components or systems are fit based on current and previous observations. In practice, the degradation is estimated using Kalman Filter (KF), Extended Kalman Filter (EKF), particle filter, etc., if not all the parameters are accessible for measurements by direct means. In broad, only external features of the systems are considered for system-level prognostics. Thus, the predicted degradation trends are intersected with the failure thresholds of the components or the system.

Finally, the motivation of this thesis is fundamentally based on the diversity of PHM approaches for complex systems. Based on the aforementioned, the reliability assessment is strongly based on the estimation of SoH of a component or a system on which the RUL forecasting is based. Indeed, the prognostics approach should consider practical applications characterized as systems with multidisciplinary components. Additionally, noises and uncertainties of sensors and degradation models crucially affect the failure prediction process. In broad, stochastic approaches are mainly employed in the literature to deal with such constraints following Gaussian distributions of

noises and uncertainties, and probabilistic failure predictions. Whereas, the degraded systems behavior with unknown noises and uncertainties necessitate to be investigated. Additionally, the CBM strategy can be optimized for system-level PHM by identifying the degradation of the critical components rather than only considering the external features of a system. Moreover, there is a remarkable rule that employ data-driven prognostics for unknown degradation models, yet it is worth investigating to which extent the RUL can be predicted without knowledge of degradation models. For these purposes, the objectives and contributions of this PhD thesis are detailed in the following section.

Objectives and Contributions

Based on the aforementioned issues, the main objective of this thesis is to formalize a model-based PHM architecture for nonlinear systems with emphasizing on a guaranteed robust degradation estimation of systems. Thus, it is essential to assess the SoH of a system by estimating the states of its critical components, especially for complex systems. Therefore, we focus on the investigation of degradation estimation through simple indicators that do not require a strong knowledge of the system for the sake of generalization. Thus, the challenges that accompany the estimation problem arise. Identification and representation of nonlinear switched-systems were encountered first by the approximation, observability, representation, and uncertainties issues. To this phase, we investigated various linearization approaches with different representation throughout this thesis until adopting a polytopic Linear Parameter-Variant (LPV) model representation that suites best for real-time prognostics applications. The main aim of employing such representation is motivated by the diversity of system identification approaches for LPV modeling, that allows the implementation of the proposed PHM with more applications with fine tuning only.

Moreover, dealing with future events has never been certain. Thus, the classical stochastic approaches that employ KF, particle filter, etc. for states and parameters estimation are accurate for estimation, yet not reliable for RUL forecasting. For these reasons, these approaches have been investigated in this thesis, and according to the observations, we intended to employ zonotopic-based approaches for both estimation and prediction. The simple implementation of zonotopes is motivated for real-time forecasting, in addition to the dynamic bounds that solve the issue of uncertainties in the stochastic approaches. In broad, the bounds provide guaranteed limits for

the estimated states and parameters that characterize the degradation precursors. Furthermore, the importance of the LPV representation can be seen through the tuning of the aforementioned zonotopic observers. In other words, we proposed to tune the LPV observers offline with the polytopic model obtained using the bounding box approach using Linear Matrix Inequality (LMI) formulation for stability, which also provides a mode reduced computational time than the classical online gain scheduling approaches. Consequently, the estimated zonotopic sets will be employed online by the RUL forecasting phase.

The ideal desired outcome of the PHM is achieved if the RUL forecasting is achieved online with high reliability from the measurement time instant until the EoL of the component or system. Building upon this hypothesis, we investigated a classical degradation prediction approach using known degradation models, as usually followed in the literature. However, as we intend to generalize the whole PHM approach, we proposed an intuitive RUL forecasting approach which does not require any previous knowledge of the degradation model. However, it has been eliminated along with the classical approach due to vital reliability concerns, model-dependency, and complex computations that consume time and effort. Therefore, we proposed a recursive zonotopic approach that follows an exponential degradation trend with no previous knowledge of the exact degradation model, that has been reduced and rewritten in a linear form to guarantee the homogeneity between the estimation and the prediction process. The later approach has been validated with unknown-but-bounded and Gaussian noises and uncertainties with a very high forecasting reliability unlike the previously-investigated predictions.

This thesis is made up by five chapters and two appendices in total, as illustrated in Figure 1. Here follows, a short description of the contents of each chapter apart from the general introduction.

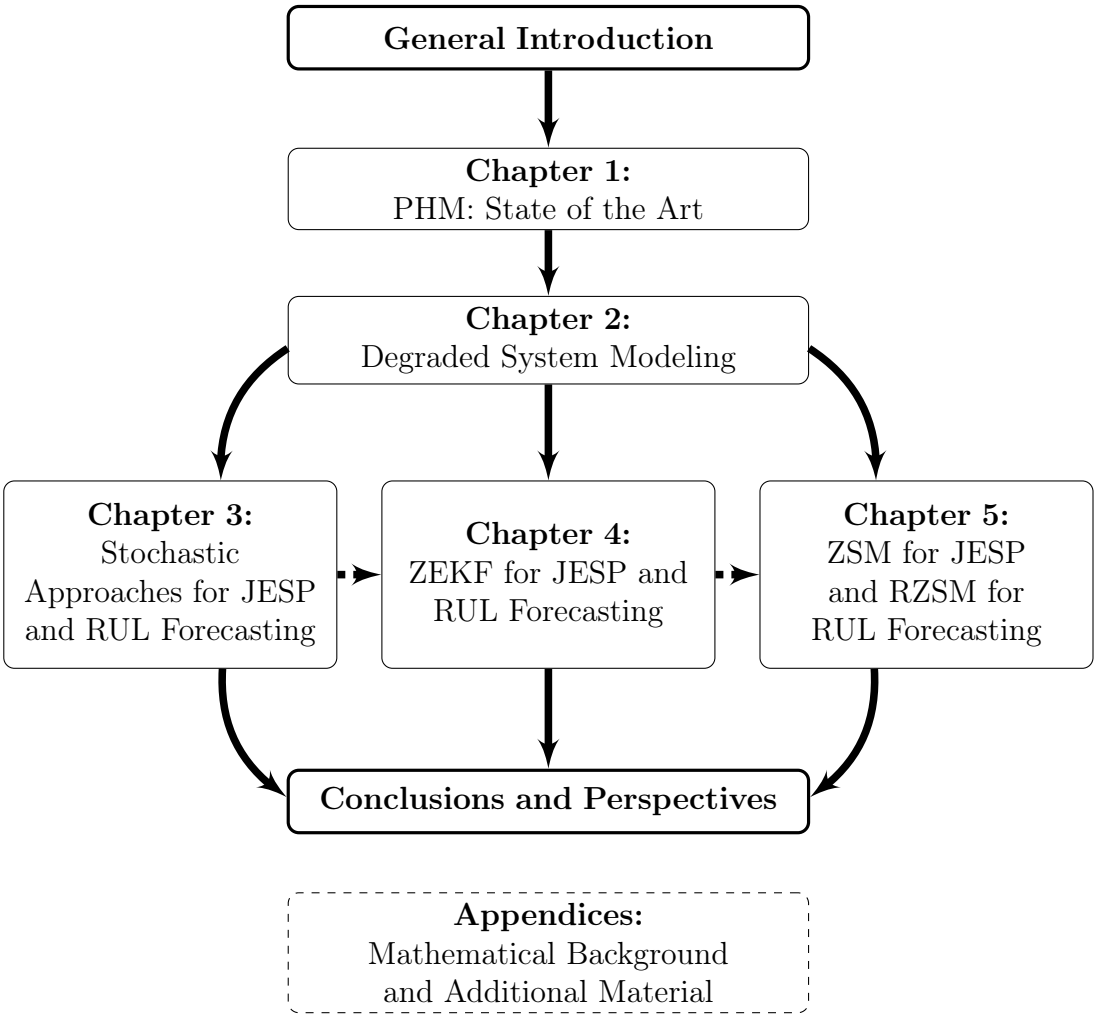

Figure 1: Thesis structure

Chapter 1: Prognostics and Health Management: State of the Art

An overview of the PHM is presented in this chapter. The various types of prognostics approaches are introduced with the required physical and numerical tools to stand against the challenges of their applications. Thus, the importance of integrating prognostics techniques with emphasis on the expenses of each type with possible cost-saving methods and improvements. Moreover, the investigation of the model-based PHM approach has been defended for the sake of applications to power electronics-rich systems. Ad-

ditionally, the proposed PHM methodology is structured and the essential roles of the stochastic and the deterministic estimation techniques have been discussed. Hence, the RUL forecasting methods have been explained, and directed to our point of view from these contributions.

Chapter 2: Degraded System: Modeling and Analysis

This chapter highlights a principal pillar of the prognostics applications. It starts by modeling a DC-DC converter that is used in electrical vehicles, and can be involved in many other engineering fields such as satellites, aircraft, power plants, etc. Alternating and average models are two representations for switched-systems, where each one can be utilized with different types of precursors for the prognostics study. However, the average model has been applied in this work in order to reduce the computational effort. Moreover, we have proposed three degradation scenarios after presenting the empirical modeling of two crucial power electronic components. The empirical models of the Metal Oxide Semiconductor Field Effect Transistor (MOSFET) and the Electrolytic Capacitor (ECAP) have been created by fitting their real accelerated aging data which are available on an online repository (Renwick, J. and Kulkarni, C. and Celaya, J. 2015; Celaya, J. R. and Saxena, A. and Saha, S. and Goebel, K. 2011). Thus, the aim of the empirical degradation is to analyze the degradation effect on the remaining components in the system and on its overall efficiency. Therefore, it allows to simulate several degradation behaviors for the sake of investigating the prognostics techniques with several case studies. Moreover, assuming that only the external measurements of the system are allowed, the model should be represented to allow the estimation of the internal parameters that describe the degradation precursors. For this reason, we propose to extract the parameters in form of regressors, apply two separate filters for states and parameters estimation, or reduce the computational efforts by employing only one filter for Joint Estimation of States and Parameters (JESP). Therefore, we adopt the augmented model representation of the dynamical model.

Chapter 3: Stochastic Approaches for PHM and RUL Forecasting

The first PHM approach based on stochastic estimation techniques is presented in this chapter. The aim of this chapter is to present the general structure of model-based prognostics by dealing with nonlinear systems, degradation estimation, and RUL forecasting. Thus, based on its wide applications in many industrial applications, we employ the EKF in order to estimate

the states and the parameters. Furthermore, parameters estimation plays a vital role in the reliability assessment of the RUL forecasting approach. The main reason refers to the proposition of unknown degradation behaviors that obliges the estimation of the degradation precursors. Hence, the first proposed RUL approach is based on the simple EoL-RUL linear relation and the estimated degradation level. The proposed approach is investigated with the scenarios of the case study for the sake of a complete assessment on the whole system. Finally, further improvements are proposed based on the obtained results, in the following chapter.

Chapter 4: Zonotopic Extended Kalman Filter Approach for PHM with Bounded RUL Forecasting

A major RUL-related issue had been analyzed and concluded from the previous chapter. The RUL is a sensitive prediction which is mainly applied to crucial, autonomous, and costly systems. Thus, as the prediction is still not happened yet, it can never follows a precise timeline for its occurrence. In consequence, we propose to provide bounded RUL forecasting by indirectly deducing the bounds from zonotopic parameters estimation using the Zonotopic Extended Kalman Filter (ZEKF) approach for JESP. Zonotopes have been selected because of the reduced computational effort in addition to the high estimation accuracy as they are combined with the widely-utilized EKF. Moreover, we propose an LMI-based optimization problem to tune the observer offline with online arithmetic computations only, that will reduce the time of the estimation and the prediction process, which could also be applied to nonlinear systems.

Chapter 5: Zonotopic Set-Membership Approach for PHM with Recursive Zonotopic-RUL Forecasting

A robust Recursive Zonotopic Set-Membership (RZSM) approach for RUL forecasting with application to LPV systems is proposed in this chapter. It addresses the JESP in a Zonotopic Set-Membership (ZSM) scheme with optimal LMI-based tuning for multi-output systems. Thus, a RZSM approach is proposed for an indirect RUL forecasting based on the prediction of the varying functions. Additionally, the issue of dealing with the nonlinearities of the parameter variations, uncertainties and noises is solved in an LPV framework. Finally, this approach is tested on the DC-DC converter case study with unknown degradation behaviors, and the obtained results show the estimation and the forecasting accuracy of this methodology.

Conclusions and Perspectives

General conclusions and proposed perspectives contributing to system-level prognostics.

Extended keywords list: System identification and modeling, degradation modeling, power electronics, DC-DC converters, electric vehicles, nonlinear systems, augmented model representation, stochastic observers, extended Kalman filter, dual extended Kalman filter, recursive least squares filter, Gaussian noises, joint estimation of states and parameters, Jacobian linearization, model-based prognostics, remaining useful life forecasting, deterministic observers, zonotopes, bounded noises and uncertainties, bounded remaining useful life forecasting, linear parameter-varying systems, linear matrix inequality optimization, zonotopic set-membership, recursive zonotopic set-membership, exponential degradation prediction.

Publications

Journals papers

1. **Ahmad Al-Mohamad**, Ghaleb Hoblos, Vicenç Puig, A hybrid system-level prognostics approach with online RUL forecasting for electronics-rich systems with unknown degradation behaviors, Microelectronics Reliability, Volume 111, 2020, 113676, ISSN 0026-2714, https://doi.org/10.1016/j.microrel.2020.113676

Papers in peer-reviewed conferences

1. **A. Al-Mohamad**, V. Puig, G. Hoblos and J. Azzam, "Robust Zonotopic Prognostics Approaches for LPV Systems Based on Set-Membership and Extended Kalman Filter," 2021 5th International Conference on Control, Automation and Diagnosis (ICCAD), Grenoble, France, 2021 (ACCEPTED).

2. **A. Al-Mohamad**, V. Puig and G. Hoblos, "Prognosis Based on the Joint Parameter/State Estimation Using Zonotopic LPV Set-Membership Approach," 2021 19th IFAC Symposium on System Identification (SYSID), Padova, Italy , 2021 (ACCEPTED).

3. **A. Al-Mohamad**, V. Puig and G. Hoblos, "Robust Zonotopic Set-Membership Approach for Model-Based Prognosis: Application on Lin-

ear Parameter-Varying Systems," 2021 19th European Control Conference (ECC), Rotterdam, The Netherlands, 2021 (ACCEPTED).

4. **A. Al-Mohamad**, V. Puig and G. Hoblos, "Zonotopic Extended Kalman Filter For RUL Forecasting With Unknown Degradation Behaviors," 2020 28th Mediterranean Conference on Control and Automation (MED), Saint-Raphaël, France, 2020, pp. 574-579, doi: 10.1109/MED48518.2020.9182829

5. A. Alyakhni, **A. Al-Mohamad** and G. Hoblos, "Joint Estimation of MOSFET Degradation in a DC-DC Converter Using Extended Kalman Filter," 2019 4th Conference on Control and Fault Tolerant Systems (SysTol), Casablanca, Morocco, 2019, pp. 319-324. doi: 10.1109/SYSTOL.2019.8864731

6. **A. Al-Mohamad**, G. Hoblos and V. Puig, "A Model-Based Prognostics Approach for RUL Forecasting of a Degraded DC-DC Converter," 2019 4th Conference on Control and Fault Tolerant Systems (SysTol), Casablanca, Morocco, 2019, pp. 312-318. doi: 10.1109/SYSTOL.2019.8864778

Pending submission papers

1. **Ahmad Al-Mohamad**, Vicenç Puig, Ghaleb Hoblos, Recursive Zonotopic Set-Membership Approach for System-Level Prognostics with Application to LPV Systems, Journal of Reliability Engineering and System Safety, volume ..., 2021, ISSN ...,

CHAPTER 1

Prognostics and Health Management: State of the Art

Contents

1.1 Introduction to Prognostics and Health Management

The major increase of complexity of the modern engineering applications has emerged an essential elaboration of new techniques for health monitoring and maintenance strategies (Elattar, Elminir, and Riad 2016; N. Kim, An, and J. Choi 2017b). In broad, these techniques emphasize on ensuring reliable operations with safety measures by continuously monitoring the health of the system, where the required decisions should be taken instantly (M. G. Pecht and Kang 2018). Thus, the continuous health monitoring of critical systems is namely referred to Fault Detection and Identification (FDI) in a diagnostic framework, where the faults are detected and located. In spite of the widespread fault diagnostics techniques, critical and complex applications (i.e. autonomous transportation, nuclear power plants, aerospace, etc.) have had necessitated upgrades to the current faults detection techniques. These upgrades consist of failure predictions, optimal maintenance scheduling, operation decision support, decision-making support, etc. Eventually, the root cause of this development lies in the importance of the maintenance strategies and the effects of such practices on the reliability of the systems. Indeed, the traditional maintenance strategy is known as the CM that takes place post-failure which is a completely passive practice that could lead to catastrophic events. Additionally, the CM is the most expensive maintenance strategy due to its unscheduled behavior that affects the life-cycle of systems. Moreover, the reliability prediction techniques that have been developed in the 1950s, focus on estimating the field-reliability of systems using analytical modeling and data acquisition (W. Denson 1998; Elattar, Elminir, and Riad 2016; N. Kim, An, and J. Choi 2017b). Such maintenance strategy is known as the PM, and considered as an active practice since it occurs at scheduled intervals of times. The PM is less expensive than the CM due to the fact that statistical and analytical analyses of the previous failure data are involved to develop these techniques that organize the maintenance needs (Luo, Namburu, and Pattipati 2003). These approaches have been elaborated in Mil-HDBK-217 (*MIL-HDBK 217 (1965)* 1965), 217-PLUS, PRISM (W.A. Denson 1999), Telcordia SR-332 (*Telcordia Technologies (2001)* 2001), and FIDES (*FIDES Group (2004)* 2004).

Moreover, the concerns about the reliability assessment have had been raised despite the safe role of the PM approaches, due to the complexity of modern critical engineering applications that does not comply efficiently with the traditional systems operation monitoring and scheduled maintenance, in order

to avoid catastrophic failures that could lead to complete systems shutdown, and loss of lives. In consequence, the CBM strategy has been elaborated in order to reduce the unnecessary maintenance that increases the total life-cycle costs, and indicates the exact damaged/faulty components or systems. The CBM strategy accounts for the least expensive strategy in terms of the life-cycle costs since it is considered as a proactive approach that is only applied when it is needed (Elattar, Elminir, and Riad 2016; Chang, Fan, et al. 2018; M. Pecht 2011; Schwabacher and K. Goebel 2007; M. Pecht 2006). An example that clarifies the concept of the CBM was given in (N. Kim, An, and J. Choi 2017b) about changing the oil of cars. It states that the conventional old method defined a range of 3000 to 5000 miles that emerges changing the engine oil. Whereas, this method can lead to huge oil waste, and the CBM solves this issue by continuously measuring the health of the oil, and prevents the driver to change it when needed only. Therefore, the CBM is carried out by the implementation of the PHM.
Figure 1.1 illustrates the maintenance strategies versus the cost.

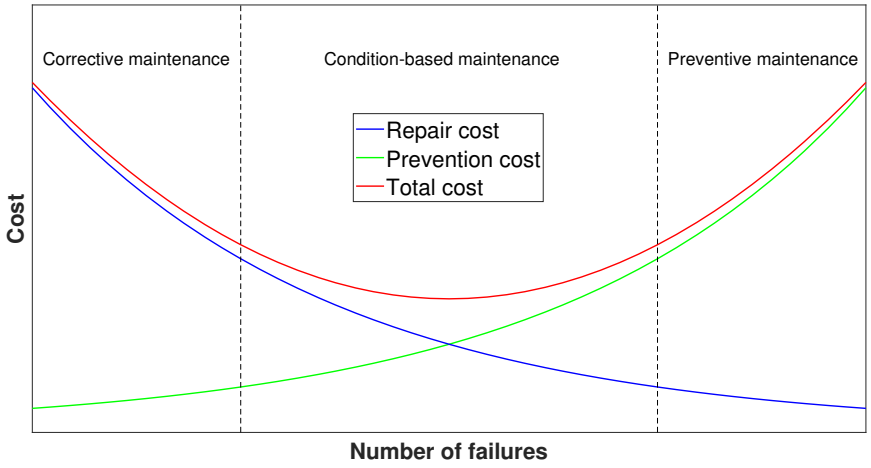

Figure 1.1: The three maintenance strategies versus cost (N. Kim, An, and J. Choi 2017b)

PHM is split into prognostics and health management of systems (Chang, Fan, et al. 2018). Health management is mainly based on the health monitoring of the system at the actual operating time (Elattar, Elminir, and Riad 2016; Chang, Fan, et al. 2018; M. Pecht 2011; Schwabacher and K. Goebel 2007; S. Zhou, L. Zhou, and P. Sun 2013; Xiong et al. 2008; Xiang, Ran, Tavner, S. Yang, et al. 2012; Xiang, Ran, Tavner, Bryant, et al. 2011; Mo-

hagheghi, Harley, and Habetler 2009). Health monitoring is considered as the in-situ fault diagnostics that reports various types of detected malfunctions in the system. Thus, the Greek word "*proginoskes*" is the modern-day prognostics that means foresight or foreknowledge (Chang, Fan, et al. 2018). In an engineering framework, prognostics is defined as the process that permits the prediction of the RUL of a component/subsystem/system that is subject to degradation due to natural or harsh operation conditions (Elattar, Elminir, and Riad 2016). Among various sources, ISO Central Secretary (2015) defined the prognostics as "*an estimation of time to failure and risk for one or more existing and future failure modes*".

The concept of the PHM was first adopted for the aerospace applications as it was initially used to reduce the helicopter accident rate by the civil aviation authority of United Kingdom in the 1980s (N. Kim, An, and J. Choi 2017b). Furthermore, the development of the PHM approaches took place in the 1990s where the desired functionalities have been achieved by Health and Usage Monitoring System (HUMS) that reduced the accident rate of helicopters by more than a half as stated in (*UK Offshore Commercial Air Transport Helicopter Safety Record (1981 – 2010)* 2011; N. Kim, An, and J. Choi 2017b).

During the same period, the Center for Advanced Life Cycle Engineering (CALCE) was established in 1986 with a great interest in reliability assessment for power electronic systems that has been elaborated under the PHM practices with physics-based failure analysis (CALCE 1986). National Aeronautics and Space Administration (NASA) Office of Space Flights also established the Integrated Vehicle Health Management (IVHM) to monitor the health of the space vehicles as a major technology of the future (Aeronautics and Technology 1992; C.D. et al. 1999). Thus, the same concept of the IVHM has been replaced by a more extensive term, the Integrated Systems Health Management (ISHM) as a universal term, where the prognostics play an essential role in its development. This establishment has pushed the boundaries of systems health management to the next level by integrating the prognostics in the ISHM (Schwabacher and K. Goebel 2007; Elattar, Elminir, and Riad 2016; N. Kim, An, and J. Choi 2017b; M. G. Pecht and Kang 2018).

The main reason behind emphasizing on developing prognostics techniques refers to avoid inaccurate predictions of failures that could affect the decision-making as in logistics and maintenance (M. G. Pecht and Kang 2018). Accordingly, the United States Department of Defense (DoD) forces the employment of PHM technologies by investing in their development by NASA Ames

Research Center and the Jet propulsion Laboratory that are game changers in this field (defense 2002).
Later on, the Prognostics Center of Excellence (PCoE) of NASA started the investigation of failure mechanisms with damage propagation for the wiring insulation and electrical and electronic components of aircraft and the avionic field in general (PCoE 1986).

The development of the prognostics has been elaborated for the sake of the employment of CBM in order to save predefined and unnecessary maintenance expenses, keep the system available, and predict an accurate and reliable RUL on a component-level or on a system-level. RUL forecasting is the most important contribution in this thesis as much as it is also one of the most challenging frontiers of PHM that provide advance warning of failures and aim for life-cycle extensions (M. Pecht 2006; B. Saha et al. 2009; M. Pecht 2011; Elattar, Elminir, and Riad 2016; Ferhat 2020). For these reasons the PHM practices address the reliability assessment despite the presence of standard-based reliability assessment (Ristow and Begovi 2008; S. E. D. Le et al. 2013; Khorshed Alam and H. Khan 2013), fault-tolerant topologies with redundant components (Tajfar and Mazumder 2012; Dat et al. 2012; A and K 2013) that do not prevent the failures from occurring.
Figure 1.2 illustrates the main elements in PHM as proposed in (K. Goebel, A. Saxena, et al. 2012).

The raw data acquired by the sensors of the system are usually processed before extracting the needed indicators for the PHM study. Despite the variety of data processing methods, the aim of this step is to analyze the useful information about the SoH of the system. It is required for the continuous assessment of fault detection using fault diagnostics techniques. non-faulty conditions do not necessarily mean a healthy system. Thus, failure prognostics are applied in order to detect and localize the degradation for the sake of RUL forecasting. finally, the accomplishment of the prognostics provides a clear image about the SoH of the system that has been provided by the enhanced diagnostics in addition to the predicted RUL which combined allow an optimized decision-making. The latter is mainly related to the required maintenance of the system (K. Goebel, A. Saxena, et al. 2012). This brief explanation of the PHM modules in general will be further explained throughout this thesis.

This chapter is structured as follows. Section 1.2 highlights the multidisciplinary benefits of PHM along with the main challenges. Thus, Section 1.3 presents the advantages and the limitations of the two prognostics approaches

and the possibility of merging them for optimal solutions. An overview of the PHM applications is provided in Section 1.4 with emphasizing on the role of electronics. Section 1.5 details the failure mechanisms of the most critical electronics components and explains their role in lifetime predictions versus the failure precursors approach. Moreover, the RUL forecasting methods are presented in Section 1.6. Additionally, a brief overview about prognostics evaluation metrics is provided in Section 1.7. We proposed a structured PHM methodology in Section 1.8. Finally, a state-of-the-art summary is provided in Section 1.9.

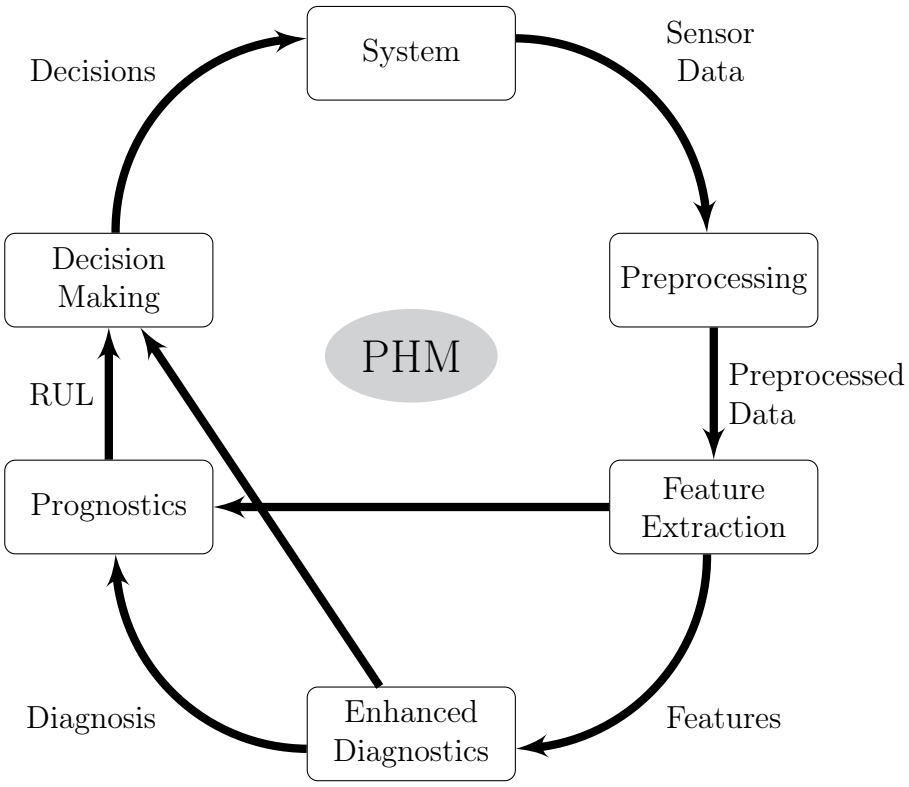

Figure 1.2: PHM overview (K. Goebel, A. Saxena, et al. 2012)

1.2 Benefits and Challenges of PHM

PHM is a multidisciplinary engineering practice which assesses the level of deviation of the system behavior from the desired operation in order to predict the system behavior and Forecast the RUL (Feather et al. 2008; M. G. Pecht and Kang 2018; N. Kim, An, and J. Choi 2017b). The aforementioned

targets are beneficial in terms of improving the system reliability, availability, operation, safety, and logistics support as well as reducing the maintenance-induced faults, time, and costs. Thus, many techniques have been developed, integrated, and validated towards enhancing the PHM aims. However, since the prognostic is not an easy task, many challenges such as uncertainties, lack of information, and false readings, accompany the PHM process and require serious development and validation. The following subsections summarize broadly, the main benefits and challenges of PHM.

1.2.1 Benefits of PHM

The benefits of the PHM are directed towards the reduction of cost-related actions such as the maintenance cost and extending the life-cycle of a system via the CBM. Thus, the cost reduction of the prognostics-based CBM is huge as claimed by General Electric, 1% efficiency improvement results in $276 billion in oil and gas, power, healthcare, aviation, and railroad industries (Evans and Annunziata 2012). Furthermore, the cost reduction will indirectly increase the revenue via the reliability. The reliability encourages more investment and trust in a product with embedded PHM system. As an example, an autonomous vehicle with reliable PHM attracts the users buyers, which increases the revenues. A more detailed analysis about the life-cycle benefits of PHM was elaborated by (B. Sun et al. 2012).

Moreover, prognostics can help the manufacturer to improve their products, by investigating their abilities via the PHM which will provide reliability-related data in various operation conditions and scenarios. Additionally, the reliability improvements along with the RUL forecasting practices can save time and costs in logistics. In other words, the future behaviors prediction with the RUL forecasting provide prior failure alarm that enables the logistics to ship the spare components and devices in advance, and avoid additional depots fees (N. Kim, An, and J. Choi 2017b; Elattar, Elminir, and Riad 2016; M. G. Pecht and Kang 2018; R. Yan et al. 2019).

Furthermore, the ability of predicting the future behavior of the complex and interconnected subsystems/systems, provides more time to the decision-makers in charge to plan and reconfigure the whole operation of the system optimally (Wheeler, Kurtoglu, and Poll 2010). Whereas, the reconfiguration process could be vital in some types of applications due to components degradation by many factors such as electrical overstress (i.e. overvoltage, overcurrent, electromagnetic field, frequency, etc.), and mechanical overstress (i.e. high temperature, vibration, friction, etc.).

The operational reliability can be improved by increasing the safety of the system which is provided by the PHM. Based on the aforementioned prognostics capability to predict the future behavior that adds more flexibility to encounter the failures, the availability of the system can be guaranteed. Thus, the risk of failures decreases and the lifetime of the whole system increases optimally with maintaining the reliable operation through the CBM practices (N. Kim, An, and J. Choi 2017b; Elattar, Elminir, and Riad 2016). Adding to the aforementioned benefits, the PHM improves the maintenance strategy from PM to a proactive CBM which by its turn reduces the processing and operation time, costs, and manpower that also reduces the risks that accompany these factors. Since the CBM minimizes the scheduled maintenance and increases the interval of maintenance which eliminates the redundant inspections and reduces the maintenance-induced faults, the cascading and secondary damages are eliminated (N. Kim, An, and J. Choi 2017b; Elattar, Elminir, and Riad 2016).

Additionally, the PHM provides continuous monitoring of the systems including black/grey box for degradation, tear, and wear slowly-evolved faults. Consequently, the operation of the system is safely guaranteed until its predicted EoL, which increases the safety of the system.

1.2.2 Challenges of PHM

Despite the multi-aspect benefits of PHM, the challenges increase with the complexity of critical systems particularly, due to the concept of prognostics that is based on predicting the future behaviors of systems. Prognostics are mostly related to observations and actual measurements, they are always affected by uncertainties, measurement-related instrumentation, and lack of information that will be detailed in the following (N. Kim, An, and J. Choi 2017b).

PHM require data acquisition either in real-time or historical measurements. They are employed for filtering and estimating the damage or for building training data-set in order to achieve the prognostics tasks. Sensors are the only link relating the system to the PHM. An optimal configuration could be achieved by implementing redundant multiple sensor for monitoring validation. Thus, considering the environmental effects with sensors degradation adds a burden to the RUL forecasting that could be affected by small uncertain measurements that could deteriorate the system and block the desired PHM outcomes (Sankararaman 2018; Robinson 2018; Cheng, Azarian, and

M. G. Pecht 2010; N. Kim, An, and J. Choi 2017b).
Moreover, prognostics uncertainties are major challenge that are related to:

- Model uncertainty which is caused by the degree of fidelity and parameters simplifications throughout the modeling process,
- RUL forecasting uncertainty affected by the aforementioned uncertain measurements due to the operation conditions and encountering environment.
- Originally-defected components and instruments by the production, can affect the whole operating behavior of the component/system that affects the forecasting process and the decision-making afterwards.

Thus, in order to encounter the effects of these uncertainties in RUL forecasting, it is crucial to develop techniques that can bound the uncertainties for guaranteed safety region while estimating and predicting the system behavior and EoL/RUL (Leao et al. 2008; J. R. Celaya, A. Saxena, S. Saha, and K. F. Goebel 2011; M. A. Djeziri, Benmoussa, and Sanchez 2018; Vachtsevanos, Lewis, M., et al. 2006; Vachtsevanos, Lewis, Roemer, et al. 2006b; Wheeler, Kurtoglu, and Poll 2010; A. Saxena et al. 2010b; Elattar, Elminir, and Riad 2016).

Furthermore, the lack of data of failures and operation conditions due to many reasons such as novel systems which are not yet experimented enough. Additionally, it is impossible to measure a crack growth or degradation of any components due to some barriers, etc. Thus, this can lead to inaccurate identification of the degradation profile.
N. Kim, An, and J. Choi (2017a) has shown an example about cracks of bearings and how difficult is to measure their evolution in order to extract degradation data from larger noisy signals in such dynamical system with harsh operation conditions.

Moreover, the post-prognostics actions are to be addressed with accurate decision-making due to the fact that they are highly-dependent on the prognostics. As for example, an automated system reconfiguration is based on the prognostics outputs, any uncertain RUL forecasting can decrease the estimated life-cycle of a system, or cause unnecessary system shut-down, false maintenance alarm, and more negative effects (B. Sun et al. 2012).

1.3 Prognostics Approaches

Three main approaches can categorize the prognostics techniques, model-based, data-driven, and hybrid. The selection of either approach depends on the specifications of the system, the availability of measurements and/or historical failures information, in addition to the implementation cost and complexity. In general, the model-based approach is more intuitive and depends on strong knowledge of the system and its parameters which are extracted as physical models. Whereas, the data-driven approach depends on training-data due to historical operations that are extrapolated with mathematical functions, and applied using statistical or soft computing approaches. Thus, the hybrid prognostics approach is the fusion between specific selections of features depending on the availability of the requirements of an application (N. Kim, An, and J. Choi 2017b; Elattar, Elminir, and Riad 2016; M. G. Pecht and Kang 2018; Robinson 2018; Luo, Namburu, and Pattipati 2003; L.H., E.L., and R.D. 2001). In broad, each of the aforementioned approaches has specific advantages in addition to some limitations. The choice of any approach depends on some criteria such as the knowledge of the system behavior, operating conditions, the degradation mechanisms, the importance of real-time forecasting, available measurement data, etc. Thus, the details about the main features of each approach are explained in the following subsections.

1.3.1 Data-driven prognostics

Data-driven techniques are basically applied to systems with PoF are difficult to model. These approaches are utilized more than other PHM approaches despite the fact that the data-driven approach performs with a relatively lower accuracy in real-time degradation estimation and RUL forecasting. The reason behind supporting this approach is that it is easy to implement in most applications, and does not require deep understanding of the PoF of the components or systems (Elattar, Elminir, and Riad 2016). Data-driven PHM is based on previously-aggregated data from similar systems, in various operation conditions and degradation behaviors. The training-data are utilized to estimate the current SoH and predict the future behaviors (Robinson 2018; Ferhat 2020). The proper amount of needed data forms a great barrier between the prediction accuracy and the computational time and effort, and it is the main challenge in developing the data-driven approaches.
Moreover, there exists several artificial intelligence and machine learning packages and already-developed algorithms that can be employed with simple tuning for prognostics.

Artificial Neural Network (ANN) is the most used approach in the data-driven methods (An, N. H. Kim, and J. Choi 2015). Vatani, Khorasani, and Meskin (2015) investigated the prognosis of gas turbine due to degradation based on recurrent neural network and nonlinear autoregressive neural network techniques. However, the authors presented some challenges that can be faced during the employment of these techniques such as the selection of parameters, the delays, the training data-set, validation, etc.

Furthermore, support vector machine and relevance vector machine techniques have been also investigated for prognostics applications. Chang, Kang, and M. Pecht (2017) proposed a relevance-vector-machine-based regression model approach for the sake of RUL prediction of light-emitting diodes. Thus, M. A. Patil et al. (2015) used the support vector machine classification method as a first stage for uncertain RUL estimation. Hence, they used support vector regressor for more accurate RUL prediction based on temperature and voltage data-sets for prognosis of lithium-ion batteries.

Gaussian process has also been used for prognostics in the literature. However, it is remarkable that this approach was mainly utilized for SoH prognosis of lithium-ion batteries i.e. (Richardson, Osborne, and Howey 2017; D. Liu et al. 2013; D. Zhou et al. 2018).

In addition to self-organizing map, principle component analysis, Hidden Markov Models, fuzzy logic techniques, and so on (M. G. Pecht and Kang 2018; Robinson 2018; Elattar, Elminir, and Riad 2016).

The main advantage of implementing the soft computing techniques over statistical, is that all hidden relations among parameters and components are considered and learned in addition to their ability of noise rejection. The failures data can be obtained through Accelerated Aging Experiments (AGEs) which are applied in real experimental testbeds, which are effective but not necessarily contain all types of failures. However, testing all types of failures with various operations can be achieved, yet it is very expensive and time-consuming as well. Failure simulation is another option that requires high-fidelity modeling of failures which is expensive and time-consuming, and not an easy task especially for complex systems (Q. Zhang, Basseville, and Benveniste 1994; P. Wang and Vachtsevanos 1999; Swanson 2001; W. Yang 2001; W. Wang and Wong 2002; Luo, Namburu, and Pattipati 2003; N. Kim, An, and J. Choi 2017b; M. G. Pecht and Kang 2018; Z. Zhang, Dong, and Xie 2018; M. Djeziri, Benmoussa, and Benbouzid 2019; R. Yan et al. 2019;

B. Yang, R. Liu, and Zio 2019; Y. Zhang et al. 2020).

1.3.2 Model-based prognostics

In model-based methods which are widely known as physics/PoF-based methods, it is assumed that the mathematical model of the degradation exists. Ordinarily, the model-based approaches are used to systems that can be modeled on micro-level as well the the macro-level in order to estimate the current degradation state and predict the RUL (Robinson 2018). In other words, the prognostics sometimes might be applied to an internal component that deteriorates the whole system, and a mathematical representation of the degradation requires a strong knowledge about the PoF of each relevant component. Hence, since the PoF can be modeled, degradation models are widely used to assess the SoH of the intended component, in addition to RUL prediction methodologies which are mainly based on statistical failures data (N. Kim, An, and J. Choi 2017b; M. G. Pecht and Kang 2018). In broad, degraded systems with inaccessible internal parameters, the degradation are mainly estimated based on failure mechanisms and/or failure precursors which are explained in details throughout this chapter.

Thus, stochastic approaches such as KF (Kalman 1960) for linear systems and its extensions such as EKF, Unscented Kalman Filter (UKF) (Wan and Van Der Merwe 2000), particle filters (Arulampalam et al. 2002) for nonlinear systems, etc. are used to estimate states and parameters of the degradation models. Mainly the particle filters are used for non-Gaussian noises whereas the Kalman-based filters are only concerned with Gaussian noise distribution. Furthermore, unknown input observers (Darouach, Zasadzinski, and Xu 1994) are possible approaches to estimate the hidden degradation as proposed in (Chelidze, Cusumano, and Chatterjee 2001).

Moreover, reliability-based assessment for standalone components were also considered with knowledge about its failure history without considering the current operating conditions. Thus, Poisson laws, Weibull analysis, and similar techniques can be used to deal with such conditions for degraded components. Thus, the residuals are also used as features of some RUL forecasting approaches that do not require to assess the degraded component on a system-level. Yet, it depends on the external cascading damage due to the degradation effects (Medjaher and Zerhouni 2009).

To sum up, the major drawback of this approach is related to costly and time-consuming of high-fidelity modeling, especially for complex systems (Elattar,

Elminir, and Riad 2016). On the other hand, the model-based prognostics provide relatively accurate RUL forecasting results based on the modeling fidelity. Moreover, such approaches are beneficial since they can be validated and verified in comparison with real degraded systems (Uckun, K. Goebel, and P. J.F. Lucas 2008). Despite that the modeling is a time-consuming practice, the models can be reused by simple parameters tuning. In broad, the model-based prognostics require the selection of the fault precursors that are identified by the identification of the failure mechanisms. Additionally, the model-based PHM can predict both the future behavior and the RUL of a component or a system (Luo, Namburu, and Pattipati 2003; Daigle and K. Goebel 2013; Elattar, Elminir, and Riad 2016; N. Kim, An, and J. Choi 2017b; Robinson 2018; M. G. Pecht and Kang 2018; Aggab et al. 2018; Ekanayake et al. 2019; Ferhat 2020).

According to the aforementioned briefing of the model-based approaches, it is seen that the techniques in the literature strongly depend on physical models of degradation. Hence, one of our objectives in this thesis is to investigate the RUL forecasting techniques in order to reduce the dependency on the time-consuming degradation modeling that could be avoided for our aim to standardize a structured system-level PHM approach. The elaboration of this investigation is consecutively explained throughout this thesis, while we dedicate this part of this chapter to review and assess the main prognostics techniques.

1.3.3 Hybrid prognostics

Hybrid prognostics approaches are the fusion between the advantages of the model-based and data-driven methods. As the model-based requires the availability of the degradation, failure, and system models and operation conditions, it compensates the lack of information that are not provided by the data-driven methods. On the other hand, the data-driven prognostics approaches can take advantage of the knowledge of the PoF when failure data are not available in order to process them in soft computing algorithms. Cheng and M. Pecht (2009) investigated a hybrid prognostics approach for RUL prediction of ceramic capacitors. The authors defined a nine-step hybridization process that can be extended to further applications.
Furthermore, K. Goebel, B. Saha, et al. (2008) proposed a hybrid prognostics approach for degraded lithium-ion batteries.
Moreover, K. Goebel, Eklund, and Bonanni (2006) applied fusion prognostics for RUL forecasting of aircraft engines bearing that have shown reliable results.

Merging the two approaches can be achieved on different levels depending on the actual needs by targeting the essential aim of RUL forecasting (Elattar, Elminir, and Riad 2016; N. Kim, An, and J. Choi 2017b; M. G. Pecht and Kang 2018; Baptista et al. 2019).

Since the hybrid prognostics approaches are not widely spread in the literature as the model-based and the data-driven, these reviews may be interesting for more information (Zio and Di Maio 2012; Daroogheh et al. 2015).

1.3.4 Summary of prognostics approaches

There is no standard rule that specifies the selection of any prognostics approaches. However, as explained above, some criteria define the requirements of each application. Modeling of complex systems is costly and time-consuming, yet physics-based prognostics approach provides accurate and reliable predictions. Whereas, if measurements and operation conditions of real systems are available, data-driven prognostics approach can be utilized due to its simple and fast implementation with no necessary knowledge of the system behavior. However, training data-sets are required and they are not always available for all applications. In other words, data-driven prognostics for latest real applications necessitate degrading real systems for data acquisition to learn the algorithms which is also a challenge to time and expenses. Table 1.1 summarizes the main advantages and limitations of model-based and data-driven prognostics approaches.

Our vision in this thesis is focused on model-based PHM practices with investigation on reduced knowledge of degradation models which can save a remarkable amount of effort and time for the sake of real-time accurate prognostics. It is essential to highlight the importance of developing a standardized PHM approach that suits modern-engineering applications with only simple tuning and no requirements of studying the failure mechanisms of the systems. Thus, this part is dedicated to a brief review about the PHM. Hence, our perspectives are extensively elaborated in this thesis after the problem statement in this chapter.

1.4 PHM Applications

The first elaborated application of an integrated PHM was intended for the aerospace field, as mentioned in Section 1.1. The main goal of contributing

Table 1.1: Advantages and limitations of prognostics techniques

Methods	Model-based	Data-driven
Advantages	• Intuitive results	• Easy and fast to implement
	• Models are reusable	• Consider all relationships without prejudice
	• Computationally acceptable to implement	
Limitations	• Requires understanding of the system and the PoF for the modeling	• Requires lots of data
	• High-fidelity models are computationally expensive	• Computationally expensive

to the development of PHM for the sake of the CBM concept, relies in the importance of the safety of critical engineering systems as well as the humans, in addition to the operations and maintenance. Failures in aerospace systems are mostly catastrophic while CM and PM are not sufficient to guarantee a reliable operation with real-time monitoring and predicted behavior assessment (Vachtsevanos, Lewis, Roemer, et al. 2006a). Moreover, as the prognostics yields to RUL forecasting, intermittent faults could not be predicted especially in electrical and electronic-based systems. In broad, the PHM in engineering applications concerns the degradation prediction of a component/subsystem/system. It is worth noting that the concept of prognostics is not a new invention since it has been applied in the weather forecast and in the medical field for prediction of the disease evolution after treatment (Abu-Hanna and Peter J. Lucas 2001), however we are interested in contributing to the PHM for complex engineering applications.

Furthermore, the PHM could be integrated with the system (plant) onboard for critical real-time applications such as outer space missions. It could be also applied offboard the system as the PHM aggregates the measured data for offline RUL forecasting for the sake of maintenance assessment, system reconfiguration, and logistics support. Thus, we can summarize that the two main prognostics outputs are the prediction of the *EoL* and/or *future behaviors* of the systems (A. Saxena et al. 2010b; Kothamasu, Huang, and VerDuin

2005). Moreover, as we previously stated, PHM is not a standardized and structured framework, yet it depends on the type of the application, the size of measured information, the location, static or dynamic system, and more factors that help optimize a suitable PHM for the desired outcomes. Rather than the faults in electronic and electrical systems, the cracks in materials can also be described as degradation where prognostics could forecast the future behavior of the crack evolution. The following are various examples of some prognostics applications in electrical, electronics, storage, healthcare, mechanical, and other critical and complex engineering fields. It is worth mentioning that these examples are a few samples of a wider prognostics-related application fields, yet not specific and cover aerial vehicles, cracks in rotating machinery, semiconductors, robotics, bearings, hydraulic pumps, nuclear plants, turbines, etc.

1.4.1 Vehicles

The automobile industry in addition to the outer space vehicles such as rockets and satellites are considered as ones of the most suitable applications for PHM that can save lives losses, and maintenance expenses. Safety first, it has started with real-time integrated diagnostics for automobiles to monitor the state of the actuators, that are all processed based on the onboard sensors readings (Elattar, Elminir, and Riad 2016). As an example, a patent for a prognostic and diagnostic system (Smith 2011) that performs online health monitoring and prognostics functions based on the sensors readings. It is also connected to a centralized database station that conserves all the information about previously diagnosed systems in order to detect any anomaly that could affect the operation of the system. The newly-measured data are compared with the central database and proper warnings about faults are sent back to the user/driver/commander of the vehicle. Then, the onboard prognostics system performs the necessary RUL forecasting and trend predictions based on the current diagnostics from the central database and the onboard Vehicle Management Computer (Smith 2011).

Moreover, NASA Ames center for diagnostic and prognostic in collaboration with the US Army and many technological institutes and universities developed PHM approaches for predicting the health of electro-mechanical actuators with online diagnostics onboard aircraft such as UH-60 Blackhawk. The relative error accuracy of the EoL forecasting did not exceed 10% (Balaban, A. Saxena, Narasimhan, Roychoudhury, and K. Goebel 2011; Balaban, A. Saxena, Narasimhan, Roychoudhury, Koopmans, et al. 2015).

Another critical device in the aircraft is the turbine engine that is vital for the safety of the whole system. PHM supports the CBM to such essential system that is described with high complexity due to the various types of internal and external components, and high-fidelity physical models are time-consuming and costly behaviors that can be avoided by the implementation of data-driven PHM approaches based on ANN (Elattar, Elminir, and Riad 2016).

1.4.2 Electronics

The electronics are engaged into many daily uses such as smartphones and computers as well as critical applications such as electric vehicles, aerial vehicles, and huge industrial applications. They are vital in any type of applications and can lead to a complete failure and system shutdown. In broad, the main challenges that affect the optimal operation of the electronic devices are thermo-electrical. The latter yield these devices to degrade with time, which accumulates in a cascading behavior to deteriorate the whole system. Thus, electronic components are most likely to deviate from their optimal rated operation, and the role of PHM is to estimate the level of this degradation and predict the RUL. However, in real applications the electronic components are integrated in electronic circuits such as converters, inverters, drives, controllers, and more that contain passive and active components, in addition to connectors, cables, switches, etc. Thus, the electronic circuit is considered as a system of many types of components that are characterized by different degradation behaviors. Each component is affected by external oversresses as well as internal damage due to the interdependency inside the circuit. This formation increases the complexity of the electronic circuits which by its turn adds a burden on the PHM to manage the transition from component-level to system-level prognostics, in addition to the uncertainties (B. Saha et al. 2009; M. Pecht 2011; Vasan and M. G. Pecht 2018; Hanif et al. 2019; Schmidt, König, and Prenosil 2012; Krebs et al. 2013). Moreover, Chang, Fan, et al. (2018) conducted research about PHM for light-emitting diodes, which shows that all types of electronic devices are concerned.

1.4.3 Lithium-ion batteries

The recent growing interest in the lithium-ion batteries in several electronics-rich system such as everyday portable electronics, electric/autonomous vehicles, and space systems, has raised the awareness of PHM and RUL forecasting for these batteries (S. Saxena, Xing, and M. G. Pecht 2018).

Stochastic filtering techniques were implemented by a novel approach developed by (D. Wang, Miao, and M. Pecht 2013), to determine the degradation of lithium-ion batteries. Least squares regression technique was used to fit the degradation models which are extrapolated in order to predict the RUL.

Hu, Youn, and Chung (2012) proposed EKF to estimate the state of charge and the capacity of batteries in a multiscale framework. Then, a particle filter was employed in order to project the estimates evolution for RUL prediction purposes with high accuracy, in (Hu, Jain, Tamirisa, et al. 2014).

Furthermore, data-driven approaches have been also proposed to estimate the capacity of lithium-ion batteries based on charging current and voltage curves by (Hu, Jain, P. Zhang, et al. 2014). The authors applied particle swamp optimization to find the optimum weight combination among previously obtained features and precursors using k-nearest neighbor regression. Finally, the capacity was estimated accurately using this data-driven approach.

Z. Wang et al. (2017) proposed voltage fault diagnosis and prognosis of battery systems of electric vehicles based on entropy and Z-score approaches. They emphasized on predicting the voltage fault through monitoring the battery voltage while operating in real-time.

1.4.4 Industrial

Huge industrial applications can benefit from the aforementioned advantages of PHM implementation in terms of increasing the system availability, the revenues, the reliability with decreasing the costs and failures risks.

Bonissone and K. Goebel (2002) employed hybrid soft computing techniques in order to develop an online prognostics approach to predict the remaining time to break of paper making machine in a particular phase.

J. Yan, Koç, and J. Lee (2004) developed an online prognostics algorithm for machine performance assessment for health monitoring and prediction of future failures behavior. This technique is implemented based on the logistics regression in order to assess the probability of failure. Thus, the RUL is predicted based on continuous monitoring in real-time autoregressive moving average.

1.4.5 Commercial aircraft

Commercial aircraft are a perfect example that shows the crucial role of PHM accompanied by safety and cost benefits. As explained in Section 1.1, the concept of PHM was applied to military helicopters, yet it has been extended to the commercial applications. To elaborate the essential role that PHM plays, it is important to emphasize on the maintenance strategy with the risks of such application. The major risk that encounters the aircraft is their availability while operating. In other words, in case of any critical failure, time is the only rescuer until safe landing. Thus, the ability of RUL forecasting of the devices of the aircraft such as the jet engines, electronics system, batteries, ans sensors, provides a prior knowledge about the health of the system which indirectly provides more time for maintenance and planning. Furthermore, commercial airliners tend to reduce the expenses in which the maintenance accounts for an important partition. For safety reasons, a part of the maintenance is made at scheduled periods rather than the detected faults by the online diagnostics that necessitates on-spot repair. The PHM system can transfer the active PM to proactive CBM that might provided an extended life-cycle of the devices of the aircraft in addition to reduced maintenance costs. Moreover, a prior planning can be made to the whole fleet in addition to optimal logistics support due to the previous knowledge of the occurring faults. A fully-detailed discussion about the role of PHM in commercial airlines was provided in (Walthall and Rajamani 2018).

These applications are a few and not the only examples which we summarized about the ability of PHM to deal with complex and critical systems, which also includes more field such as healthcare (Capelli-Schellpfeffer, Kang, and M. G. Pecht 2018), subsea cables (Flynn et al. 2018), etc. Moreover, we intended to express the PHM for vehicles, electronics, engines, sensors, batteries, and mechanical disciplines in order to show the major role of the electronic circuits in such applications. The electronic circuits have become common and essential in all engineering fields, and their failures cause the failure of the whole system. Consequently, it is vital to increase their reliability as components/subsystems/systems with the proper PHM methodology to guarantee the availability of the whole system. For these reasons, the PHM tools for critical power electronic components are investigated along with their failure mechanisms on component and system levels, in Section 1.5.

1.5 Failures and Prognostics of Electronic Devices

Motivated by the importance of the electronics in modern-engineering applications, this section is dedicated to elaborate the causes of failures, their types, and necessary practices of PHM for electronics.

Modern power electronic devices have discrete characteristics and are expected to live longer due to the advanced technologies in this field (Qingchuan et al. 2017). However, they are exposed to harsh operating conditions which lead to system-failure throughout the time. Whereas, the intermittent faults fall outside the scope of the prognostics application, the focus is on the slow degradation of the most effective power electronic components in the system. Thus, statistical studies have shown that the ECAPs are the most fragile followed by the power switching devices such as MOSFET and Insulated Gate Bipolar Transistor (IGBT), as illustrated in Figure 1.3 (Wolfgang 2007; S. Yang et al. 2010). The remaining failures are circuit-related such as the solder joints, connectors, and the printed circuit board, and others. Consequently, due to the fact that around 51% of the failures in the electronic devices occur in the ECAPs and the power semiconductors, it is crucial to review the PoF of both active and passive power electronic components.

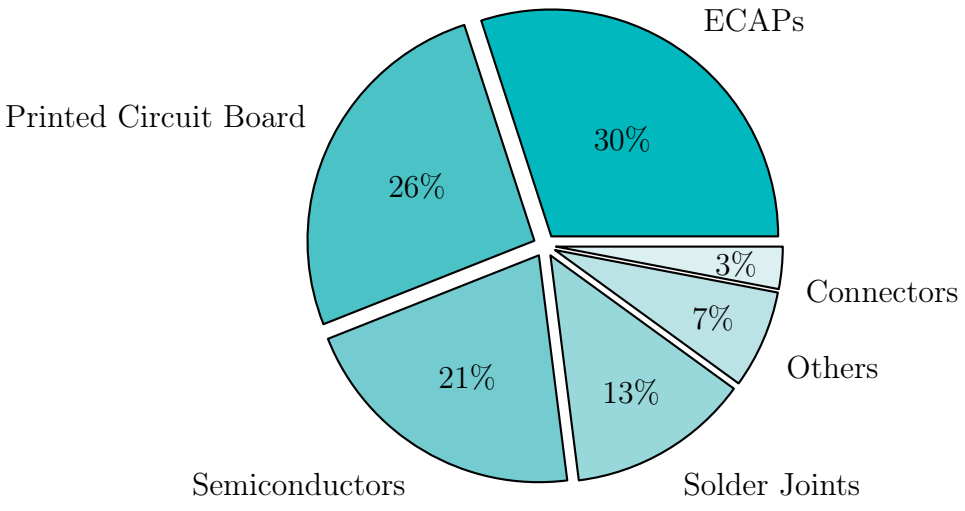

Figure 1.3: Failures in electronic devices (Wolfgang 2007; S. Yang et al. 2010)

1.5.1 Accelerated aging experiments

The electronic components are investigated by run-to-failure experiments, which are also known as accelerated life tests or as AGEs, in order to establish the root causes of the occurred faults. Thus, the *failure mechanisms* of each power electronic component are explained physically thanks to the AGEs which allow to accelerate the degradation process different electrical and thermal conditions. The fundamental interest of such practices is the derivation of degradation models, aggregation of measurements of the degradation profiles, and most importantly, the definition of the *failure precursors* of power switches (Hanif et al. 2019; Anderson, Cox, and O'Connor 2013; Samavatian, Avenas, and Iman-Eini 2018) and ECAPs (C. S. Kulkarni et al. 2012; C. Kulkarni, J. Celaya, G. Biswas, et al. 2011; J. Celaya et al. 2011; Chen et al. 2008).

The AGEs are powerful techniques to test the reliability of electronic components, examine their failure mechanisms, identify their failure precursors, parameterize their degradation behaviors, etc. Although the power electronic devices run through harsh operating conditions and degrade, they serve the system for a relatively long time. The AGEs allow easier investigation of the faults through degradation and examine the capabilities of the components being tested. Furthermore, the PoF assessment is based on the run-until-failure tests with several measurements at different precursors of the system, which will be further explained in the following subsections (Hanif et al. 2019). The AGEs are performed throughout electrical and thermal cycling to shorten the timescale of the electronic components such as ECAPs and power semiconductor switches. The performed in-situ measurements reports the occurred variations to illustrate their evolution (Z. Li, Zheng, and Outbib 2018; J. R. Celaya, A. Saxena, S. Saha, Vashchenko, et al. 2011a; J. R. Celaya, A. Saxena, S. Saha, and K. F. Goebel 2011; Jose R Celaya et al. 2010; S. Saha et al. 2011; J. R. Celaya, Wysocki, et al. 2010).

1.5.2 Failure mechanisms and precursors of MOSFETs and IGBTs

The power switching modules are accelerated in thermal testbeds that aim to stress the gate oxide, solder joints, and bond-wires of MOSFETs and IGBTs. Defined cycles of thermal swing amplitudes run for specific time intervals until failure, while measuring their parameters using a curve tracer machine. The parameters that vary with the degradation of the components/circuits are considered as failure precursors. These parameters are

monitored throughout different AGEs setups. For these reasons, there exists industrial standards such as IEC 60747, IEC 60749, IEC 60068, AEC-Q101, and JESD-47 in order to formalize the AGEs for semiconductors (Hanif et al. 2019).
A thermal chamber was used in (Katsis and van Wyk 2001) to degrade and monitor high-power MOSFETs using thermal cycling. The MOSFETs were heated up from 55°C to 100°C by a DC current for 3 minutes, then turn off the DC current for 2 minutes to complete the cycles.

Another AGE example was accomplished by (Dusmez and Akin 2015a), where the drain current was set at 5.2A while varying the junction temperature at three different conditions: 210°C, 220°C, and 240°C.

Another AGE was intended to monitor the reliability of MOSFETs and IGBTs of motor drive, was accomplished in (Pippola et al. 2015). The chamber was maintained at 85°C and 85% humidity level.

Therefore, the major failure precursors of MOSFETs and IGBTs are illustrated in Table 1.2.

Table 1.2: Fault precursors of electronic components

Electronic components	Failure precursors
MOSFET	• ON-resistance R_{ON}: Increases • Gate threshold voltage V_{th}: Increases
IGBT	• Gate threshold voltage V_{th}: Increases • Rise and fall time: Increases • ON-state collector-emitter voltage $V_{\text{CE}_{\text{ON}}}$: Increases or decreases • Turn-OFF time

A significant increase of the R_{ON} by around 17%, and the V_{th} of MOSFETs have been observed in (Dupont et al. 2007; J. R. Celaya, A. Saxena, S. Saha, Vashchenko, et al. 2011b; Azoui et al. 2012; Dusmez, Duran, and Akin 2016; Dusmez and Akin 2015b). The observed failure precursors of IGBTs have been characterized via the AGEs under more possibilities as shown in Table 1.2.
Thus, the increase of V_{th} is a major failure precursor for IGBTs as observed in (N. Patil et al. 2009).

The OFF-time has been identified as a precursor for latch-up failures in (Brown et al. 2012).
The $V_{CE_{ON}}$ does not reflect always the degradation of IGBT since it has shown voltage drop in (N. Patil et al. 2009), as well as voltage increase in (Smet et al. 2013; U. Choi, Jørgensen, and Blaabjerg 2016; Eleffendi and Johnson 2015; Xiong et al. 2008).
In addition to breakdown voltage, leakage current, body diode avalanche voltage, gate charge, parasitic capacitance, body diode voltage drop (Dusmez, Ali, et al. 2017; B. Saha et al. 2009; S. Saha et al. 2011; Dusmez and Akin 2015b; Dupont et al. 2007; Vasan and M. G. Pecht 2018).

Each failure is assigned to fault causes and might affect parameters over others, as the thermal overstress can increase the leakage current, cause short and open circuit, and loss of gate controls of the power switching devices. The failures location, causes modes, and the affected parameters are reviewed in details by Hanif et al. (2019) and Valentine, Das, and P. M. Pecht (2015). Consequently, the researchers have categorized the failures of power switching devices into extrinsic (package-related) such as bond-wire fatigue, solder fatigue, and Aluminum reconstruction and intrinsic (chip-related) faults such as electrical overstress, electro-migration, latch-up, and dielectric breakdown (Hanif et al. 2019; Anderson, Cox, and O'Connor 2013; S. Saha et al. 2011; J. R. Celaya, Wysocki, et al. 2010; Valentine, Das, and P. M. Pecht 2015; Ciappa 2002).
Figure 1.4 illustrates the typical structure of a power module (Hanif et al. 2019).

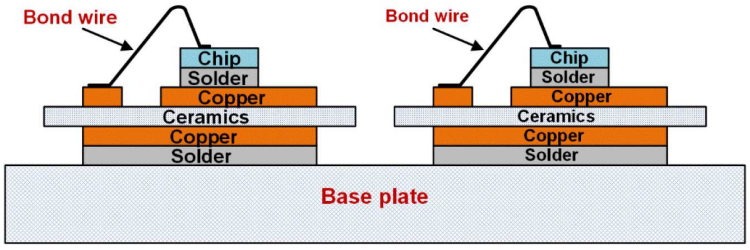

Figure 1.4: Multilayer structure of a power module by (Hanif et al. 2019)

Chip-related failures

- *Electro-migration:* The degradation caused by such failure mechanism is less likely to happen. It creates a void among metal connections which causes resistance increment. Consequently, it results a high cur-

rent density in silicon interconnections which is the main responsible of the degradation (Hanif et al. 2019).

- *Latch-Up:* Overvoltage, irradiation and high electric field may cause loss in the control gate of IGBTs and MOSFETs, if the bipolar junction transistor is triggered. Hence, any high current can destroy the device if it is not cleared immediately (Hanif et al. 2019). In this case, the affected parameter is the $V_{\mathrm{CE_{ON}}}$ (Valentine, Das, and P. M. Pecht 2015).

- *Dielectric Breakdown:* It affects the gate oxide degradation of the dielectric (Hanif et al. 2019). It introduces different failure mechanisms such as anode hole injection, trap creation and impact ionization (Lombardo et al. 2005). Therefore, the MOSFET experiences an increased gate current and decreased drain current after the dielectric breakdown (Nasrin, Khan, and Alam 2014). This results in loss of gate control and short-circuit caused by over voltages, high temperature and high electric field. The fault precursor in this case is V_{th} (Hanif et al. 2019; Valentine, Das, and P. M. Pecht 2015).

- *Electrical Overstress:* Due to overvoltages and overcurrents, the heat affects the device functionality (Hanif et al. 2019).

Package-related failures

- *Bond wire fatigue:* There exists two types of bond wire failures. the bond wire lift-off that creates a crack between the Silicon and Aluminum surfaces, is caused by the mismatch of the thermal expansion coefficient between them. And, the bond wire heel is caused by the fracture fatigue (Ciappa 2002). Thus, the high current density and high temperature may result open-circuit fault and affect $V_{\mathrm{CE_{ON}}}$ (Valentine, Das, and P. M. Pecht 2015).

- *Solder fatigue:* The overheating of the device, also known as thermal and power cycling creates cracks in the layer attached by solder. Hence, the thermal impedance increases which accelerates the propagation of voids (Hanif et al. 2019). Similar to the bond wire fatigue, the solder fatigue is affected by the same causes and results similar faults.

- *Aluminum reconstruction:* The metallization layer of the Silicon chips are subject to degradation process that causes the Aluminum reconstruction (Hanif et al. 2019).

1.5.3 Failure mechanisms and precursors of ECAPs

Similar to the power semiconductor switches, the ECAPs are one of the major responsible of the electronic-system failures. Therefore, the electrical and thermal overstresses cause major perturbation in the capacitor normal functionality. Thus, the ECAP can be expressed by its capacitance and its Equivalent Series Resistance (ESR) as shown in the lumped model in Figure 1.5.

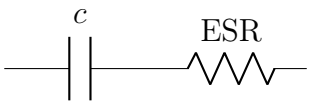

Figure 1.5: Lumped model of ECAP

Moreover, the failure mechanisms of the ECAPs are extrapolated by electrical and thermal overstresses through AGEs.

In (C. Kulkarni, J. Celaya, G. Biswas, et al. 2011), a controlled thermal chamber was used to raise the temperature of the ECAPs above their maximum rated storage temperature of 85°C. The authors followed a gradual increase of temperature of 25°C in order to avoid permanent shocks with 15 minutes intervals until reaching a constant 125°C. Thus, using the proper instrumentation techniques it was noticeable by direct measurement that the ESR of the degraded ECAP increases, where the computed capacitance decreases.

In (C. S. Kulkarni et al. 2012), the AGEs were conducted to electrically-overstress the ECAPs in order to extract the features of their failure mechanisms. A batch of the same ECAPs rated at 10V were continuously charging and discharging at 12V with a square voltage waveform of 20 mHz frequency. The experiments have shown that the ECAPs fail at 20% degradation of their initial rated capacitance.

Moreover, the electrolyte inside the capacitor unit evaporates which increases the pressure and decreases the oxide area. The ESR is the sum of the resistance due to the parameters of the capacitor itself such as the aluminum Oxide layer, the electrolyte, the electrodes, and the spacer. Figure 1.6 illustrates the physical model of ECAP that shows the affected parameters due to the aforementioned failure mechanisms (Chetan Kulkarni, Gautam Biswas, X. Koutsoukos, et al. 2010).

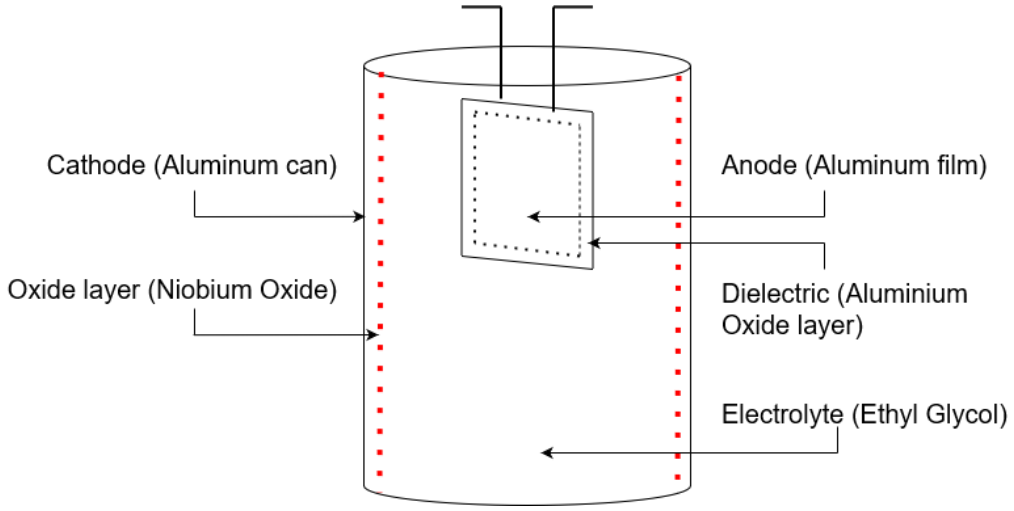

Figure 1.6: Physical model of ECAP (Chetan Kulkarni, Gautam Biswas, X. Koutsoukos, et al. 2010)

Table 1.3 illustrates the observed failure precursors of ECAPs.

Table 1.3: Fault precursors of ECAPs

Electronic component	Failure precursors
ECAPs	• Capacitance • ESR • Leakage current/resistance • Radio frequency noise • Dissipation factor

Therefore, the degradation of ECAPs is characterized by an increase of the ESR while the capacitance decreases which deteriorates and leads to a complete failure (C. Kulkarni, J. Celaya, G. Biswas, et al. 2011; Vasan and M. G. Pecht 2018). Thus, the main degradation mechanisms are related to the following effects (Chetan Kulkarni, Gautam Biswas, X. Koutsoukos, et al. 2010; J. Celaya et al. 2011):

- *High voltage:* The capacitance of ECAPs decreases while the ESR increases due to a supplied voltage higher than the rated value.
- *High ripple current:* The ECAPs age gradually due to high ripple current that increases the internal heat which increases the core temperature.

- *Transients:* High leakage-current occurs due to transients that can cause internal short-circuits.

- *Reverse bias:* The capacitance can be totally lost and the ESR increases due to the induced high leakage-current of the reverse bias.

- *Strong vibrations:* Mechanical damages can affect many parameters of ECAPs such as internal short-circuits, open-circuits, high leakage current, increase in ESR, and capacitance loss.

1.5.4 Failure precursors of other components

The failure precursors are parameters that indicate variations in an electronic component/circuit. Thus, the main fault precursors of more active and passive components in electronic circuits, that can be measured by direct means or observed by filtering techniques, are provided in Table 1.4.

Table 1.4: Potential failure precursors for electronic components (M. G. Pecht and Kang 2018)

Electronic components	Failure precursors
Diodes	• Forward voltage drop • Power dissipation • Thermal resistance • Radio frequency noise • Reverse leakage current
Cables and connectors	• Impedance changes • Physical damage • High-energy dielectric breakdown
Switching power supply	• Ripples • Efficiency • DC output • Duty cycle • Leakage current • Radio frequency noise

1.5.5 Failure predictions methods

The *failure mechanisms* in Section 1.5 and the *failure precursors* in Table 1.4 are the foundation methods for PHM of electronic components. The assessment of each method is not straightforward and requires accurate analysis for reliable predictions. Evidently, the electronic components/circuits can be modeled due to the strong knowledge of their manufacturing and failure mechanisms which makes the model-based PHM for electronics a favorable approach to investigate, test, and simulate different failures and degradation scenarios. However, the data-driven PHM approaches are also advantageous and can be explored with multidisciplinary systems, or with highly complex electronics-rich systems, especially that the degradation and test data can be aggregated and simulated for this purpose.

Failure mechanisms-based prognostics

The failure mechanisms can be described by *empirical models* or *PoF models*. Table 1.5 summarizes the main features of the different failure methods (Hanif et al. 2019; W. Denson 1998).

Table 1.5: Failure methods: PoF versus empirical

Methods	Physics-of-failure	Empirical
Advantages	• Allows modeling of specific failure mechanisms	• Provides a wider image of the failures and their occurrences
	• Reliable with prognostics implementation	• Accurate indicator for reliability assessment
Limitations	• Complex, expensive, and time-consuming to obtain and employ	• Requires updates with novel technologies in electronics and power electronics
	• Unpractical for system-level reliability assessment	• Requires collection of an important amount of degradation

Hence, as illustrated in Table 1.5, both modeling methods can be elaborated depending on the type of the application, the fidelity level, the size of the system, etc. However, it is worth noting that the failure modeling that is based on the failure mechanisms of the components is normally treated by

number of cycles. Whereas, the failure precursors-based modeling allow expressing the degradation process in real time such as days, minutes, etc. Moreover, we intend to show a brief example of the two failure precursors of ECAPs, the capacitance (C) and the ESR are obtained based on the PoF of the failure mechanisms as shown in (1.1).

Example 1.5.1.

$$C = \frac{2\ \varepsilon_R\ \varepsilon_o\ A_o}{t_o}, \tag{1.1a}$$

$$\text{ESR} = \frac{\rho_E\ t_o\ P_E}{2\ L\ W}, \tag{1.1b}$$

where ε_R is the relative dielectric constant, ε_o is the permittivity of free space, A_o is the oxide area, t_o is the oxide thickness, ρ_E is the electrolyte resistivity, L and W are the physical parameters of the anode area, P_E is the correlation factor related to electrolyte space porosity and average liquid path-away (C. Kulkarni, J. Celaya, G. Biswas, et al. 2011; Chetan S. Kulkarni, Gautam Biswas, José R. Celaya, et al. 2012).

As shown in Example 1.5.1, it is complex to consider all the failure mechanisms with many parameters in function of the PoF since it requires a strong knowledge.

Failure precursors-based prognostics

The failure precursors are physical parameters of the electronic components which reflect the degradation level on the micro-level or the macro-level. However, the failure precursors-based prognostic is not a straightforward approach, since the measurement of these parameters is challenging. The barriers arise especially for online circuits such as converters, or black-box systems that make the direct measurement difficult to perform. It also requires special instrumentation to measure resistance, capacitance, temperature as well as voltage and current. However, for the RUL forecasting, the intended failure precursors can be estimated which also can create more challenges with respect to the uncertainties and the complexity of the system.

The failure mechanisms-based prognostics and the failure precursors-based prognostics are two approaches that can be carried out for model-based, data-driven, and hybrid PHM. The failure mechanisms-based approach requires more knowledge of the components and becomes highly complex for bigger systems. On the other hand, the failure precursors-based approach reflects the degradation with a wider image with no strong interest of internal parameters monitoring of the component.

The final assessment of the aforementioned approaches and our perspective with respect to the RUL forecasting is detailed in Section 1.6.

1.6 Remaining Useful Life Forecasting: Component Versus System-level

The background review of the PHM and the value which the prognostics add to the maintenance strategy show many benefits that involves the operational reliability, the expenses, the system availability, the logistics. Moreover, many challenges such as uncertainties, modeling fidelity, data acquisition, and more obstruct the fast development and standardization of PHM. Despite that, the PHM involve multidisciplinary applications such as land and outer space vehicles, batteries, industrial applications, healthcare, electronics, etc. Hence, the main role of the PHM in these applications is to forecast the RUL and/or predict the future behavior of a component/subsystem/system which are subject to degradation that deviates their operation from their optimal operating. The degradation of a component deteriorates a whole system due to its cascading effect.

Thus, it is worth noting that the electronics are one common, yet essential devices that control, measure, observe, and protect the aforementioned applications. For these reasons, we intend to investigate the PHM role in modern-days electronics. Furthermore, the PHM in broad can be addressed by model-based or data-driven approaches that can be merged together in a hybrid method depending on the type of application. Thus, due to the fact that the electronic devices are widely utilized and their modeling is mainly practical to a certain level of system complexity, the model-based PHM for electronics is a favorable approach to adopt in this thesis. The data-driven approaches exist to address the same problems, however they require more information and test data as measurements in normal and in degraded operations. Whereas, our aim is to contribute to a generalized structured strategy for model-based PHM that can be applicable to various systems with trivial tuning and reduced knowledge about the PoF.

• For all of the above-mentioned reasons, we have adopted the model-based PHM approach for further investigations and contributions in this thesis.

Moreover, as stated in Section 1.5, ECAPs and power switching devices as MOSFETs and IGBTs are the major responsible of systems failure due

to their degradation that is affected by electrical and thermal overstresses. Hence, we have briefed the main degradation causes from the failure mechanisms perspective, and explained the different methods of lifetime predictions by exploiting the empirical and PoF modeling methods of the failure mechanisms, or by the failure precursors approach.

Additionally, in practice, these components are not applied as standalone devices, they are integrated in complete circuits such as converters, inverters, drives, etc. Evidently, the level of complexity of these systems is considered high enough that makes the failure precursors-based prediction a preferred approach in this thesis. The reasons of eliminating the failure mechanisms-based prediction are related the features extraction of the internal parameters of each component, which requires strong knowledge of all failures, and is strictly specific to each type of failure. Thus, this approach is not recommended for big circuits where all the components interconnect.

• It is worth noting that the conventional RUL forecasting approaches are based on stochastic regression of observed degradation data that predict degradation profiles until reaching the failure Threshold (TH). Our propositions concerning this approach are discussed in Section 1.8.

• Therefore, we have considered the failure precursors-based prognostics of a switching converter with degraded MOSFET and ECAP to be investigated under different scenarios with unknown degradation models and generalized prediction approach.

1.6.1 Component-level prognostics approaches

The RUL forecasting is the main objective which is based on constructive phases that are targeted towards the failure precursors. The failure precursors are crucial indicators of the SoH of any system. Yet, online aggregating of their measurements is not a trivial task in most applications.

• We intend to generalize the utilization of our contributions to systems with no direct access to the internal parameters.

Therefore, the failure precursors are required to be estimated either in a standalone application or as critical parameters of a system.

In the literature, C. Kulkarni, J. Celaya, K. Goebel, et al. (2012) developed empirical models of the capacitance and the ESR of ECAPs based on

their current SoH for failure predictions.

Moreover, Kwon, Azarian, and M. Pecht (2015) and Kwon and Yoon (2016) used particle filtering technique in order to predict the RUL based on failure mechanisms of solder joints using the radio frequency impedance analysis and Gaussian process regression using a model.

Nishad Patil, Das, and Michael Pecht (2012) and J. R. Celaya, A. Saxena, S. Saha, and K. F. Goebel (2011) employed statistical filtering with known empirical models of IGBTs in order to predict their failures based on the collector-emitter resistance. These methods aim for CRUL forecasting on a micro-level, and mostly based on stochastic approaches with statistical regression for the failure predictions.

1.6.2 System-level prognostics approaches

As was discussed above, in practice, the electronics are embedded in a circuit scheme which increases the complexity of the prognostics. Additionally, the analysis of the SoH of a circuit which represents a system, is based on the interdependent electronic components and their failure mechanisms (Vasan and M. G. Pecht 2018; Goodman, Hofmeister, and Judkins 2007).

Some studies as in (Sai Sarathi Vasan, Long, and M. Pecht 2013; M. Li et al. 2013; C. Zhang et al. 2014; J. Zhou, Tian, and C. Yang 2014), have employed machine learning techniques in order to estimate the SoH of the whole circuit which becomes the system that contains many electronic components. The SoH of the whole system has been estimated using a distance-based method and known empirical models of extracted features with particle filter of relevance vector machine. The extracted features such as statistical, time-domain, wavelet, and more are assessed to estimate the health of the whole electronic circuit using Mahalanobis distance in (Sai Sarathi Vasan, Long, and M. Pecht 2013). C. Zhang et al. (2014) and M. Li et al. (2013) used a regression technique for RUL prediction. Whereas, C. Zhang et al. (2014) employed the relevance vector machine model for RUL predictions instead of regression fit. However, this technique assumes a Gaussian distribution for the random variables of the RUL model. C. Zhang et al. (2014) and J. Zhou, Tian, and C. Yang (2014) employed the same health indicator assumption technique that is based on calculating the cosine and sine of the distance between the deviated features and their rated values. However, this technique lacks the ability of considering the induced measurement noises that affect the prognostics.

Qingchuan et al. (2017) contributed to the prognostics of a DC-DC converter by estimating its SoH based on the output voltage as a failure precursor. A defined percentage of the deviation of the rated output voltage at different temperatures was considered as the main failure criterion. Hence, the RUL was predicted based on an empirical model of the output voltage.

Samavatian, Avenas, and Iman-Eini (2018) contributed to the self and coupling thermal influences of power semiconductors of a DC-DC converter. They analyzed the thermal deviation point of an IGBT and a diode due to degradation.

Chen et al. (2008) conducted an online failure prediction method for ECAPs in an LC filter of a DC-DC converter. Only the capacitor voltage was required for the health estimation due to the fact that the ESR of the ECAP is reflected by the output ripple of the converter. This failure prediction method requires a band-pass filter, a rectifier, a low-pass filter, a hysteresis comparator, and a time-delay, and it is dedicated to the ESR of the ECAP only.

1.6.3 Summary and problem statement

To sum up, the component-level prognostics are effective and mainly based on statistical techniques. Additionally, their assessment is specific and accomplished by implementing known empirical degradation models for each chosen failure precursor or failure mechanisms. Despite the promising results of such approaches, they may depend on strong knowledge of the degraded components. Thus, stochastic filtering techniques are usually used along with previous observations in order to predict the degradation behaviors. Moreover, most of the existing techniques consider only Gaussian uncertainties due to the implementation of the stochastic filters.

Moreover, the system-level prognostics approaches exploit the predictions based on the health assessment of the whole system by monitoring external precursors of the system that reflect the overall interdependency of the internal interconnected parameters. The presented techniques monitor the electronic circuit and estimate its deviation with respect to the optimal operation. However, they lack the identification of the main responsible parameters of the degradation, in most cases. This feature is sensitive and crucial for the CBM, an overall system prognostic requires maintenance for the whole system if the failed parameters were not identified and repaired, which is the

core of the PHM with the CBM strategy.

Furthermore, the given examples of modern-engineering applications have shown the diversity of the implementation of various prognostics techniques with known degradation behaviors that elaborate the model-based approaches, and unknown degradation behaviors that elaborate the data-driven approaches. In (N. Kim, An, and J. Choi 2017d), they presented the least squares regression as an approach to estimate and fit the degradation data to provide a prior prediction of failure. Then, the RUL is computed by comparing the predicted degradation model with the TH of the parameter. In the case of known degradation model, the parameters of the model are mostly unknown due to the effects of the measurement noises and other uncertainties. Thus, the parameters are identified using the Bayesian approaches for real-time degradation estimation, in (N. Kim, An, and J. Choi 2017d). Additionally, (N. Kim, An, and J. Choi 2017c) emphasized on the same RUL prediction approach by propagating the degradation until failure, after identifying the parameters. Moreover, (Gavin 2020) employed the nonlinear least squares technique for the parameters identification of the degradation models. And other approaches that considers the Gaussian noises such as the KF (Kalman 1960) for linear systems, and EKF, UKF, particle filter, and more for nonlinear systems (Ristic, Arulampalm, and Gordon 2004; Julier and Uhlmann 2004).

As discussed above, the model-based PHM necessitates parameters estimation for the degradation models in order to propagate the model until failure for the sake of RUL prediction. In broad, the conducted studies employ stochastic and statistical approaches for parameter estimation and the derivatives of the least squares for fitting of the degradation models.

Figure 1.7 illustrates most of the RUL forecasting methodologies for component- and system-level prognostics that already carried out in the literature.
Therefore, we intended to investigate the following:

- The possibility of RUL forecasting with partial or without knowledge of the degradation models without the use of training data-sets.
- Apply system-level prognostics by predicting the RUL of the internal critical components instead of employing external features such as input/output voltage and current.
- The ability of replacing the statistical RUL confidence interval by a dynamical online bounded RUL via the estimated SoH of the critical

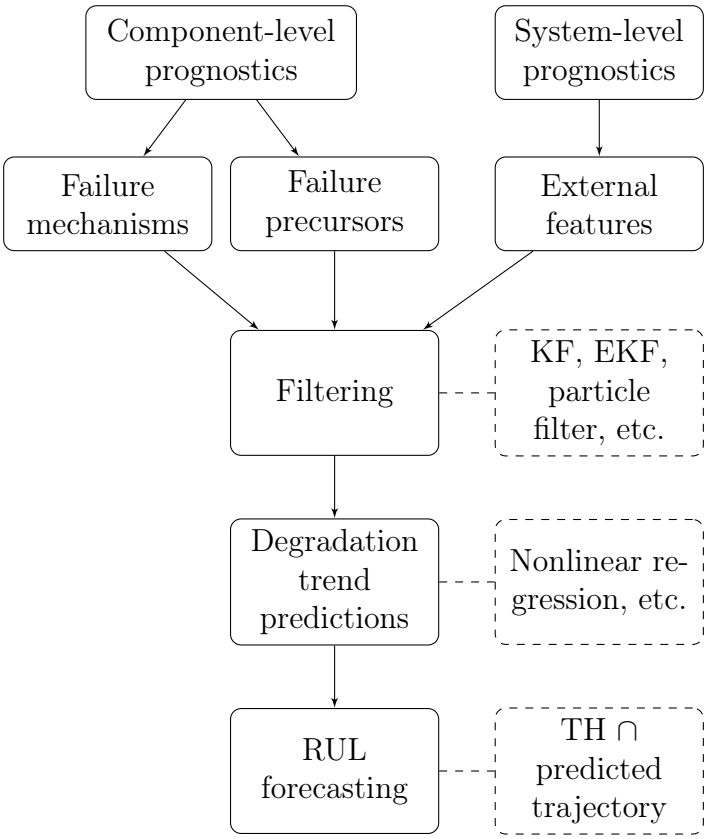

Figure 1.7: A broad overview about most of the existing model-based prognostics structures

components of a system.

- The performance of deterministic observers with different types of uncertainties rather than classical Gaussian distribution.
- Guaranteeing the observers stability.

1.7 Prognostics Evaluation Metrics

The RUL forecasting is the final step of the PHM before the maintenance-related decision-making. Thus, it is crucial to evaluate the performance of the prognostic in order to guarantee a safe operation of the system and a reliable decision for the CBM. Although there exist various performance evaluation techniques, they lack the standardization due to difference of applications,

the prognostics approaches, the constraints, online or offline, etc. (A. Saxena et al. 2010b; D. Zhang 2018; Robinson 2018; N. Kim, An, and J. Choi 2017d). Furthermore, some of these metrics are employed to evaluate the prognostic performance such as the accuracy, robustness, precision, steadiness, and convergence as summarized below with some metrics:

- *Prognostic Horizon (PH)*: It defines the time when the prediction successfully occurs in a safe zone with respect to the real RUL. PH is the difference in time between the successful prediction and the true EoL. Thus, reliable EoL and therefore RUL forecasting are accomplished with larger PH which allows early-time prediction (A. Saxena et al. 2010b; N. Kim, An, and J. Choi 2017d; D. Zhang 2018).

- $\alpha-\lambda$ *Accuracy*: It determines if the prediction occurs in a safe accuracy zone. Unlike the constant accuracy zone of the PH, the accuracy zone shrinks with time as a cone while converging towards the EoL (A. Saxena et al. 2010b; A. Saxena et al. 2010a; N. Kim, An, and J. Choi 2017d; D. Zhang 2018; Rigamonti, Baraldi, and Zio 2018).

- *Relative Accuracy (RA)*: It quantifies the estimation/prediction accuracy with respect to the real values (A. Saxena et al. 2010b; N. Kim, An, and J. Choi 2017d; D. Zhang 2018).

- *Convergence*: It is defined by the Euclidean distance between the origin and the centroid area of a curve that characterizes accuracy or precision metrics. The convergence index can be calculated with the relative error for example, and as the convergence speed increases as the distance decreases (A. Saxena et al. 2010b; N. Kim, An, and J. Choi 2017d).

1.8 Proposed PHM Methodology: Positioning and Discussions

We previously confirmed that for electronics applications, we intend to investigate the model-based approaches due to the advanced knowledge of modeling the electronic circuits such as switching power converters, and especially a DC-DC converter in this thesis.

Moreover, the studies that contribute to the model-based PHM generally base their degradation assessment on known degradation models. The parameters of these models are usually estimated using stochastic approaches and propagated until reaching the defined TH. In broad, Gaussian noises are

concerned with these techniques that utilize KF for linear systems and its derivatives for nonlinear systems. Particle filter can be implemented to nonlinear systems with non-Gaussian noises (Robinson 2018). Moreover, these approaches employ failure precursors of electronic components for RUL predictions, such as capacitance, resistance, voltage, current, etc. Hence, for electronic circuits which are considered as systems, the failure precursors are mainly dedicated to external features such as output voltage, ripples, etc. The latter methods are promising for indicating the health of the whole circuit, however the root target of prognostics in which we are interested, is to perform the CBM for internal components for the sake of extending the lifetime of the system and reduce the expenses. Additionally, we observe that employing the output voltage as a failure precursor of a circuit lacks the condition of closed-loop converters which regulates the output voltage and the varying parameter become the duty cycle which can be monitored for degradation assessment.

Thus, the main problematic involves the current SoH estimation of the critical components which are the internal parameters of the system, and predict their future behavior regardless of the degradation models. The latter are the base of the model-based prognostics since the run-until-failure data are not available for all systems and not reliable for online PHM practices.

Consequently, we propose to estimate the degradation of the critical components of the multicomponent system instead of estimating the SoH of the system itself.

Moreover, we assume that we do not have any direct access the internal components of the system in order to mimic real applications. Eventually, we are required to measure the inputs and/or outputs of the system for the sake of estimating the internal parameters in real-time without previous knowledge of any degradation model or failure mechanisms.

As we previously mentioned that the studies in the literature address this problematic depending on stochastic methods with Gaussian noises and regression techniques to predict the RUL with decisions based on the Probability Density Function (PDF). We intend to investigate the RUL forecasting methods based on the estimated critical components which are parameters of the system. In other words, instead of statistically process the estimation and predict the RUL, we opted for assessing a guaranteed bounded degradation estimation towards the RUL forecasting. We initiated this research in order to:

- Estimate the degradation of the critical components of a system by online monitoring of the input/output sensors only.
- Consider different types of uncertainties.
- Forecast the RUL based on the estimated SoH of the internal parameters regardless of the knowledge of the degradation models.
- Consider bounded RUL forecasting which could be exploited to encounter the uncertainties of the modeling and the measurements, by only propagating bounded estimated parameters that represent the degraded components.
- Structurize the model-based PHM methodology for multicomponent nonlinear systems.
- Minimize the computational time for online PHM.

1.8.1 Phase 1

The key point of model-based PHM is the modeling phase. This phase is the first in our proposed structure, and consists of the following:

1. Definition of the model characteristics. The system in this thesis is a power converter that can describe any dynamical system with degraded components. The characteristics can be defined by the sensors locations, the most critical components, the complexity of the model, etc.
2. Representation of the subsystems of the dynamical model. Some applications such as switched-systems consist of two or more subsystems that operate consecutively. Thus, it is essential to model the subsystems without any degradation effect at first.
3. Nonlinear representation of the dynamical system. The subsystems could be averaged into one system or kept. Despite the advantages and the limitations of each method, we recommend an average representation for the sake of reducing the computational effort. Therefore, the nonlinear dynamical system is represented with varying parameters that describe the degraded critical components. Thus, based on the assumption of no direct measurement is provided, the model requires parameters and/or states estimation for degradation assessment. Hence, the possibilities can vary among separate observers, joint estimation,

etc. Such representation depends on the system itself and the number of critical degraded components.

4. In order to proceed to the second structured phase of the PHM, it is required to linearize the dynamical model. Hence, among many linearization techniques, we proposed a generalized and effective linearization approach that can be utilized with any nonlinear system and does not require high computational effort, after investigating and presenting different techniques throughout this thesis.

The modeling phase is explained in details in Chapter 2. We suggest to utilize the model of the system instead of modeling the critical components based on their failure mechanisms or PoF, and estimate their failure precursors. The case study is modeled in a state-space representation. Then, we discussed the possibilities of different nonlinear representation and their formalities with our generalization intentions. A linearized model is presented in Chapter 3 that highlights stochastic PHM approaches. Thus, we adopted an upgraded linearization technique that will be explained in details in Chapter 4. We aim to emphasize on the importance of unifying the linearized representation due to our intentions of extending the proposed PHM structure to more applications such as automatic control.

Moreover, we previously mentioned that we suggest to investigate to reduce the knowledge of degradation models of the selected failure precursors of the critical components, in order to estimate the value of the precursor instead of the parameters of its model. It is worth noting that in this phase we obtained the empirical models of the failure precursors for two reasons:

1. To mimic the various degradation scenarios in simulation which will provide us the reference to investigate our proposed approaches.

2. To obtain the EoL TH of these precursors based on real AGEs that are provided by the online repository of NASA PCoE (Renwick, J. and Kulkarni, C. and Celaya, J. 2015; Celaya, J. R. and Saxena, A. and Saha, S. and Goebel, K. 2011).

Thus, the empirical degradation models are only utilized for degradation simulation and not considered as known nor integrated in any part of the proposed PHM approaches in the following phases.

1.8.2 Phase 2

Degradation estimation by employing the failure precursors of the most critical components without knowledge of the degradation models is the core of this PHM phase. Thus, it is dedicated to estimate the current SoH of the critical components and then of the whole system. An online assessment of the estimated failure precursors is accomplished to either trigger an alarm for fault or to continue towards the prognostics. This phase can be extended to FDI along with the estimation process, for a robust fault diagnosis and prognosis assessment.

Therefore, we propose to employ estimation techniques for parameters and states by real-time measuring voltages and/or currents of the input/output sensors. Alternating subsystems or average modeling are two representations that open the gate towards many estimation techniques which consist of separate states and parameters estimation or joint approaches. These approaches are discussed in Chapter 2.

Thus, RUL forecasting is based on the current estimation of the critical degraded parameters of the system. In consequence, the studies focus on estimating the parameters of the failure precursors models, whereas we proposed to estimate the failure precursors states. Stochastic approaches were our starting point in Chapter 3 with Gaussian noises and uncertainties, where we implemented EKF for nonlinear systems in order to estimate the states and the parameters of the model. Moreover, we upgraded the proposed approach in Chapter 4 to implement a deterministic observer by merging zonotopes with EKF for many benefits on the estimation and the prediction levels. Then, finally we investigated the ZSM in Chapter 5 as the main observer due to the proven similarities with the ZEKF to a certain level, whereas the two observers are designed differently. Further details will be explained in the following chapters.
Figure 1.8 illustrates the main stochastic and deterministic states and parameters estimation techniques, and pinpoints the approaches in which we are interested to investigate.

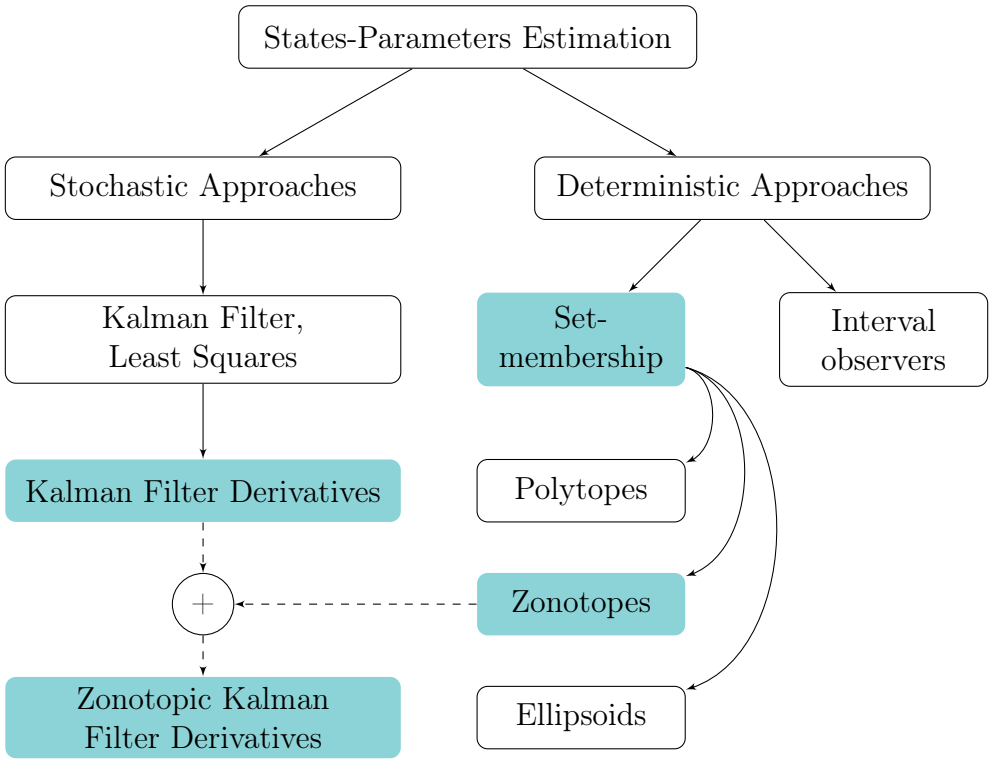

Figure 1.8: States-parameters estimation approaches

1.8.3 Phase 3

The last phase in the PHM methodology is crucial for the decision-making and the CBM which are based on the RUL forecasting of the component/-subsystem/system. The methods of RUL forecasting in the literature differ among regression techniques for model-based component-level prognostics and machine learning based on data-set for data-driven prognostics, and more approaches depending on each application as explained in Section 1.3. In this thesis, the classical degradation prediction and RUL forecasting approach using known degradation model has been applied in order to investigated two proposed approaches.

1. RUL forecasting with unknown degradation behavior based on the linear relation between RUL, EoL, and the current time. It requires partial knowledge of statistical PM for EoL acknowledgment. This proposed approach is examined in Chapter 3 and extended to bounded RUL forecasting in Chapter 4 without predicting the degradation behaviors.

2. Homogeneous RUL forecasting approach based on the critical system

parameters estimation with recursive prediction of their behavior using an exponential regressor that describes the degradation trends in broad. This approach provides bounded RUL forecasting for risk prevention with very high reliability and guaranteed convergence. It is elaborated in Chapter 5.

The EoL-RUL relation is:

$$t_{\mathrm{RUL}} = t_{\mathrm{EoL}} - t_{\mathrm{current}}, \tag{1.2}$$

where t_{EoL}, t_{RUL}, and t_{current} denote the time of EoL, RUL, and the measurement at the current time respectively.

Furthermore, it is crucial to emphasize the uncertainty effect on RUL forecasting as illustrated in Figure 1.9. The divergence of the predicted degradation trajectories due to uncertainties negatively affect the RUL forecasting which can reduce the lifecyle of the system or lead to a complete failure. According to this effect, the two proposed approaches are motivated for investigation, by either eliminating the phase of predicting the degradation trajectories, or by bounding the prediction using a robust estimation approach with reduced degradation model for real-time applications.

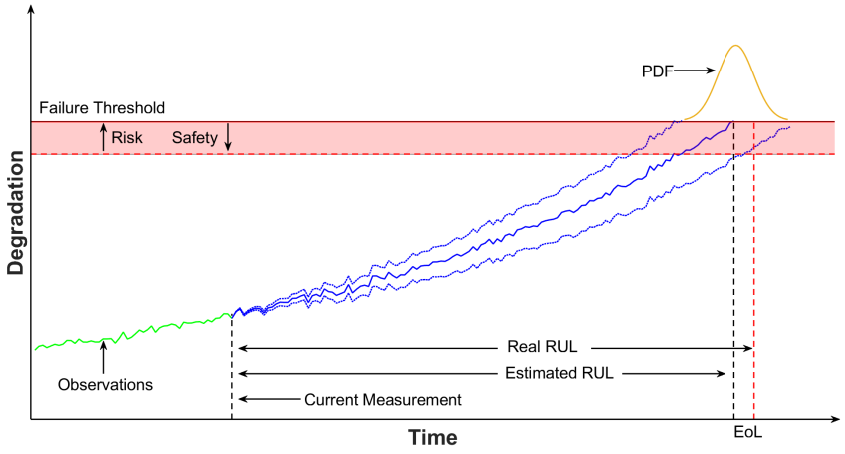

Figure 1.9: Uncertainty effects on RUL forecasting

Finally, Figure 1.10 illustrates the proposed threefold PHM methodology that consists of:

1. *Modeling:* Model a parameter-varying system without previous knowledge of the degradation models nor their statistical data. Hence, represent a linearized model of the system for further interests and possible extensions to various nonlinear applications. It is worth reminding that data-driven approaches with training-data are usually used when the degradation models are not used, however we are not employing any historical data in the PHM. The historical data are only used to simulate different degradation scenarios to mimic the real AGEs.

2. *Degradation estimation:* Estimate the varying parameters that describe the degraded components by only measuring input/output features of the system. In addition to the assessment of the current health of the system.

3. *RUL forecasting:* Apply a classical RUL forecasting approach with stochastic methods, and investigate two proposed approaches to improve the performance and reduce the uncertainty effect on RUL forecasting. The proposed approaches are only based on the previously-estimated varying parameters, and the RUL forecasting is accomplished online at each measurement.

1.9 Summary

This chapters presents the state of the art of PHM with focusing on system-level power electronics applications. We first provided a general background review about prognostics and the importance of the maintenance strategies. Then, we highlighted the main benefits and challenges that face the PHM in various fields of applications. Moreover, the failure mechanisms of ECAPs and MOSFETs/IGBTs are explained with the possible modeling methods based on their PoF or empirical modeling, in addition to their most accurate failure precursors. Finally, we discussed our positioning regarding the existing studies by explaining our investigations that consider deterministic estimation approaches and bounding the predicted RUL without implementing the PoF models. This chapter is essential to pinpoint our contributions towards multicomponent systems prognostics in a structured PHM methodology. The latter consists of the modeling phase that considers a common linearized representation of nonlinear systems for future extensions to more applications. Then, the failure precursors estimation with online health monitoring. Hence, the RUL forecasting and/or degradation behaviors predictions which are strongly based on the online degradation estimation.

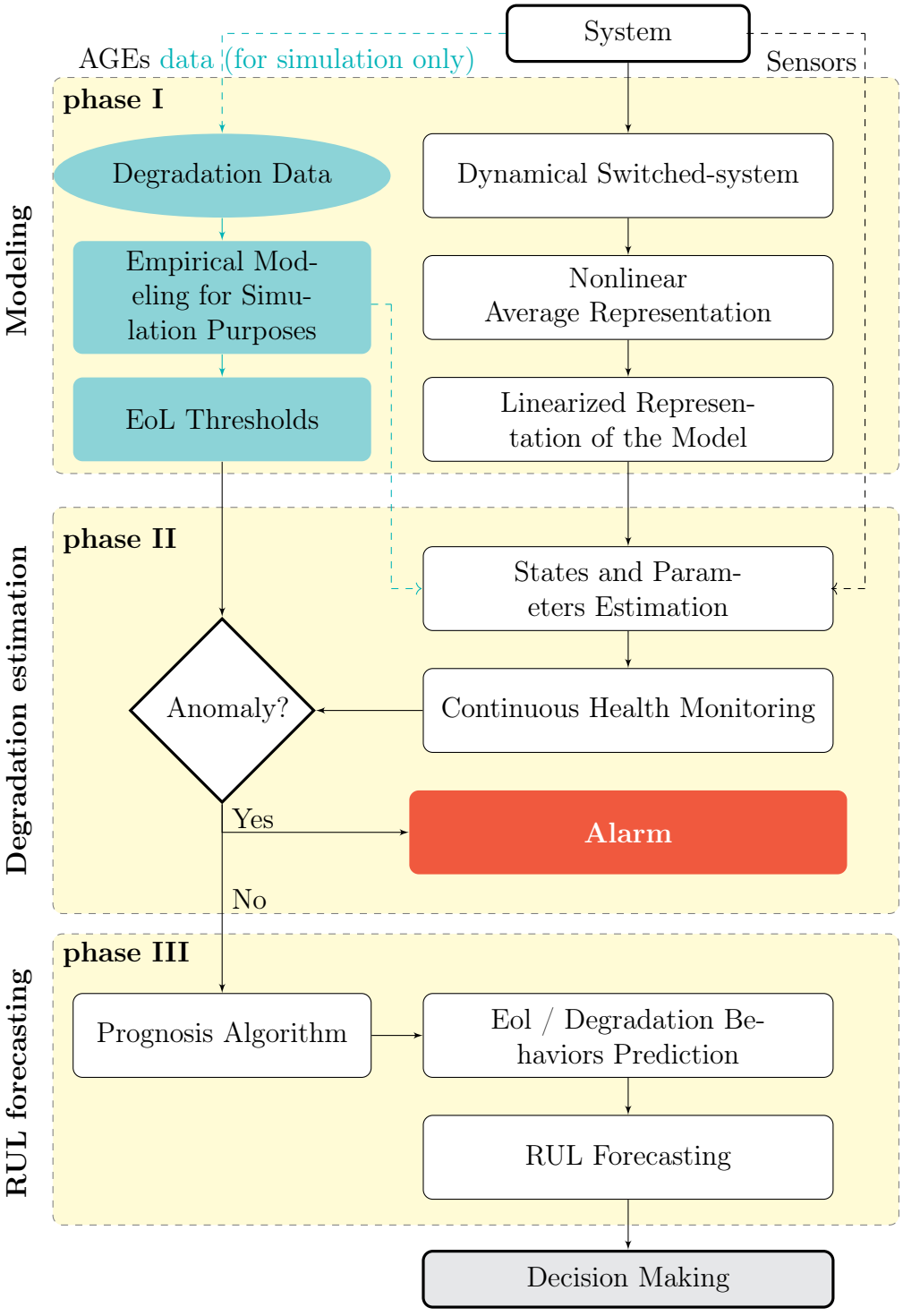

Figure 1.10: Proposed Model-based PHM Methodology

This page is intentionally left blank

CHAPTER 2

Degraded System: Modeling and Analysis

Contents

2.1 Introduction

The foundation of model-based PHM approaches relies on accurate modeling for the sake of achieving the intended objective of methodology generalization as shown in the proposed PHM structure in Figure 1.10. Thus, the prognostics applications do not embrace intermittent faults, and are more directed towards predicting the RUL of components, devices, and systems, as stated in Chapter 1. Based on the fact that slowly-varying systems such as degraded power electronic devices, or cracks in mechanical and structural systems are the most suitable case studies for prognostics, we have selected a DC-DC converter that is used in some architectures for electric vehicles, due to the following reasons:

- In broad, the power electronic systems are integrated in most of the modern engineering applications.
- The ability to analytically model such converter with high accuracy, and validate the results in simulation and on real systems.
- The availability of real degradation data of power electronic components on open-source repositories.
- The ability to operate in harsh operation conditions, and examine the proposed PHM approaches under various working conditions.
- The ability to extend the micro-level model to a macro-level by considering sources, and loads and different components, in order to extend the prognostics applications.

Harsh operation conditions, uncertainties, perturbations, noises, and overstresses could affect the desired operation conditions of any system whether in control, automation, protection, diagnosis and prognosis fields of applications. Moreover, electronics-rich systems are interestingly gaining attention in applications such as electric vehicles, aircraft industry, satellites, and huge industrial applications where critical decisions and expensive maintenance are requisite (Tidriri et al. 2019). Furthermore, by excluding the intermittent faults for their unpredictable behaviors, the power electronic systems are subject to failures characterized by slow degradation behaviors of particular components that lead to cascading damage and affect the efficiency

This chapter is included in all the publications related to this thesis.

of the whole system. These reasons motivate investigating the CBM in a prognostics framework.

Moreover, the adopted case study for the PHM investigation is a bi-directional buck-boost converter that is used in some of the architectures of electric vehicles as a bridge between the bank of batteries and the inverter of the electric motor (Al-Sheikh, Bennouna, and Hoblos 2014). Thus, such converters correspond to the aim of our research of reassessing the prognostics perspective from a component-level towards a system-level with a great interest in the internal critical components. Moreover, ECAPs followed by power semiconductors such as MOSFETs and IGBTs are the most vulnerable components that are responsible of the failure occurrences in the electronics-rich systems (S. Yang et al. 2010). In broad, the failures in power electronic systems are widely investigated in (Hanif et al. 2019; M. Pecht 2006; B. Saha et al. 2009). Additionally, the authors in (J. Celaya et al. 2011; Chetan S. Kulkarni, Gautam Biswas, and Xenofon Koutsoukos 2009; Chetan S. Kulkarni, Gautam Biswas, José R. Celaya, et al. 2012; Chetan Kulkarni, Gautam Biswas, X. Koutsoukos, et al. 2010; C. Kulkarni, J. Celaya, G. Biswas, et al. 2011; C. S. Kulkarni et al. 2012; Chetan Kulkarni, Gautam Biswas, Jose Celaya, et al. 2011) have extensively investigated the degradation behaviors of ECAPs under thermal and electrical overstresses in AGEs, and characterized their failure mechanisms. Similarly, the authors in (Z. Li, Zheng, and Outbib 2018; Jose R Celaya et al. 2010; J. R. Celaya, A. Saxena, S. Saha, and K. F. Goebel 2011; Hanif et al. 2019) have also examined the MOSFETs under thermal overstress in AGEs framework and classified various types of failure precursors as mentioned in Chapter 1. The degradation precursors of power electronic devices could vary among voltage, current, and flux indications, or physical parameters of the components themselves such as resistance and capacitance. Thus, the failure precursors play an essential role in the prognostics framework, since their variations indicate the degradation level of the system, which leads to the RUL forecasting that will be extensively discussed in the following chapters. Furthermore, phase I of the proposed model-based PHM approach consists of the model identification in addition to its accurate representation that enables the transition to phase II.

In this chapter, the normal operation of the application is first modeled and investigated. Hence, the degradation integration and its effects are analyzed under three scenarios. The degradation has been simulated using empirical degradation models of the aforementioned critical components of the case study. The empirical models of the failure precursors have been modeled based on aggregated data of real AGEs from online open-source repositories

(Renwick, J. and Kulkarni, C. and Celaya, J. 2015; Celaya, J. R. and Saxena, A. and Saha, S. and Goebel, K. 2011), and their behaviors have been fitted in order to examine our case study. It is worth noting that the empirical degradation analysis is the key to run multiple degradation scenarios on the system-level to test our proposed PHM approaches with reference to the aggregated data.

Therefore, the degradation integration raises the problem of model representation which is crucial for the health assessment of the system. Decreasing the modeling uncertainties and computational time and effort, is the main objective of this phase. Thus, the nonlinear dynamical nature of the time-varying parameters which are represented by the failure precursors of the model, affects the genuine Linear Time-Invariant (LTI) model of the normal operation of the system. Additionally, this representation considers the degradation estimation of the internal parameter of the system in order to contribute the CBM on a component-level as well as a system-level. For there reasons, various model representations have been proposed for investigation by considering the aforementioned objectives with regards to the estimation burdens.

Finally, the main aim of this phase is to reproduce a linearized and an observable model that highlights the critical parameters of the degraded system. It is essential to estimate the degradation while their failure precursors are unknown, in addition to guaranteeing a less uncertain and time-consuming model in order to cope with the target of the system-level prognostics and online RUL forecasting. thus, among many linearization and approximations possibilities, a generalized model has been selected for our proposed PHM approaches that can describe any real degraded application. These possibilities will be further explained in the following chapters along with the proper degradation estimation approaches.

This chapter is structured as follows. Section 2.2 is dedicated to the DC-DC converter modeling in normal operation. Thus, the degradation analysis is investigated with different scenarios in Section 2.3. Then, the model representations approaches for degradation estimation purposes are explained in Section 2.4. Finally, the conclusions are drawn in Section 2.5

2.2 DC-DC Converter Modeling

The DC-DC converter is used in electric vehicles (Al-Sheikh, Bennouna, and Hoblos 2014) and represents an application towards system-level prognostics. The first step of this phase consists of modeling the converter in normal operation. The adopted DC-DC converter is a bridge Buck-Boost between the batteries and the motor of some of the architectures of the electric vehicles. Hence, only the Boost operation is employed and explained in this thesis for the sole reason of similarities with the Buck operation, from the modeling point of view. We have examined the buck converter in (Alyakhni, Al-Mohamad, and Hoblos 2019).
Figure 2.1 shows the circuit diagram of the Boost converter.

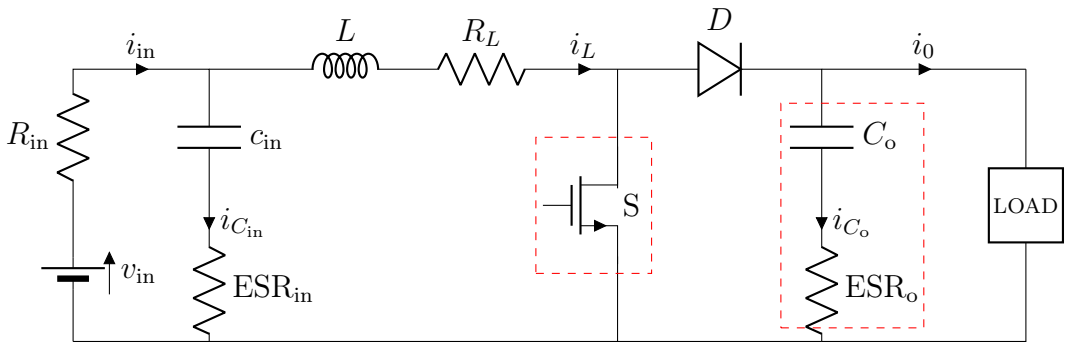

Figure 2.1: Boost converter circuit

2.2.1 Switched-system modeling

Such types of converters are known as switched-systems due to their switching behavior resulting two split subsystems in this case. Thus, the power switch S is fired during a duty cycle d that describes the ON-state of the MOSFET S which is characterized by its internal resistance R_{ON}, and *subsystem 1* is operational. Oppositely, *subsystem 2* describes the OFF-state of the MOSFET S (Al-Sheikh, Bennouna, Hoblos, and Moubayed 2014; Hart 2010).

Subsystem 1: MOSFET ON-state

The circuit diagram of subsystem 1 during the ON-state of the MOSFET is shown in Figure 2.2:

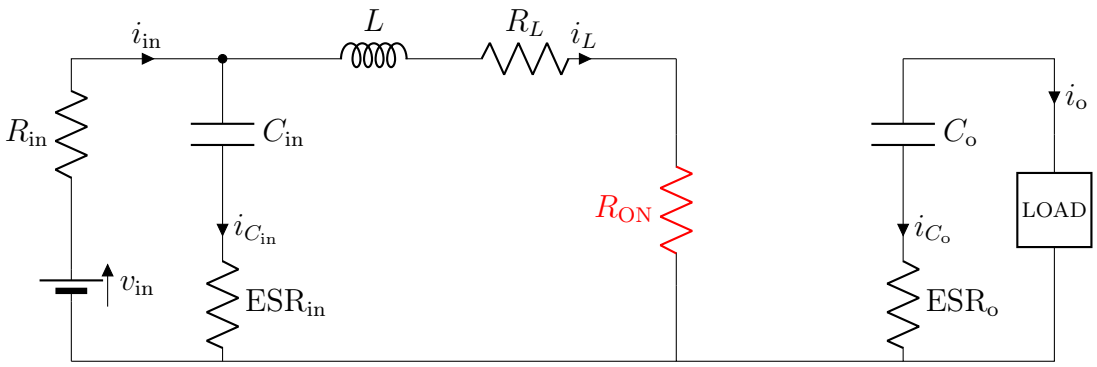

Figure 2.2: Subsystem 1 during the ON-state of the MOSFET

Applying the Kirchhoff's Voltage Law (KVL) to the three loops of the subsystem 1 circuit in Figure 2.2:

$$-v_{\text{in}} + (R_{\text{in}} i_{\text{in}}) + v_{C_{\text{in}}} + (\text{ESR}_{\text{in}} i_{C_{\text{in}}}) = 0, \tag{2.1a}$$
$$-(\text{ESR}_{\text{in}} i_{C_{\text{in}}}) - v_{C_{\text{in}}} + v_L + (R_L i_L) + (R_{\text{ON}} i_L) = 0, \tag{2.1b}$$
$$v_{\text{o}} - (\text{ESR}_{\text{o}} i_{C_{\text{o}}}) - v_{C_{\text{o}}} = 0, \tag{2.1c}$$

next, by applying Kirchhoff's Current Law (KCL) to the same circuit, we obtain:

$$i_{\text{in}} - i_{C_{\text{in}}} - i_L = 0, \tag{2.2a}$$
$$i_{C_{\text{o}}} + i_{\text{o}} = 0. \tag{2.2b}$$

Then, given the measurement equations of the output vector $\mathbf{y}$ as follows:

$$\mathbf{y} = \begin{cases} i_{\text{in}} = i_L + C_{\text{in}} \dfrac{dv_{C_{\text{in}}}}{dt}, & \text{(2.3a)} \\ v_{\text{o}} = v_{C_{\text{o}}} - \text{ESR}_{\text{o}} i_{\text{o}}, & \text{(2.3b)} \end{cases}$$

the state equations are then obtained by restructuring (2.1) with the substitution of (2.2) and (2.3):

$$\begin{aligned} \frac{dv_{C_{\text{in}}}}{dt} &= \frac{-v_{C_{\text{in}}} - (R_{\text{in}} i_{\text{in}}) + v_{\text{in}}}{C_{\text{in}} \text{ESR}_{\text{in}}}, \\ &= \frac{-v_{C_{\text{in}}} - (R_{\text{in}} C_{\text{in}} \frac{dv_{C_{\text{in}}}}{dt}) - v_{\text{in}}}{C_{\text{in}} \text{ESR}_{\text{in}}}, \\ &= \frac{-v_{C_{\text{in}}} - R_{\text{in}} i_L + v_{\text{in}}}{C_{\text{in}}(R_{\text{in}} + \text{ESR}_{\text{in}})}, \end{aligned} \tag{2.4a}$$

$$\begin{aligned}
\frac{di_L}{dt} &= \frac{\mathrm{ESR_{in}} C_{\mathrm{in}} \frac{dv_{C_{\mathrm{in}}}}{dt} + v_{C_{\mathrm{in}}} - (R_L + R_{\mathrm{ON}}) i_L}{L}, \\
&= \frac{1}{L(R_{\mathrm{in}} + \mathrm{ESR_{in}})} [R_{\mathrm{in}} v_{C_{\mathrm{in}}} \\
&\quad - (R_{\mathrm{in}} \mathrm{ESR_{in}} + (R_L + R_{\mathrm{ON}})(R_{\mathrm{in}} + \mathrm{ESR_{in}})) i_L \\
&\quad + \mathrm{ESR_{in}} v_{\mathrm{in}}], \qquad (2.4b) \\
\frac{dv_{C_{\mathrm{o}}}}{dt} &= \frac{v_{\mathrm{o}} - v_{C_{\mathrm{o}}}}{\mathrm{ESR_o} C_{\mathrm{o}}}, \\
&= -\frac{i_{\mathrm{o}}}{C_{\mathrm{o}}}. \qquad (2.4c)
\end{aligned}$$

Thus, the states matrices $\mathbf{A}_1$ and $\mathbf{B}_1$ of subsystem 1 are created by rewriting the differential equations of the states (2.4) and the input vector $\mathbf{u}$ as:

$$\overbrace{\begin{bmatrix} \frac{dv_{C_{\mathrm{in}}}}{dt} \\ \frac{di_L}{dt} \\ \frac{dv_{C_{\mathrm{o}}}}{dt} \end{bmatrix}}^{\dot{\mathbf{x}}} = \overbrace{\begin{bmatrix} \frac{-1}{C_{\mathrm{in}}(R_{\mathrm{in}}+\mathrm{ESR_{in}})} & \frac{-R_{\mathrm{in}}}{C_{\mathrm{in}}(R_{\mathrm{in}}+\mathrm{ESR_{in}})} & 0 \\ \frac{R_{\mathrm{in}}}{L(R_{\mathrm{in}}+\mathrm{ESR_{in}})} & \frac{-(R_{\mathrm{in}}\mathrm{ESR_{in}}+(R_L+R_{\mathrm{ON}})(R_{\mathrm{in}}+\mathrm{ESR_{in}}))}{L(R_{\mathrm{in}}+\mathrm{ESR_{in}})} & 0 \\ 0 & 0 & 0 \end{bmatrix}}^{\mathbf{A}_1} \overbrace{\begin{bmatrix} v_{C_{\mathrm{in}}} \\ i_L \\ v_{C_{\mathrm{o}}} \end{bmatrix}}^{\mathbf{x}} + \underbrace{\begin{bmatrix} \frac{1}{C_{\mathrm{in}}(R_{\mathrm{in}}+\mathrm{ESR_{in}})} & 0 \\ \frac{\mathrm{ESR_{in}}}{L(R_{\mathrm{in}}+\mathrm{ESR_{in}})} & 0 \\ 0 & \frac{-1}{C_o} \end{bmatrix}}_{\mathbf{B}_1} \underbrace{\begin{bmatrix} v_{\mathrm{in}} \\ i_{\mathrm{o}} \end{bmatrix}}_{\mathbf{u}}. \qquad (2.5)$$

Moreover, the KVL equations (2.1) are rewritten in function of the output vector $\mathbf{y}$ (2.3) as:

$$\begin{aligned}
0 &= v_{\mathrm{in}} + (R_{\mathrm{in}} i_{\mathrm{in}}) + v_{C_{\mathrm{in}}} + \mathrm{ESR_{in}}(i_{\mathrm{in}} - i_L), \\
i_{\mathrm{in}} &= \frac{\mathrm{ESR_{in}} i_L + v_{\mathrm{in}} - v_{C_{\mathrm{in}}}}{R_{\mathrm{in}} \mathrm{ESR_{in}}}, \qquad (2.6a) \\
v_{\mathrm{o}} &= v_{C_{\mathrm{o}}} - \mathrm{ESR_o} i_{\mathrm{o}}, \qquad (2.6b)
\end{aligned}$$

Hence, the matrices $\mathbf{C}_1$ and $\mathbf{D}_1$ are obtained by rewriting (2.6) in function of $\mathbf{x}$ and $\mathbf{u}$ as:

$$\overbrace{\begin{bmatrix} i_{\text{in}} \\ v_{\text{o}} \end{bmatrix}}^{\mathbf{y}} = \overbrace{\begin{bmatrix} \frac{-1}{(R_{\text{in}}+\text{ESR}_{\text{in}})} & \frac{\text{ESR}_{\text{in}}}{(R_{\text{in}}+\text{ESR}_{\text{in}})} & 0 \\ 0 & 0 & 1 \end{bmatrix}}^{\mathbf{C}_1} \overbrace{\begin{bmatrix} v_{C_{\text{in}}} \\ i_L \\ v_{C_{\text{o}}} \end{bmatrix}}^{\mathbf{x}} + \underbrace{\begin{bmatrix} \frac{1}{(R_{\text{in}}+\text{ESR}_{\text{in}})} & 0 \\ 0 & -\text{ESR}_{\text{o}} \end{bmatrix}}_{\mathbf{D}_1} \underbrace{\begin{bmatrix} v_{\text{in}} \\ i_{\text{o}} \end{bmatrix}}_{\mathbf{u}}. \tag{2.7}$$

Finally, the state-space matrices of subsystem 1 during the ON-state of the Boost converter are represented as follows:

$$\mathbf{A}_1 = \begin{bmatrix} \frac{-1}{C_{\text{in}}(R_{\text{in}}+\text{ESR}_{\text{in}})} & \frac{-R_{\text{in}}}{C_{\text{in}}(R_{\text{in}}+\text{ESR}_{\text{in}})} & 0 \\ \frac{R_{\text{in}}}{L(R_{\text{in}}+\text{ESR}_{\text{in}})} & \frac{-(R_{\text{in}}\text{ESR}_{\text{in}}+(R_L+R_{\text{ON}})(R_{\text{in}}+\text{ESR}_{\text{in}}))}{L(R_{\text{in}}+\text{ESR}_{\text{in}})} & 0 \\ 0 & 0 & 0 \end{bmatrix}, \tag{2.8a}$$

$$\mathbf{B}_1 = \begin{bmatrix} \frac{1}{C_{\text{in}}(R_{\text{in}}+\text{ESR}_{\text{in}})} & 0 \\ \frac{\text{ESR}_{\text{in}}}{L(R_{\text{in}}+\text{ESR}_{\text{in}})} & 0 \\ 0 & \frac{-1}{C_o} \end{bmatrix}, \tag{2.8b}$$

$$\mathbf{C}_1 = \begin{bmatrix} \frac{-1}{(R_{\text{in}}+\text{ESR}_{\text{in}})} & \frac{\text{ESR}_{\text{in}}}{(R_{\text{in}}+\text{ESR}_{\text{in}})} & 0 \\ 0 & 0 & 1 \end{bmatrix}, \tag{2.8c}$$

$$\mathbf{D}_1 = \begin{bmatrix} \frac{1}{(R_{\text{in}}+\text{ESR}_{\text{in}})} & 0 \\ 0 & -\text{ESR}_{\text{o}} \end{bmatrix}. \tag{2.8d}$$

Subsystem 2: MOSFET OFF-state

The circuit diagram of subsystem 2 of the Boost converter during the OFF-state of the MOSFET is illustrated in Figure 2.3.
Applying KVL to the loops of the OFF-state circuit in Figure 2.3 yields to:

$$-v_{\text{in}} + (R_{\text{in}} i_{\text{in}}) + v_{C_{\text{in}}} + (\text{ESR}_{\text{in}} i_{C_{\text{in}}}) = 0, \tag{2.9a}$$

$$-(\text{ESR}_{\text{in}} i_{C_{\text{in}}}) - v_{C_{\text{in}}} + v_L + (R_L i_L) + v_{C_{\text{o}}} + (\text{ESR}_{\text{o}} i_{C_{\text{o}}}) = 0, \tag{2.9b}$$

$$-(\text{ESR}_{\text{o}} i_{C_{\text{o}}}) - v_{C_{\text{o}}} + v_{\text{o}} = 0, \tag{2.9c}$$

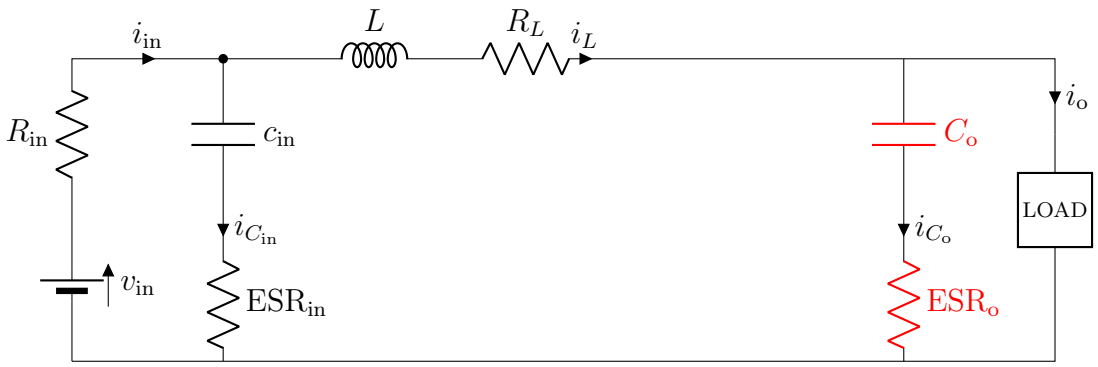

Figure 2.3: Boost converter OFF

Then, by applying the KCL to the same circuit, we obtain:

$$i_{in} - i_{C_{in}} - i_L = 0, \tag{2.10a}$$
$$i_L - i_{C_o} - i_o = 0. \tag{2.10b}$$

Therefore, the state equations of subsystem 2 are obtained by restructuring (2.9) with the substitution of (2.10) and (2.3) as:

$$\begin{aligned}
\frac{dv_{C_{in}}}{dt} &= \frac{-v_{C_{in}} - (R_{in}i_{in}) + v_{in}}{C_{in}ESR_{in}}, \\
&= \frac{-v_{C_{in}} - (R_{in}C_{in}\frac{dv_{C_{in}}}{dt}) - v_{in}}{C_{in}ESR_{in}}, \\
&= \frac{-v_{C_{in}} - R_{in}i_L + v_{in}}{C_{in}(R_{in} + ESR_{in})},
\end{aligned} \tag{2.11a}$$

$$\begin{aligned}
\frac{di_L}{dt} &= \frac{ESR_{in}\frac{v_{in}-(R_{in}i_{in})-v_{C_{in}}}{ESR_{in}} + v_{C_{in}} - (R_L i_L) - v_{C_o} - (ESR_o(i_L - i_o))}{L}, \\
&= \frac{1}{L(R_{in} + ESR_{in})}[R_{in}v_{C_{in}} \\
&- (R_{in}ESR_{in} + (R_L + ESR_o)(R_{in} + ESR_{in}))i_L \\
&- \frac{1}{L}v_{C_o} + ESR_{in}v_{in} + \frac{ESR_o}{L}i_o],
\end{aligned} \tag{2.11b}$$

$$\begin{aligned}\frac{dv_{C_o}}{dt} &= \frac{v_o - v_{C_o}}{\mathrm{ESR_o} C_o}, \\ &= \frac{v_{C_o} + \mathrm{ESR_o}(i_{C_o} - i_L)}{C_o \mathrm{ESR_o}}, \\ &= \frac{i_o}{C_o} - \frac{i_L}{C_o}.\end{aligned} \tag{2.11c}$$

Thus, the state-space matrices $\mathbf{A}_2$ and $\mathbf{B}_2$ of subsystem 2 are obtained by rewriting the equations (2.4) as:

$$\overbrace{\begin{bmatrix} \frac{dv_{C_{in}}}{dt} \\ \frac{di_L}{dt} \\ \frac{dv_{C_o}}{dt} \end{bmatrix}}^{\dot{\mathbf{x}}} = \overbrace{\begin{bmatrix} \frac{-1}{C_{in}(R_{in}+\mathrm{ESR_{in}})} & \frac{-R_{in}}{C_{in}(R_{in}+\mathrm{ESR_{in}})} & 0 \\ \frac{R_{in}}{L(R_{in}+\mathrm{ESR_{in}})} & \frac{-(R_{in}\mathrm{ESR_{in}}+(R_L+\mathrm{ESR_o})(R_{in}+\mathrm{ESR_{in}}))}{L(R_{in}+\mathrm{ESR_{in}})} & \frac{-1}{L} \\ 0 & \frac{1}{C_o} & 0 \end{bmatrix}}^{\mathbf{A}_2} \overbrace{\begin{bmatrix} v_{C_{in}} \\ i_L \\ v_{C_o} \end{bmatrix}}^{\mathbf{x}} + \underbrace{\begin{bmatrix} \frac{1}{C_{in}(R_{in}+\mathrm{ESR_{in}})} & 0 \\ \frac{\mathrm{ESR_{in}}}{L(R_{in}+\mathrm{ESR_{in}})} & \frac{\mathrm{ESR_o}}{L} \\ 0 & \frac{-1}{C_o} \end{bmatrix}}_{\mathbf{B}_2} \underbrace{\begin{bmatrix} v_{in} \\ i_o \end{bmatrix}}_{\mathbf{u}}. \tag{2.12}$$

Moreover, the KVL equations of subsystem 2 (2.9) are rewritten in function of the output equations (2.3) as:

$$i_{in} = \frac{v_{in} - v_{C_{in}} + \mathrm{ESR_{in}} i_L}{R_{in} + \mathrm{ESR_{in}}}, \tag{2.13a}$$

$$v_o = v_{C_o} + \mathrm{ESR_o} i_L - \mathrm{ESR_{in}} i_o. \tag{2.13b}$$

Hence, the matrices $\mathbf{C}_2$ and $\mathbf{D}_2$ are obtained by rewriting (2.13) in function of $\mathbf{x}$ and $\mathbf{u}$ as:

$$\overbrace{\begin{bmatrix} i_{in} \\ v_o \end{bmatrix}}^{\mathbf{y}} = \overbrace{\begin{bmatrix} \frac{-1}{(R_{in}+\mathrm{ESR_{in}})} & \frac{\mathrm{ESR_{in}}}{(R_{in}+\mathrm{ESR_{in}})} & 0 \\ 0 & \mathrm{ESR_o} & 1 \end{bmatrix}}^{\mathbf{C}_2} \overbrace{\begin{bmatrix} v_{C_{in}} \\ i_L \\ v_{C_o} \end{bmatrix}}^{\mathbf{x}} + \underbrace{\begin{bmatrix} \frac{1}{(R_{in}+\mathrm{ESR_{in}})} & 0 \\ 0 & -\mathrm{ESR_o} \end{bmatrix}}_{\mathbf{D}_2} \underbrace{\begin{bmatrix} v_{in} \\ i_o \end{bmatrix}}_{\mathbf{u}}. \tag{2.14}$$

Finally, the state-space matrices of subsystem 2 during the OFF-state of the Boost converter are represented as follows:

$$\mathbf{A}_2 = \begin{bmatrix} \frac{-1}{C_{\text{in}}(R_{\text{in}}+\text{ESR}_{\text{in}})} & \frac{-R_{\text{in}}}{C_{\text{in}}(R_{\text{in}}+\text{ESR}_{\text{in}})} & 0 \\ \frac{R_{\text{in}}}{L(R_{\text{in}}+\text{ESR}_{\text{in}})} & \frac{-(R_{\text{in}}\text{ESR}_{\text{in}}+(R_L+\text{ESR}_{\text{o}})(R_{\text{in}}+\text{ESR}_{\text{in}}))}{L(R_{\text{in}}+\text{ESR}_{\text{in}})} & \frac{-1}{L} \\ 0 & \frac{1}{C_{\text{o}}} & 0 \end{bmatrix}, \tag{2.15a}$$

$$\mathbf{B}_2 = \begin{bmatrix} \frac{1}{C_{\text{in}}(R_{\text{in}}+\text{ESR}_{\text{in}})} & 0 \\ \frac{\text{ESR}_{\text{in}}}{L(R_{\text{in}}+\text{ESR}_{\text{in}})} & \frac{\text{ESR}_{\text{o}}}{L} \\ 0 & \frac{-1}{C_{\text{o}}} \end{bmatrix}, \tag{2.15b}$$

$$\mathbf{C}_2 = \begin{bmatrix} \frac{-1}{(R_{\text{in}}+\text{ESR}_{\text{in}})} & \frac{\text{ESR}_{\text{in}}}{(R_{\text{in}}+\text{ESR}_{\text{in}})} & 0 \\ 0 & \text{ESR}_{\text{o}} & 1 \end{bmatrix}, \tag{2.15c}$$

$$\mathbf{D}_2 = \begin{bmatrix} \frac{1}{(R_{\text{in}}+\text{ESR}_{\text{in}})} & 0 \\ 0 & -\text{ESR}_{\text{o}} \end{bmatrix}. \tag{2.15d}$$

2.2.2 Average representation of the switched-systems

The switched-systems can be expressed by *alternating* or *averaged* models. The alternating model conserves the switching between the original subsystems according to the period of the duty cycle. Whereas, the averaged model is obtained by averaging the subsystems to extract only one model. The alternating model representation can represent the degradation on a system-level, due to the kept varying ripples. Whereas, we intend to forecast the CRUL as well as the SRUL of a system while minimizing the computational effort and time for real-time applications, as we proposed in Chapter 1. Consequently, we propose to employ the averaged model representation due to its reduced computations by half. Additionally, we intend to investigate the parameters of the system as the failure precursors, and not the external indicators such as the output voltage ripples. Consequently, only one model is obtained following the illustrated subsystems switching in Figure 2.4. The averaged state-space matrices are computed as:

$$\mathbf{A}_{\text{avg}} = \mathbf{A}_1 d + \mathbf{A}_2(1-d), \tag{2.16a}$$
$$\mathbf{B}_{\text{avg}} = \mathbf{B}_1 d + \mathbf{B}_2(1-d), \tag{2.16b}$$
$$\mathbf{C}_{\text{avg}} = \mathbf{C}_1 d + \mathbf{C}_2(1-d), \tag{2.16c}$$
$$\mathbf{D}_{\text{avg}} = \mathbf{D}_1 d + \mathbf{D}_2(1-d). \tag{2.16d}$$

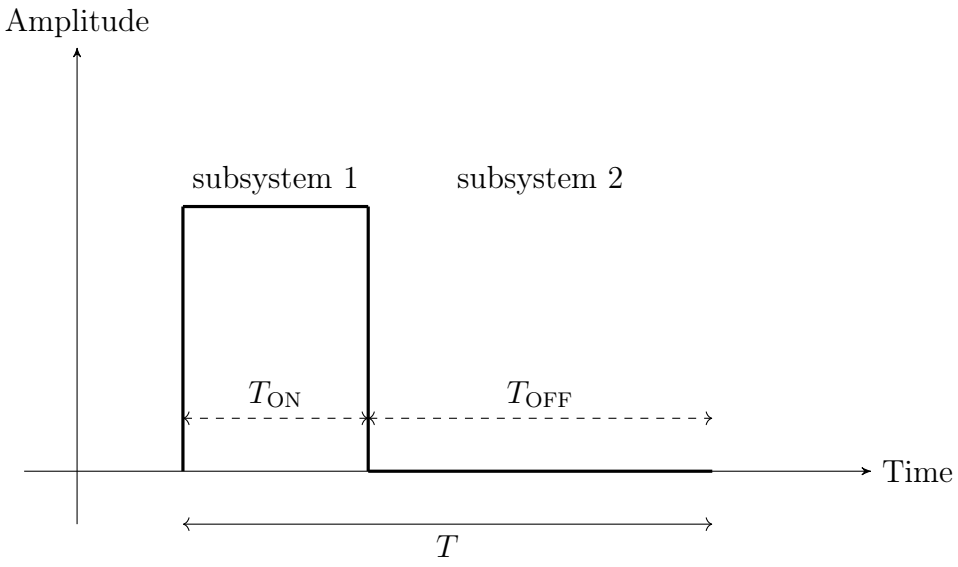

Figure 2.4: Subsystems switching

Remark 2.2.1. It is worth noting that the alternating and the averaged models have been examined and presented in Chapter 3.

The average state-space representation of an LTI system is:

$$\begin{cases} \dot{\mathbf{x}}(t) = \mathbf{A}_{\text{avg}}\mathbf{x}(t) + \mathbf{B}_{\text{avg}}\mathbf{u}(t), & \text{(2.17a)} \\ \mathbf{y}(t) = \mathbf{C}_{\text{avg}}\mathbf{x}(t) + \mathbf{D}_{\text{avg}}\mathbf{u}(t), & \text{(2.17b)} \end{cases}$$

where $\mathbf{x}(t) \in \mathbb{R}^{n_x}$, $\mathbf{y}(t) \in \mathbb{R}^{n_y}$, and $\mathbf{u}(t) \in \mathbb{R}^{n_u}$ denote the state, output, and input vectors respectively.

$$\mathbf{u} = \begin{bmatrix} v_{\text{in}} & i_{\text{o}} \end{bmatrix}^{\intercal}, \quad \text{(2.18a)}$$

$$\mathbf{y} = \begin{bmatrix} i_{\text{in}} & v_{\text{o}} \end{bmatrix}^{\intercal}, \quad \text{(2.18b)}$$

$$\mathbf{x} = \begin{bmatrix} v_{C_{\text{in}}} & i_L & v_{C_{\text{o}}} \end{bmatrix}^{\intercal}, \quad \text{(2.18c)}$$

where the variable v_{in} denotes the input source voltage of the circuit, i_{o} is the output load current, i_{in} is the input current and v_{o} is the output voltage. Thus, the states are the input capacitor voltage $v_{C_{\text{in}}}$, the inductor current i_{L} and $v_{C_{\text{o}}}$ the output capacitor voltage.

Remark 2.2.2. For the sake of simplicity, the average state-space matrices (i.e. $\mathbf{A}_{\text{avg}}$, etc.) are henceforth denoted without the subscripts (i.e. $\mathbf{A}$, etc.).

In the normal operation mode, $\mathbf{A} \in \mathbb{R}^{n_x \times n_x}$ represents the state matrix with $\dim[\mathbf{A}(\cdot)] = 3\times3$, $\mathbf{B} \in \mathbb{R}^{n_x \times n_u}$ is the input matrix with $\dim[\mathbf{B}(\cdot)] = 3\times2$,

$\mathbf{C} \in \mathbb{R}^{n_y \times n_x}$ is the output matrix with $\dim[\mathbf{C}(\cdot)] = 2 \times 3$ and $\mathbf{D} \in \mathbb{R}^{n_y \times n_u}$ represents the feed-through matrix of the system with $\dim[\mathbf{D}(\cdot)] = 2 \times 2$.

Moreover, the model is discretized following the zero-order hold assumption for the input:

$$\mathbf{A}_d = e^{\mathbf{A}T_s}, \tag{2.19a}$$
$$\mathbf{B}_d = \mathbf{A}^{-1}(\mathbf{A}_d - \mathbf{I})\mathbf{B}, \tag{2.19b}$$
$$\mathbf{C}_d = \mathbf{C}, \tag{2.19c}$$
$$\mathbf{D}_d = \mathbf{D}. \tag{2.19d}$$

Furthermore, the exact discretization is approximated based on the *Euler method* to reduce the computational effort of the exponential calculation:

$$\mathbf{A}_d = e^{\mathbf{A}T_s} \qquad \approx \mathbf{I} + \mathbf{A}T_s, \tag{2.20a}$$
$$\mathbf{B}_d = \mathbf{A}^{-1}(\mathbf{A}_d - \mathbf{I})\mathbf{B} \approx T_s\mathbf{B}. \tag{2.20b}$$

Finally, the discrete-time state-space model is obtained as:

$$\begin{cases} \mathbf{x}_{k+1} = \mathbf{A}_d\mathbf{x}_k + \mathbf{B}_d\mathbf{u}_k, & \text{(2.21a)} \\ \mathbf{y}_k = \mathbf{C}_d\mathbf{x}_k + \mathbf{D}_d\mathbf{u}_k, & \text{(2.21b)} \end{cases}$$

Remark 2.2.3. Different types of noises and uncertainties are considered and investigated in the following chapters.

2.2.3 Numerical application: normal operation of the Boost converter

The components and the parameters of the proposed DC-DC converter are presented in Table 2.1.
Moreover, the switching frequency is rated at $f_s = 15000$ Hz, and the duty cycle is set at $d = 0.35$ to control the gate of the MOSFET.
The input vector is initialized as:

$$\mathbf{u}_0 = \begin{bmatrix} v_{\text{in}_0} \\ i_{\text{o}_0} \end{bmatrix} = \begin{bmatrix} 200 \\ 100 \end{bmatrix}, \tag{2.22}$$

and the states are initialized as:

$$\mathbf{x}_0 = \begin{bmatrix} v_{C_{\text{in}_0}} \\ i_{L_0} \\ v_{C_{\text{o}_0}} \end{bmatrix} = \begin{bmatrix} 200 \\ 150 \\ 300 \end{bmatrix}. \tag{2.23}$$

Table 2.1: Converter parameters

Component	Symbol	Value	Unit
Input resistance	R_{in}	0.01	Ω
Input capacitance	C_{in}	80	mF
Input capacitor resistance	ESR_{in}	100	mΩ
Inductance	L	146	μH
Inductor internal resistance	R_L	5	mΩ
MOSFET ON-resistance	R_{ON}	0.2	Ω
Output capacitance	C_{o}	5	mF
Output capacitor resistance	ESR_{o}	80	mΩ

The numerical state-space matrices (2.24) and (2.25) represent the models of subsystem 1 and subsystem 2 respectively in continuous-time in normal operation condition of the Boost converter as:

$$\mathbf{A}_1 = \begin{bmatrix} -113636 & -1136.36 & 0 \\ 622.665 & -1466.37 & 0 \\ 0 & 0 & 0 \end{bmatrix}, \quad \mathbf{B}_1 = \begin{bmatrix} 113636 & 0 \\ 6226.65 & 0 \\ 0 & -200 \end{bmatrix},$$
$$\mathbf{C}_1 = \begin{bmatrix} -9.09 & 0.909 & 0 \\ 0 & 0 & 1 \end{bmatrix}, \quad \mathbf{D}_1 = \begin{bmatrix} 9.09 & 0 \\ 0 & -0.08 \end{bmatrix}, \tag{2.24}$$

$$\mathbf{A}_2 = \begin{bmatrix} -113636 & -1136.36 & 0 \\ 622.665 & -644.45 & -6849.315 \\ 0 & 200 & 0 \end{bmatrix}, \quad \mathbf{B}_2 = \begin{bmatrix} 113636 & 0 \\ 6226.65 & 547.94 \\ 0 & -200 \end{bmatrix},$$
$$\mathbf{C}_2 = \begin{bmatrix} -9.0909 & 0.90909 & 0 \\ 0 & 0.08 & 1 \end{bmatrix}, \quad \mathbf{D}_2 = \begin{bmatrix} 9.0909 & 0 \\ 0 & -0.08 \end{bmatrix}. \tag{2.25}$$

Hence, the average continuous-time state-space matrices of subsystem 1 (2.24) and subsystem 2 (2.25) are:

$$\mathbf{A} = \begin{bmatrix} -113636 & -1136.36 & 0 \\ 622.665 & -932.12 & -4452.054 \\ 0 & 130 & 0 \end{bmatrix}, \quad \mathbf{B} = \begin{bmatrix} 113636 & 0 \\ 6226.65 & 356.16 \\ 0 & -200 \end{bmatrix},$$
$$\mathbf{C} = \begin{bmatrix} -9.0909 & 0.90909 & 0 \\ 0 & 0.052 & 1 \end{bmatrix}, \quad \mathbf{D} = \begin{bmatrix} 9.0909 & 0 \\ 0 & -0.08 \end{bmatrix}, \tag{2.26}$$

Then, by discretizing the average continuous-time model (2.26) with a sampling frequency $F_s = 15000$ Hz, we obtain:

$$\mathbf{A}_d = \begin{bmatrix} 0.00046 & -0.00945 & 0.0025 \\ 0.00518 & 0.93817 & -0.2876 \\ 0.00004 & 0.00839 & 0.99874 \end{bmatrix}, \quad \mathbf{B}_d = \begin{bmatrix} 0.99568 & -0.00021 \\ 0.43728 & 0.02494 \\ 0.00189 & -0.01322 \end{bmatrix},$$
$$\mathbf{C}_d = \begin{bmatrix} -9.0909 & 0.90909 & 0 \\ 0 & 0.052 & 1 \end{bmatrix}, \quad \mathbf{D}_d = \begin{bmatrix} 9.0909 & 0 \\ 0 & -0.08 \end{bmatrix}. \tag{2.27}$$

The three states are illustrated in Figures 2.5, 2.6, and 2.7 based on the simulation of the discrete-time average state-space model (2.27) in normal operation condition without noises.

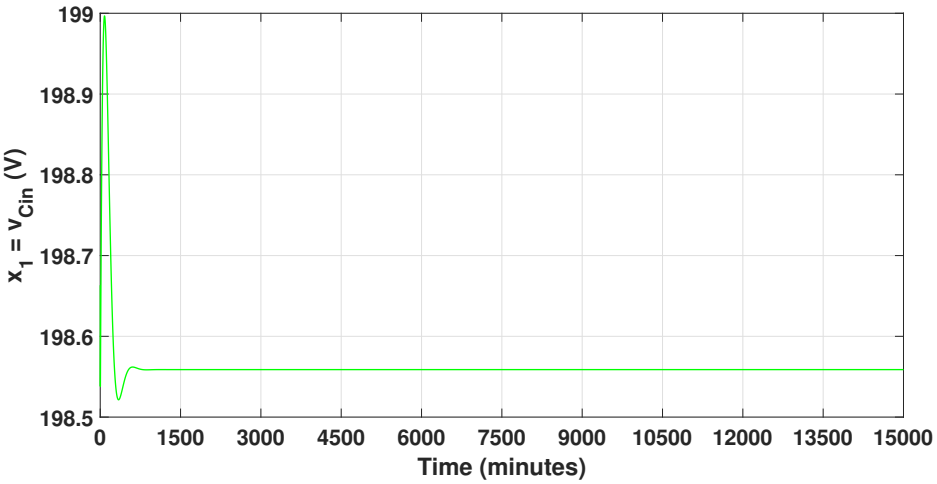

Figure 2.5: x_1 in normal operation of the Boost converter

2.3 Degradation Modeling and Analysis

The degradation integration in the model on a system-level requires a detailed-component level analysis first. As previously mentioned in Chapter 1, the MOSFET and the output ECAP are the most crucial power electronic components that can affect the health of the converter due to their degradation behaviors. For this reason, we propose to consider the parameters of the aforementioned components as their failure precursors as well as for the system itself. Thus, the interdependency of these parameters will be observed by the cascading damage, following this strategy. Therefore, the very first step of the degradation analysis consists of the degradation modeling in a

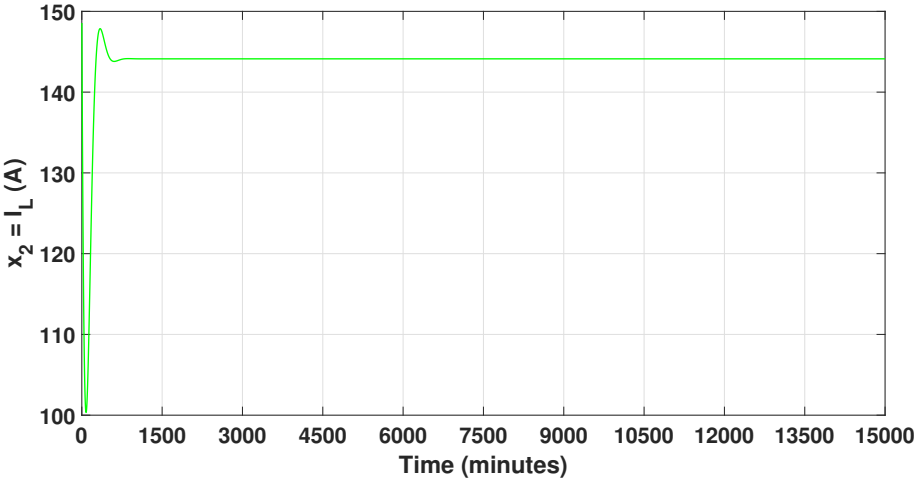

Figure 2.6: x_2 in normal operation of the Boost converter

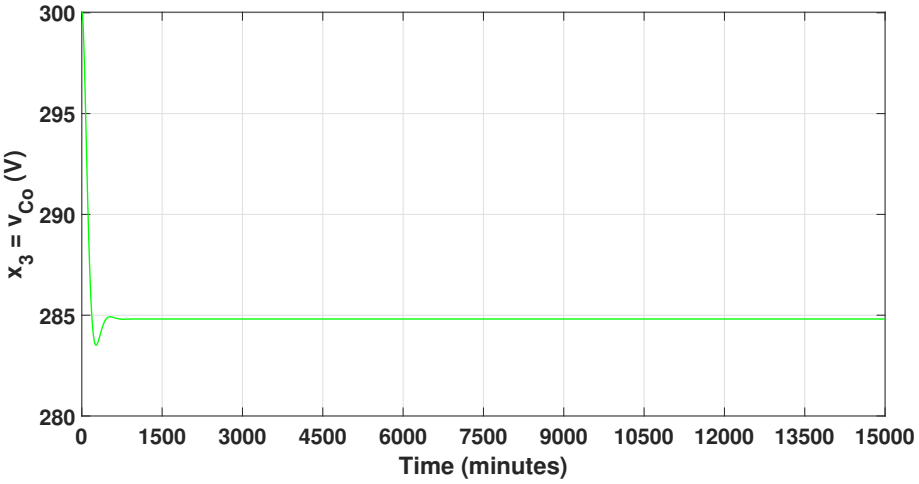

Figure 2.7: x_3 in normal operation of the Boost converter

deterministic interval of time of the AGEs on each component (Renwick, J. and Kulkarni, C. and Celaya, J. 2015; Celaya, J. R. and Saxena, A. and Saha, S. and Goebel, K. 2011). The acquired measurements of the AGEs play an essential role in the degradation simulation, since they represent accelerated degradation data of real power electronic components. Finally, a numerical fitting has been accomplished in order to obtain empirical models of the degradation for simulation purposes and investigations only.

Remark 2.3.1. By recalling that the SRUL forecasting with unknown degra-

dation behaviors is one of the main objectives of this research, the empirical degradation analysis is essential to assess the effects on different operations and scenarios. In other words, the empirical assessment and its integration on the system-level is employed to simulate different scenarios of degradation that will be used as case studies for the application of our proposed PHM approaches.

Proposition 2.3.1 (Degradation scenarios to investigate the direct and mutual effects of the critical components on the whole system)**.** Due to the fact that the degradation precursors are parameters of the system itself, we proposed three scenarios for this assessment by considering the MOSFET and the ECAP as degraded components.

- *Scenario 1:* The converter is degraded by the MOSFET which is represented by its precursor R_{ON}. Among the various degradation precursors of power electronic switches, the choice of R_{ON} refers to our intention of targeting real applications that always matters in this thesis. In other words, designing such degradation scenario without harming the model in addition to an easy access to the internal components would be much easier by embedding a resistor to emulate the degradation behavior of the MOSFET or other power electronic components. Additionally, the R_{ON} is an accurate failure precursor for MOSFETs in specific, as stated in Chapter 1.

- *Scenario 2:* The converter is degraded by the output ECAP which is represented by its precursor $\mathrm{ESR_o}$. The choice of the ESR instead of the capacitance as a precursor refers to our intention to investigate the proposed approaches with different degradation behaviors. In other words, the R_{ON} precursor follows an exponential increase throughout the degradation process as well as the capacitance of the ECAP. Whereas, the ESR follows a double exponential functions that could be approximated as linear increase, which can provide a different type of variation to examine. In addition to the aforementioned reason of the advantages of dealing with resistors rather than other precursors in real applications.

- *Scenario 3:* The converter is degraded by the MOSFET and the output ECAP components at the same time which are represented by their precursors R_{ON} and $\mathrm{ESR_o}$ respectively. The aim of this scenario is to assess the mutual effect of multiple critical components in a system for the sake of developing the prognostics approaches of such systems that characterize most of the real applications.

The LTI models of (2.8) and (2.15) become dynamical due to the integration of the time-varying parameters that represent the failure precursors as mentioned in the proposed scenarios. Thus, the system has been simulated as a black-box without any additional transformation, in order to observe the effect of each scenario on the components as well as the whole system.

Therefore, the empirical modeling of the acquired measurement data for the MOSFET and the output ECAP will be detailed in the following subsections.

Remark 2.3.2. The approximation $\approx$ is used with the empirical models to emphasize on the fact that they are obtained from real measurements of AGEs that have been numerically fit and approximated in an accelerated time (Renwick, J. and Kulkarni, C. and Celaya, J. 2015; Celaya, J. R. and Saxena, A. and Saha, S. and Goebel, K. 2011).

2.3.1 MOSFET degradation

The ON-resistance R_{ON} of the MOSFET is considered as the precursor of degradation. Although there exists different possibilities to choose a proper degradation precursor such as the gate and collector-emitter voltages and currents, the R_{ON} has been selected for a very important reason that suites our proposed prognostics method. Other precursors are not directly represented in the system identification, in another meaning, the R_{ON} is a fundamental parameter of the model that differentiates between the switching states. Thus, its empirical model is only utilized to simulate the degradation behavior of the converter and not included in the estimation process. The empirical continuous-time non-linear model of the degradation of R_{ON} has been derived based on the AGEs of thermal overstress accomplished in (J. R. Celaya, A. Saxena, C. S. Kulkarni, et al. 2012; J. R. Celaya, A. Saxena, S. Saha, and K. F. Goebel 2011; Celaya, J. R. and Saxena, A. and Saha, S. and Goebel, K. 2011), and approximated as follows:

$$\Delta R_{\text{ON}_{\text{emp}}}(t) \approx R_{\text{ON}_{\text{emp}}}(t) - R_{\text{ON}_0} = \alpha(e^{\beta t} - 1), \tag{2.28a}$$

$$R_{\text{ON}_{\text{emp}}}(t) \approx R_{\text{ON}_0} + \alpha(e^{\beta t} - 1), \tag{2.28b}$$

where $\Delta R_{\text{ON}_{\text{emp}}}$ denotes the empirical variation resulted during an accelerated degradation process. $\alpha \approx 0.0003332$ and $\beta \approx 0.0003331$ denote the parameters of the empirical degradation model. Therefore, α is smaller than a very small value denoted by ϵ, the degradation equation can be rewritten

in the following manner (Alyakhni, Al-Mohamad, and Hoblos 2019):

$$\Delta R_{\mathrm{ON}_{\mathrm{emp}}}(t) \approx \alpha e^{\beta t}, \qquad \text{for } \alpha << \epsilon, \tag{2.29a}$$

$$R_{\mathrm{ON}_{\mathrm{emp}}}(t) \approx R_{\mathrm{ON}_0} + \alpha e^{\beta t}, \tag{2.29b}$$

Figure 2.8 illustrates the degradation variation % in function of the available degradation data which are fitted for 15000 accelerated minutes. As stated in Chapter 1, the TH that defines the maximum EoL of MOSFETs could vary between 10% and 17% increase in R_{ON}. For safety reasons, the 10% increase has been selected to define the TH of R_{ON}.

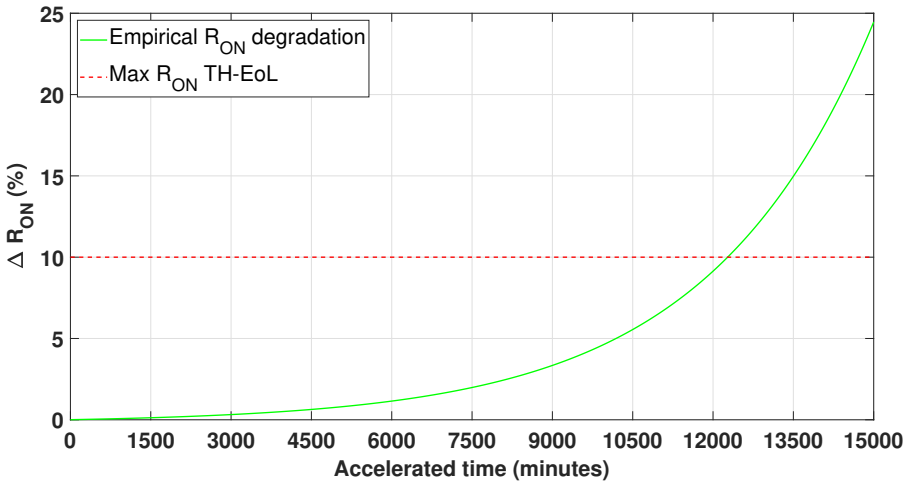

Figure 2.8: MOSFET ON-resistance variation due to degradation using empirical model.

2.3.2 ECAP degradation

The empirical models of capacitance loss and ESR increase are given by the following equations based on (J. Celaya et al. 2011; Chetan S. Kulkarni, Gautam Biswas, and Xenofon Koutsoukos 2009; Chetan S. Kulkarni, Gautam Biswas, José R. Celaya, et al. 2012; Chetan Kulkarni, Gautam Biswas, X. Koutsoukos, et al. 2010; C. Kulkarni, J. Celaya, G. Biswas, et al. 2011; C. S. Kulkarni et al. 2012; Chetan Kulkarni, Gautam Biswas, Jose Celaya, et al. 2011):

$$C_{\mathrm{emp}}\%(t) \approx e^{at} + b, \tag{2.30a}$$

$$C_{\mathrm{emp}}(t) \approx C_0 \left(1 - \frac{C_{\mathrm{emp}}\%(t)}{100}\right) = C_0 \left(1 - \frac{e^{at} + b}{100}\right), \tag{2.30b}$$

where $a = 0.8815$ and $b = 0.0003158$ are the parameters of the fitted empirical models of the capacitance degradation. The capacitance degradation percentage is denoted by $C_{\text{emp}}\%(t)$, and represents the degradation percentage increase. $C_{\text{emp}}(t)$ denotes the capacitance degradation which decreases exponentially.
Moreover, unlike the capacitance, the ESR of the ECAP increases with the degradation, and refitted from polynomial models and remodelled in the following exponential form:

$$\text{ESR}_{\text{emp}}\%(t) \approx a_1 e^{b_1 t} + c_1 e^{d_1 t}, \tag{2.31a}$$

$$\text{ESR}_{\text{emp}}(t) \approx \text{ESR}_0(1 + \frac{\text{ESR}_{\text{emp}}\%(t)}{100}), \tag{2.31b}$$

where $a_1 = 22.02$, $b_1 = 9.62.10^{-5}$, $c_1 = -21.72$, and $d_1 = -0.0004157$ are the parameters of the empirical degradation model. $\text{ESR}_{\text{emp}}\%(t)$ denotes the increase percentage of the ESR throughout the degradation of the ECAP. $\text{ESR}_{\text{emp}}(t)$ denotes the increase of the ESR starting from its initial rated value. Thus, Figures 2.9a and 2.9b illustrate the evolution of the empirical models considering the capacitance degradation and ESR increase percentages. A 20% decrease in the capacitance value results in around 57% increase in the the ESR, that represent their failure TH respectively.

2.3.3 Numerical application: empirical degradation analysis

The empirical degradation models of the failure precursors $R_{\text{ON}_{\text{emp}}}$ and ESR_{emp} are integrated without any model transformation as mentioned in Proposition 2.3.1. Figures 2.10a, 2.10b and 2.10c illustrate the empirical degradation effect on the states in the three scenarios.
The simulation of the empirical degradation on the system-level has clearly shown the effect of the cascading damage on the remaining components of the system. The first two scenarios show almost similar degradation rate with a different evolution, as shown in Figures 2.10a, 2.10b and 2.10c. Whereas, the degradation impact in scenario 3 is more important on the three states of the DC-DC converter. Additionally, the degradation effect on the input capacitance voltage represented by x_1 is negligible as the voltage increases between 0.02 V and 0.04 V with respect to the initial value of 198.54 V in the three scenarios. The inductor current x_2 drops between 2 A in the first two scenarios and 4 A in the third scenario, during the whole degradation process. Finally, the output capacitance voltage drops between approximately 3 V to 7 V in the first two scenarios and the third scenario respectively.

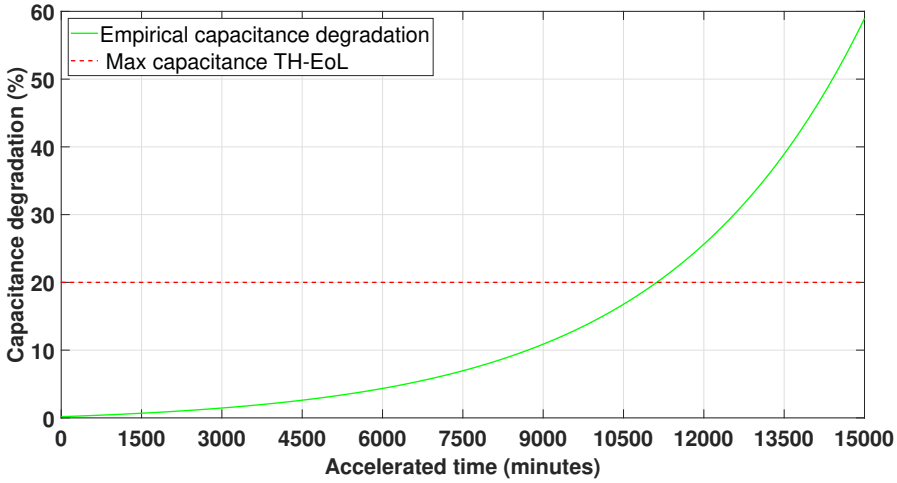

(a) Evolution of capacitance degradation using empirical model.

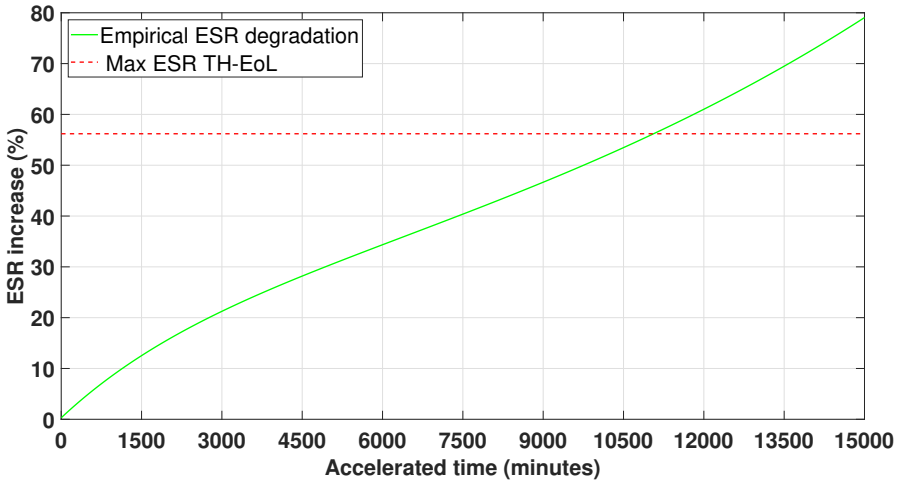

(b) Evolution of ESR using empirical model.

Figure 2.9: Evolution of the lumped model of ECAPs

The observation of the degradation effects on the components of the system is essential for the next step in this phase, where different model transformation approaches are investigated for the sake of creating a structured modeling approach that can be generalized with further real applications. The main aim of the following step is to emphasize on the critical components of the system in order to facilitate the assessment of the system-level prognostics via the critical components and not the external features, as proposed in

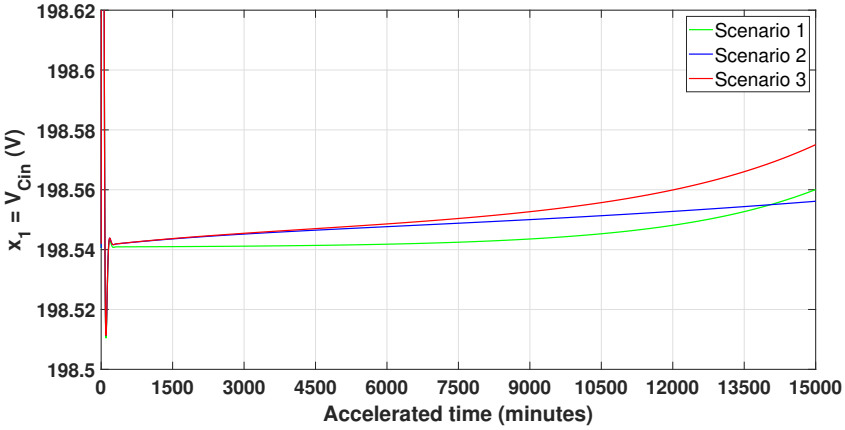

(a) x_1 during the three degradation scenarios

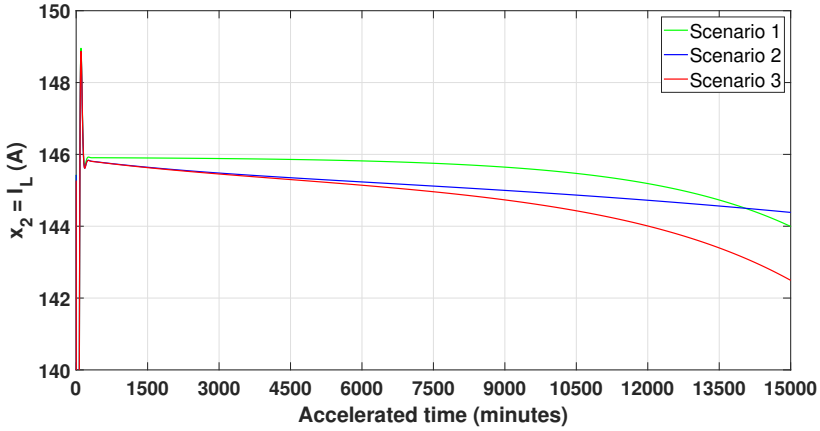

(b) x_2 during the three degradation scenarios

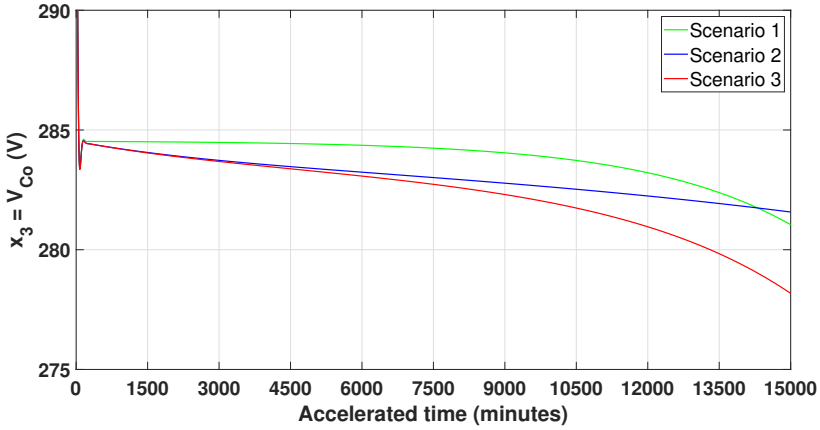

(c) x_3 during the three degradation scenarios

Figure 2.10: The states during the three degradation scenarios

Chapter 1. Additionally, this aim can not be achieved without considering less computational effort and time with high modeling accuracy, in order to decrease the cost and the modeling uncertainties.

2.4 Model Representation with Degradation Integration for Estimation Purposes

In broad, rather than the technical perspective, the prognostics approaches depend on *time* which is one of the triads of universe by which the *past*, the *present*, and the *future* are defined. In the context of our research and the importance of time in prognostics applications, the past consists of all the degradation actions that happened and affected the present time which is characterized by uncertain observations of the system. Furthermore, the main goal of the RUL *forecasting* depends on projecting from the present to the future with exponentially increasing unknown uncertainties (D. W. Boyd 2001a). Moreover, only the components with degraded profiles in the past referring to the present are concerned in the forecasting process. Although the forecasting is based on the present observations, we assume that we do not have any direct access to measure the parameters of the system. Consequently, parameters estimation is the proposed solution to overcome the observation barrier. It is worth noting to differentiate between the parameters which describe real physical components such as resistance and capacitance, and the variables which are defined as the independent energy-storage elements.

Wherefore, it has become crucial to put forward a systematical method for parameters estimation for model-based prognostics applications in the interest of generalization to other applications. Thus, the ideal estimation and forecasting results can be obtained if less computations are required.

To this point we are only responsible of structuring the estimation methodology with respect to the three degradation scenarios. Thus, the *endogenous* parameters where the variations occur internally, follow either stochastic, constant, logical, Malthusian, or exponential forms (D. W. Boyd 2001b). Therefore, based on previous experimental observations of the AGEs for power electronic devices, the degraded components show in general either exponential growth (i.e. the resistance) or exponential decline (i.e. the capacitance) as shown in Section 2.3.

Therefore, we present an overview about three model representation approaches that have been investigated for the parameters extraction for estimation purposes. Stochastic or deterministic estimation approaches could be implemented, yet they are not detailed in this section since the focus is on synthesizing the modeling phase of the general PHM approach.

Remark 2.4.1. Henceforth, the degradation precursors such as R_{ON} and $\mathrm{ESR_o}$ are included in the parameter vector ρ.

2.4.1 Hybrid states estimation and parameters regression

Proposition 2.4.1 (States estimation and parameters regression using one observer)**.** This strategy combines the state estimation of the genuine dynamical model and compute the varying parameters in function of the states, input, and/or output components as illustrated in the diagram of Figure 2.11.

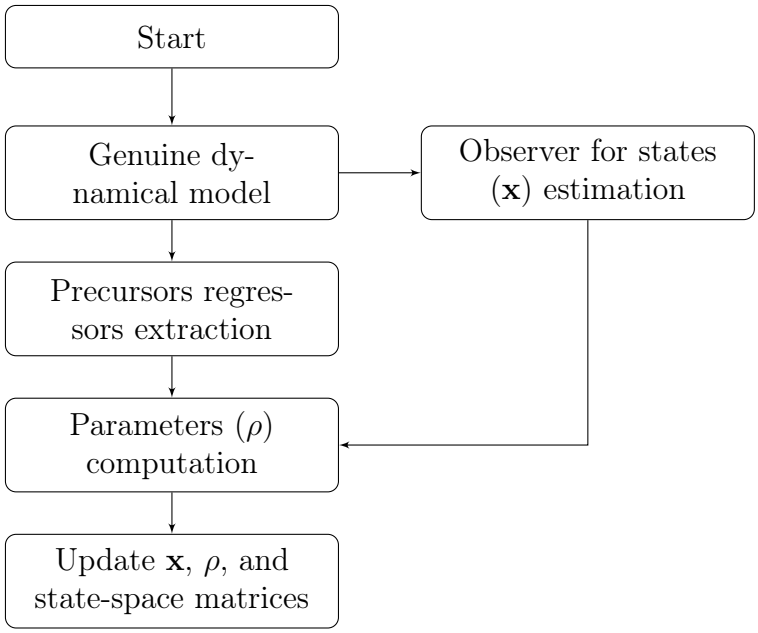

Figure 2.11: Hybrid states estimation and parameters regression approach

The parameters ρ are extracted as regressors from the main state-space model. The observer is only used for states estimation that will update the regressors online.

Let us consider scenario 1 as a demonstrating example with the degraded MOSFET. The modeling phase in normal operation condition has shown that the R_{ON} precursor is only shown in the matrix $\mathbf{A}_1$ of the subsystem 1 (2.5).

Example 2.4.1. The state equation in function of R_{ON} is:

$$\begin{aligned}\dot{x}_2(t) = &\frac{R_{\mathrm{in}}}{L(R_{\mathrm{in}}+\mathrm{ESR}_{\mathrm{in}})}x_1(t)\\ &-\frac{(R_{\mathrm{in}}\mathrm{ESR}_{\mathrm{in}}+(R_L+R_{\mathrm{ON}}(t))(R_{\mathrm{in}}+\mathrm{ESR}_{\mathrm{in}}))}{L(R_{\mathrm{in}}+\mathrm{ESR}_{\mathrm{in}})}x_2(t)\\ &+\frac{\mathrm{ESR}_{\mathrm{in}}}{L(R_{\mathrm{in}}+\mathrm{ESR}_{\mathrm{in}})}u_1(t),\end{aligned} \tag{2.32}$$

then, the regressor equation of $R_{\mathrm{ON}}(t)$ is rewritten as:

$$\begin{aligned}R_{\mathrm{ON}}(t) = &\left(\frac{1}{R_{\mathrm{in}}+\mathrm{ESR}_{\mathrm{in}}}\right)\left[\left(\frac{L(R_{\mathrm{in}}+\mathrm{ESR}_{\mathrm{in}})}{x_2(t)}\right)\right.\\ &\left(\frac{R_{\mathrm{in}}}{L(R_{\mathrm{in}}+\mathrm{ESR}_{\mathrm{in}})}x_1(t)+\frac{\mathrm{ESR}_{\mathrm{in}}}{L(R_{\mathrm{in}}+\mathrm{ESR}_{\mathrm{in}})}u_1(t)-\dot{x}_2(t)\right)\\ &\left.-R_{\mathrm{in}}\mathrm{ESR}_{\mathrm{in}}\right]-R_L.\end{aligned} \tag{2.33}$$

The major drawback in the regressor equation (2.33) is that this representation is accompanied by regression error with no correction step. Additionally, for scenario 2 and 3 the complexity of forming the regression increases with the number of variables and the correlation among the equations become unrealistic. Consequently, this method has not been considered further since that no concessions in accuracy and reliability are accepted in the prognostics applications.

2.4.2 Dual observers for separate states and parameters estimation or for switched-systems

Proposition 2.4.2 (Multifunctional dual-observer approaches)**.** As the parameter regression in Proposition 2.4.1 lacks the correction step in the parameter computation, another observer can be dedicated for the parameter estimation in order to improve its accuracy, following the average representation of the main model.
Moreover, dual observers can also be used in a different approach for switched-systems, by alternating between the two subsystems. In other words, if the

external features are considered as the failure precursors for system-level prognostics, the dual-observer approach provides ripples estimation of the states.
Figure 2.12 illustrates the proposed improved approach of the dual-observers for separate states and parameters estimation.

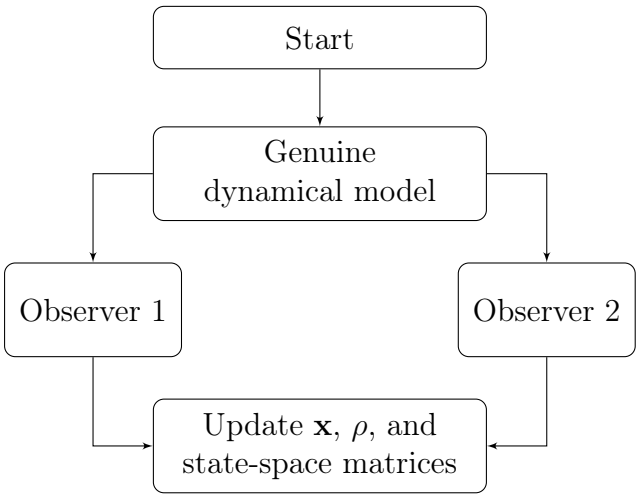

Figure 2.12: Dual-Observers for Separate States and Parameters Estimation Approach or Switched-Systems

Table 2.2 shows two different approaches that can be employed with the dual-observer technique for system-level prognostics.

Table 2.2: Dual-observer approaches

Observer	Approach 1: Average model	Approach 2: Alternating model
Observer 1	states ($\mathbf{x}$) estimation	states ($\mathbf{x}$) estimation for subsystem 1
Observer 2	parameters (ρ) estimation	states ($\mathbf{x}$) estimation for subsystem 2

Both approaches require two separate observers which increases the computational time and effort. Without detailing the observers design in this section, this approach has been also tried and therefore eliminated due to the unsatisfactory estimation results. The design and the results of the dual-observer approaches are presented in Chapter 3 in addition to a third approach that combines the dual-observer with Proposition 2.4.3.

2.4.3 Augmented representation for joint estimation of states and parameters

Proposition 2.4.3 (Joint states and parameters estimation for an augmented representation using only one observer)**.** The correction issue in Proposition 2.4.1 and the double computational effort using two observers in Proposition 2.4.2 can be solved by joining the states and the varying parameters together. This technique provides direct availability of the parameters as part of the state vector and requires only one observer for the joint estimation. However, the augmented representation of the model extends its size. Figure 2.13 illustrates the flowchart of the augmentation process and its representation with the observer.

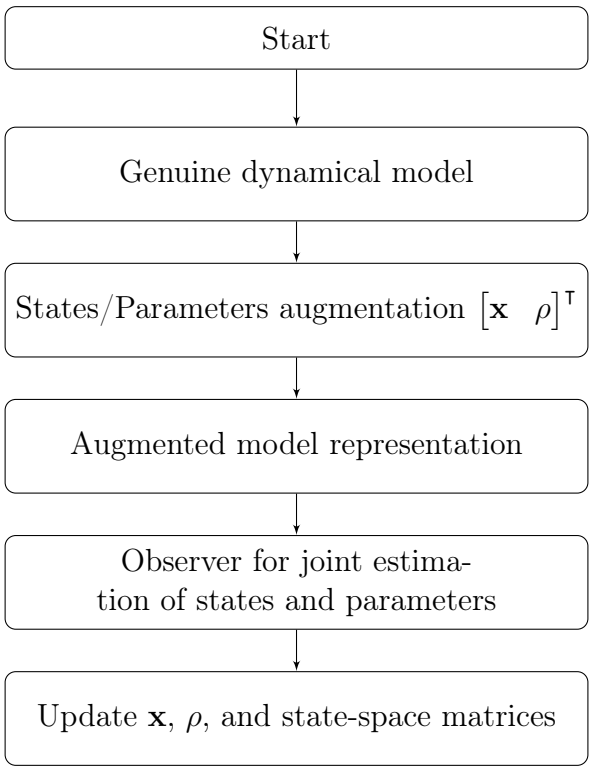

Figure 2.13: Proposed augmented model representation for JESP

The augmented state vector with the varying parameters $\rho_1, \ldots, \rho_{n_\rho}$ which describe the degradation precursors in our case, becomes:

$$\mathbf{x}^{\text{aug}} = \begin{bmatrix} x_1 & \ldots & x_{n_x} & \rho_1 & \ldots & \rho_{n_\rho} \end{bmatrix}^\intercal, \tag{2.34}$$

Then, by considering the three scenarios of the case study, the state vectors become:

$$\mathbf{x}^{\mathrm{S1}} = \begin{bmatrix} v_{C_{\mathrm{in}}} & i_L & v_{C_{\mathrm{o}}} & R_{\mathrm{ON}} \end{bmatrix}^{\intercal}, \tag{2.35a}$$

$$\mathbf{x}^{\mathrm{S2}} = \begin{bmatrix} v_{C_{\mathrm{in}}} & i_L & v_{C_{\mathrm{o}}} & \mathrm{ESR}_{\mathrm{o}} \end{bmatrix}^{\intercal}, \tag{2.35b}$$

$$\mathbf{x}^{\mathrm{S3}} = \begin{bmatrix} v_{C_{\mathrm{in}}} & i_L & v_{C_{\mathrm{o}}} & \mathrm{ESR}_{\mathrm{o}} & R_{\mathrm{ON}} \end{bmatrix}^{\intercal}. \tag{2.35c}$$

Remark 2.4.2. Henceforth, the augmented representation will be adopted in this thesis, and the augmented state vector $\mathbf{x}^{\mathrm{aug}}$ will be denoted as $\mathbf{x}$ for the sake of notation simplification.

Proposition 2.4.3 is therefore adopted for the implementation with the model of the case study. Consequently, due to the augmentation process, the dynamical nonlinear state-space model is represented in function of the time-varying parameters as:

$$\begin{cases} \dot{\mathbf{x}}(t) = \mathbf{A}(t)\mathbf{x}(t) + \mathbf{B}(t)\mathbf{u}(t), & (2.36a) \\ \mathbf{y}(t) = \mathbf{C}(t)\mathbf{x}(t) + \mathbf{D}(t)\mathbf{u}(t), & (2.36b) \end{cases}$$

and after discretization as:

$$\begin{cases} \mathbf{x}_{k+1} = \mathbf{A}(\rho_k)\mathbf{x}_k + \mathbf{B}(\rho_k)\mathbf{u}_k, & (2.37a) \\ \mathbf{y}_k = \mathbf{C}(\rho_k)\mathbf{x}_k + \mathbf{D}(\rho_k)\mathbf{u}_k. & (2.37b) \end{cases}$$

For notation simplification purposes, the state-space matrices $\mathbf{A}(\rho_k)$, $\mathbf{B}(\rho_k)$, $\mathbf{C}(\rho_k)$, and $\mathbf{D}(\rho_k)$ will be denoted by $\mathbf{A}_k$, $\mathbf{B}_k$, $\mathbf{C}_k$, and $\mathbf{D}_k$, respectively.

2.4.4 Numerical application: Augmented models

The average numerical models of the three scenarios with the augmentation process are shown below.

Augmented model of scenario 1

The numerical averaged augmented dynamical model of scenario 1 is obtained by averaging the two subsystems (B.1) and (B.2) as in (2.16), and shown in

(2.38).

$$\mathbf{A}^{\mathrm{S1}}(t) = \left[\begin{array}{ccc:c} -113636 & -1136.363 & 0 & 0 \\ 622.665 & -2397.26\boxed{R_{\mathrm{ON}}(t)} - 452.677 & -4452.054 & 0 \\ 0 & 130 & 0 & 0 \\ \hdashline 0 & 0 & 0 & 1 \end{array}\right], \tag{2.38a}$$

$$\mathbf{B}^{\mathrm{S1}}(t) = \left[\begin{array}{cc} 113636 & 0 \\ 6226.65 & 356.164 \\ 0 & -200 \\ \hdashline 0 & 0 \end{array}\right], \tag{2.38b}$$

$$\mathbf{C}^{\mathrm{S1}}(t) = \left[\begin{array}{ccc:c} -9.0909 & 0.90909 & 0 & 0 \\ 0 & 0.052 & 1 & 0 \end{array}\right], \tag{2.38c}$$

$$\mathbf{D}^{\mathrm{S1}}(t) = \begin{bmatrix} 9.0909 & 0 \\ 0 & -0.08 \end{bmatrix}. \tag{2.38d}$$

It is clearly shown that the augmented parameter $R_{\mathrm{ON}}(t)$ only affects the matrix $\mathbf{A}_1^{\mathrm{S1}}$, and therefore $\mathbf{A}^{\mathrm{S1}}$.

Augmented model of scenario 2

The numerical augmented dynamical averaged model of scenario 2 is obtained by averaging the two subsystems (B.6) and (B.7) as in (2.16), and shown in (2.39).

$$\mathbf{A}^{\mathrm{S2}}(t) = \left[\begin{array}{ccc:c} -113636 & -1136.36 & 0 & 0 \\ 622.665 & -4452.054\boxed{\mathrm{ESR_o}(t)} - 98.9103 & -4452.054 & 0 \\ 0 & 0 & 130 & 0 \\ \hdashline 0 & 0 & 0 & 1 \end{array}\right], \tag{2.39a}$$

$$\mathbf{B}^{\mathrm{S2}}(t) = \left[\begin{array}{cc} 113636 & 0 \\ 6226.65 & 4452.054\boxed{\mathrm{ESR_o}(t)} \\ 0 & -200 \\ \hdashline 0 & 0 \end{array}\right], \tag{2.39b}$$

$$\mathbf{C}^{\mathrm{S2}}(t) = \left[\begin{array}{ccc:c} -9.0909 & 0.909 & 0 & 0 \\ 0 & 0 & 0.65\boxed{\mathrm{ESR_o}(t)} & 0 \end{array}\right], \tag{2.39c}$$

$$\mathbf{D}^{\mathrm{S2}}(t) = \begin{bmatrix} 9.0909 & 0 \\ 0 & -\boxed{\mathrm{ESR_o}(t)} \end{bmatrix}. \tag{2.39d}$$

It is remarkable that the $\mathrm{ESR_o}$ precursor has a larger effect on more matrices than the case of the MOSFET degradation.

Augmented model of scenario 3

The numerical augmented dynamical averaged model of scenario 3 is obtained by averaging the two subsystems (B.10) and (B.11) as in (2.16), and shown in (2.40).

$$\mathbf{A}^{\mathrm{S3}}(t) = \left[\begin{array}{ccc:cc} -113636 & -1136.36 & 0 & 0 & 0 \\ 622.665 & \boxed{a_{22}^{\mathrm{S3}}} & -4452.054 & 0 & 0 \\ 0 & 130 & 0 & 0 & 0 \\ \hdashline 0 & 0 & 0 & 1 & 0 \\ 0 & 0 & 0 & 0 & 1 \end{array}\right], \tag{2.40a}$$

$$\mathbf{B}^{\mathrm{S3}}(t) = \left[\begin{array}{cc} 113636 & 0 \\ 6226.65 & 4452.054\boxed{\mathrm{ESR_o}(t)} \\ 0 & -200 \\ \hdashline 0 & 0 \\ 0 & 0 \end{array}\right], \tag{2.40b}$$

$$\mathbf{C}^{\mathrm{S3}}(t) = \left[\begin{array}{ccc:cc} -9.09 & 0.909 & 0 & 0 & 0 \\ 0 & 0.65\boxed{\mathrm{ESR_o}(t)} & 1 & 0 & 0 \end{array}\right], \tag{2.40c}$$

$$\mathbf{D}^{\mathrm{S3}}(t) = \begin{bmatrix} 9.09 & 0 \\ 0 & -\boxed{\mathrm{ESR_o}(t)} \end{bmatrix}, \tag{2.40d}$$

where, $a_{22}^{\mathrm{S3}} = -4452.04\boxed{\mathrm{ESR_o}(t)} - 2397.26\boxed{R_{\mathrm{ON}}(t)} - 96.513$.

2.4.5 Inspection of the augmented model representation

The augmented states/parameters representation of the model is an effective method to extract all the endogenous parameters that are subject to estimation. Based on the fact that the system is dynamic with nonlinear varying parameters that represent the degradation precursors, the augmented model is therefore nonlinear. Additionally, we intend to use only one observer for the JESP by adopting the augmented representation, as shown in Figure 2.13. Degradation estimation is the second phase of the proposed PHM approaches, however it is crucial to represent an accurate linearized model compared to the original for efficient estimation results. Since the online estimation is required, the first inspection of the augmented models has resulted nonobservable systems in all three scenarios. The observability matrix

is computed as follows:

$$\mathcal{O} = \begin{bmatrix} \mathbf{C} \\ \mathbf{CA} \\ \mathbf{CA}^2 \\ \vdots \\ \mathbf{CA}^{n_x-1} \end{bmatrix}. \tag{2.41}$$

The system is observable $\iff$ $\text{rank}(\mathcal{O}) = n_x + n_\rho$. Whereas, $\text{rank}(\mathcal{O})$ of all the three scenarios with the augmented model representation have resulted 3, which yields only successful states estimation with nonobservable parameters. The following examples demonstrate the observability matrices of the augmented models of the three scenarios at the initial conditions.

Example 2.4.2. The observability matrix of the augmented model of scenario 1 is $\mathcal{O}^{\text{S1}}$((2.38a), (2.38c)):

$$\mathcal{O}^{\text{S1}} = \begin{bmatrix} -0.000001 & 0 & 0 & 0 \\ 0 & 0 & 0 & 0 \\ 0.10336 & 0.00094 & -0.0004 & 0 \\ 0.000003 & 0.000008 & -0.00002 & 0 \\ -11745.1357 & -118.39383 & -4.22196 & 0 \\ -0.36286 & -0.01428 & -0.03629 & 0 \\ 1334600799.4944 & 13456554.7228 & 527095.8348 & 0 \\ 41225.4065 & 420.9431 & 63.6134 & 0 \end{bmatrix} 10^7. \tag{2.42}$$

Example 2.4.3. The observability matrix of the augmented model of scenario 2 is $\mathcal{O}^{\text{S2}}$((2.39a), (2.39c)):

$$\mathcal{O}^{\text{S2}} = \begin{bmatrix} -0.000001 & 0 & 0 & 0 \\ 0 & 0 & 0 & 0 \\ 0.10336 & 0.00099 & -0.0004 & 0 \\ 0.000003 & 0.00001 & -0.00002 & 0 \\ -11745.10876 & -117.96117 & -4.41504 & 0 \\ -0.361317 & -0.011528 & -0.04734 & 0 \\ 334598000.249184 & 13399821.69554 & 525169.59071 & 0 \\ 41051.59858 & 409.67951 & 51.32355 & 0 \end{bmatrix} 10^7. \tag{2.43}$$

Example 2.4.4. The observability matrix of the augmented model of sce-

nario 3 is $\mathcal{O}^{S3}$((2.40a), (2.40c)):

$$\mathcal{O}^{S3} = \begin{bmatrix} 0 & 0 & 0 & 0 & 0 \\ 0 & 0 & 0 & 0 & 0 \\ 0.000001 & 0 & 0 & 0 & 0 \\ 0 & 0 & 0 & 0 & 0 \\ -0.11745 & -0.00118 & -0.00004 & 0 & 0 \\ -0.000004 & 0 & 0 & 0 & 0 \\ 13346.008 & 134.5668 & 5.271 & 0 & 0 \\ 0.4135 & 0.0042 & 0.0006 & 0 & 0 \\ -1516508035.0543 & -0.01529 & -0.00059 & 0 & 0 \\ -46992.35891 & -0473.8081 & -18.8002 & 0 & 0 \end{bmatrix} 10^{12}. \quad (2.44)$$

The observability issue appears in the last column of $\mathcal{O}^{S1}$ and $\mathcal{O}^{S2}$, and the last two columns of $\mathcal{O}^{S3}$ which are null. Hence, evidently the rank($\mathcal{O}$) = 3 in all scenarios, and the augmented models are not able to be employed without transformation. In consequence, the nonlinear and nonobservable augmented models require a transformed model representation that will be extensively explained in each application in the following chapters.

2.5 Conclusions

This chapter highlights the essential role of system modeling in the PHM. The presented case study is widely utilized in many engineering applications that necessitate the employment of prognostics techniques, since the power electronics systems are essential in electric vehicles, satellites, power plants, and other huge industrial applications. Firstly, a DC-DC converter has been modeled in the normal operation mode, and the average model representation has been adopted to minimize the computational effort of such switched-systems. Secondly, three degradation scenarios have been proposed for investigation purposes after obtaining the empirical models of the most crucial power electronic components in the case study. Eventually, the cascading effects of the degraded components on the system have been assessed. Furthermore, the different propositions concerning the states and parameters estimation have been explained and discussed for the sake of employing the most convenient model representation that allows the states and parameters estimation with high accuracy and reduced computational effort. Consequently, the augmented model representation has been adopted for the JESP. Whereas, such representation with the integration of the time-varying parameters can face nonobservablity barriers in addition to the nonlinearities. Therefore, this issue will be carried out in the following chapters. Figure 2.14 illustrates

the adopted procedures of phase I of the proposed PHM approach, that can be generalized to similar real applications of dynamical systems with degraded behaviors. Finally, the following chapters will discuss the second and the third phases with proper model representations, estimation approaches, tuning, and RUL forecasting.

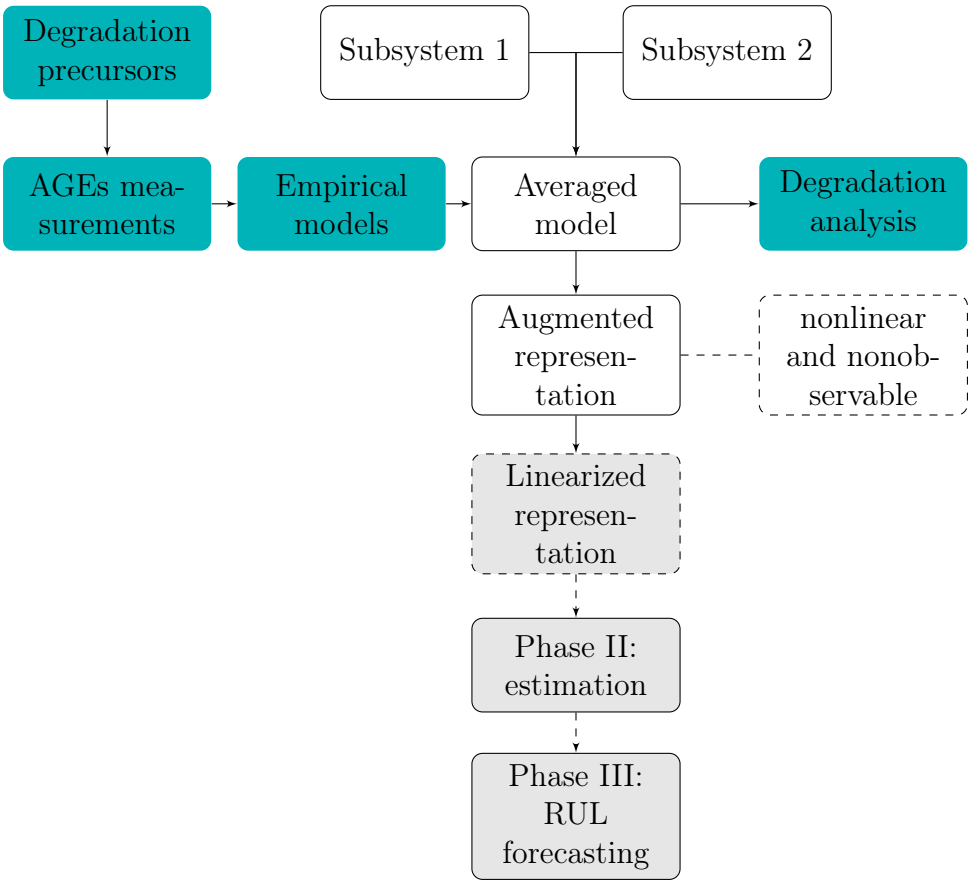

Figure 2.14: Diagram showing the formulation of the modeling phase

CHAPTER 3

Stochastic Approaches for PHM and RUL Forecasting

Contents

3.1 Introduction

The proposed PHM methodology for model-based applications requires a reliable degradation estimation method, on which the RUL forecasting approach relies, as shown in Figure 1.10. For this reason each proposed approach in this thesis is mainly based on the state and parameter estimation techniques for nonlinear systems, in order to establish the most reliable threefold methodology for prognostics. In Chapter 1, we elaborated the importance of estimating the internal parameters of the system for an efficient CBM. Additionally, we proposed the JESP of the augmented model representation as a technique that encounters most of the components and the failure precursors of a system. As mentioned earlier, the modeling, estimation, and RUL forecasting phases are investigated for nonlinear systems with degraded behaviors as shown in the proposed case study in Chapter 2.

We adopted a stochastic technique for JESP in the first proposed approach for the sake of emphasizing on the development of the RUL forecasting method from the literature perspective. In other words, the stochastic observers such as KF and its extensions (EKF, UKF, dual KF, sigma-point KF, square-root sigma-point KF etc.), are widely utilized in industrial applications for state and parameter estimation purposes (Kalman 1960; He et al. 2018; Merhy 2019). For these reasons, they are employed in the prognostics applications for degradation estimation. Furthermore, we can endorse the nontrivial fast and accurate simultaneous estimation by the application of the EKF to the augmented state-space representation of the dynamical model (Blanchard, A. Sandu, and C. Sandu 2007). This motivation allows the investigation of our proposed structured PHM approach with the stochastic observers for nonlinear systems on a macro level.

Therefore, we intend to employ the estimated parameters that describe the physical degraded components, in the RUL forecasting phase. In broad, the later is accomplished by predicting the degradation trajectories using their known polynomial, or exponential models for model-based prognostics, as stated in Chapter 1. However, in the case of unknown degradation models with no historical measurements acquired, we assume that the estimated

This chapter is based on the following publications: (Al-Mohamad, Hoblos, and V. Puig 2020; Alyakhni, Al-Mohamad, and Hoblos 2019; Al-Mohamad, Hoblos, and V. Puig 2019).

varying failure precursors are the indicators for the RUL forecasting. In other words, we intend to investigate the possibility of RUL forecasting based on the estimated critical parameters without predicting their behaviors nor using their models. The aforementioned conventional technique has been investigated along with the EoL-RUL approach that will be detailed throughout this chapter.

In this chapter, we intend to focus on the linear EoL-RUL forecasting approach, that refers to the linear relation between EoL and the RUL, despite the investigation of another approach in Chapter 5. Given the stochastic nature of the JESP, Gaussian noises and uncertainties are considered in order to complete the full proposed threefold PHM structure. Thus, the aim of assessing the stochastic approaches of the literature with our proposed threefold PHM strategy, is to contribute to its development towards system-level prognostics with unknown degradation models. It is worth recalling the importance of improving the forecasting reliability by improving the estimation accuracy in real-time applications.

This chapter is structured as follows. Section 3.2 presents the problem formulation of the PHM approach based on stochastic estimation. The augmented EKF for JESP is explained in Section 3.3. Thus, Section 3.4 is dedicated to the RUL forecasting approaches using a known degradation model and the proposed approach of linear EoL-RUL relation. The full algorithm of the PHM is explained in Section 3.5. Section 3.6 shows the implementation of the Dual Extended Kalman Filter (DEKF) for switched-systems. The application of the proposed PHM approach to the case study is shown in Section 3.7. Finally, the conclusions are drawn with an assessment in Section 3.8.

3.2 PHM Problem Formulation in a Stochastic Framework

As stated in the introduction, in this chapter we intend to formulate the proposed PHM approach with stochastic estimation techniques for nonlinear systems. The direct method of the RUL forecasting approach using the estimated degradation level to compute the EoL, and therefore the RUL, is henceforth called the linear EoL-RUL approach. As well, the classical prediction approach with known degradation models is tested. Figure 3.1 broadly highlights the employed methodology for the prognostics in this chapter.

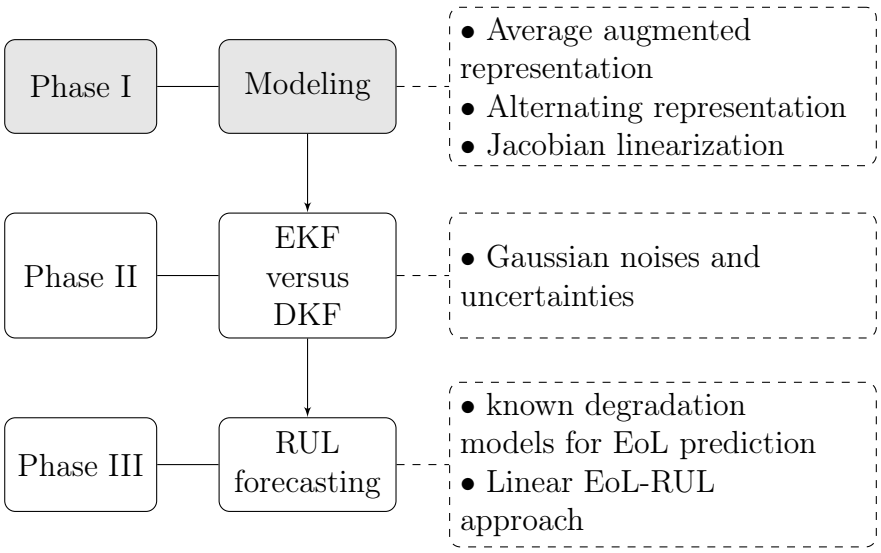

Figure 3.1: Stochastic-based proposed PHM methodology

1. *System modeling:* The modeling phase has been carried out in Chapter 2, where we adopted the average augmented representation of the model. Whereas, the switched approach is also explained and investigated since it keeps the ripples characteristics, which could open more possibilities of RUL forecasting development based on such external features. However, for computational effort reduction and fast estimation purposes, we propose to adopt the averaged model in this thesis.

2. *EKF for JESP and dual-observer for switched-systems:* The accurate estimation of the varying parameters is the core of the model-based prognostics. Therefore, the well-known stochastic EKF has been employed for the JESP, applied to the average augmented model with online Jacobian linearization. On the other hand, the SoH of the system is assessed continuously due to the knowledge of the physical TH of the fault precursors, as explained in Chapter 2. The JESP is assessed at each measurement, and the RUL forecasting follows if the TH is not crossed. Furthermore, the dual-observer approach for switched-systems has been investigated for research purposes, despite the fact that we motivate the augmented representation for its beneficial features.

3. *RUL forecasting:* The RUL forecasting is the main objective of the whole PHM methodology, on which the maintenance-related decision making is based. To cope with this fundamental role, we proposed to

directly compute the EoL of each varying parameter that describes the precursor of a degraded component in our case study. Consequently, the estimated parameter, its rated value, and its breakdown TH are needed for this process. Therefore, the RUL is then obtained online at each measurement. We proposed in 3.2.1 that the SRUL is the CRUL based on the First Critical Component to Fail (FCCF). Moreover, this strategy is compared to the degradation trajectory prediction with known polynomial models of the failure precursors. Thus, an Recursive Least Squares (RLS) filter has been employed to estimate the parameters of the degradation models and predict their behaviors until failure to obtain their EoL.

Proposition 3.2.1 (FCCF)**.** The SRUL is the CRUL of the FCCF. Technically, the EoL of the system is decided based on the component that reaches the TH first. It should be noted that this strategy is followed since no maintenance is being considered at this point of this thesis.

3.3 Augmented EKF for JESP

The EKF is specifically used for nonlinear systems, which follows the same procedure as the standard KF with the Jacobian linearization of the state-space equations, as mentioned in Section 3.2. Moreover, Gaussian noises and uncertainties are considered in Assumption 3.3.1.

Assumption 3.3.1. The process and measurement noises and uncertainties are denoted by $\omega \in \mathbb{R}^{n_x}$ and $\upsilon \in \mathbb{R}^{n_y}$ respectively. They are assumed to follow a Gaussian distribution with independent zero-mean, and no cross-correlations with covariances $\mathbf{Q}$ and $\mathbf{R}$. Thus, they are considered unknown at each time-step as (Kalman 1960; Ma et al. 2020):

$$\omega_k \sim N(0, \mathbf{Q}), \tag{3.1a}$$
$$\upsilon_k \sim N(0, \mathbf{R}), \tag{3.1b}$$

where the expectations are:

$$E[\omega_k] = 0, \tag{3.2a}$$
$$E[\upsilon_k] = 0, \tag{3.2b}$$
$$E[\omega_k \omega_k^\intercal] = \mathbf{Q}, \tag{3.2c}$$
$$E[\upsilon_k \upsilon_k^\intercal] = \mathbf{R}. \tag{3.2d}$$

Thus, the process and measurement covariances are discretized as:

$$\mathbf{Q}_d = \int_{\tau}^{T_s} e^{\mathbf{A}\tau} \mathbf{Q} e^{\mathbf{A}^\intercal \tau} d\tau, \tag{3.3a}$$

$$\mathbf{R}_d = \mathbf{R}\frac{1}{T_s}. \tag{3.3b}$$

Finally, the discrete-time state-space model is obtained as:

$$\begin{cases} \mathbf{x}_{k+1} = \mathbf{A}\mathbf{x}_k + \mathbf{B}\mathbf{u}_k + \omega_k, & (3.4a) \\ \mathbf{y}_k = \mathbf{C}\mathbf{x}_k + \mathbf{D}\mathbf{u}_k + \upsilon_k, & (3.4b) \end{cases}$$

The nonlinear discrete-time state-space model can be represented as:

$$\mathbf{x}_{k+1} = \mathbf{f}\left(\mathbf{x}_k, \mathbf{u}_k, \omega_k\right), \tag{3.5a}$$

$$\mathbf{y}_k = \mathbf{g}\left(\mathbf{x}_k, \mathbf{u}_k, \upsilon_k\right), \tag{3.5b}$$

where $\mathbf{f}\left(\mathbf{x}_k, \mathbf{u}_k, \omega_k\right)$ is the state transition matrix, and $\mathbf{g}\left(\mathbf{x}_k, \mathbf{u}_k, \upsilon_k\right)$ is the observation matrix. Recalling that that the varying parameter $\rho_k \in \mathbf{x}_k$, as discussed in (2.34) for notations simplification purposes. Thus, $\mathbf{f}$ is written as:

$$\mathbf{f}\left(\begin{bmatrix} x_1 \\ \vdots \\ x_{n_x} \\ \rho_1 \\ \vdots \\ \rho_{n_\rho} \end{bmatrix}\right) = \begin{bmatrix} \mathbf{f}_1(x_1, \ldots, x_{n_x}, \rho_1, \ldots, \rho_{n_\rho}) \\ \vdots \\ \mathbf{f}_{n_x}(x_1, \ldots, x_{n_x}, \rho_1, \ldots, \rho_{n_\rho}) \\ \mathbf{f}_{\rho_1}(x_1, \ldots, x_{n_x}, \rho_1, \ldots, \rho_{n_\rho}) \\ \vdots \\ \mathbf{f}_{n_\rho}(x_1, \ldots, x_{n_x}, \rho_1, \ldots, \rho_{n_\rho}) \end{bmatrix}, \tag{3.6}$$

and similarly for $\mathbf{g}$.
Then, based on the Assumption 3.3.1 of Gaussian noises and uncertainties, the prediction process can be approximated as:

$$\tilde{\mathbf{x}}_{k+1|k} = \mathbf{f}\left(\hat{\mathbf{x}}_{k|k}, \mathbf{u}_k, 0\right), \tag{3.7a}$$

$$\tilde{\mathbf{y}}_{k+1|k} = \mathbf{g}\left(\tilde{\mathbf{x}}_{k+1|k}, \mathbf{u}_k, 0\right), \tag{3.7b}$$

where $\tilde{\mathbf{x}}_{k+1|k}$ and $\tilde{\mathbf{y}}_{k+1|k}$ denote the predicted state and measurement vectors respectively. Thus, $\hat{\mathbf{x}}_k$ denotes the posteriori state estimate.

Remark 3.3.1. For notations simplification purposes, the $(\tilde{\star})$, and $(\hat{\star})$ are henceforth denoting predicted and estimated elements, respectively.

Therefore, the states and the measurements vectors are predicted as follows:

$$\tilde{\mathbf{x}}_{k+1|k} = \mathbf{A}_k \hat{\mathbf{x}}_{k|k} + \mathbf{B}_k \mathbf{u}_k, \tag{3.8}$$

$$\tilde{\mathbf{y}}_{k+1|k} = \mathbf{C}_k \tilde{\mathbf{x}}_{k+1|k} + \mathbf{D}_k \mathbf{u}_k. \tag{3.9}$$

Thus, it is required to compute the Jacobian matrices for $\mathbf{f}$ and $\mathbf{g}$ in order to proceed with the following filtering steps as:

$$\mathbf{J}(x_1, \ldots, x_{n_x}, \rho_1, \ldots, \rho_{n_\rho}) = \begin{bmatrix} \bigtriangledown^\intercal \mathbf{f}_1 \\ \vdots \\ \bigtriangledown^\intercal \mathbf{f}_{n_x} \\ \bigtriangledown^\intercal \mathbf{f}_{\rho_1} \\ \vdots \\ \bigtriangledown^\intercal \mathbf{f}_{n_\rho} \end{bmatrix} = \begin{bmatrix} \frac{\partial \mathbf{f}_1}{\partial x_1} & \cdots & \frac{\partial \mathbf{f}_1}{\partial x_{n_x}} & \frac{\partial \mathbf{f}_1}{\partial x_{\rho_1}} & \cdots & \frac{\partial \mathbf{f}_1}{\partial x_{\rho n_\rho}} \\ \vdots & \ddots & \vdots & \vdots & \ddots & \vdots \\ \frac{\partial \mathbf{f}_{n_\rho}}{\partial x_1} & \cdots & \frac{\partial \mathbf{f}_{n_\rho}}{\partial x_{n_x}} & \frac{\partial \mathbf{f}_{n_\rho}}{\partial \rho_1} & \cdots & \frac{\partial \mathbf{f}_{n_\rho}}{\partial \rho_{n_\rho}} \end{bmatrix}. \tag{3.10}$$

Next, the prediction of the filter error covariance is computed as:

$$\mathbf{P}_{k+1|k} = \left[\frac{\partial \mathbf{f}_k}{\partial \mathbf{x}}\right] \mathbf{P}_{k|k} \left[\frac{\partial \mathbf{f}_k}{\partial \mathbf{x}}\right]^\intercal + \mathbf{Q}_k. \tag{3.11}$$

Then, the filter gain matrix is computed as:

$$\mathbf{K}_{k+1} = \mathbf{P}_{k+1|k} \left[\frac{\partial \mathbf{g}_k}{\partial \mathbf{x}}\right]^\intercal \left(\left[\frac{\partial \mathbf{g}_k}{\partial \mathbf{x}}\right] \mathbf{P}_{k+1|k} \left[\frac{\partial \mathbf{g}_k}{\partial \mathbf{x}}\right]^\intercal + \mathbf{R}_{k+1} \right)^{-1}, \tag{3.12}$$

to perform the filter update as:

$$\hat{\mathbf{x}}_{k+1|k+1} = \tilde{\mathbf{x}}_{k+1|k} + \mathbf{K}_{k+1} \left(\mathbf{y}_{k+1} - \tilde{\mathbf{y}}_{k+1|k} \right). \tag{3.13}$$

Finally, the prediction error covariance is updated as:

$$\mathbf{P}_k = \left(\mathbf{I} - \mathbf{K}_k \left[\frac{\partial \mathbf{g}_k}{\partial \mathbf{x}}\right] \right) \tilde{\mathbf{P}}_k. \tag{3.14}$$

Remark 3.3.2. The initial value of the error covariance diagonal matrix $\mathbf{P}_0 \in \mathbb{R}^{n_x \times n_x}$ defines how much confidence we have regarding the model. A low $\mathbf{P}_0$ indicates more confidence in the inputs than the estimation, and vice-versa. However, it should be noted that high values of $\mathbf{P}_0$ could lead to numerical instability in the filtering process. Whereas, a moderately lower values could lead to faster filtering convergence. Moreover, $\mathbf{Q}$ can be found intuitively depending on each application, and the dynamics and the parameters uncertainties that are not modeled, are generally included in the process noise. However, $\mathbf{R}$ can be computed by a straightforward processing of measurements while keeping the outputs constant (Ma et al. 2020).

Finally, the estimated states and parameters are obtained in order to assess the SoH of the system, and proceed to the online RUL forecasting which only employs the estimated augmented parameters. Furthermore, the observability issue that was faced with the augmented model representation, has been solved with the Jacobian linearization that restructured the model as will be shown in Section 3.7.

Remark 3.3.3. Coping with real-time prognostics is a crucial mission in this study. One of the main objectives of this thesis is to structurize the PHM strategy for real applications with only fine tuning. Thus, the online linearization using the Jacobian is a widely-used approximation approach for dynamical systems. However, it requires a relatively high computational time that can burden the estimation and the prediction practices. Additionally, for future extensions of the PHM with automated control and larger applications, this approximation approach of the model will be developed to a generalized form that can suit many modern engineering applications. The later problem set-up is detailed in Chapter 4 and used as well in Chapter 5, while the Jacobian linearization is adopted in this chapter for investigation purposes.

3.4 RUL Forecasting Based on Stochastic Approaches

This section is dedicated to the classical RUL forecasting strategies and the proposed linear EoL-RUL approach that will be investigated throughout this thesis.

3.4.1 Classical RUL forecasting with known degradation models

In broad, the SoH assessment is related to the critical components. As mentioned in Chapter 2, the degradation of the critical components usually follows exponential or double exponential evolution. Thus, these degradation models can be used exactly with a dedicated filter for parameter estimation, in order to predict their behaviors. Hence, with known TH of each degraded component and predicted behavior using the known models and their estimated parameters, the two are intersected in order to obtain the EoL. This existing strategy has been illustrated in Figure 1.7.

In this thesis, we propose the employment of an RLS filter to estimate the

parameters of a defined-degree polynomial equation equivalent to the exponential degradation models. Thus, the failure precursors of the critical components will be expressed following the polynomial form as:

$$\rho(t) = p_n t^n + p_{n-1} t^{n-1} + \cdots + p_2 t^2 + p_1 t + p_0, \tag{3.15}$$

where $p_n, \ldots, p_0$ are the parameters that will be estimated using the RLS. Thus, the model will be refitted using the same polynomial model and intersected with the proper known TH.
Moreover, the degradation prediction uncertainties can affect the EoL prediction due to measurements and modeling uncertainties, as shown in Figure 1.9.

3.4.2 Proposed RUL forecasting based on the linear EoL-RUL approach

The slowly-degraded components have a long-term impact on the efficiency of the whole system, as we analyzed the cascading damage in Chapter 2. Thus, the SoH of the system could be predicted in order to keep the desired operation, with the advantages of reducing the scheduled maintenance expenses at the first place. Therefore, the first proposed RUL forecasting approach is based on the following linear EoL-RUL relation:

$$t_{\text{RUL}} = t_{\text{EoL}} - t_{\text{current}}, \tag{3.16}$$

where t_{current} can be replaced by k that represents the actual measurement time instant in discrete-time.
Additionally, the breakdown TH of each component is known and the degradation level is estimated.

Proposition 3.4.1 (RUL forecasting based on the EoL-RUL relation without degradation prediction)**.** Given the degradation variation level equation based on the estimated parameters with respect to its rated value as:

$$\hat{\text{deg}}_{\%_k} = \frac{\hat{\mathbf{x}}_k - \mathbf{x}_0}{\mathbf{x}_0} \times 100. \tag{3.17}$$

where $\hat{\mathbf{x}}_k$ denotes the estimated augmented vector of states and parameters which is previously-obtained from the EKF. Thus, the main aim is to relate the estimated degradation level $\hat{\text{deg}}_{\%}$ (3.17) with the linear EoL-RUL equation (3.16). Hence, a linear degradation level equations is assumed as:

$$\hat{\text{deg}}_{\%_k} \approx a_k k + b_k, \tag{3.18}$$

where a_k and b_k denote the parameters of the linear equation at each measurement instant k.

Therefore, it is known that the EoL occurs once the TH of each parameter has been crossed. Consequently, the EoL can be obtained by replacing this statement with the parameters of (3.18) as:

$$\tilde{\text{EoL}}_k \approx \frac{\text{TH} - b_k}{a_k}. \tag{3.19}$$

Remark 3.4.1. It is worth noting that $\tilde{\text{EoL}}_k$ is in discrete-time due to the simulation purposes. Whereas, the final value will be referred again to the real time in minutes.

After relating the EoL-RUL equation with the TH and the degradation level, it is necessary to compute the parameters a_k and b_k. A parameter estimation technique such as RLS can be employed in order to estimate the parameters a_k and b_k. However, the filter is not built on concrete accurate information, which will delay the converging process due to Assumption 3.4.1, which allows us to eliminate such filtering technique if no other information is provided [1].

Assumption 3.4.1. The initial condition of each parameter that describes a critical component is assumed to be 100% healthy in the case no further information provided about any previous working conditions, times, and maintenance.

Consequently, by eliminating the parameter estimation of (3.19), it is required to assume an initial condition based on previous maintenance experiences for such systems, rated information, inspections, or any other information. This condition states that the system will be fully-degraded (100%) after an assumed $\breve{\text{EoL}}$. In other words, an EoL will be assumed based on previous experiences from the manufacturers of the critical components, without knowing the degradation behaviors.
It is essential to note that the investigation of this approach considers an extreme case where no degradation models nor previous measurements data are known.
Thus, a drawback of this assumption is that it could be too conservative in a way that $\breve{\text{EoL}} < \text{EoL}$, or too optimistic-but-hazardous such that $\breve{\text{EoL}} > \text{EoL}$. The main aim of employing such technique in this chapter, is to show how critical is the RUL forecasting problem set-up in such conditions.

[1] A recursive approach for degradation behavior prediction is employed in Chapter 5.

Furthermore, a system of linear equations is formed as:

$$\begin{cases} a_k \breve{\text{EoL}} + b_k \approx 100\%, & \text{(3.20a)} \\ a_k k + b_k \approx \hat{\text{deg}}_{\%_k}. & \text{(3.20b)} \end{cases}$$

Hence, based on the aforementioned assumptions, $\breve{\text{EoL}}$ is assumed for a longer duration that the empirical EoL, to push the RUL forecasting algorithm to the limits while investigating.
Finally, after computing the parameters, the predicted $\tilde{\text{RUL}}$ is obtained in discrete-time as:

$$\tilde{\text{RUL}}_k \approx \tilde{\text{EoL}}_k - k \approx \frac{\text{TH} - b_k}{a_k} - k. \tag{3.21}$$

Where k is the current sample, the shown RUL forecasting results will be related to the accelerate time in minutes in this case study as:

$$\tilde{t}_{\text{RUL}} = \tilde{t}_{\text{EoL}} - t_{\text{current}}, \tag{3.22}$$

3.5 Algorithm of the Proposed PHM Approach

Algorithm 1 presents the implementation of the EKF for JESP and the online RUL forecasting.
This approach is simple to implement and the JESP is accurate and reliable. The overall performance of this proposition will be further numerically-investigated and analyzed in Section 3.7.

3.6 Dual Observers Approaches for Degradation Estimation of Switched-Systems

According to the statements in Section 3.1 and in Chapter 2, there exist possible estimation approaches. Separate states and parameters estimation using the average model or for genuine one-model systems, or achieving states estimation of each subsystem of switched-systems.
Moreover, a third approach can be investigated using the augmented representation for JESP of alternating systems. In other words, the subsystems can be augmented with the critical parameters and implemented with two separate observers as detailed in Algorithm 2 that employs the DEKF for JESP of switched-systems.

Algorithm 1: Stochastic algorithm for JESP and RUL forecasting

Result: $\hat{\mathbf{x}}$, $\tilde{\mathrm{RUL}}_k$
initialization: $\mathbf{x}_0$, ρ_0, ω_0, υ_0, $\mathbf{Q}_0$, $\mathbf{R}_0$, $\mathbf{P}_0$;
for $k = 1 : N$ **do**
  Compute:
  $\mathbf{A}_k, \mathbf{B}_k, \mathbf{C}_k, \mathbf{D}_k$;
  The predicted state vector $\tilde{\mathbf{x}}_{k+1|k}$ as in (3.8);
  The Jacobian matrices (3.10);
  The predicted measurement vector $\tilde{\mathbf{y}}_{k+1|k}$ (3.9);
  The filter covariance $\mathbf{P}_{k+1|k}$ (3.11);
  The filter gain matrix $\mathbf{K}_{k+1}$ (3.12);
  The filter update $\hat{\mathbf{x}}_{k+1|k+1}$ (3.13);
  The prediction error covariance $\mathbf{P}_k$ (3.14);
  The estimated degradation percentage $\hat{\mathrm{deg}}_{\%}$ (3.18);
  Solve the system of equations (3.20);
  Predict $\tilde{\mathrm{RUL}}_k$ (3.21);
  Illustrate the predicted RUL in real time $\tilde{t}_{\mathrm{RUL}}$ (3.22);
  Update $\mathbf{A}_k, \mathbf{B}_k, \mathbf{C}_k, \mathbf{D}_k$ with $\hat{\rho}_k$, $\hat{\mathbf{x}}_k$ and repeat;
end

Remark 3.6.1. Although the alternating approach estimate the ripples that can play an important role in the SoH assessment, it arises the burden of the computational effort in addition to the closed-loop regulations and variable loads that can affect the ripples levels.
For all these reasons, the dual-observer approach has been examined in this thesis despite the aforementioned limitations in order to establish an efficient PHM structure with reliable estimation and prediction.

The results of the alternating approach with separate states estimation are shown in Section 3.7. Algorithm 2 and approach 1 in Table 2.2 are not shown since, the DEKF is similar to the JESP using the EKF in the parameters estimation framework. We propose to compare the KF-based dual-observer approach for alternating states estimation with the JESP using EKF for the sake of assessing the efficiency of the proposed JESP against the Dual Kalman Filter (DKF) (KF-based dual-observer). Additionally, this comparison emphasizes on the importance of the estimation of the critical parameters in addition to the external features for the SoH assessment and specifically for the CBM.

Algorithm 2: DEKF for switched-systems

Result: JESP

initialization: $\mathbf{x}_0$, ω_0, υ_0, $\mathbf{Q}_0$, $\mathbf{R}_0$, $\mathbf{P}_0$;

for $k = 1 : N$ **do**

Predict the states of subsystem 1: $\tilde{\mathbf{x}}_{1_{k+1|k}} = \mathbf{A}_{1_k}\hat{\mathbf{x}}_{1_{k|k}} + \mathbf{B}_{1_k}\mathbf{u}_k$;

Predict the outputs of subsystem 1: $\tilde{\mathbf{y}}_{1_{k+1|k}} = \mathbf{C}_{1_k}\tilde{\mathbf{x}}_{1_{k+1|k}} + \mathbf{D}_{1_k}\mathbf{u}_k$;

Compute the error covariance of subsystem 1:

$\mathbf{P}_{1_{k+1|k}} = \left[\frac{\partial \mathbf{f}_{1_k}}{\partial \mathbf{x}}\right]\mathbf{P}_{1_{k|k}}\left[\frac{\partial \mathbf{f}_{1_k}}{\partial \mathbf{x}}\right]^{\intercal} + \mathbf{Q}_k$;

Compute the gain of subsystem 1:

$\mathbf{K}_{1_{k+1}} = \mathbf{P}_{1_{k+1|k}}\left[\frac{\partial \mathbf{g}_{1_k}}{\partial \mathbf{x}}\right]^{\intercal}\left(\left[\frac{\partial \mathbf{g}_{1_k}}{\partial \mathbf{x}}\right]\mathbf{P}_{1_{k+1|k}}\left[\frac{\partial \mathbf{g}_{1_k}}{\partial \mathbf{x}}\right]^{\intercal} + \mathbf{R}_{k+1}\right)^{-1}$;

Estimate the states of subsystem 1:

$\hat{\mathbf{x}}_{1_{k+1|k+1}} = \tilde{\mathbf{x}}_{1_{k+1|k}} + \mathbf{K}_{1_{k+1}}\left(\mathbf{y}_{1_{k+1}} - \tilde{\mathbf{y}}_{1_{k+1|k}}\right)$;

Update the error covariance of subsystem 1 for subsystem 2:

$\mathbf{P}_{1_k} = \left(\mathbf{I} - \mathbf{K}_{1_k}\left[\frac{\partial \mathbf{g}_{1_k}}{\partial \mathbf{x}}\right]\right)\tilde{\mathbf{P}}_{1_k}$;

Predict the states of subsystem 2 in function of the estimated state of subsystem 1 ($\hat{\mathbf{x}}_{1_{k+1|k+1}}$): $\tilde{\mathbf{x}}_{2_{k+1|k}} = \mathbf{A}_{2_k}\hat{\mathbf{x}}_{1_{k+1|k+1}} + \mathbf{B}_{2_k}\mathbf{u}_k$;

Predict the outputs of subsystem 2: $\tilde{\mathbf{y}}_{2_{k+1|k}} = \mathbf{C}_{2_k}\tilde{\mathbf{x}}_{2_{k+1|k}} + \mathbf{D}_{2_k}\mathbf{u}_k$;

Compute the error covariance of subsystem 2 in function of the updated error covariance 1: $\mathbf{P}_{2_{k+1|k}} = \left[\frac{\partial \mathbf{f}_{2_k}}{\partial \mathbf{x}}\right]\mathbf{P}_{1_k}\left[\frac{\partial \mathbf{f}_{2_k}}{\partial \mathbf{x}}\right]^{\intercal} + \mathbf{Q}_k$;

Compute the gain of subsystem 2:

$\mathbf{K}_{2_{k+1}} = \mathbf{P}_{2_{k+1|k}}\left[\frac{\partial \mathbf{g}_{2_k}}{\partial \mathbf{x}}\right]^{\intercal}\left(\left[\frac{\partial \mathbf{g}_{2_k}}{\partial \mathbf{x}}\right]\mathbf{P}_{2_{k+1|k}}\left[\frac{\partial \mathbf{g}_{2_k}}{\partial \mathbf{x}}\right]^{\intercal} + \mathbf{R}_{k+1}\right)^{-1}$;

Estimate the states of subsystem 2:

$\hat{\mathbf{x}}_{2_{k+1|k+1}} = \tilde{\mathbf{x}}_{2_{k+1|k}} + \mathbf{K}_{2_{k+1}}\left(\mathbf{y}_{2_{k+1}} - \tilde{\mathbf{y}}_{2_{k+1|k}}\right)$;

Update the error covariance for the sake of repeating the process with subsystem 1: $\mathbf{P}_{1_k} = \left(\mathbf{I} - \mathbf{K}_{2_k}\left[\frac{\partial \mathbf{g}_{2_k}}{\partial \mathbf{x}}\right]\right)\tilde{\mathbf{P}}_{2_k}$;

end

3.7 Case Study: Results and Analysis

The proposed PHM approach in this chapter is applied to the DC-DC converter case study. The augmentation process with the time-varying parameters that describe the degraded critical electronic components have been extensively explained in Chapter 2. Thus, the stochastic estimation approaches of the second phase of the proposed PHM are simulated using the EKF-based JESP and the DKF for switched-systems. Hence, the classical degradation prediction approach with known models has been investigated along with the

proposed linear EoL-RUL forecasting.
Firstly, the empirical degradation models have been simulated in order to obtain the measurements vector online. As we previously mentioned, the empirical models are only used to degrade the model with real critical components with AGEs data.
Secondly, the EKF for JESP has been applied to the augmented state-space average model in each scenario, noting that it has been linearized using the Jacobian technique. Thus, the DKF with the switched-system have been applied to scenario 2 as an illustrative example and to avoid repetitions since it is not adopted in this thesis.
Thirdly, after retrieving the estimated varying parameter(s) at each time instant k, the RUL forecasting algorithm using the system of linear equations is solved to predict the EoL and therefore the RUL of each component. Finally, based on the FCCF proposition, the SRUL is the first CRUL.
The assessment of the model representation, estimation technique and proposed RUL methodology is discussed in the following subsections.

3.7.1 Scenario 1

The nonlinear continuous-time R_{ON}-augmented state-space model[2] is:

$$\left[\begin{array}{c|c} \mathbf{A}^{\text{S1}}(2.38\text{a}) & \mathbf{B}^{\text{S1}}(2.38\text{b}) \\ \hline \mathbf{C}^{\text{S1}}(2.38\text{c}) & \mathbf{D}^{\text{S1}}(2.38\text{d}) \end{array}\right]. \tag{3.23}$$

Recalling that the model (3.23) is nonlinear, only $\mathbf{A}^{\text{S1}}$ is parameter-dependent while the remaining matrices are LTI. Thus, the Jacobian matrix of $\mathbf{A}^{\text{S1}}$ is computed as in (4.1), and obtained as:

$$\mathbf{J}_{\mathbf{A}}{}^{\text{S1}}(t) = \begin{bmatrix} -1.13610^5 & -1.13610^3 & 0 & 0 \\ 6.22610^2 & \boxed{a_{22}^{\text{S1}}(t)} & -4.45210^3 & -2.39710^3\boxed{x_2(t)} \\ 0 & 130 & 0 & 0 \\ 0 & 0 & 0 & 1 \end{bmatrix}, \tag{3.24}$$

where $a_{22}^{\text{S1}}(t) = -2.39710^3\boxed{R_{\text{ON}}(t)} - 4.52610^2$. As clearly shown that the model depends on the state x_2 in addition to the parameter R_{ON}.
Hence, the observability matrix is checked after obtaining the discrete couple

[2]The model is discretized during the estimation and the forecasting process.

$(\mathbf{J_A}^{S1}, \mathbf{C}^{S1})$ as:

$$\mathcal{O}^{S1}(\mathbf{J_A}^{S1}, \mathbf{C}^{S1}) = \begin{bmatrix} -9.090909 & 0.90909 & 0 & 0 \\ 0 & 0.052 & 1 & 0 \\ -0.931904 & 0.972644 & -0.085055 & -6.869962 \\ 0.00026 & 0.053605 & 0.995298 & -0.379778 \\ -0.091261 & 0.96253 & -0.171341 & -13.839433 \\ 0.000295 & 0.055166 & 0.990455 & -0.770947 \\ -0.004729 & 0.944938 & -0.256276 & -20.699851 \\ 0.000306 & 0.056685 & 0.985475 & -1.173201 \end{bmatrix}. \tag{3.25}$$

Therefore, $\text{rank}(\mathcal{O}^{S1}(\mathbf{J_A}^{S1}, \mathbf{C}^{S1})) = 4$, which yields a fully-observable model in this case.

Remark 3.7.1. It should be noted that the observability matrix has been computed and verified $\forall k$, and (3.25) shows only the initial time instant as a representative numerical example.

Results of the JESP using the EKF

The EKF has been applied as explained in Section 3.3 to the augmented model of the presented case study. Figures 3.2a, 3.2b, and 3.2c show the states estimation in comparison with the empirically-degraded model with Gaussian noises.
The estimated states follow the empirical degradation with high accuracy. Furhtermore, the augmented parameter R_{ON} is simultaneously estimated with the states using the JESP technique. Eventually, the parameter estimation is as accurate as the state estimation as shown in Figure 3.3.

RLS-based degradation prediction using known models of the failure precursors

According to Section 3.4, the existing RUL forecasting approach by predicting the degradation trajectories, has been investigated in this chapter. The exponential degradation model (2.29) of the augmented R_{ON} of scenario 1 has been rewritten in a 5-degree polynomial equation in order to apply a RLS filter for parameters estimation. The empirical polynomial degradation model of R_{ON} is written in (3.26) with R-square = 1.

$$\begin{aligned} \Delta R_{\text{ON}_{\text{poly}}}(t) \approx\ & 1.615.10^{-22}t^5 - 3.465.10^{-18}t^4 + 3.684.10^{-14}t^3 \\ & -1.247.10^{-10}t^2 + 3.575.10^{-7}t - 7.607.10^{-5}. \end{aligned} \tag{3.26}$$

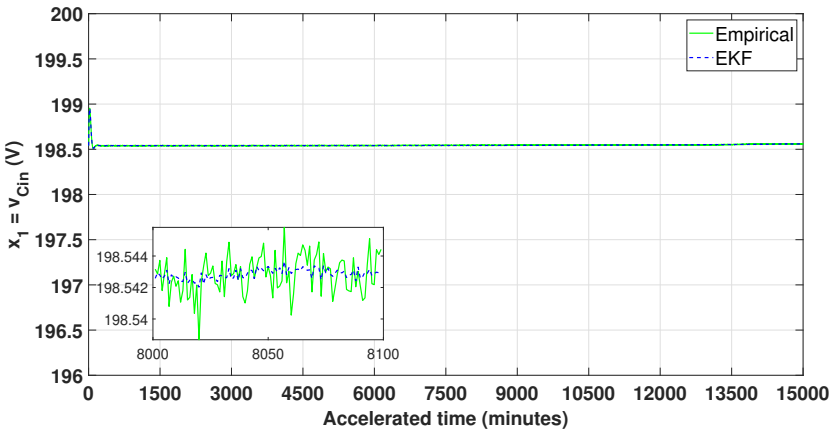

(a) $\hat{\mathbf{x}}_1$ versus empirical degradation in scenario 1

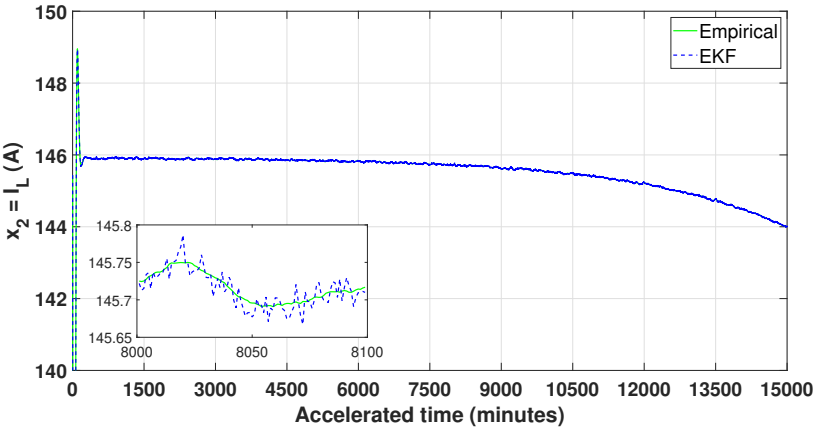

(b) $\hat{\mathbf{x}}_2$ versus empirical degradation in scenario 1

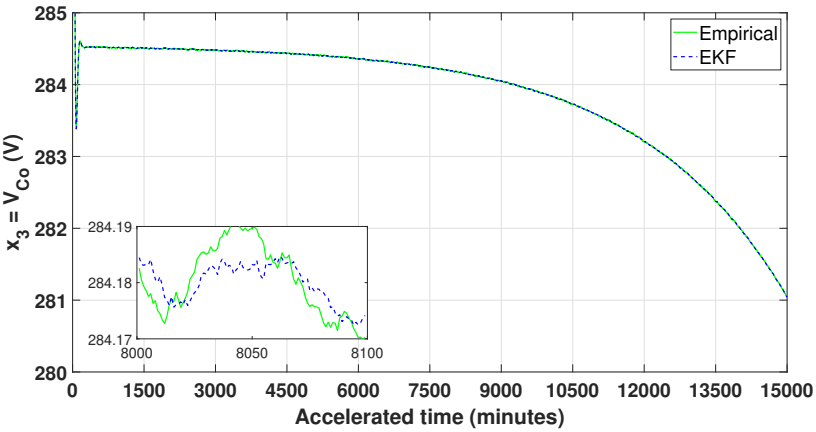

(c) $\hat{\mathbf{x}}_3$ versus empirical degradation in scenario 1

Figure 3.2: The estimated states versus the corresponding empirical degradation in scenario 1

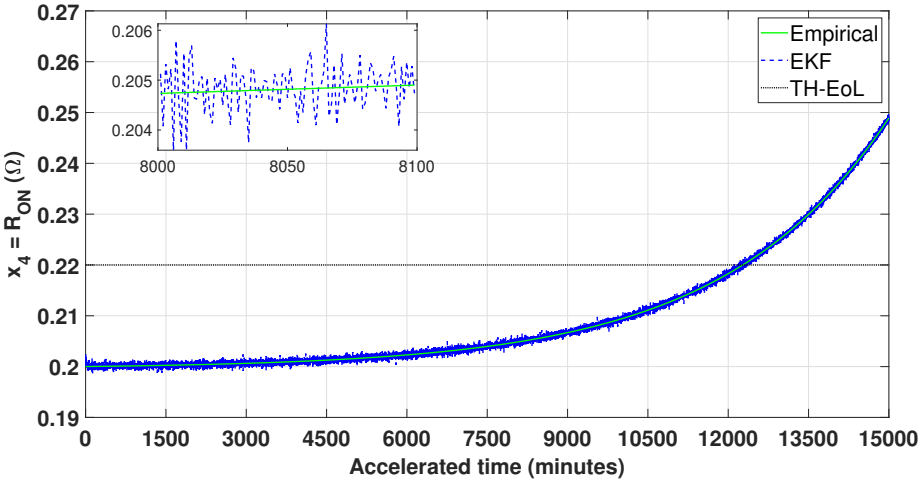

Figure 3.3: $\hat{\mathbf{x}}_4$ versus empirical degradation in scenario 1

The EKF estimates the states and the parameters, then the RLS filter is employed to estimate the parameters of the polynomial degradation model and predict the future behavior until reaching the TH.

Figures 3.4 illustrates the evolution of the degradation prediction based on the existing estimated critical parameter R_{ON}. It is clearly shown that the predicted degradation converges with more available observations. In other words, it took around 8000 accelerated minutes in order to forecast the EoL with high precision. Thus, we conclude that this approach can forecast the RUL to a relatively short time before the real EoL of the system, based on the obtained results. It is worth mentioning that the prediction uncertainties increase with the presence of the considered noises.
Table 3.1 shows the predicted EoL using the classical approach at the four illustrated measurements.

Table 3.1: RLS-based EoL prediction in scenario 1

Online measurements (minutes)	2000	4000	6000	8000
$\tilde{\text{EoL}}$ (minutes)	3274	6781	10625	12029

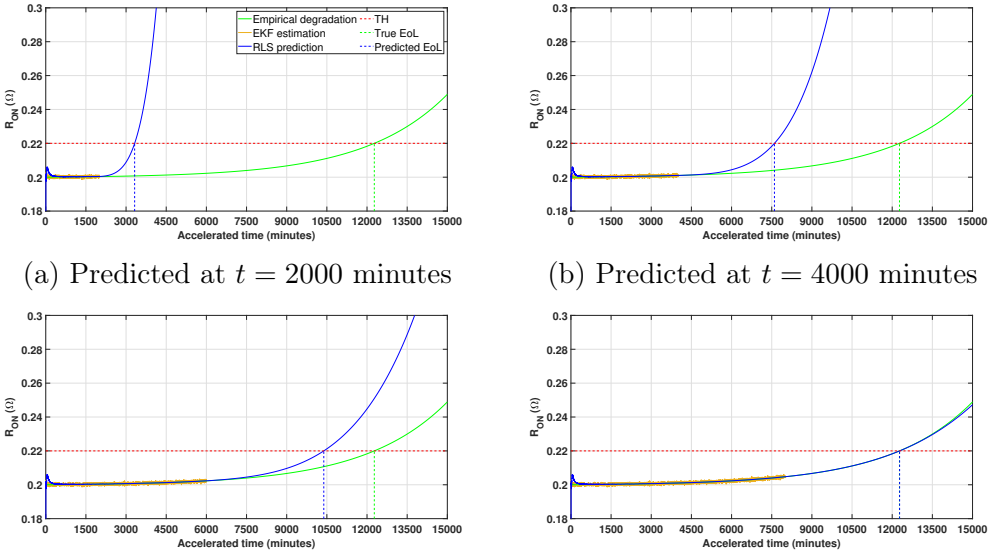

(a) Predicted at $t = 2000$ minutes

(b) Predicted at $t = 4000$ minutes

(c) Predicted at $t = 6000$ minutes

(d) Predicted at $t = 8000$ minutes

Figure 3.4: Degradation and EoL prediction of R_{ON} using RLS filter

RUL forecasting using the linear EoL-RUL approach

Figure 3.5 illustrates the predicted RUL in scenario 1, compared to the empirical RUL until the EoL. It is shown that the predicted RUL in scenario 1,

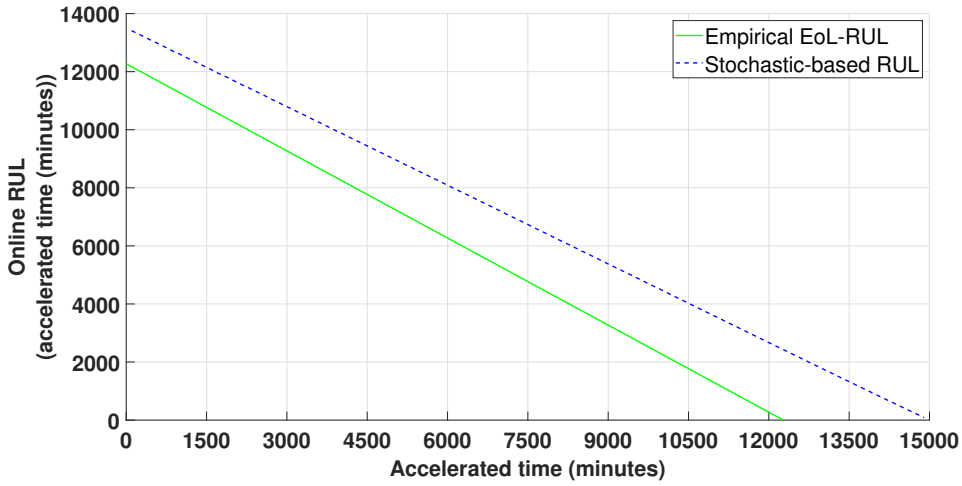

Figure 3.5: $\tilde{\mathrm{RUL}}$ versus empirical RUL in scenario 1

diverges using the linear EoL-RUL approach. It can be explained due to the initialized expected EoL that can reduce the prediction accuracy.
Therefore, Table 3.2 shows the online RUL forecasting of both approaches at four measurements, for illustration purposes. Consequently, the RLS-based

Table 3.2: RUL forecasting comparison in scenario 1

Measurement time (minutes)	True RUL (minutes)	RLS-based $\tilde{\text{RUL}}$ (minutes)	Proposed $\tilde{\text{RUL}}$ (minutes)
2000	10272	1274	11698.4
4000	8272	2781	9892.6
6000	6272	4625	8085.48
8000	4272	4029	6281.45

degradation prediction approach for RUL forecasting has shown inaccurate results compared to the proposed forecasting based on the linear EoL-RUL approach.

3.7.2 Scenario 2

The nonlinear ESR_o-augmented state-space model[3] is:

$$\left[\begin{array}{c|c} \mathbf{A}^{\text{S2}}(2.39\text{a}) & \mathbf{B}^{\text{S2}}(2.39\text{b}) \\ \hline \mathbf{C}^{\text{S2}}(2.39\text{c}) & \mathbf{D}^{\text{S2}}(2.39\text{d}) \end{array}\right]. \tag{3.27}$$

Unlike scenario 1, the state-space matrices of scenario 2 are all parameter-dependent, and the observability matrix is computed based on the Jacobian couple $(\mathbf{J_A}^{\text{S2}}, \mathbf{J_C}^{\text{S2}})$ as:

$$\mathbf{J_A}^{\text{S2}}(t) = \begin{bmatrix} -113636 & -1136.36 & 0 & 0 \\ 622.665 & \boxed{a_{22}^{\text{S2}}(t)} & -4452.054 & -4452.054\boxed{x_2(t)} \\ 0 & 130 & 0 & 0 \\ 0 & 0 & 0 & 1 \end{bmatrix}, \tag{3.28a}$$

$$\mathbf{J_C}^{\text{S2}}(t) = \begin{bmatrix} -9.09 & 0.909 & 0 & 0 \\ 0 & 0.65\boxed{\text{ESR}(t)} & 1 & 0.65\boxed{x_2(t)}, \end{bmatrix}. \tag{3.28b}$$

[3]The model is discretized during the estimation and the forecasting process.

where $a_{22}^{S2} = -4452.054\boxed{\text{ESR}(t)} - 575.9$.
Thus, the observability matrix at the initial condition is obtained as follows:

$$\mathcal{O}^{S2}(\mathbf{J_A}^{S2}, \mathbf{J_C}^{S2}) = \begin{bmatrix} -9.090909 & 0.90909 & 0 & 0 \\ 0 & 0.052 & 1 & -2.5 \\ -0.931904 & 0.972644 & -0.085055 & -12.758501 \\ 0.00026 & 0.053605 & 0.995298 & -3.205352 \\ -0.091261 & 0.96253 & -0.171341 & -25.701804 \\ 0.000295 & 0.055166 & 0.990455 & -3.931859 \\ -0.004729 & 0.944938 & -0.256276 & -38.442581 \\ 0.000306 & 0.056685 & 0.985475 & -4.678952 \end{bmatrix}. \tag{3.29}$$

Results of the JESP using the EKF

Similar to scenario 1, the same approaches have been investigated for states and parameters estimation, in scenario 2. Figure 3.6a, 3.6b, and 3.6c illustrate the estimated states.
The performance of the EKF for JESP in states estimation have proven its ability for both scenarios. Hence, Figure 3.7 illustrates the estimated augmented parameter ESR_o, compared to the empirical degradation that also shows an accurate parameter estimation.

RLS-based degradation prediction using known models of the failure precursors

According to the aforementioned strategy as explained in scenario 1, the RLS filter has been employed to predict the parameters of the polynomial degradation model of the failure precursor based on the estimated parameter using the EKF for JESP. The empirical 4-degree polynomial degradation model of the ESR increase that is equivalent to the exponential model in (2.31), is given in (3.30) with R-square = 1.

$$\begin{aligned} \Delta\text{ESR}_{\text{poly}}(t) \approx -1.106.10^{-18}t^4 + 5.047.10^{-14}t^3 - 7.086.10^{-10}t^2 \\ +7.171.10^{-6}t + 0.0005673. \end{aligned} \tag{3.30}$$

Nevertheless, we propose a linear model with only two unknown parameters for the ESR increase, since the double exponential model can be fit with such model with R-square = 0.9952. The reasons behind this proposition are referred to the investigation a model with reduced unknown parameters with the RLS filter prediction. In other words, the results of scenario 1 with the 5-degree polynomial model were not accurate for the degradation

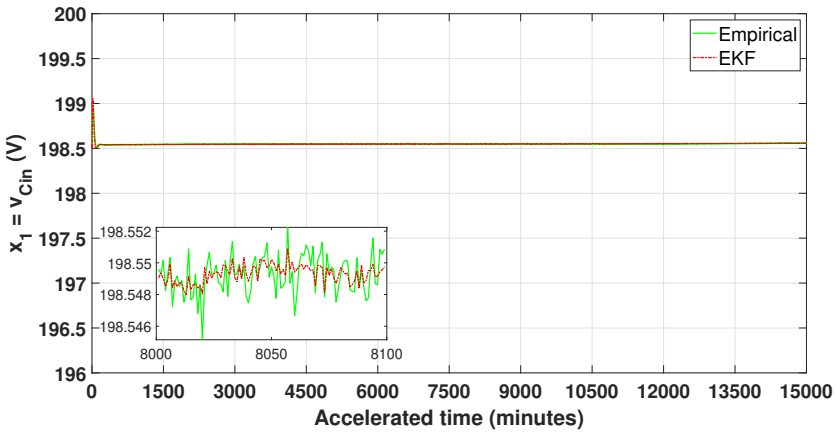

(a) $\hat{\mathbf{x}}_1$ versus empirical degradation in scenario 2

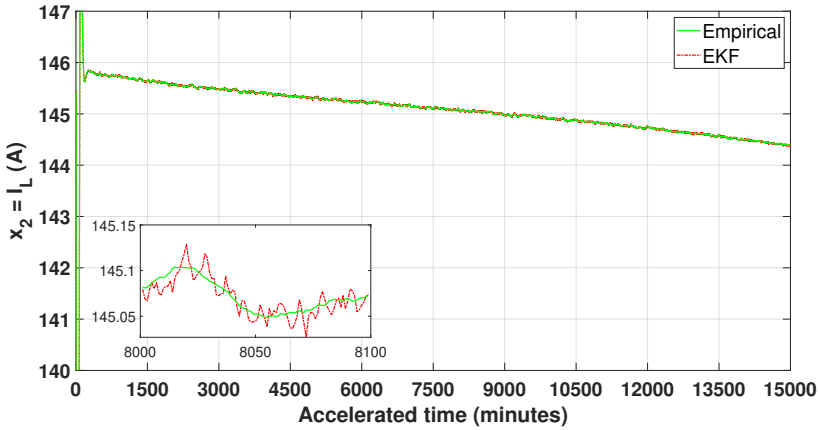

(b) $\hat{\mathbf{x}}_2$ versus empirical degradation in scenario 2

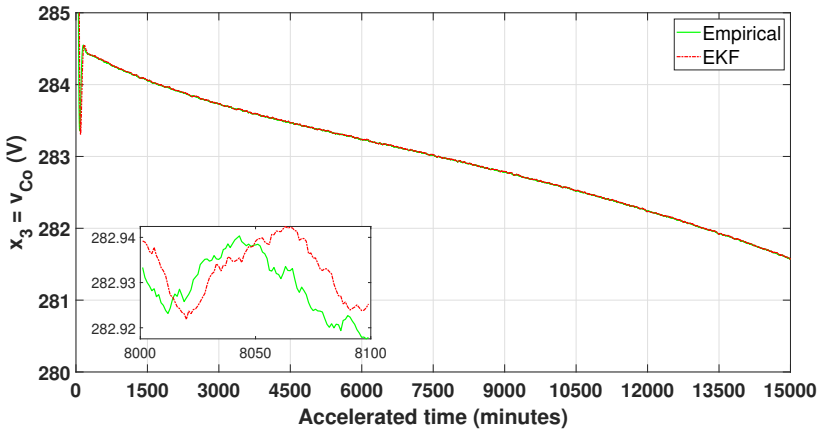

(c) $\hat{\mathbf{x}}_3$ versus empirical degradation in scenario 2

Figure 3.6: The estimated states versus the corresponding empirical degradation in scenario 2

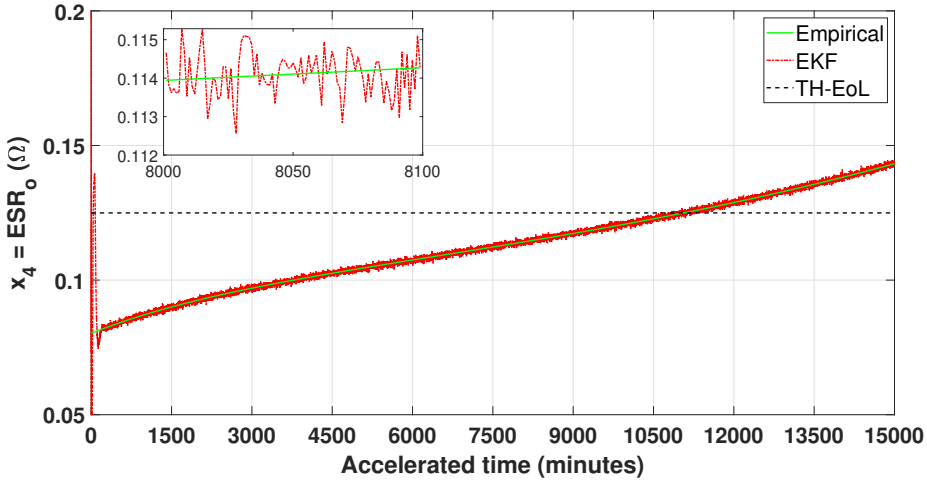

Figure 3.7: $\hat{\mathbf{x}}_4$ versus empirical degradation in scenario 2

prediction and affected the RUL forecasting. Thus, this can be repeated in this scenario, whereas we intend to reduce the computations with keeping a high R-square. Therefore, we propose to estimate the following linear model of the ESR variation as given in (3.31).

$$\Delta \mathrm{ESR}_{\mathrm{linear}}(t) \approx p_1 t + p_2, \tag{3.31}$$

where p_1 and p_2 are the unknown parameters that will be estimated using an RLS filter, and the EKF provides the estimated value of $\hat{\mathrm{ESR}}_{\mathrm{o}}$.
Thus, Figure 3.8 illustrates the predicted degradation until the TH of the $\mathrm{ESR}_{\mathrm{o}}$.
Due to the fact that the double-exponential evolution of the $\mathrm{ESR}_{\mathrm{o}}$ is similar to a linear evolution, the prediction results using the RLS filter have shown better results in scenario 2 than in scenario 1.
Table 3.3 shows the predicted EoL using the classical approach at the four illustrated measurements.

Table 3.3: RLS-based EoL prediction in scenario 2

Online measurements (minutes)	2000	4000	6000	8000
$\tilde{\mathrm{EoL}}$ (minutes)	11619	9508	10101	10641

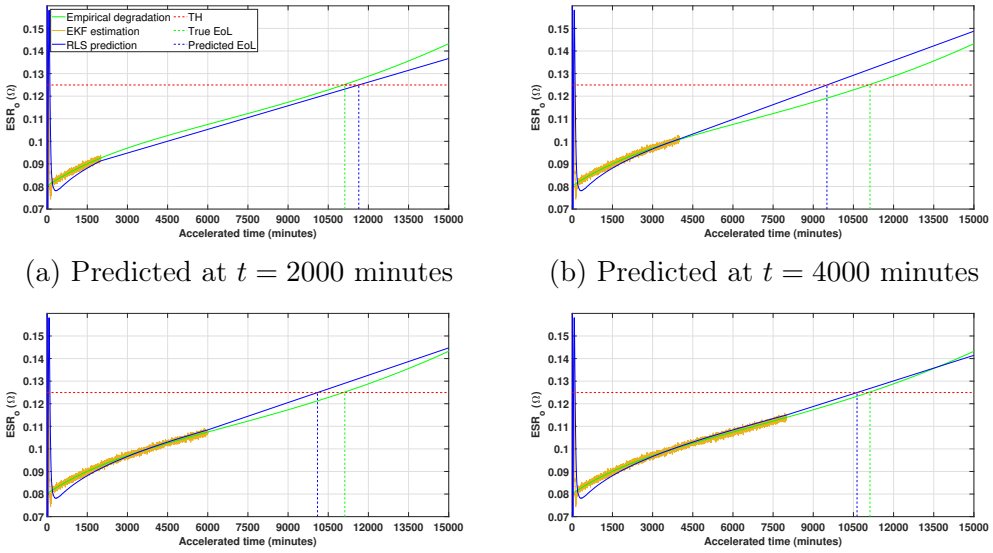

(a) Predicted at $t = 2000$ minutes

(b) Predicted at $t = 4000$ minutes

(c) Predicted at $t = 6000$ minutes

(d) Predicted at $t = 8000$ minutes

Figure 3.8: Degradation and EoL prediction of ESR_o using RLS filter

RUL forecasting using the linear EoL-RUL approach

Figure 3.9 shows the predicted RUL.

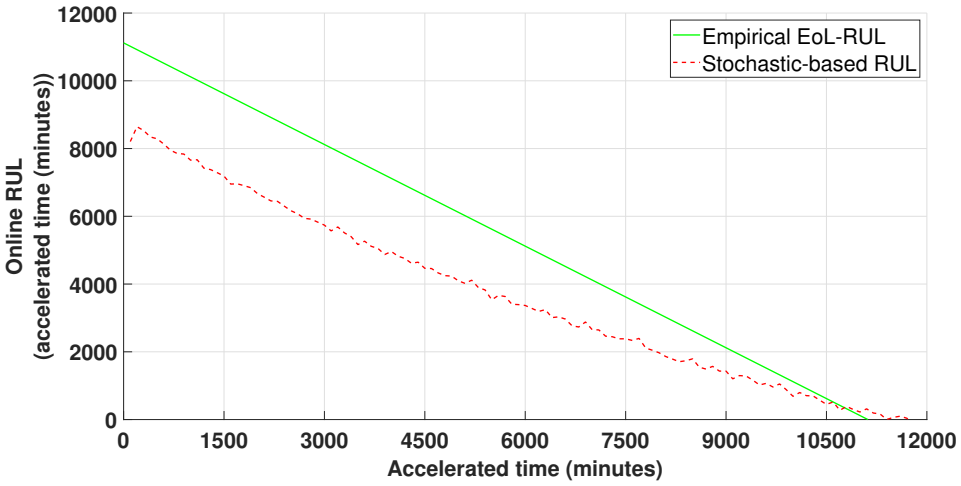

Figure 3.9: $\tilde{\mathrm{RUL}}$ versus empirical RUL in scenario 2

Therefore, Table 3.4 shows the online RUL forecasting of both approaches at

four measurements, for illustration purposes.

Table 3.4: RUL forecasting comparison in scenario 2

Measurement time (minutes)	True RUL (minutes)	RLS-based $\tilde{\text{RUL}}$ (minutes)	Proposed $\tilde{\text{RUL}}$ (minutes)
2000	9119	9619	6183.63
4000	7119	5508	4455.74
6000	5119	4101	2914.94
8000	3119	2641	1524.9

Unlike scenario 1, the RLS-based approach has shown better RUL forecasting than the proposed approach with respect to the empirical RUL, due to the reduced number of the unknown parameters of the proposed degradation model.

DKF for switched-systems in scenario 2

One of the main objectives of this chapter is to examine various approaches in order to define a roadmap for structured PHM practices. Thus, we proposed to investigate a DKF for states estimation of the proposed switched-system without the estimation of any critical component.
The rate of change of the estimated alternating states is not remarkable as seen in the illustrated results.

3.7.3 Scenario 3

Two parameters are augmented to the states vector in scenario 3 as shown in (2.35c). Thus, the nonlinear continuous-time augmented state-space model[4] of scenario 3 is represented in (3.32) as:

$$\left[\begin{array}{c|c} \mathbf{A}^{\text{S3}}(2.40\text{a}) & \mathbf{B}^{\text{S3}}(2.40\text{b}) \\ \hline \mathbf{C}^{\text{S3}}(2.40\text{c}) & \mathbf{D}^{\text{S3}}(2.40\text{d}) \end{array}\right]. \tag{3.32}$$

[4]The model is discretized during the estimation and the forecasting process.

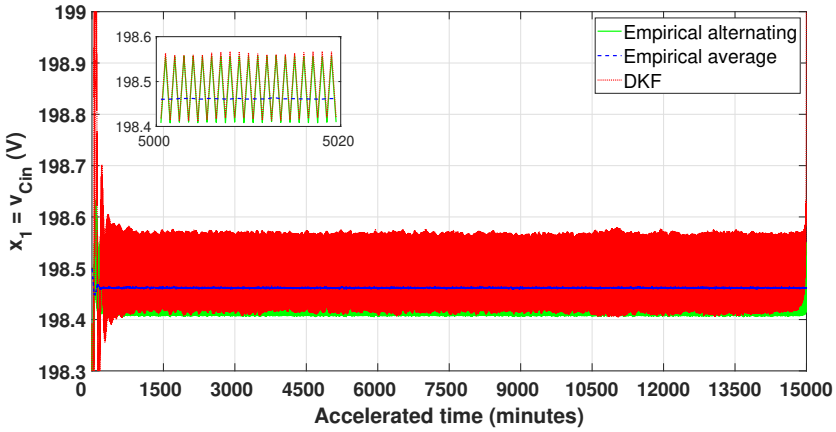

(a) DKF-based $\hat{\mathbf{x}}_1$ versus empirical degradation and EKF estimation in scenario 2

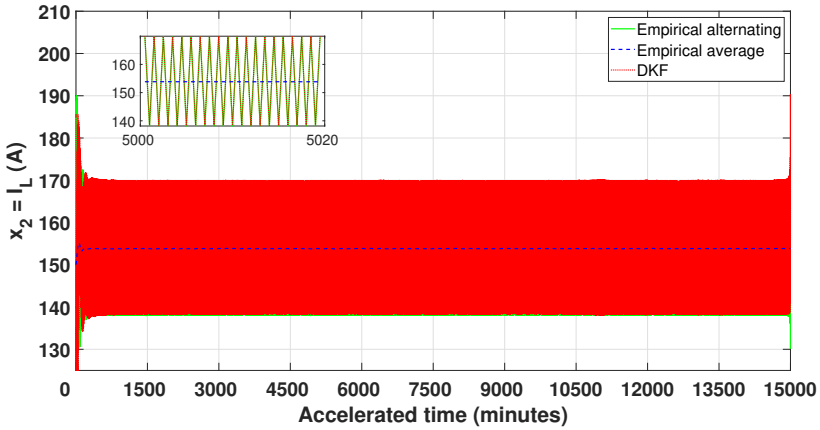

(b) DKF-based $\hat{\mathbf{x}}_2$ versus empirical degradation and EKF estimation in scenario 2

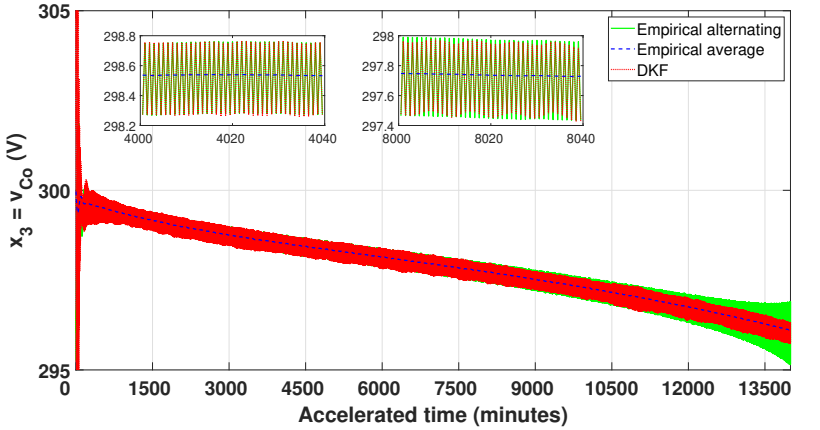

(c) DKF-based $\hat{\mathbf{x}}_3$ versus empirical degradation and EKF estimation in scenario 2

Figure 3.10: DKF-based estimated states versus the corresponding empirical degradation and the EKF in scenario 2

Moreover, the Jacobian of the couple $(\mathbf{J_A}^{S3}, \mathbf{J_C}^{S3})$ becomes:

$$\mathbf{J_A}^{S3}(t) = \begin{bmatrix} -113636 & -1136.36 & 0 & 0 & 0 \\ 622.665 & \boxed{a_{22}^{sys}(t)} & -4452.04 & -4452.04\boxed{x_2(t)} & -2397.26\boxed{x_2(t)} \\ 0 & 130 & 0 & 0 & 0 \\ 0 & 0 & 0 & 1 & 0 \\ 0 & 0 & 0 & 0 & 1 \end{bmatrix}, \tag{3.33a}$$

$$\mathbf{J_C}^{S3}(t) = \begin{bmatrix} -9.09 & 0.909 & 0 & 0 & 0 \\ 0 & 0.65\boxed{\text{ESR}(t)} & 1 & 0.65\boxed{x_2(t)} & 0 \end{bmatrix}. \tag{3.33b}$$

Therefore, the full-rank observability matrix at $k = 1$, as an example, is obtained as:

$$\mathcal{O}^{S3} = \begin{bmatrix} -9.0909 & 0.90909 & 0 & 0 & 0 \\ 0 & 0.052 & 1 & 97.5 & 0 \\ -0.9319 & 0.97264 & -0.08505 & -12.75850 & -6.86996 \\ 0.0002 & 0.05360 & 0.99529 & 96.79664 & -0.37977 \\ -0.0912 & 0.96253 & -0.17134 & -25.70180 & -13.83943 \\ 0.0002 & 0.05516 & 0.99045 & 96.07214 & -0.77094 \\ -0.0047 & 0.94493 & -0.25627 & -38.44258 & -20.69985 \\ 0.0003 & 0.05668 & 0.98547 & 95.32704 & -1.17320 \\ 0.0040 & 0.92668 & -0.33960 & -50.94242 & -27.43053 \\ 0.0003 & 0.05816 & 0.98036 & 94.56192 & -1.58623 \end{bmatrix} \tag{3.34}$$

Results of the JESP using the EKF

Figures 3.11a, 3.11b, 3.11c, 3.12a, and 3.12b illustrate the estimated states and parameters of scenario 3 that simulate a case of multiple-components degradation which increases the mutual effects on a system-level.
Based on the estimated parameters in scenario 3 using the EKF for JESP, the RUL forecasting has not been assessed due to the estimation errors that will be reflected negatively on the RUL forecasting as seen in scenario 1 and 2. For these reasons, we propose to improve this approach but guaranteeing a reliable parameters estimation in order to improve the efficiency of the RUL forecasting. A proposition is explained in the following part to be investigated in the following chapters concerning the assessment of the stochastic-based prognostics.

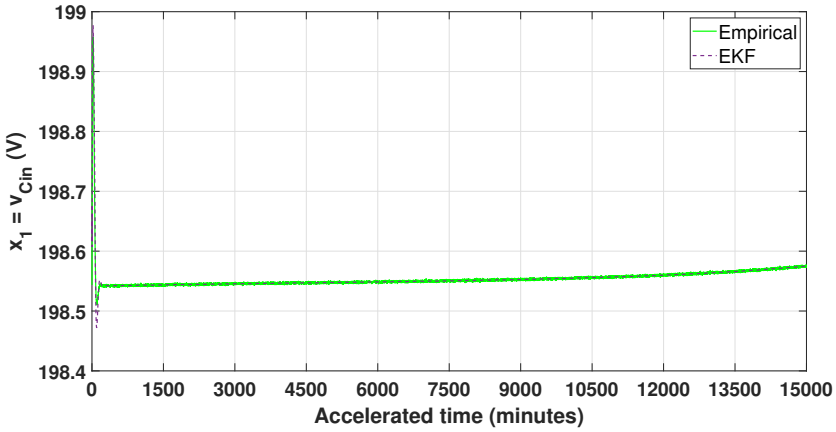

(a) $\hat{\mathbf{x}}_1$ versus empirical degradation in scenario 3

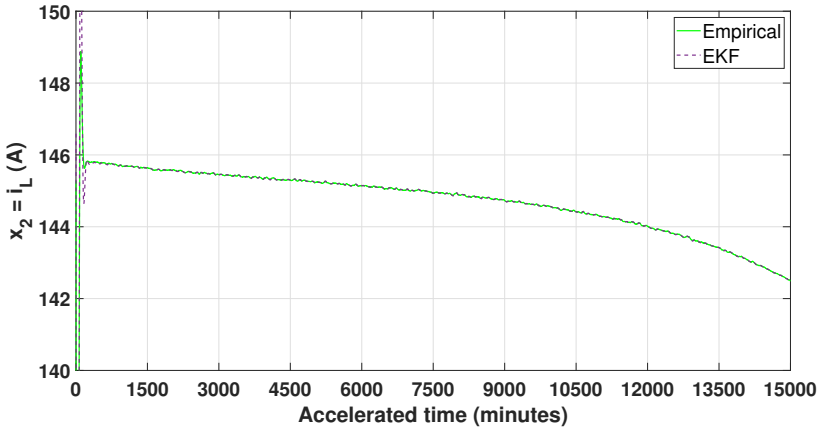

(b) $\hat{\mathbf{x}}_2$ versus empirical degradation in scenario 3

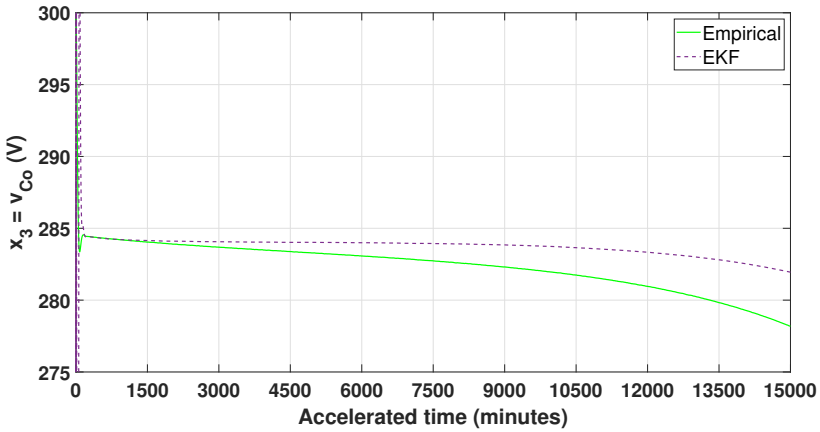

(c) $\hat{\mathbf{x}}_3$ versus empirical degradation in scenario 3

Figure 3.11: The estimated states versus the corresponding empirical degradation in scenario 3

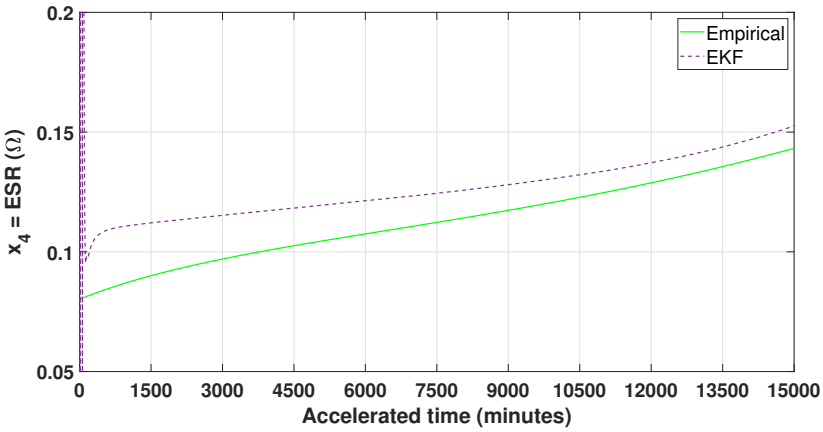

(a) $\hat{\mathbf{x}}_4$ versus empirical degradation in scenario 3

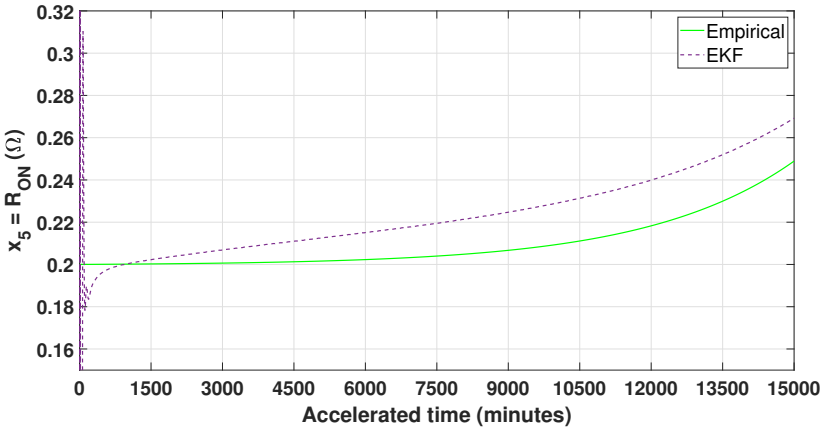

(b) $\hat{\mathbf{x}}_5$ versus empirical degradation in scenario 3

Figure 3.12: The estimated parameters versus the corresponding empirical degradation in scenario 3

3.7.4 Assessment of the proposed approaches

In broad, the JESP using the augmented EKF has shown accurate estimation results for the investigated scenarios. Thus, the RA in (3.35) can assess the estimation and the prediction accuracy.

$$\text{RA} = \frac{\mathbf{x} - |\mathbf{x} - \hat{\mathbf{x}}|}{\mathbf{x}} \times 100. \tag{3.35}$$

Table 3.5 illustrates the average RA for the estimated states and parameters.

Table 3.5: The average RA of the JESP by EKF of the investigated scenarios

States and Parameters	RA^{S1} %	RA^{S2} %	RA^{S3} %
$\hat{\mathbf{x}}_1$	99.99999	99.99991	99.99997
$\hat{\mathbf{x}}_2$	99.99996	99.99722	99.99670
$\hat{\mathbf{x}}_3$	99.99995	99.98934	95.81004
$\hat{\mathbf{x}}_4$	99.99089	99.89643	90.93163
$\hat{\mathbf{x}}_5$	-	-	93.82725

The average RA of the first two scenarios show accurate and robust JESP, however the parameters estimation in scenario 3 have been affected due to the multiple degradation integration and the average RA has been decreased up to 90%.
Table 3.6 shows the average RA of the RUL forecasting through the proposed linear EoL-RUL approach. The average RA has been calculated until 80% of the actual EoL in order to provide the last 20% of the EoL as a safety margin.

Table 3.6: Average RA of RUL forecasting of the investigated scenarios for 80% of the actual EoL

$\tilde{\text{RUL}}$	RUL^{S1}	RUL^{S2}
RA %	69.6655	61.4503

Therefore, the three simulated scenarios are based on the EKF for JESP and

dual-observer approach for external features assessment, in addition to the classical RLS-based degradation and EoL prediction with known degradation behaviors against the proposed linear EoL-RUL approach.

According to the obtained results, the EKF has shown accurate and reliable results in the first two scenarios, where the estimation accuracy has decreases by around 10% for the third scenario, specifically for the parameters. The dual-observer approach has been examined and can be further optimized and developed for prognostics in future work, since our intention is to reduce all the time and computational burdens for a better estimation-prediction performance.

Moreover, the classical approach of RUL that predict the degradation and therefore the EoL, is limited to the knowledge of the degradation models that necessitate a parameter estimation filter such as the RLS filter in order to predict their behaviors. The polynomial degradation model as seen in scenario 1, has not provided a long-term EoL prediction prior to the true EoL. This condition is explained due to the provided or observed information in addition to the uncertainties in measuring, estimating, modeling, etc. However, we examined a linear model in scenario 2 that is approximated of the 4-degree true polynomial model of the ESR degradation, in order to reduce the computations. Eventually, the prediction efficiency is more efficient that scenario 1.

On the other hand, the proposed linear EoL-RUL approach does not depend on the knowledge of the degradation behavior, yet it is limited to an EoL expectation based on previous experiences from the manufacturers, users, etc. The forecasting results in general have shown a difference gap compared to the true RUL, whether too pessimistic or optimistic.

To sum up, the stochastic-based approaches require a development in the uncertainty management for RUL forecasting which is mainly based on the online degradation estimation in this case. The major drawback in such approaches is that they deal with the future events with strict decisions. For all these reasons, and following the objectives of this thesis towards generalized system-level prognostics, we intend to bound the estimated parameters using zonotopic approaches in order to overcome the faced issue in scenario 3 along with resulting a bounded RUL. Indirect bounding of the predicted RUL by propagating bounded parameters will increase the efficiency and provide flexible forecasting that can be assessed using prognostics metrics for post-prognosis decisions. Moreover, it is also essential to examine the estimation-

prediction performance with unknown-but-bounded noises and uncertainties rather than the Gaussian distribution.

3.8 Conclusions

This chapter highlights the application of the proposed model-based PHM structure for RUL forecasting based on stochastic estimation and prediction approaches. The aim of investigating the existing RUL forecasting approach with known degradation models along with the proposed linear EoL-RUL approach, is to endorse the advantages of each approach and contribute to the development of a generalized RUL forecasting approach based on the examined limitations. The RLS-based degradation and EoL prediction depends on known degradation models and has shown its availability to a relatively short time before the real EoL occurs as seen in scenario 1. However, it has shown better results than the proposed EoL-RUL approach in scenario 2 due to the linear degradation model adopted. In other words, both approaches are limited by whether a required knowledge of the degradation models or a rough EoL expectations from previous experiments. Moreover, throughout the roadmap towards the generalization of a structured PHM, we intended to investigate a nonlinear system with focusing on the estimation of the critical components unlike most of the existing system-level approaches that emphasize on the external features only. The JESP with Gaussian noises and uncertainties reduces the computational time and effort in comparison with the dual-observer approach as seen throughout this chapter, yet its efficiency for parameters estimation has decreased with multiple-degradation. Consequently, both RUL forecasting approaches are limited and require improvements for a guaranteed reliability. Therefore, we propose to indirectly bound the predicted RUL by employing a bounded JESP in a zonotopic framework merged with the EKF considering unknown-but-bounded noises. This approach provides less computations and guaranteed estimation with optimized bounded RUL forecasting unlike the existing statistical bounds. The following chapter contributes to the improved PHM approach towards more reliable system-level prognostics with our proposed linear EoL-RUL forecasting technique.

This page is intentionally left blank

CHAPTER 4

Zonotopic Extended Kalman Filter Approach for PHM with Bounded RUL Forecasting

Contents

4.1 Introduction

The core rule of the proposed model-based PHM approach states that the RUL forecasting strictly depends on the estimated varying parameters. Despite the fact that the EKF has shown accurate JESP, the proposed RUL forecasting was supposed to prove higher reliability than the obtained results. The reason refers to the pessimistic condition of the EoL assumption or to the knowledge of the exact degradation models, as seen in Chapter 3. The main concern is not linked to the parameter estimation accuracy as much as the flexibility of the RUL technique under some constraints. Therefore, based on the methodology assessment made in Section 3.8, we proposed to bound the predicted RUL using the linear EoL-RUL approach instead of extending the complexity of the polynomial system that opposes the fast estimation-prediction constraint. In consequence, we aim to merge the advantages of the EKF for JESP with the deterministic zonotopic approach in a ZEKF framework for JESP that will result in bounded states and parameters. Hence, the proposed RUL forecasting approach is examined with propagated zonotopic sets. Additionally, the online Jacobian approximation of the nonlinear system attributed to the stochastic approach has been improved in this chapter for the sake of endorsing more modern-engineering applications rather than the reliability-related field of study. In other words, we propose an LPV transformation of the nonlinear model that copes with reduced computations due to a proposed LMI-based optimization of the ZEKF observer that will be detailed throughout this chapter with proven improved performance.

Unlike stochastic observers, the uncertainties, the perturbations, and the measurement noises are modeled as bounded convex sets in a zonotopic scheme (Schweppe 1968). The complexity arises from the geometrical sets approximation (V. Le et al. 2013a; Merhy 2019). The sets can be represented with different degrees of complexity and approximations depending on their utilization, i.e. *polytopes* (such as box and parallelotopes) (E. Walter and Piet-Lahanier 1989; Vicino and Zappa 1996; Vicenç Puig, Saludes, and Joseba Quevedo 2003) could show good estimation results with linear models, *ellipsoids* (Schweppe 1968; Witsenhausen 1968; Bertsekas and Rhodes 1971; Durieu, É. Walter, and Polyak 2001; Becis-Aubry and Ramdani 2012) are

This chapter is based on the following publications: (Al-Mohamad, V. Puig, and Hoblos 2021b; Al-Mohamad, V. Puig, and Hoblos 2021c; Al-Mohamad, V. Puig, and Hoblos 2020).

simply implemented, whatsoever their lack of flexibility might lead to pessimistic estimation, and *zonotopes* (V. Puig, Cugueró, and J. Quevedo 2001; Combastel 2003; T. Alamo, Bravo, and Camacho 2005; T. Alamo, Bravo, Redondo, et al. 2008) have become extensively applied for the sake of their simple arithmetic operations, in addition to their flexibility compared to the other geometrical sets (V. Le et al. 2013a; Merhy 2019). Additionally, the author in (Kühn 1998) showed more precise results due to the reduced wrapping effects in a zonotopic estimation. The geometrical shape of zonotopes allows the reduction of the computational complexity while propagating the estimated sets of states and parameters, by employing simple calculations (Y. Wang, Vicenç Puig, and Cembrano 2018; S. E. D. Le et al. 2013; M. Pourasghar, V. Puig, and Ocampo-Martinez 2016; Masoud Pourasghar et al. 2019; V. Le et al. 2013b). Thus, the authors in (T. Alamo, Bravo, and Camacho 2005) proposed possible solutions for the sake of minimizing the zonotopes, such as *segments* and *volume minimization* techniques. The *segments minimization method* is mainly based on minimizing the $F-$radius of the estimated zonotope, which provides an improved accuracy and reduced vertices in the zonotopic sets. The *volume minimization method* is solved by a convex optimization problem, and showed improved estimation, yet its complexity could lead to increased computations and narrow zonotopic sets. Moreover, the *$P-$radius minimization* (proposed in (Vu Tuan Hieu Le et al. 2013)) is an efficient technique that guarantees the zonotopic inclusion and can be extended to multi-output systems. The author in (Combastel 2003) introduced a reduction operator which limits the maximum number of columns of the generator matrix of the zonotopic sets, as explained in Property A.2.8. Thus, it was improved in (Combastel 2005) with a weighting strictly positive definite matrix that can benefit from the same advantages of the previously mentioned $P-$radius minimization technique, when applied to the F_W-radius as defined in A.2.19 in an LMI framework (Combastel 2015).

According to the fact that the RUL forecasting is based on critical parameters estimation, the PHM approach is therefore based on the utilized observer. For this purpose, we propose to optimally tune the observer in an LMI framework for guaranteed JESP. Additionally, a polytopic LPV is solved offline with the LMI-based optimization for the sake of an improved real-time estimation and prediction, that can be applied to any nonlinear system with bounded parameters.

This chapter is structured as follows. Section 4.2 presents the problem set-up of the ZEKF-based approach in an LPV framework. Section 4.3 is dedicated for the ZEKF observer design with an LMI-based optimal tuning. Thus, the

improved zonotopic RUL forecasting approach is determined in Section 4.4. Moreover, the algorithm of the ZEKF-based JESP and bounded RUL forecasting is detailed in Section 4.5. The results of the adopted case study are shown in Section 4.6. Finally, the conclusions are drawn in Section 4.7.

4.2 PHM Problem Formulation in a ZEKF Framework

Based on the assessment of the previous stochastic PHM approach, we propose to increase the reliability of the linear EoL-RUL approach for RUL forecasting by indirectly bounding the prediction through extending the EKF for JESP to a zonotopic framework. Thus, by emphasizing on the reliability concerns based on the aforementioned flaws and limitations which have had been faced with the stochastic-based PHM approach, a few major upgrades have been introduced to the ZEKF-based PHM approach. The Jacobian representation of the dynamical model has been transformed into an LPV representation which will be explained in Section 4.2.1. Thus, unknown-but-bounded noises and uncertainties have been considering instead of the Gaussian distribution. Moreover, an offline LMI-based optimization problem has been integrated due to the presence of bounded parameters that can provide robust observer functionality and reduce the processing time. Finally, only the zonotopic linear EoL-RUL approach is examined due to the lower obtained overall efficiency with the RLS-based that requires the knowledge of the degradation models. Figure 4.1 highlights the proposed PHM methodology with the current upgrades and adaptations.

1. *System modeling:* The nonlinear modeling phase has been carried out in Chapter 2, where we adopted the augmented representation of the model. Hence, a polytopic LPV representation has been employed for an accurate model approximation with the bounding box approach that considers the bounds of the varying parameters. The main advantage of such representation is related to the following LMI-based optimization problem that will be solved offline for the sake of real-time application, in addition to the possible extensions of LPV-based models towards more engineering applications.

2. *ZEKF for JESP:* The second phase is the core of the model-based PHM. The ZEKF observer has been adopted due to its post-effect on the RUL forecasting. As the EKF has been proved in many applications, and the zonotopes require simple implementation, they are merged in a

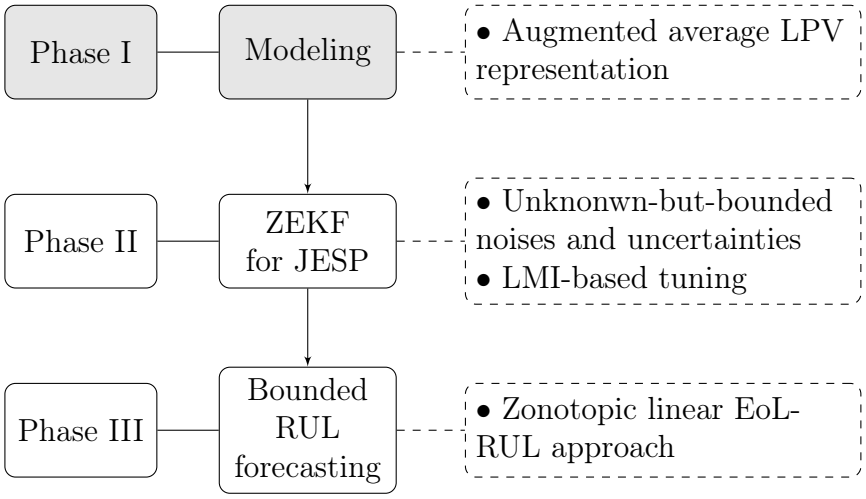

Figure 4.1: ZEKF-based PHM

ZEKF observer (Combastel 2015). The aim is to estimate zonotopic states and parameters, where the bounds of the estimated zonotopic varying parameters are retrieved at each time instant and provided as inputs of the RUL forecasting algorithm. Moreover, the unknown-but-bounded noises and uncertainties are considered in this approach which has been optimally tuned based on an LMI approach for robust stability and expressed in a polytopic LPV representation.

3. *Bounded RUL forecasting:* The third phase strongly depends on the previously estimated zonotopic parameters. The linear EoL-RUL approach is now bounded due to the propagated zonotopic parameters.

4.2.1 Problem set-up in an LPV framework

The previously-derived augmented model characterizes most of the real dynamical applications in terms of nonlinearities. Additionally, the nonobservable model in its augmented form can not accomplish its role for degradation estimation in the following phase of the proposed PHM structure. Thus, the observability challenge in the three scenarios highlights the key issue of the parameter augmentation that necessitates a model transformation in order to overcome the null rows as demonstrated in Chapter 2. Therefore, nonlinear embedding or other approximation techniques can be applied in order to linearize the model and solve the aforementioned issues. A high-accuracy approximation technique should be employed in order to successfully vali-

date the model representation in the presence of perturbations, noises and uncertainties to reach the goal of an accurate estimation. By gathering the information from all the previously-explained barriers and constraints in the previous chapters, it has been observed that the online Jacobian linearization requires relatively high computations that can be improved by adopting different representations.

Moreover, the varying parameters characterize the critical degraded components of the system which can be described as the operating points. To deal with the variations of the operating points, the gain-scheduling technique has become popular for industrial control applications due to the interpolation of local LTI models in an LPV framework (Rugh 1991). Despite the fact that LPV models are widely used in many engineering applications such as gain-scheduling control (Packard 1994; Shamma and Athans 1992), and fault-tolerant control (Tudón-Martínez et al. 2013; O. Sename, Tudon-Martinez, and S. Fergani 2013), etc., there is not a single structured strategy to transform a nonlinear system into an LPV (Tóth 2010). Additionally, the LPV identification is mainly framed by the nonlinear augmented model which is the starting point of the transformation process, following our proposition of a standardized PHM architecture. Thus, the state-space representation of the LPV is adopted in this thesis rather than input-output, or series-expansion methods thanks to its appreciation in the automatic control applications. Another fact that characterizes the transformation process, is that multi-varying-parameters with different types of noises parametrize the model that can be generalized to non-exceptional case study. Next, the model estimation is a crucial criterion that should be guaranteed in the LPV transformation.

The LPV modeling is inspired by the LTI representation with more flexibility in noise types integration in the LPV and an extension of the Linear Time-Variant (LTV) models (Tóth 2010). The state-space representation of MIMO LPV models can be categorized under different approaches. The *full state measurement approaches* assume the the states are measurable in an Linear Fractional Transformation (LFT) framework, and mainly applicable with linear regression and stochastic approaches with Gaussian noises using RLS filters for the estimation (Nemani, Ravikanth, and B. A. Bamieh 1995; M. C. Mazzaro, Movsichoff, and Pena 1999). The *gradient methods* are nonlinear-optimization-based techniques that are formulated for the estimation of the varying parameters (L. H. Lee and Poolla 1996; Verdult, Ljung, and Verhaegen 2002). Moreover, classical gain-scheduling techniques applied in intuitive manners are categorized under *multiple model approaches*. Some methods of these approaches transform the local LTI models into canoni-

cal state-space forms for the interpolation computation. Other methods are dedicated to reduce the LTI models before interpolation, LTI discretization (Groot Wassink et al. 2005; Yung 2001; Steinbuch, van de Molengraft, and van der Voort 2003), and pole location (Paijmans et al. 2008). Moreover, the authors in (Sznaier, C. Mazzaro, and Inanc 2000) proposed an LPV representation with known noise model with a moving average structure, and the estimation of the LTI models is formulated as an *LMI-based optimization problem*. Thus, the *global subspace techniques* are created based on the LTI multi-variable output-error state-space algorithms where the state evolution and the state-space matrices are being estimated (Verhaegen 1994). Moreover, the *observer-based grey-box techniques* identify the LPV transformation based on a parameter estimation problem of known nonlinear models (Gaspar, Szabo, and Bokor 2005; Gaspar, Szabo, and Bokor 2007).

Heretofore, the possible methods to transform the nonlinear augmented model into an LPV representation have been reviewed above. Thus, it is remarkable that the observer-based grey-box techniques can be employed in this case study, since they are tailored to the same augmented model representation of nonlinear models, similar to what has been accomplished in Chapter 3. However, such techniques along with the full-state measurement approaches depend on the knowledge of the noise models that burden our proposition of dealing with unknown-but-bounded noises as will be explained henceforth. Moreover, the remaining techniques require high computational effort which does not match the real-time estimation-prediction requirement for online prognostics.

Furthermore, Considering that the nonobservability issue is located and identified, we intended to apply substitution-based transformation approach by interchanging among the coefficients of the state-space matrices to reshape them. This intuitive transformation could be applied to nonlinear systems, whereas in this case-study, the system remains nonobservable after testing due to the overall combination of elements.

In an optimization-based trial, we intended to extract the time-varying degradation parameters from the nonlinear model in form of polynomial parameter-dependent approximation as a way of nonlinear embedding approach. However, a few constraints have not motivated the implementation of such technique. As we assumed that the degradation behaviors are unknown, that means that our system is a grey-box and we can only estimate the variations. However, if we suppose that the degradation behavior is known as an exponential evolution as previously stated, and we assume that the poly-

nomial regression approximation is acceptable, we obtain polynomial degradation equations up to order 5 as shown in Chapter 3. The complexity of the problem increases with the more varying parameters. In consequence, we eliminated this trial of nonlinear embedding technique for the last constraint of solving the optimization-based problem for LPV approximation for the sake of its polynomial formulation that contradicts our trade-off between complexity and estimation speed.

It is worth mentioning that the nonlinear embedding can be accomplished to various nonlinear systems, whereas the aim is to transform the dynamical system to an LPV representation. Whereas, each technique could fit better in some nonlinear models than others in the LPV model approximation. Hence, under these conditions and the fact the augmented nonlinear model cope with the observer-based grey-box techniques, we intend to transform the previously-adopted Jacobian approximation approach in Chapter 3 into an LPV model. This transition permits to investigate the same approximation of the nonlinear model for comparison assessment using the bounding box approach to obtain an LPV model. This transformation is not unique, however it is motivated in this thesis given all the aforementioned constraints, in addition to the problem description that characterizes the degraded components which are bounded between their rated value and the EoL TH. According to (Tóth 2010), such model approximation is capable to perform with high accuracy with the slowly-varying parameters. Moreover, since the Jacobian approximation provides a parameter-varying model (Tóth 2010; Rugh and Shamma 2000; Shamma and Athans 1990; Hyde and Glover 1993; Rugh 1991; Shamma and Athans 1990; Åström and Wittenmark 1898), an interpolation with the bounding box approach is accomplished to obtain a polytopic LPV model representation with bounded parameters (Olivier Sename and Soheib Fergani 2017; Lovera, Bergamasco, and Casella 2013; B. Bamieh and Giarre 2002; Rugh and Shamma 2000).

Finally, the aim of adopting the LPV representation is motivated by further extension of the prognostics to control-related applications. Assumption 4.2.1 characterizes the type of the degradation parameters which are bounded in their operational interval.

Assumption 4.2.1. The degradation parameters are bounded between their rated values and the maximum TH.

Moreover, the dynamical averaged model is locally linearized using the first order linearization technique (Jacobian) around the varying parameters

ρ_i for $i = 1, \ldots, n_\rho$:

$$\begin{aligned} \mathbf{A}_i &= \frac{\partial \mathbf{f}}{\partial \mathbf{x}}(\rho_i), \quad \mathbf{B}_i = \frac{\partial \mathbf{f}}{\partial \mathbf{u}}(\rho_i), \\ \mathbf{C}_i &= \frac{\partial \mathbf{g}}{\partial \mathbf{x}}(\rho_i), \quad \mathbf{D}_i = \frac{\partial \mathbf{g}}{\partial \mathbf{u}}(\rho_i). \end{aligned} \tag{4.1}$$

Furthermore, a local LTI model is obtained around each equilibrium parameter ρ_i, and the first-order Taylor expansion of f and g are applied to approximate the state and output vectors as:

$$\dot{\breve{\mathbf{x}}} \approx \mathbf{A}_i(\mathbf{x} - \mathbf{x}_i) + \mathbf{B}_i(\mathbf{u} - \mathbf{u}_i), \tag{4.2a}$$
$$\breve{\mathbf{y}} \approx \mathbf{C}_i(\mathbf{x} - \mathbf{x}_i) + \mathbf{D}_i(\mathbf{u} - \mathbf{u}_i) + g(\rho_i), \tag{4.2b}$$

where $\breve{\mathbf{x}}$ and $\breve{\mathbf{y}}$ are the approximated state and output vectors, respectively. Hence, the parameter-varying representation is rewritten with a scheduling function μ is introduced as $\sum_{i=1}^{N} \mu_i(\rho) = 1 \; \forall \; \rho$:

$$\dot{\breve{\mathbf{x}}} = \sum_{i=1}^{N} \mu_i(\rho)(\mathbf{A}_i\breve{\mathbf{x}} + \mathbf{B}_i\mathbf{u}) - \overbrace{\sum_{i=1}^{N} \mu_i(\rho)(\mathbf{A}_i\mathbf{x}_i + \mathbf{B}_i\mathbf{u}_i)}^{\gamma_x(\rho)}, \tag{4.3a}$$
$$\breve{\mathbf{y}} = \sum_{i=1}^{N} \mu_i(\rho)(\mathbf{C}_i\breve{\mathbf{x}} + \mathbf{D}_i\mathbf{u}) - \underbrace{\sum_{i=1}^{N} \mu_i(\rho)(\mathbf{C}_i\mathbf{x}_i + \mathbf{D}_i\mathbf{u}_i - g(\rho_i))}_{\gamma_y(\rho)}, \tag{4.3b}$$

where $\gamma_x(\rho)$ and $\gamma_y(\rho)$ are the remainder terms of the approximation process. It should be noted that (4.3) is not an LPV representation, yet the LPV is obtained by either including $\gamma_x(\rho)$ and $\gamma_y(\rho)$ as additional perturbations and measurement noises, or by locally eliminating them and then interpolate them with the global model. Therefore, to conserve the adequate approximation of the LPV model, $\gamma_x(\rho)$ and $\gamma_y(\rho)$ are included in ω and υ respectively (Tóth 2010).

The polytopic coordinates μ_i are computed with respect to the bounded parameters $[\underline{\rho}_{1,\ldots,n_\rho}, \overline{\rho}_{1,\ldots,n_\rho}]$ by interpolation. For the case study of this work, the maximum number of the augmented parameters is two. Then, the poly-

topic coordinates are obtained:

$$\mu_1 = \left(\frac{\overline{\rho_1} - \rho_1}{\overline{\rho_1} - \underline{\rho_1}}\right)\left(\frac{\overline{\rho_2} - \rho_2}{\overline{\rho_2} - \underline{\rho_2}}\right), \tag{4.4a}$$

$$\mu_2 = \left(\frac{\overline{\rho_1} - \rho_1}{\overline{\rho_1} - \underline{\rho_1}}\right)\left(\frac{\rho_2 - \underline{\rho_2}}{\overline{\rho_2} - \underline{\rho_2}}\right), \tag{4.4b}$$

$$\mu_3 = \left(\frac{\rho_1 - \underline{\rho_1}}{\overline{\rho_1} - \underline{\rho_1}}\right)\left(\frac{\overline{\rho_2} - \rho_2}{\overline{\rho_2} - \underline{\rho_2}}\right), \tag{4.4c}$$

$$\mu_4 = \left(\frac{\rho_1 - \underline{\rho_1}}{\overline{\rho_1} - \underline{\rho_1}}\right)\left(\frac{\rho_2 - \underline{\rho_2}}{\overline{\rho_2} - \underline{\rho_2}}\right). \tag{4.4d}$$

Finally, the LPV is represented in the following polytopic form for the case of two varying parameters:

$$\begin{aligned}
&\left[\begin{array}{c|c} \mathbf{A}(\rho_1,\rho_2) & \mathbf{B}(\rho_1,\rho_2) \\ \hline \mathbf{C}(\rho_1,\rho_2) & \mathbf{D}(\rho_1,\rho_2) \end{array}\right] = \\
&\mu_1 \left[\begin{array}{c|c} \mathbf{A}(\underline{\rho}_1,\underline{\rho}_2) & \mathbf{B}(\underline{\rho}_1,\underline{\rho}_2) \\ \hline \mathbf{C}(\underline{\rho}_1,\underline{\rho}_2) & \mathbf{D}(\underline{\rho}_1,\underline{\rho}_2) \end{array}\right] + \mu_2 \left[\begin{array}{c|c} \mathbf{A}(\underline{\rho}_1,\overline{\rho}_2) & \mathbf{B}(\underline{\rho}_1,\overline{\rho}_2) \\ \hline \mathbf{C}(\underline{\rho}_1,\overline{\rho}_2) & \mathbf{D}(\underline{\rho}_1,\overline{\rho}_2) \end{array}\right] \\
+&\mu_3 \left[\begin{array}{c|c} \mathbf{A}(\overline{\rho}_1,\underline{\rho}_2) & \mathbf{B}(\overline{\rho}_1,\underline{\rho}_2) \\ \hline \mathbf{C}(\overline{\rho}_1,\underline{\rho}_2) & \mathbf{D}(\overline{\rho}_1,\underline{\rho}_2) \end{array}\right] + \mu_4 \left[\begin{array}{c|c} \mathbf{A}(\overline{\rho}_1,\overline{\rho}_2) & \mathbf{B}(\overline{\rho}_1,\overline{\rho}_2) \\ \hline \mathbf{C}(\overline{\rho}_1,\overline{\rho}_2) & \mathbf{D}(\overline{\rho}_1,\overline{\rho}_2) \end{array}\right].
\end{aligned} \tag{4.5}$$

Remark 4.2.1. For the sake of notations simplification, the approximated state $\breve{\mathbf{x}}$ and output $\breve{\mathbf{y}}$ vectors are written in the following as $\mathbf{x}$ and $\mathbf{y}$, respectively.

Finally, the discrete-time LPV state-space representation is written as:

$$\begin{cases} \mathbf{x}_{k+1} &= \mathbf{A}_k\mathbf{x}_k + \mathbf{B}_k\mathbf{u}_k + \mathbf{E}_\omega\omega_k, \\ \mathbf{y}_k &= \mathbf{C}_k\mathbf{x}_k + \mathbf{D}_k\mathbf{u}_k + \mathbf{E}_\upsilon\upsilon_k. \end{cases} \tag{4.6}$$

Assumption 4.2.2. The disturbances and measurement noises are assumed to be zonotopes as:

$$\mathcal{W} = \omega_c \oplus \mathbf{E}_\omega\mathcal{B}^{n_x}, \tag{4.7a}$$

$$\mathcal{V} = \upsilon_c \oplus \mathbf{E}_\upsilon\mathcal{B}^{n_y}, \tag{4.7b}$$

where $\mathbf{E}_\omega \in \mathbb{R}^{n_x \times n_x}_{\neq 0}$ and $\mathbf{E}_\upsilon \in \mathbb{R}^{n_y \times n_y}_{\neq 0}$ are nonzero diagonal generator matrices of the zonotopes $\mathcal{W}$ and $\mathcal{V}$ respectively. $\mathcal{B}^{n_x}$ and $\mathcal{B}^{n_y}$ are unitary boxes. Thus, $\omega_k \in \mathbb{R}^{n_\omega}$ and $\upsilon_k \in \mathbb{R}^{n_\upsilon}$ are the process and output measurement noises

respectively, and they are bounded by a unitary hypercube centered at 0 as:

$$\omega_k \in \langle 0, \mathbf{I}_{n_\omega} \rangle, \quad \forall k \geq 0, \tag{4.8a}$$
$$\upsilon_k \in \langle 0, \mathbf{I}_{n_\upsilon} \rangle, \quad \forall k \geq 0. \tag{4.8b}$$

Remark 4.2.2. The model (4.6) is a polytopic LPV with varying parameters bounded by intervals denoted by $[\underline{\rho_k}, \overline{\rho_k}]$. Using this representation, the pair $(\mathbf{A}_k, \mathbf{C}_k)$ becomes observable at each time instant k.

4.3 ZEKF Observer Design for JESP

The ZEKF observer is based on the stochastic EKF that propagates the states in a zonotopic scheme. Thus, the Gaussian PDF in the conventional KF and its extensions can be replaced by zonotopic sets in order to design the ZEKF observer (Combastel 2015).

Thus, by introducing a varying tuning matrix (λ) to the model (4.6), the states vector of the observer is written as:

$$\mathbf{x}_{k+1} = \mathbf{A}_k\mathbf{x}_k + \mathbf{B}_k\mathbf{u}_k + \mathbf{E}_\omega\omega_k + \lambda_k(\mathbf{y}_k - (\mathbf{C}_k\mathbf{x}_k + \mathbf{D}_k\mathbf{u}_k + \mathbf{E}_\upsilon\upsilon_k)). \tag{4.9}$$

Hence, the estimated center $\hat{\mathbf{x}}$ and the estimated generator matrix $\mathbf{G}$ of the ZEKF observer are written as:

$$\hat{\mathbf{x}}^c_{k+1} = (\mathbf{A}_k - \lambda_k\mathbf{C}_k)\hat{\mathbf{x}}^c_k - (\mathbf{B}_k - \lambda_k\mathbf{D}_k)\mathbf{u}_k + \lambda_k\mathbf{y}_k, \tag{4.10a}$$
$$\hat{\mathbf{G}}_{k+1} = \begin{bmatrix}(\mathbf{A}_k - \lambda_k\mathbf{C}_k) \downarrow_{q,W} \hat{\mathbf{G}}_k & \mathbf{E}_\omega & -\lambda_k\mathbf{E}_\upsilon\end{bmatrix}, \tag{4.10b}$$

where $\hat{\mathbf{x}}^c_k$ denotes the estimated state vector center at time instant k, and $\hat{\mathbf{G}}_k$ denotes its estimated generator matrix. Thus, $\downarrow_{q,W} \hat{\mathbf{G}}_k$ is the reduced generator matrix that is computed based on the Property A.2.8 (Combastel 2015). It should be noted that the states are initialized at $k = 0$ based on the zonotopic inclusion property as $\mathbf{x} \in \langle \mathbf{x}^c_k, \mathbf{G}_k \rangle$, and similarly assumed $\forall k > 0$. The following subsection explains the implementation of an LMI-based optimization problem in order to guarantee a robust tuning of the ZEKF observer.

4.3.1 LMI-based Optimization of the tuning matrix

Divergence, numerical instability and other problems could be resulted due to the negative effect of uncertainties on the generator matrix as shown in

(4.10b). Therefore, there exists a few methods to compute the tuning parameter for optimal enclosures. Online and offline techniques have been carried out with remarkable performances. However, to avoid computational stress and delays in the online estimation process, an offline LMI-based optimization problem has been proposed especially to guarantee the robustness of the ZEKF observer. Hence, using the F_W-radius minimization property as shown in Definition A.2.18, an optimal tuning parameter λ^*_{LMI} is obtained by solving an optimization problem in an LMI framework.

Proposition 4.3.1 (A robust LMI-based optimization of the tuning matrices of the ZEKF observer)**.** Given the LPV model in (4.6) and following the structure of the ZEKF for JESP (5.1), the optimal tuning matrix $\lambda^*{}_{\text{LMI}}$ is computed based on the feasible solutions $\mathbf{\Psi}$ and $\mathbf{W}$ if there exists a positive scalar γ such that:

$$\lambda^{\star}_{\text{LMI}} = \mathbf{\Psi}^{-1}\mathbf{W}. \tag{4.11}$$

Hence, by introducing the matrices $\mathbf{Q} = \mathbf{Q}^\intercal$ and $\mathbf{R} = \mathbf{R}^\intercal$ as tuning parameters, the proposed optimization problem is solved[1] following this form:

$$\underset{\mathbf{W},\,\mathbf{\Psi}}{\text{minimize}} \quad \gamma \tag{4.12a}$$

subject to

$$\begin{bmatrix} \gamma\mathbf{I} & \mathbf{I} \\ \mathbf{I} & \mathbf{\Psi} \end{bmatrix} \succ 0, \tag{4.12b}$$

$$\begin{bmatrix} -\mathbf{\Psi} & \mathbf{\Psi}\mathbf{A} - \mathbf{W}\mathbf{C} & \mathbf{\Psi}\sqrt{Q}^\intercal & \mathbf{W} \\ \star & -\mathbf{\Psi} & \mathbf{0} & \mathbf{0} \\ \star & \star & -\mathbf{I} & \mathbf{0} \\ \star & \star & \star & -\mathbf{R}^{-1} \end{bmatrix} \prec 0 \tag{4.12c}$$

where $\star$ denotes symmetrical elements.

Proof. Based on the (Combastel 2015), minimizing the $F-$radius of zonotope is equivalent to minimizing the trace of its covariation $cov(\downarrow_{q,W} \mathbf{G})$. Moreover, the author also proved by analogy, that minimizing the F_W-radius is equivalent to the non-weighted case. The advantages of the size minimization based on the F_W-radius with the consistency of the reduction operator $\downarrow_{q,W}$, are similar to the $P-$radius minimization method (Vu Tuan Hieu Le et al. 2013). Both approaches provide robust stability analysis in an optimal LMI framework. Thus minimizing the F_W-radius is computed as follows:

$$J_W = \|\mathbf{G}_{k+1}\|^2_{F,W} = tr(\mathbf{G}_{k+1}\mathbf{G}^\intercal_{k+1}), \tag{4.13}$$

[1]The LMI-based optimization problem is solved in MATLAB using YALMIP toolbox https://yalmip.github.io/

where J_W denotes the weighted Frobenius function of the covariation of the generator matrices of a zonotope. Thus, a possible optimal solution of the tuning matrix $\lambda^\star$ is obtained by achieving (4.13) is being lower than a given scalar γ. Hence, by considering the Lyapunov function:

$$\mathbf{V}(x) = \mathbf{x}^\intercal \mathbf{P} \mathbf{x}. \tag{4.14}$$

If there exists a positive definite matrix $\mathbf{P} \succ 0 \in \mathbb{R}^{n_x \times n_x}$, we get a weighted norm $\sqrt{\mathbf{x}^\intercal \mathbf{P} \mathbf{x}} = \sqrt{\mathbf{V}(x)}$ that represents the distance from the origin $x = 0$. Furthermore, the system is stable if the weighting norm is decreasing such that (Alamo et al. 2006):

$$\begin{aligned} \frac{d}{dt}(\mathbf{V}(x)) &= \frac{d}{dt}(\mathbf{x}^\intercal \mathbf{P} \mathbf{x}) \\ &= \dot{\mathbf{x}}^\intercal \mathbf{P} \mathbf{x} + \mathbf{x}^\intercal \mathbf{P} \dot{\mathbf{x}}^\intercal \\ &= \mathbf{x}^\intercal \mathbf{A}^\intercal \mathbf{P} \mathbf{x} + \mathbf{x}^\intercal \mathbf{P} \mathbf{A} \mathbf{x} \\ &= \mathbf{x}^\intercal (\mathbf{A}^\intercal \mathbf{P} + \mathbf{P} \mathbf{A}) \mathbf{x} < 0, \quad \forall x \neq 0. \end{aligned} \tag{4.15}$$

Hence, by introducing the following conditions with the weighting norm is less than the scalar γ, and the variations are less than the F_W-radius as (M. Pourasghar, V. Puig, and Ocampo-Martinez 2019):

$$\mathbf{V}(x_0) = \mathbf{x_0}^\intercal \mathbf{P} \mathbf{x_0} < \gamma, \tag{4.16a}$$

$$\mathbf{V}(x_{k+1}) - \mathbf{V}(x_k) + J_W < 0, \tag{4.16b}$$

with the evolution of the system is confined in the following ellipsoid:

$$\{\ \mathbf{x}\ :\ \mathbf{x}_0^\intercal \mathbf{P} \mathbf{x}_0 < \gamma\ \}. \tag{4.17}$$

Hence, by introducing $\Psi = \mathbf{P}^{-1}$, the condition in (4.16a) becomes:

$$\gamma - \mathbf{x_0}^\intercal \Psi^{-1} \mathbf{x_0} > 0, \tag{4.18}$$

and by applying the *Schur complement* to (4.18), the LMI is obtained as:

$$\begin{bmatrix} \gamma & \mathbf{x}_0^\intercal \\ \mathbf{x}_0 & \boldsymbol{\Psi} \end{bmatrix} \succ 0. \tag{4.19}$$

Then, we multiply (4.19) by $\mathbf{I}_{n_x \times n_x}$, we obtain the first constraint in (4.11). Hence, by substituting (5.2a) with (4.15), and considering (4.16b), the LMI of (4.15) is thus rewritten as:

$$(\mathbf{A} - \lambda \mathbf{C}) \mathbf{P} + \mathbf{P} (\mathbf{A} - \lambda \mathbf{C})^\intercal + \mathbf{Q} + \lambda \mathbf{R} \lambda^\intercal \prec 0. \tag{4.20}$$

Then, by multiplying (4.20) by $\Psi = \mathbf{P}^{-1}$, and introducing $\mathbf{W} = \Psi\lambda^{\star}$, it becomes:

$$\Psi\mathbf{A} - \mathbf{W}\mathbf{C} + \mathbf{A}^{\intercal} - \mathbf{C}^{\intercal}\mathbf{W}^{\intercal} + \Psi\mathbf{Q}\Psi + \mathbf{W}\mathbf{R}\mathbf{W}^{\intercal} \prec 0. \tag{4.21}$$

Finally, Eq. (4.21) is reformulated as:

$$-\Psi + \begin{bmatrix}\Psi\mathbf{A} - \mathbf{W}\mathbf{C} & \Psi\sqrt{\mathbf{Q}} & \mathbf{W}\end{bmatrix} \begin{bmatrix}-\Psi & \mathbf{0} & \mathbf{0} \\ \mathbf{0} & -\mathbf{I} & \mathbf{0} \\ \mathbf{0} & \mathbf{0} & -\mathbf{R}^{-1}\end{bmatrix} \begin{bmatrix}\mathbf{A}^{\intercal}\Psi - \mathbf{C}^{\intercal}\mathbf{W}^{\intercal} \\ \sqrt{\mathbf{Q}}\Psi \\ \mathbf{W}^{\intercal}\end{bmatrix} \prec 0. \tag{4.22}$$

Consequently, the LMI (4.12c) is obtained from (4.22) and (4.19), where $\mathbf{Q} = \mathbf{E}_{\omega}$ and $\mathbf{R} = \mathbf{E}_{\upsilon}$. Furthermore, $\mathbf{\Psi}$ and $\mathbf{W}$ are the feasible solutions and the optimal tuning parameter $\lambda^{\star}$ is computed as in (4.11). □

Proposition 4.3.2 (A polytopic offline solving of the LMI optimization problem)**.** A polytopic approach is proposed to solve the LMI optimization problem offline considering only the vertices of varying parameters intervals. Based on the augmented model (4.6), ρ_{i_k} denotes the varying parameters in zonotopic form as:

$$\rho_{i_k} \in \langle \rho_{0_i}, \mathbf{G}_{\rho_{i_k}} \rangle, \tag{4.23}$$

where ρ_{0_i} denotes the rated value of the parameter ρ_i.

$$\rho_{i_k} \in \mathbb{R}_{+}^{n_\rho} : |\rho_{i_k} - \rho_{0_k}| \leq \rho_i^{\mathrm{TH}}, \quad \forall k > 0, \tag{4.24}$$

where ρ_i^{TH} is the value of the statistically and experimentally obtained TH of the physical components as explained in Chapter 2 (Celaya, J. R. and Saxena, A. and Saha, S. and Goebel, K. 2011; Renwick, J. and Kulkarni, C. and Celaya, J. 2015). Thus, the polytopic representation of (4.6) is obtained using the bounding box approach and considering the range of variation of the varying parameters.

$$\mathbf{x}_{k+1} = \sum_{i=1}^{N} \mu_i\left(\rho_{i_k}\right)\left(\mathbf{A}_i\mathbf{x}_k + \mathbf{B}_i\mathbf{u}_k\right), \tag{4.25}$$

$$\mathbf{y}_k = \sum_{i=1}^{N} \mu_i\left(\rho_{i_k}\right)\left(\mathbf{C}_i\mathbf{x}_k + \mathbf{D}_i\mathbf{u}_k\right), \tag{4.26}$$

where μ_i are the coefficients of the polytopic decomposition such that:

$$\sum_{i=1}^{N} \mu_i\left(\rho_{i_k}\right) = 1, \;\; \mu_i(\rho_{i_k}) \geq 0, \forall i = 1, \ldots, N \tag{4.27}$$

Furthermore, the interval limits $[\underline{\lambda}^{\star}_{\text{LMI}}, \overline{\lambda}^{\star}_{\text{LMI}}]$ of the tuning matrix $\lambda^{\star}$ are obtained such that:

$$\underline{\lambda}^{\star}_{\text{LMI}_i} = \min\ \lambda^{\star}_{\text{LMI}_i}, \quad \overline{\lambda}^{\star}_{\text{LMI}_i} = \max\ \lambda^{\star}_{\text{LMI}_i}, \tag{4.28}$$

where $\lambda^{\star}_{\text{LMI}_i}$ is represented as:

$$\lambda^{\star}_i = M_{1_i}(\lambda^{\star}_i)\underline{\lambda}^{\star}_i + M_{2_i}(\lambda^{\star}_i)\overline{\lambda}^{\star}_i, \tag{4.29}$$

with respect to the following condition:

$$M_{1_i}(\lambda^{\star}_i) + M_{2_i}(\lambda^{\star}_i) = 1, \tag{4.30}$$

where the membership functions are calculated as:

$$M_{1_i}(\lambda^{\star}_i) = \frac{\overline{\lambda}^{\star}_i - \lambda^{\star}_i}{\overline{\lambda}^{\star}_i - \underline{\lambda}^{\star}_i}, \quad M_{2_i}(\lambda^{\star}_i) = \frac{\lambda^{\star}_i - \underline{\lambda}^{\star}_i}{\overline{\lambda}^{\star}_i - \underline{\lambda}^{\star}_i}. \tag{4.31}$$

Finally, a varying value for the tuning matrix (4.11) is obtained as follows:

$$\lambda^{\star}(\rho_{i_k}) = \sum_{i=1}^{N} \mu_i\left(\rho_{i_k}\right) \lambda^{\star}_i, \tag{4.32}$$

where $\lambda^{\star}_i$ are obtained by solving (4.12c) at the vertices of the polytopic model (4.25)-(4.26).

The principal advantage of this LMI-based approach for the computation of the tuning matrix of the ZEKF, is that the optimization problem (4.12c) is solved offline. Consequently, the maximum number of optimization computations is reduced to N, and only the interpolation of the offline-obtained tuning matrices is computed online at each estimation operation.

Remark 4.3.1. It is worth mentioning that the same tuning matrices of the offline LMI-optimization have been obtained by solving the same problem online. Nevertheless, it is preferable to adopt the offline polytopic interpolation that provides reduced computational time and memory consumption.

4.3.2 Classical approach for online tuning of the observer

There exists a classical online method to compute the tuning matrix of the ZEKF observer, based on the minimization of the Frobenius norm of the generator vertices. Additionally, the proof of the computation of the optimal λ^{*} has shown its independence of the weighting matrix (Combastel 2015).

Proposition 4.3.3 (Classical online approach to tune the observer gain (Combastel 2015; V. T. H. Le et al. 2013; Y. Wang, Vicenç Puig, and Cembrano 2018)). λ_{c}^{*} denotes the tuning matrix of the online classical approach and is determined as follows:
Decompose the generator matrix $\hat{\mathbf{G}}_k(\lambda_{\mathrm{c}})$ as (T. Alamo, Bravo, and Camacho 2005; V. Le et al. 2013a):

$$\hat{\mathbf{G}}_k(\lambda_{\mathrm{c}}) = \mathbf{M} + \lambda_{\mathrm{c}}\theta^{\intercal}, \tag{4.33}$$

where $\mathbf{M} = [\tilde{\mathbf{G}}_k \quad 0]$, $\theta^{\intercal} = [-\mathbf{C}^{\intercal}\tilde{\mathbf{G}}_k\mathbf{E}_v]$. Thus, the Frobenius norm of $\hat{\mathbf{G}}_k(\lambda_{\mathrm{c}})$ is calculated as follows:

$$\begin{aligned}
\|\hat{\mathbf{G}}_k\|_F^2 &= \|\mathbf{M} + \lambda_{\mathrm{c}}\theta^{\intercal}\|_F^2 \\
&= tr((\mathbf{M}^{\intercal} + \theta\lambda_{\mathrm{c}}^{\intercal})(\mathbf{M} + \lambda_{\mathrm{c}}\theta^{\intercal})) \\
&= tr(\mathbf{M}^{\intercal}\mathbf{M}) + tr(\theta\lambda_{\mathrm{c}}^{\intercal}\mathbf{M}) + tr(\mathbf{M}^{\intercal}\lambda_{\mathrm{c}}\theta^{\intercal} + tr(\theta\lambda_{\mathrm{c}}^{\intercal}\lambda_{\mathrm{c}}\theta^{\intercal}) \\
&= 2\lambda_{\mathrm{c}}^{\intercal}\mathbf{M}\theta + \theta^{\intercal}\theta\lambda_{\mathrm{c}}^{\intercal}\lambda_{\mathrm{c}} + tr(\mathbf{M}^{\intercal}\mathbf{M}),
\end{aligned} \tag{4.34}$$

The minimum value of $\|\hat{\mathbf{G}}(\lambda_{\mathrm{c}})\|_F^2$ is obtained as:

$$\begin{aligned}
\frac{\mathrm{d}\|\hat{\mathbf{G}}(\lambda_{\mathrm{c}})\|_F^2}{\mathrm{d}\lambda_{\mathrm{c}}} &= 0, \\
\frac{\mathrm{d}(2\lambda_{\mathrm{c}}^{\intercal}\mathbf{M}\theta + \theta^{\intercal}\theta\lambda_{\mathrm{c}}^{\intercal}\lambda_{\mathrm{c}} + tr(\mathbf{M}^{\intercal}\mathbf{M}))}{\mathrm{d}\lambda_{\mathrm{c}}} &= 0,
\end{aligned} \tag{4.35}$$

consequently,

$$2\mathbf{M}\theta + 2\theta^{\intercal}\theta\lambda^{*} = 0. \tag{4.36}$$

Finally, the optimal tuning matrix is obtained online as:

$$\lambda_{\mathrm{c}}^{*} = \frac{-\mathbf{M}\theta}{\theta^{\intercal}\theta} \equiv \frac{\tilde{\mathbf{G}}_k\tilde{\mathbf{G}}_k^{\intercal}\mathbf{C}_k}{\mathbf{C}_k^{\intercal}\tilde{\mathbf{G}}_k\tilde{\mathbf{G}}_k^{\intercal}\mathbf{C}_k + \mathbf{E}_v\mathbf{E}_v^{\intercal}}. \tag{4.37}$$

It is remarkable that the optimal tuning matrix obtained in (4.37) is similar to the statistical gain of the KF as shown in Chapter 3 (Combastel 2015).

Remark 4.3.2. It is advised to employ the proposed LMI-based approach in Section 4.3.1 over the classical online approach (4.37) for its applicability to nonlinear systems, in addition to the reduced online computations.

4.4 Bounded RUL Forecasting in a Zonotopic Framework

As we previously discussed in this chapter, the aim of implementing the ZEKF is to make use of the bounds of the estimated zonotopic parameters. Therefore, in order to test the validity of the improved bounded RUL proposition based on zonotopes, the same approach of linear EoL-RUL (3.20) in Section 3.4, has been implemented with bounded parameters.

The estimated parameters bounds are:

$$\left[\underline{\hat{\mathbf{G}}}(\rho_{i_k}),\ \overline{\hat{\mathbf{G}}}(\rho_{i_k})\right], \quad \forall k \in \mathbb{N} \tag{4.38}$$

Thus, the estimated degradation level are bounded as:

$$\begin{cases} \underline{\hat{\text{deg}}}_{\%_k} = \dfrac{\underline{\hat{\mathbf{G}}}(\rho_{i_k}) - \mathbf{x}_0}{\mathbf{x}_0} \times 100, & (4.39a) \\ \overline{\hat{\text{deg}}}_{\%_k} = \dfrac{\overline{\hat{\mathbf{G}}}(\rho_{i_k}) - \mathbf{x}_0}{\mathbf{x}_0} \times 100. & (4.39b) \end{cases}$$

Next, the bounded systems for linear EoL-RUL computation are:

$$\begin{cases} \underline{a}_{i_k} \breve{\text{EoL}}_i + \underline{b}_{i_k} \approx 100\%, & (4.40a) \\ \underline{a}_{i_k} k + \underline{b}_{i_k} \approx \underline{\hat{\text{deg}}}_{\%_k}, & (4.40b) \end{cases}$$

$$\begin{cases} \overline{a}_{i_k} \breve{\text{EoL}}_i + \overline{b}_{i_k} \approx 100\%, & (4.41a) \\ \overline{a}_{i_k} k + \overline{b}_{i_k} \approx \overline{\hat{\text{deg}}}_{\%_k}. & (4.41b) \end{cases}$$

Finally, the bounded RUL is predicted as:

$$\begin{cases} \underline{\tilde{\text{RUL}}}_{i_k} \approx \dfrac{\text{TH}_i - \underline{b}_{i_k}}{\underline{a}_{i_k}} - k, & (4.42a) \\ \overline{\tilde{\text{RUL}}}_{i_k} \approx \dfrac{\text{TH}_i - \overline{b}_{i_k}}{\overline{a}_{i_k}} - k, & (4.42b) \end{cases}$$

where i refers to the selection of each augmented parameter. Hence, k refers to t_{current} of the accelerated degradation time in this case study, and the bounded predicted RUL of (4.42) are then presented as $[\underline{\tilde{t}}_{\text{RUL}}, \overline{\tilde{t}}_{\text{RUL}}]$.

4.5 ZEKF-based Algorithm for JESP and RUL Forecasting

This section is dedicated to summarize the computation of the ZEKF-based approach for JESP and RUL forecasting.

Algorithm 3: ZEKF-based Algorithm for JESP and RUL Forecasting

Result: $[\underline{\tilde{\text{RUL}}}, \overline{\tilde{\text{RUL}}}]$
Initialization:$\hat{\mathbf{x}}^c$, $\hat{\mathbf{G}}$,$\mathbf{E}_\omega$, $\mathbf{E}_\upsilon$, $\mathcal{W}$, $\mathcal{V}$, ρ;
Solve the LMI-based optimization problem and return $2^{n_\rho}\lambda$ (4.12c);
for $k = 1 : N$ **do**
  Compute $\mathbf{A}_k, \mathbf{B}_k, \mathbf{C}_k, \mathbf{D}_k$;
  Run the online bounding box approach to calculate $\lambda^\star_{i_k}$ (4.32);
  Compute the reduced generator matrix $\downarrow_{q,W} \hat{\mathbf{G}}_k$;
  Prediction of the state vector center $\hat{\mathbf{x}}^{\text{c}}_{k+1}$ (4.10a) and the generator matrix $\hat{\mathbf{G}}_{k+1}$ (4.10b) of $\hat{\mathcal{X}}_k$;
  return $\hat{\mathcal{X}}_k$;
  Compute the estimated bounds of the augmented parameters as in (4.38);
  Compute the bounded estimation of the degradation level as in (4.39);
  Solve the systems of linear EoL-RUL equations (4.40) and (4.41);
  Predict the bounded RUL as in (4.42);
  return $\left[\underline{\tilde{\text{RUL}}}_{i_k}, \overline{\tilde{\text{RUL}}}_{i_k}\right]$
end

4.6 Case Study: Results and Analysis

The DC-DC converter case study has been tested for the ZEKF-based PHM approach as well as the stochastic-based. Thus, the polytopic LPV model has been employed as shown in Section 4.2.1. The augmented parameters are bounded between the rated value and the TH of each, for the sake of the application of the polytopic LPV model. Hence, the parameters of the bounding box approach are defined as $[R_{\text{ON}_0}, R^{\text{TH}}_{\text{ON}}]$ and $[\text{ESR}_{\text{o}_0}, \text{ESR}^{\text{TH}}_{\text{o}}]$. Given that the LPV model is observable according to the linearization approach

that has proven its functionality against the previously-faced numerical constraints. Thus, the ZEKF has been implemented as explained in 4.3 where the zonotopic states and parameters are returned. The estimated zonotopic parameters are bounded at each time instant for the sake of the implementation of the proposed RUL forecasting approach as presented in Section 4.4. The dual-observer approach for switched-systems is not examined for the reasons that have been mentioned in the previous chapters.

It is worth noting that the ZEKF-based observer for JESP is tuned using the offline LMI-based optimization as explained in Section 4.3.1 and compared to the classical online tuning approach as shown in Section 4.3.2.

4.6.1 Scenario 1

The direction matrices of the unknown-but-bounded noises and uncertainties are defined as:

$$\mathbf{E}_{\omega} = diag(0.01,\ 0.01,\ 0.01,\ 0.0005), \tag{4.43a}$$

$$\mathbf{E}_{v} = diag(0.1,\ 0.1). \tag{4.43b}$$

Results of the JESP using the ZEKF

Figures 4.2a, 4.2b, 4.2c, and 4.3 illustrate the estimated zonotopic states and parameter R_{ON} of degradation scenario 1.
The JESP using the ZEKF approach has proven its accuracy by the illustrated results. The online classical (λ_{c}^{*}) and the offline LMI-based optimization ($\lambda_{\mathrm{LMI}}^{*}$) tuning approaches have both optimally tuned the observer where the zonotopic bounds always enclose the empirical degradation that describes the true accelerated aging of the critical components. Yet, $\lambda_{\mathrm{LMI}}^{*}$ is motivated due to its reduced computations in an offline optimization, in addition to the ability of adding constraints of the physical system to the LMIs. Table 4.1 shows the average RA of the ZEKF-based JESP tuned by both approaches against the EKF for JESP. Therefore, the average RA is very reliable using any of the aforementioned approaches. However, it is essential to characterize the advantages of that the LMI-based JESP using the ZEKF provide such as the offline optimization and the propagated bounds. As mentioned, the bounds of the estimated parameters are the foundation of the RUL forecasting. Thus, by recalling our objective to estimate the degradation of the critical components in a system unlike most of the system-level prognostics approaches, it is crucial to emphasize on Figure 4.3 that represents the parameter estimation and is employed for the RUL forecasting approach.

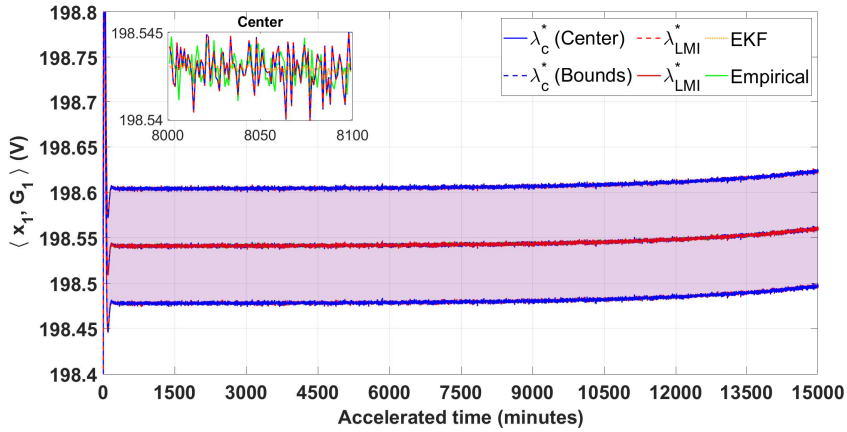

(a) ZEKF-based $\hat{\mathcal{X}}_1$ with both tuning approaches versus the stochastic estimation and the empirical degradation in Scenario 1

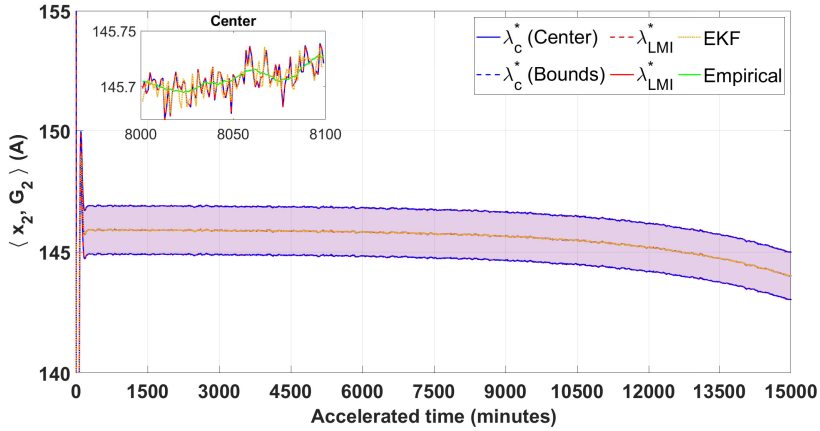

(b) ZEKF-based $\hat{\mathcal{X}}_2$ with both tuning approaches versus the stochastic estimation and the empirical degradation in Scenario 1

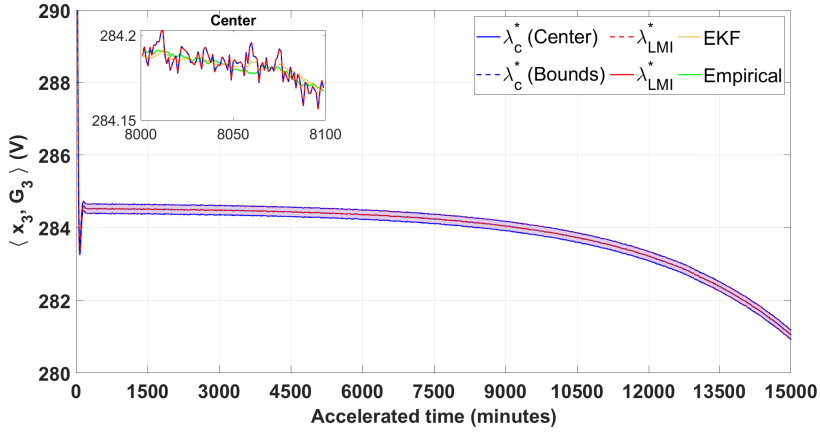

(c) ZEKF-based $\hat{\mathcal{X}}_3$ with both tuning approaches versus the stochastic estimation and the empirical degradation in Scenario 1

Figure 4.2: ZEKF-based states estimation with both tuning approaches versus the stochastic estimation and the empirical degradation in Scenario 1

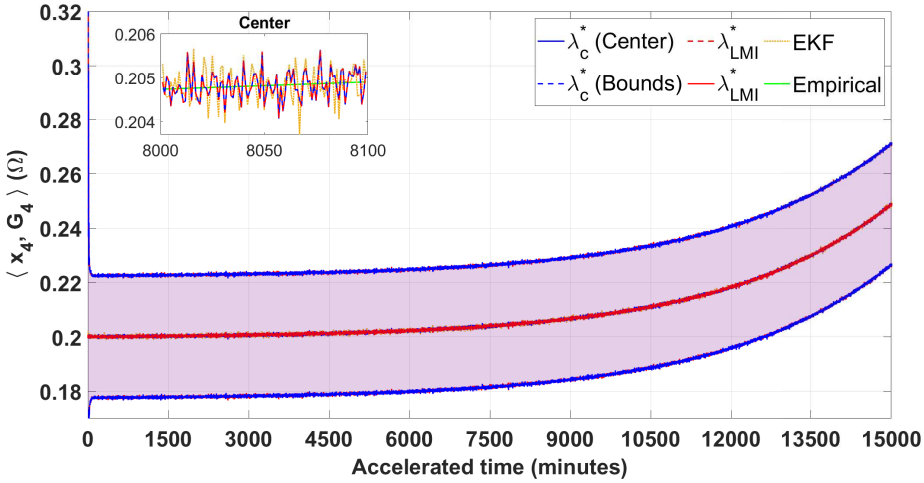

Figure 4.3: ZEKF-based $\hat{\mathcal{X}}_4$ with both tuning approaches versus the stochastic estimation and the empirical degradation in Scenario 1

Table 4.1: Average RA of the estimated centers of states and parameters by ZEKF versus EKF in scenario 1

States and Parameters	RA^{S1} %		
	ZEKF: λ^*_{LMI}	ZEKF: λ^*_c	EKF
$\hat{\mathcal{X}}_1$	99.99950	99.99950	99.99999
$\hat{\mathcal{X}}_2$	99.99276	99.99276	99.99996
$\hat{\mathcal{X}}_3$	99.99818	99.99818	99.99995
$\hat{\mathcal{X}}_4$	99.85852	99.85852	99.99089

RUL forecasting using the zonotopic linear EoL-RUL approach

The linear EoL-RUL approach has been applied based on the ZEKF as shown in Figure 4.4.

Remark 4.6.1. It is essential to recall throughout this thesis that the RLS-based approach with known degradation models could have been also applied using the zonotopic approach. However, we intend to examine, provide, and show a generalized case with unknown degradation behaviors on a system-level in order to characterize the threefold proposed PHM. Noting that a general degradation approach using recursive zonotopic prediction is proposed

in Chapter 5.

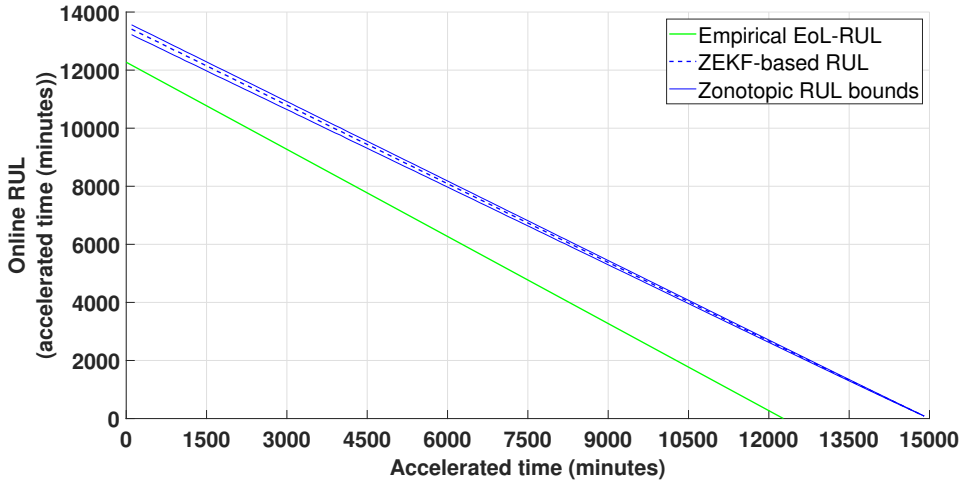

Figure 4.4: ZEKF-based RUL forecasting using the linear EoL-RUL approach versus the empirical RUL in Scenario 1

It is eventually clear that the gap difference between the true empirical RUL and the predicted RUL is larger than the safe zonotopic bounds. Consequently, the limitation of the unknown degradation behaviors could not guarantee a reliable RUL forecasting following the linear EoL-RUL approach in this scenario, despite the guaranteed zonotopic states and parameters. Consequently, these limitations build up the problematic that will be contributed to and solved in Chapter 5.

Nevertheless, scenario 3 will show different results due to the interdependent mutual degradation effects that will be explained in the following subsection.

4.6.2 Scenario 3

The empirical degradation models have been employed in order to simultaneously simulate the varying behaviors of the parameters as accomplished in the previous scenarios. Unknown-but-bounded noises and uncertainties have been defined as explained in (4.8). Thus, we intend in this scenario to test the reliability of the ZEKF for JESP with multiple-component degradation with a larger weight of noises compared to scenario 1, in order to emphasize on the robustness of the ZEKF observer. Hence, the direction matrices that

weigh the noises and uncertainties are given as:

$$\mathbf{E}_{\omega} = diag(1,\ 1,\ 2,\ 0.003,\ 0.035), \tag{4.44a}$$
$$\mathbf{E}_{\upsilon} = diag(0.01,\ 0.09). \tag{4.44b}$$

Results of the JESP by the ZEKF

The varying parameters in scenario 3 are propagated in form of zonotopes as $\hat{\mathrm{ESR}}_{\mathrm{o}} \in \hat{\mathcal{X}}_4$ and $\hat{R}_{\mathrm{ON}} \in \hat{\mathcal{X}}_5$. Thus, Figures 4.5a, 4.5b, and 4.5c illustrate the estimation of the zonotopic states using the ZEKF approach for JESP. Both tuning approaches have shown similar bounds in the first two estimated states along with the estimation of the EKF that follow the empirical degradation of the same states. However, as shown in Figure 4.5c, state 3 is bounded with some differences, the LMI-based tuning approach using λ^*_{LMI} has shown complete bounding during the whole degradation process as well as the classical online tuning approach using λ^*_{c}. Whereas, the upper bounds are close to the initial value of $\mathbf{x}_3$ using λ^*_{c}, opposing to the λ^*_{LMI}. The estimated bounds of the zonotope $\hat{\mathcal{X}}_3$ will not affect the RUL forecasting process nor the accuracy of the results since they cover all the degradation in an optimal way.

Moreover, Figures 4.6a, and 4.6b illustrate the estimated augmented parameters in form of zonotopes, and compared to the EKF estimation with the empirical degradation reference.
As shown in Figure 4.6a, the λ^*_{c}-tuned ZEKF has shown too conservative upper bounds which intersect the empirically-degraded model. Whereas, the λ^*_{LMI}-tuned approach has shown better results in terms estimated bounds that cover the whole degradation process with no violations. The estimated bounds using both tuning approaches have shown better results as shown in Figure 4.6b. The EKF clearly shows the least accurate JESP compared to the ZEKF, where the main focus is on the estimated parameters bounds that will be utilized in the following phase of RUL forecasting.

The previously illustrated results are evaluated in Table 4.2 by calculating the average RA to the center of the bounds using both tuning approaches, and the EKF estimation in comparison with the empirically-degraded states and parameters. Recalling that the estimated parameters are essential for RUL forecasting, the RA in the zonotopic approach is not essential since the estimated bounds are guaranteed starting from the healthy operation until reaching the EoL of each critical component. Thus, the zonotopic linear Eol-RUL approach is examined in the following part.

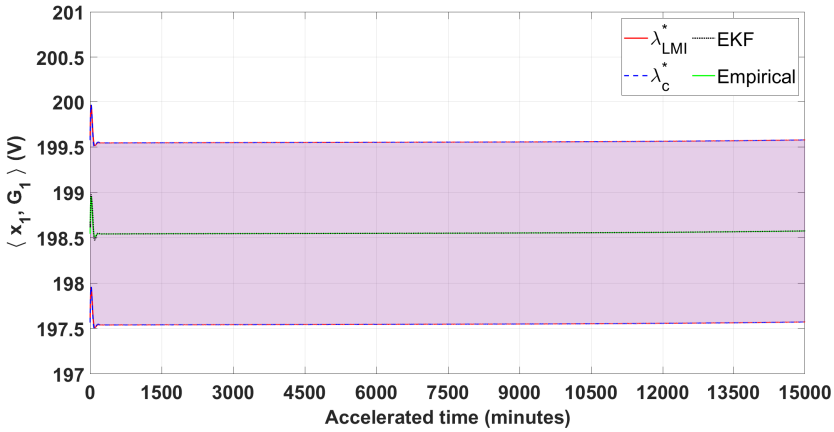

(a) $\hat{\mathcal{X}}_1$ with both tuning approaches versus the stochastic estimation and the empirical degradation in scenario 3

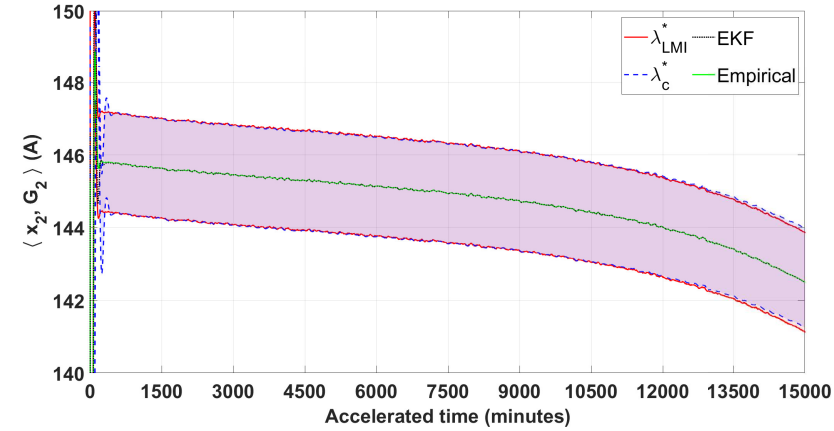

(b) $\hat{\mathcal{X}}_2$ with both tuning approaches versus the stochastic estimation and the empirical degradation in scenario 3

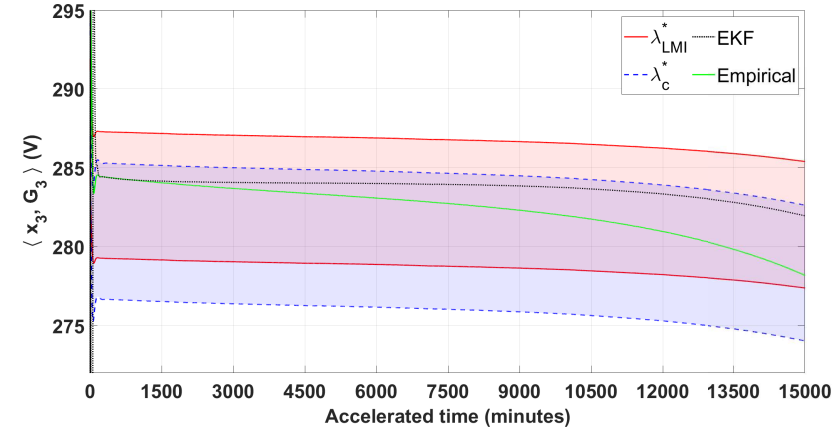

(c) $\hat{\mathcal{X}}_3$ with both tuning approaches versus the stochastic estimation and the empirical degradation in scenario 3

Figure 4.5: The estimated zonotopic states versus the corresponding stochastic estimation and the empirical degradation in scenario 3

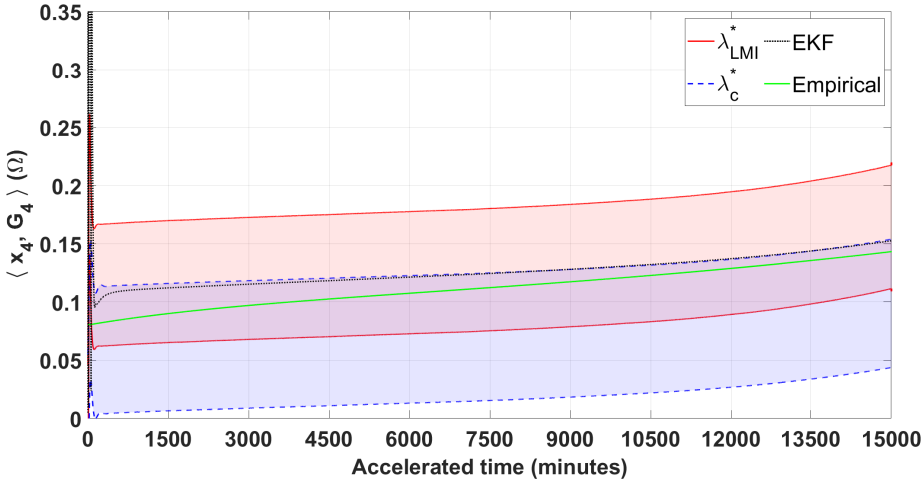

(a) $\hat{\mathcal{X}}_4$ with both tuning approaches versus the stochastic estimation and the empirical degradation in scenario 3

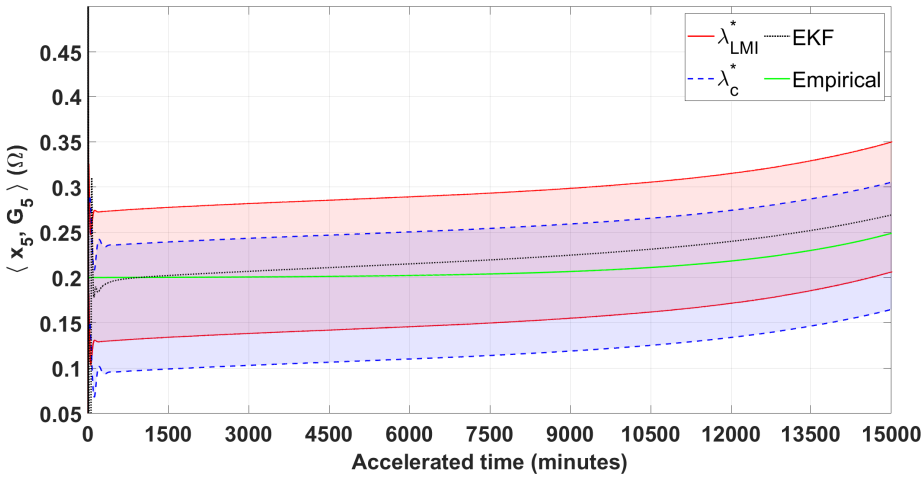

(b) $\hat{\mathcal{X}}_5$ with both tuning approaches versus the stochastic estimation and the empirical degradation in scenario 3

Figure 4.6: The estimated zonotopic parameters versus the corresponding stochastic estimation and the empirical degradation in scenario 3

Table 4.2: Average RA of the estimated centers of the zonotopic states and parameters by ZEKF versus EKF in scenario 3

States and Parameters	RA^{S3} %		
	ZEKF: λ^*_{LMI}	ZEKF: λ^*_c	EKF
$\hat{\mathcal{X}}_1$	99.99962	99.99954	99.99997
$\hat{\mathcal{X}}_2$	99.99033	99.89536	99.99670
$\hat{\mathcal{X}}_3$	95.63094	97.58018	95.81004
$\hat{\mathcal{X}}_4$	82.07027	64.81468	90.93163
$\hat{\mathcal{X}}_5$	91.84298	89.88081	93.82725

Zonotopic linear EoL-RUL approach for RUL forecasting

The application of the RUL forecasting approach depends on the estimated bounds of the augmented parameters $[\underline{\hat{\mathbf{G}}}_4, \overline{\hat{\mathbf{G}}}_4]$ and $[\underline{\hat{\mathbf{G}}}_5, \overline{\hat{\mathbf{G}}}_5]$.
Thus, Figure 4.7 illustrates the bounded RUL forecasting. As stated in Proposition 3.2.1, the SRUL is assumed to follow the CRUL of the FCCF. In this case, without considering any scheduled maintenance, the ESR_o has a shorter lifespan compared to the R_{ON}.

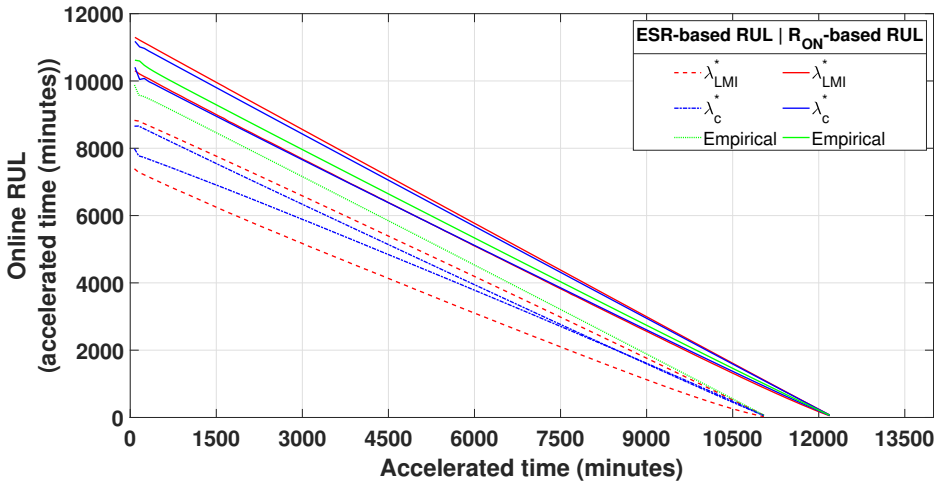

Figure 4.7: $[\underline{\tilde{\text{RUL}}}, \overline{\tilde{\text{RUL}}}]$ with both tuning approaches versus empirical RUL in scenario 3

Adopting the ZEKF-based estimation has affected the linear EoL-RUL approach, specifically in scenario 3. The RUL at each online measurement is bounded and converges towards the estimated EoL. The R_{ON}-based RUL forecasting shows complete bounding of the empirical EoL-RUL, with tighter bounds obtained using the classical online tuning approach of ZEKF. Furthermore, the ESR-based RUL forecasting has shown more conservative results with respect to the empirical EoL-RUL. For this reason, following the predicted RUL via the FCCF leads to a completely safe prediction, yet not optimal due to the major weakness of the intuitive expectation of the EoL, as mentioned in Chapter 3.

Table 4.3: The average RA of RUL forecasting of the scenario 3 for 80% of the actual EoL

Zonotopic EoL-RUL Approach	ESR-based $\tilde{\mathrm{RUL}}^{\mathrm{S3}}$ RA %	$R_{\mathrm{ON}}-$based $\tilde{\mathrm{RUL}}^{\mathrm{S3}}$ RA %
LMI-based tuning	82.033	97.7702
Classical online tuning	86.017	96.8746

Moreover, a numerical example of an online measurement at 6000 minutes is shown in Table 4.4, in order to compare among the predicted RUL and the empirical RUL.

Table 4.4: RUL forecasting intervals at an online measurement at 6000 minutes

Critical parameters at 6000 minutes		$\underline{\tilde{\mathrm{RUL}}}$	$\overline{\tilde{\mathrm{RUL}}}$	Empirical RUL
$\mathrm{ESR_o}$	λ^*_{LMI}	3091	4189	4491
	λ^*_{c}	3781	3940	
R_{ON}	λ^*_{LMI}	5120	5795	5600
	λ^*_{c}	5134	5704	

Therefore, the FCCF-based RUL interval at 6000 minutes of the acceler-

ated online measurement using the LMI-based approach, is $[\underline{\hat{\text{RUL}}}, \overline{\hat{\text{RUL}}}] = [3091, 4189]$ minutes.

4.6.3 Assessment of the proposed approaches

The main motivation of bounding the estimated parameters using zonotopic approaches have been investigated due to the unreliable parameters estimation of scenario 3 using the stochastic-based approaches. We based our proposition on the linear EoL-RUL relation that can forecast without the need of degradation models and reduced computations. For these reasons, we adopted the ZEKF in order to bound the estimated parameters which will indirectly provide bounded RUL prediction. By this proposition, we intended to guarantee a RUL enclosure. However, the zonotopes have shown a very reliable effect on the JESP in all conditions and scenarios, while the main issue is still related to the RUL forecasting approach which is affected by the EoL expectations in this case. As shown, the ESR-based RUL forecasting in scenario 3 has shown increased safety with reduced predicted lifecycle of the component. On the other hand, the RUL is still overpredicted in scenario 1 which increases the risk of a complete failure in the system.

To sum up, the zonotopes have provided a remarkable advantage by bounding the estimated parameters. The linear EoL-RUL approach is still affected by the EoL expectation and the RLS-based approach is a model-dependent technique and strongly related to the observed data. Therefore, it is crucial to keep the bounding of the JESP for the sake of guaranteed safety, in addition to the optimization advantages and the simple and reduced computations of zonotopes. Thus, it is also essential to develop a RUL forecasting approach that considers a general degradation model with reduced computations in order to provide predicted degradation and EoL. The aforementioned limitations will be developed in Chapter 5 in order to obtain a guaranteed RUL forecasting with guaranteed estimation in a generalized manner to achieve the main target of this thesis.

4.7 Conclusions

In this chapter, the RUL forecasting has been improved by providing a bounded safety margin for each concerned critical parameter of the system. The main contribution refers to the degradation estimation phase, where a ZEKF has been employed for JESP. The ZEKF merges between the reliability of the stochastic EKF and the deterministic zonotopic sets that deal with unknown-but-bounded noises and uncertainties. Additionally, this approach has been tuned by an LMI-based optimization problem that is solved offline with reduced computations. The main aim of adopting this approach was motivated by the unreliable degradation estimation resulted in scenario 3 for multiple-component degradation using the stochastic EKF. Moreover, the RUL forecasting can be improved by either stated approaches.

Furthermore, the online linearization of the nonlinear model has been improved for several reasons, and opted for an LPV representation. The later has been transformed from the Jacobian linearization as accomplished using the EKF, into a polytopic LPV for reduced computations and counting on the bounded parameters that characterize one of the pillars of the PHM features. In addition to that, an LPV model can be designed by various approaches in order to be employed for different engineering applications.

In conclusion, the elaboration of the ZEKF does not require complex implementation, and increases the overall efficiency of the JESP in addition to the bounded RUL forecasting. However, in scenario 3, the RUL forecasting was more conservative on a parameter over the other. The main reason behind this observation refers to the EoL-RUL approach condition as explained in Chapter 3. In consequence, we have proposed to investigate an approach that recursively predicts the degradation behaviors of the augmented parameters in a zonotopic framework with a general degradation model with reduced computations. This approach will follow the same structure of the ZEKF with considering each measured output separately and eliminating any intuitive condition. Chapter 5 is dedicated to explain the improvements on both the JESP and the zonotopic RUL forecasting approaches.

This page is intentionally left blank

CHAPTER 5

Zonotopic Set-Membership Approach for PHM with Recursive Zonotopic RUL Forecasting

Contents

5.1 Introduction

Building upon the proposed approaches in the previous chapters, this chapter contributes the RUL forecasting from a different perspective. The zonotopic integration in the estimation process has improved the RUL forecasting as well as the JESP by providing guaranteed bounds enclosure. Thus, as the linear EoL-RUL approach is based on an partially intuitive assumption, the RUL forecasting based on the EKF estimation were not reliable in terms of high fidelity to the prediction. Furthermore, the improved zonotopic RUL forecasting based on the ZEKF for JESP, has shown an interesting bounded RUL forecasting, specifically in scenario 3 where the EKF could not perform as reliable as the ZEKF approach. However, the improved reliability was too conservative in the zonotopic approach, which raises the importance of eliminating all the intuitive conditions. In other words, a trade-off between an increased complexity that yields a high reliability is essential to be adopted. For that reason, a ZSM for multi-output systems is implemented in this approach for JESP. Additionally, the RUL forecasting is reformulated for the sake of degradation prediction of the critical varying parameters.

The ZSM observer has been proposed for the JESP in this approach rather than the accuracy of the ZEKF as shown in Chapter 4. The set-based deterministic approach is based on a Luenberger observer and simply follows three main steps, the prediction, the measurement, and the correction. The main intention of implementing the ZSM observer is to investigate the effect of each measurement of the system on the JESP. Additionally, the states and parameters are estimated based on an intersection between certain sets of states and parameters, and the measurements at the current time instant. On the other hand, the ZEKF-based approach considers measurements from a previous time instant and follows the structure of an EKF. Moreover, the unknown-but-bounded noises are also considered in this case study as well as in many engineering applications (Schweppe 1968; Witsenhausen 1968; Bertsekas and Rhodes 1971; V. Le et al. 2013a; Merhy 2019).

The proposed RUL forecasting approach is the turning point in this chapter. Hence, we recursively reformulated the steps of the second and third phases of the proposed model-based PHM approach. Furthermore, instead of directly

This chapter is based on the following publications: (Al-Mohamad, V. Puig, and Hoblos 2021b; Al-Mohamad, V. Puig, and Hoblos 2021a).

implementing the polynomial approach using the RLS filter for degradation prediction, or following the intuitive linear EoL-RUL approach, we have proposed to indirectly forecast the linear RUL with reduced computations using a generalized degradation model that can cope with such applications. The most common degradation evolution follows an exponential decay which will add a complex computational burden to design a recursive observer that can be avoidable for the sake of real-time prognostics. Therefore, a RZSM approach has been proposed in order to homogenize the degradation estimation via the ZSM for JESP with the degradation and EoL prediction following a general degradation model with reduced computations. The main objective of such implementation is to employ the same estimation technique for the prediction as well in a zonotopic framework that provides bounded RUL. Finally, the predicted degradation bounds are intersected with the TH of each critical component, and the EoL is then predicted online at each measurement instant.

Moreover, according to previous statements, the LPV model representation is practically and theoretically efficient to be employed for the prognostics applications. Thus, the ZSM observer that allows the estimation of states and parameters by intersecting with each output measurement of the system is provided to guarantee the zonotopic inclusion. Hence, the ZSM observer for JESP is also tuned using the LMI-based optimization, as explained in Chapter 4.

In this context, the aim of this chapter is to guarantee the zonotopic inclusion for JESP and predict the degradation recursively, with reduced effort for real-time applications in a homogeneous deterministic approach.

This chapter is structured as follows. Section 5.2 addresses the problem formulation. Hence, the multi-output ZSM observer is designed in Section 5.3. Section 5.4 is dedicated to the recursive zonotopic RUL forecasting. The algorithm of this proposed methodology is shown in Section 5.5. Thus, a case-study featuring a DC-DC converter with degraded components is assessed, and the results are illustrated in Section 5.6. Finally, the conclusions are drawn in Section 5.7.

5.2 PHM Problem Formulation in ZSM and RZSM Framework

Based on the aforementioned improvements regarding the ZSM for JESP and the homogenization with the RUL forecasting approach, this chapter extensively investigates a ZSM-RZSM approach in a zonotopic LPV framework. The major key points in this chapter are related to the multi-output observer structure that requires several intersection, in addition to the RZSM for parameters estimation design for a general degradation model.
Thus, Figure 5.1 highlights the improved overall proposed model-based PHM approach of this chapter.

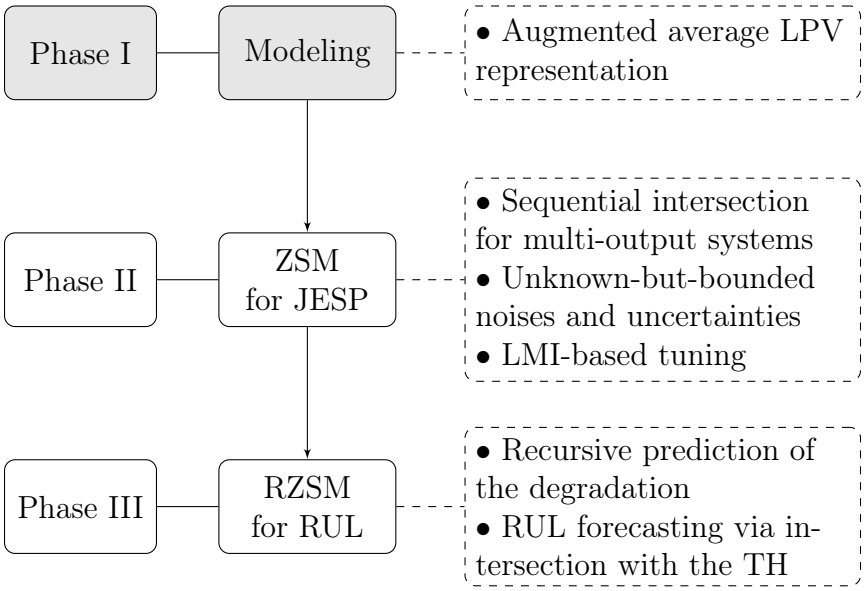

Figure 5.1: ZSM-based PHM

1. *System modeling:* The system is represented in an LPV framework as explained in Chapter 4.

2. *ZSM for JESP:* The most crucial phase in the model-based PHM approach has been handled by the proposed ZSM observer that is specially designed for multi-output systems. It predicts uncertain states and parameters that will be intersected with a measurement strip of each output at the current time instant, in order to estimate the certain zonotopic states and parameters. Similar to the ZEKF, the ZSM is also

tuned with an LMI-based optimization approach and compared to the online gain scheduling method.

3. *RZSM for RUL forecasting:* The RZSM for degradation prediction and RUL forecasting is designed based on the investigations of the previous chapters. Firstly, the linear EoL-RUL approach is intuitive and is not guaranteed in some situations. Secondly, the classic RUL forecasting approach depends on the exact known models, and the degradation prediction is misleading with less observations. For all these reasons, we propose to adopt a general exponential degradation model in a logarithmic form to recursively predict the degradation. Thus, zonotopes play an important role in this approach due to the fact that the estimation is guaranteed in ZSM which will guarantee the parameter estimation in the RZSM. Finally, the bounded RUL forecasting is accomplished online in a zonotopic homogeneous framework.

The contribution to such challenging approaches requires strong knowledge of systems being dealt with. The cascading damage caused by the degradation of a critical component, affects the behavior of the whole system including the internal parameters, the input, and the output variables. Moreover, since no direct measurement is considered at a component-level, the degradation estimation plays an essential role in the RUL prediction towards a system-level. Additionally, the promising applications of zonotopes lead to a step further from estimation to prediction by designing a RZSM observer. The latter shows some technical similarities with the RLS filter, and it is employed to predict the degradation equations without prior knowledge and based on estimated data only. Finally, the aforementioned characteristics are designed and implemented in an LPV model with the assumption of unknown-but-bounded noises and uncertainties.

5.3 ZSM-based JESP observer design for multi-output systems

Given the multi-output LPV model in (4.6), the consistent state-bounding zonotope $\hat{\mathcal{X}}_{i_k}$ at each component of the measured output y_{i_k} can be obtained based on *Luenberger observer* as follows:

$$\hat{\mathcal{X}}_{i_k} = \hat{\mathbf{x}}^{\mathrm{c}}_{i_k} \oplus \hat{\mathbf{G}}_{i_k} \mathcal{B}^{m+n_x+n_y}, \tag{5.1}$$

where,

$$\hat{\mathbf{x}}^{\mathrm{c}}_{i_k} = \tilde{\mathbf{x}}^{\mathrm{c}}_{i_k} + \lambda_{i_k}(y_{i_k} - (\mathbf{C}_{i_k}\tilde{\mathbf{x}}^{\mathrm{c}}_{i_k} + \mathbf{D}_{i_k}\mathbf{u}_k)), \tag{5.2a}$$

$$\hat{\mathbf{G}}_{ik} = [(\mathbf{I} - \lambda_{i_k}\mathbf{C}_{i_k})\tilde{\mathbf{G}}_{i_k} \quad -\lambda_{i_k}\mathbf{E}_{\upsilon}], \tag{5.2b}$$

with,

$$\tilde{\mathbf{x}}^{\mathrm{c}}_{k} = \mathbf{A}_{k-1}\hat{\mathbf{x}}^{\mathrm{c}}_{k-1} + \mathbf{B}_{k-1}\mathbf{u}_{k-1}, \tag{5.3a}$$

$$\tilde{\mathbf{G}}_{k} = [\mathbf{A}_{k-1}\hat{\mathbf{G}}_{k-1} \quad \mathbf{E}_{\omega}], \tag{5.3b}$$

where $\hat{\mathbf{x}}^{\mathrm{c}}_k$ is the estimated center of the consistent state-bounding zonotope, $\hat{\mathbf{G}}_k$ denotes its generator matrix, $\tilde{\mathbf{x}}^{\mathrm{c}}_k$ denotes the center of the uncertain predicted zonotope $\tilde{\mathcal{X}}_k$, and λ is the tuning matrix that is extensively explained throughout this section. i refers to the i^{th} output component at each time sample k.

Remark 5.3.1. For simplification purposes $\hat{\mathbf{x}}^{\mathrm{c}}_k$ will be denoted by the states vector $\hat{\mathbf{x}}_k$ which is considered as the center of the state zonotopic set $\hat{\mathcal{X}}_k$, and similarly for $\tilde{\mathbf{x}}^{\mathrm{c}}_k$ and all the other zonotopes in this chapter.

Figure 5.2 illustrates the JESP using ZSM approach. It shows the intersection between the predicted state-bounding zonotope at k based on the $k-1$ exact estimation with the measurement strip at k.

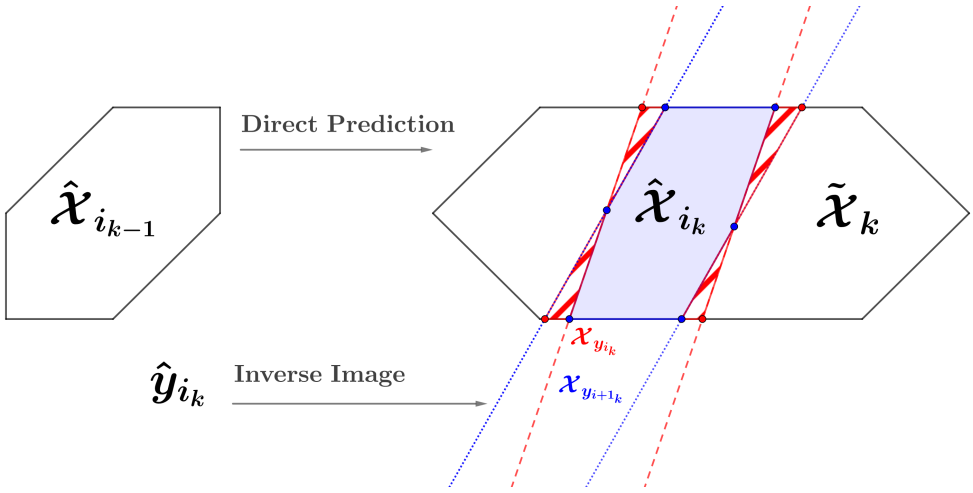

Figure 5.2: Diagram of the ZSM approach for multi-output systems

In broad, the consistent state-bounding zonotope $\hat{\mathcal{X}}_{i_k}$ is estimated by intersecting the *predicted state set* $\tilde{\mathcal{X}}_k$ with the *consistent measurement state set* $\mathcal{X}_{\mathbf{y}_{i_k}}$ using the known measurement $\mathbf{y}_{i_k}$. Therefore, the three required steps for a guaranteed estimation are explained in the following.

Theorem 5.3.1 (*Prediction* (T. Alamo, Bravo, and Camacho 2005; Combastel 2005; V. Le et al. 2013a; V. Le et al. 2013b))**.** *The predicted state set* $\tilde{\mathcal{X}}_k = \langle \tilde{\mathbf{x}}_k, \tilde{\mathbf{G}}_k \rangle$*, is bounded in a zonotopic form to limit the number of uncertain states in the prediction based on the previous exact uncertain estimation* $\hat{\mathcal{X}}_{k-1}$*, and on an actual output measurement* $\mathbf{y}_k$ *(Combastel 2003). Thus, the predicted state set is defined as follows:*

$$\begin{aligned}
\tilde{\mathcal{X}}_k &= \mathbf{A}_{k-1}\hat{\mathcal{X}}_{k-1} + \mathbf{B}_{k-1}\mathbf{u}_{k-1} \oplus \mathcal{W} \\
&= \mathbf{A}_{k-1}(\hat{\mathbf{x}}_{k-1} \oplus \hat{\mathbf{G}}_{k-1}\mathcal{B}^m) + \mathbf{B}_{k-1}\mathbf{u}_{k-1} \oplus \mathbf{E}_\omega \mathcal{B}^{n_x} \\
&= \mathbf{A}_{k-1}\hat{\mathbf{x}}_{k-1} \oplus \mathbf{A}_{k-1}\hat{\mathbf{G}}_{k-1}\mathcal{B}^m + \mathbf{B}_{k-1}\mathbf{u}_{k-1} \oplus \mathbf{E}_\omega \mathcal{B}^{n_x} \\
&= (\mathbf{A}_{k-1}\hat{\mathbf{x}}_{k-1} + \mathbf{B}_{k-1}\mathbf{u}_{k-1}) \oplus [\mathbf{A}_{k-1}\hat{\mathbf{G}}_{k-1} \quad \mathbf{E}_\omega]\mathcal{B}^{m+n_x} \\
&= \tilde{\mathbf{x}}_k \oplus \tilde{\mathbf{G}}_k \mathcal{B}^{m+n_x},
\end{aligned} \tag{5.4}$$

where $\tilde{\mathbf{x}}_k = \mathbf{A}_{k-1}\hat{\mathbf{x}}_{k-1} + \mathbf{B}_{k-1}\mathbf{u}_{k-1}$ and $\tilde{\mathbf{G}}_k = [\mathbf{A}_{k-1}\hat{\mathbf{G}}_{k-1} \quad \mathbf{E}_\omega]$ are the center and the generator matrix of the prediction state set $\tilde{\mathcal{X}}_k$ respectively.

Remark 5.3.2. The computation of the predicted state set is similar for single-output and multi-output systems.

Theorem 5.3.2 (*Measurement Strip* (T. Alamo, Bravo, and Camacho 2005; Combastel 2005; V. Le et al. 2013a; V. Le et al. 2013b))**.** *Given each measurement* y_{i_k} *of the measurements vector* $\mathbf{y}_k$ *at time instant* k *of the same model, the consistent measurement set* $\mathcal{X}_{y_{i_k}}$ *denoting the strip, is computed as follows:*

$$\mathcal{X}_{y_{i_k}} = \{\mathbf{x} \in \mathbb{R}^{n_x} : |y_{i_k} - (\mathbf{C}_{i_k}\mathbf{x}_k + \mathbf{D}_{i_k}\mathbf{u}_k)| \leq \mathbf{E}_{v_i}\}, \tag{5.5}$$

where $\mathbf{C}_{i_k}^\intercal$ *is a vector of the* i^{th} *row of the matrix* $\mathbf{C}_k$ *at time instant* k*. Based on Definition A.2.13, the estimated consistent zonotope* (5.1) *is obtained by intersecting the uncertain predicted zonotope* (5.4) *and the strip* (5.5) *as:*

$$\begin{aligned}
\hat{\mathcal{X}}_{i_k} &= \tilde{\mathcal{X}}_k \cap \mathcal{X}_{\mathbf{y}_{i_k}} \\
&= \langle \hat{\mathbf{x}}_{i_k}, \hat{\mathbf{G}}_{i_k} \rangle,
\end{aligned} \tag{5.6}$$

Proposition 5.3.1 (Multiple strip intersection for multiple outputs (T. Alamo, Bravo, and Camacho 2005))**.** For a guaranteed zonotopic inclusion, the intersection between the measurement strip $\mathcal{X}_{y_{i_k}}$ of each of the output components, and the predicted state-bounding set $\tilde{\mathcal{X}}_k$ is successively repeated for $i = 1, \ldots, n_y$ at each time sample k.

Proof. The guaranteed state estimation set $\hat{\mathcal{X}}_k$ for multi-output systems is obtained by repeating the zonotopic intersection between the strip of a particular output component $y_{k,i}$ and the uncertain predicted state set $\tilde{\mathcal{X}}_k$ (Vu Tuan Hieu Le et al. 2013; V. T. H. Le et al. 2013). Thus, the output vector $\mathbf{y}_k$ for n_y measured components is defined as follows:

$$\mathbf{y}_k = \sum_{i=1}^{n_y} \mathbf{C}_i \mathbf{x}_{i_k} + \mathbf{D}_{i_k} \mathbf{u}_k + \mathbf{E}_{v_i} v_{i_k}, \quad i = 1, \ldots, n_y. \tag{5.7}$$

The first intersection between the strip of the first output component $\mathcal{X}_{y_{i_k}}$ and the predicted sate set $\tilde{\mathcal{X}}_k$ results the following consistent estimated zonotopic state set:

$$\hat{\mathcal{X}}_{1_k}(\lambda_{1_k}) = \hat{\mathbf{x}}_{1_k}(\lambda_{1_k}) \oplus \hat{\mathbf{G}}_{1_k}(\lambda_{1_k}) \mathcal{B}^{m+n_x+1}, \tag{5.8}$$

where,

$$\begin{aligned} \hat{\mathbf{x}}_{1_k}(\lambda_{1_k}) &= \mathbf{A}_{k-1}\hat{\mathbf{x}}_{k-1} + \mathbf{B}_{k-1}\mathbf{u}_{k-1} \\ &\quad + \lambda_{1_k}(y_{1_k} - (\mathbf{C}_{1_k}(\mathbf{A}_{k-1}\hat{\mathbf{x}}_{k-1} + \mathbf{B}_{k-1}\mathbf{u}_{k-1}) + \mathbf{D}_{1_k}\mathbf{u}_k)), \end{aligned} \tag{5.9a}$$

$$\hat{\mathbf{G}}_{1_k}(\lambda_{1_k}) = [(\mathbf{I} - \lambda_{1_k}\mathbf{C}_{1_k})\mathbf{A}_{k-1}\hat{\mathbf{G}}_{k-1} \quad (\mathbf{I} - \lambda_{1_k}\mathbf{C}_{1_k})\mathbf{E}_{\omega_1} \quad -\lambda_{1_k}\mathbf{E}_{v_1}], \tag{5.9b}$$

therefore, the obtained $\hat{\mathcal{X}}_{k,1}(\lambda_{k,1})$ from the first intersection at k will be intersected with the strip of the following output component $y_{k,2}$ as follows:

$$\hat{\mathcal{X}}_{2_k}(\lambda_{1_k}, \lambda_{2_k}) = \hat{\mathbf{x}}_{2_k}(\lambda_{1_k}, \lambda_{2_k}) \oplus \hat{\mathbf{G}}_{2_k}(\lambda_{1_k}, \lambda_{2_k}) \mathcal{B}^{m+n_x+2}, \tag{5.10}$$

where,

$$\hat{\mathbf{x}}_{2_k}(\lambda_{1_k}, \lambda_{2_k}) = \hat{\mathbf{x}}_{1_k}(\lambda_{1_k}) + \lambda_{2_k}(y_{2_k} - (\mathbf{C}_{2_k}\hat{\mathbf{x}}_{1_k} + \mathbf{D}_{2_k}\mathbf{u}_k), \tag{5.11a}$$

$$\hat{\mathbf{G}}_{2_k}(\lambda_{1_k}, \lambda_{2_k}) = [(\mathbf{I} - \lambda_{2_k}\mathbf{C}_{2_k})\hat{\mathbf{G}}_{1_k}(\lambda_{1_k}) \quad -\lambda_{2_k}\mathbf{E}_{v_2}]. \tag{5.11b}$$

Then, repeat this correction step with every output component $y_{k,i}$ of $\mathbf{y}_k$ until n_y in order to obtain the consistent estimated state zonotopic set with guaranteed inclusion, at each time instant k as:

$$\hat{\mathcal{X}}_{n_{y_k}}(\lambda_1, \ldots, \lambda_{n_y}) = \hat{\mathbf{x}}_{n_{y_k}}(\lambda_1, \ldots, \lambda_{n_y}) \oplus \hat{\mathbf{G}}_{n_{y_k}}(\lambda_1, \ldots, \lambda_{n_y}) \mathcal{B}^{m+n_x+n_y}, \tag{5.12}$$

where,

$$\begin{aligned} \hat{\mathbf{x}}_{n_{y_k}}(\lambda_{\mathbf{1}}, \ldots, \lambda_{n_y}) &= \hat{\mathbf{x}}_{n_y-1_k}(\lambda_{\mathbf{1}}, \ldots, \lambda_{n_y-1}) \\ &\quad + \lambda_{n_{y_k}}(y_{n_{y_k}} - (\mathbf{C}_{n_{y_k}}\hat{\mathbf{x}}_{n_y-1_k}(\lambda_{\mathbf{1}}, \ldots, \lambda_{n_y}) + \mathbf{D}_{n_{y_k}}\mathbf{u}_k), \end{aligned} \tag{5.13a}$$

$$\hat{\mathbf{G}}_{n_{y_k}}(\lambda_{\mathbf{1}}, \ldots, \lambda_{n_y}) = [(\mathbf{I} - \lambda_{n_{y_k}}\mathbf{C}_{n_{y_k}})\hat{\mathbf{G}}_{n_y-1_k}(\lambda_1, \ldots, \lambda_{n_y}) \quad -\lambda_{n_{y_k}}\mathbf{E}_{v_{n_y}}]. \tag{5.13b}$$

Hence, the guaranteed state zonotopic set is finally obtained as in (5.1). □

Moreover, the tuning matrix λ is crucial to guarantee the inclusion of the zonotopes A.2.7, in addition to the size reduction operator that provides less computational complexity for the benefits of real-time estimation and forecasting. The following subsection is dedicated to characterize this matter.

5.3.1 ZSM observer tuning

The proposed LMI-based optimization problem is also employed to tune the ZSM observer as shown in Subsection 4.3.1, and has been compared to the classical tuning approach as shown in Subsection 4.3.2.

5.4 RZSM for RUL Forecasting

The objectives of the RZSM are fulfilled by the following steps:

1. Proposition of an exponential degradation model with unknown parameters (α).
2. Transformation of the exponential degradation model into a state-space model.
3. Estimation of the parameters α using the ZSM approach for parameters estimation.
4. Propagation of the bounds of the estimated zonotopic degradation parameters.
5. Prediction of the bounded degradation trajectories using the RZSM approach.
6. Intersection between the predicted profiles and the TH of each component to obtain the bounded EoL.
7. Forecasting of the bounded RUL of the system.

5.4.1 Prediction of degradation trajectories

The proposed strategy of RUL forecasting in this chapter is the improved version of the previously-investigated approaches in Chapters 3 and 4. The main difference between the classical polynomial approach and the proposed RZSM is that the 5-degree polynomial degradation model has been eliminated by transforming a general exponential decay form into a logarithmic regressor. Hence, the later is then modeled in a state-space representation

in order to employ the zonotopic parameters estimation. The main motivation of this approach is based on the fact that the electronic components degrade with exponential trend. Consequently, this approach can be utilized to predict the degradation of the critical components through their failure precursors. Most importantly, since the parameters estimation is guaranteed, the RUL forecasting reliability will increase compared to the previous approaches. Thus, it is worth mentioning that the logarithmic representation of the degradation requires less computation with reduced unknown parameters.

Assumption 5.4.1. The degradation behavior of each and every parameter is always considered as an unknown exponential trend. Consequently, the historical degradation data and EoL expectations are not needed for any part of the RUL forecasting step.

Proposition 5.4.1 (Degradation trajectory prediction using a linearized general exponential degradation model)**.** The final discrete-time state-space model that describes an exponential degradation is written as:

$$\mathbf{x}_{\alpha_{i_{k+1}}} = \mathbf{A}_{\alpha}\mathbf{x}_{\alpha_{i_k}}, \tag{5.14a}$$

$$y_{\alpha_{i_k}} = \mathbf{C}_{\alpha_k}\alpha_{i_k}, \tag{5.14b}$$

where,

$$\mathbf{A}_{\alpha} = \mathbf{I}, \tag{5.15a}$$

$$y_{\alpha_{i_k}} = \ln\left(\hat{\rho}_{i_k} - \rho_{0_i}\right), \tag{5.15b}$$

$$\mathbf{C}_{\alpha_k} = \begin{bmatrix} 1 & kT_s \end{bmatrix}, \tag{5.15c}$$

with $\hat{\rho}_{i_k}$ is the previously estimated parameter using the ZSM approach. $\mathbf{x}_{\alpha_{i_k}}$ is the parameter vector of the exponential degradation equation.

Proof. Let the following exponential equation describe the degradation of each augmented component denoted by ρ_i, and previously estimated as a zonotope using the JESP using the ZSM approach:

$$\Delta\rho_i(t) \equiv \rho_i(t) - \rho_{0_i} = \alpha_{1_i} e^{\alpha_{2_i} t}, \tag{5.16}$$

where $\Delta\rho_i(t)$ is the difference between the actual value of the parameter ρ_i at time instant t and the rated value of the same parameter ρ_{0_i}. It should be noted that α_1 and α_2 are the two unknown parameters that will be estimated using the RZSM applied to the state-space model (5.14).
Thus, it is rewritten in a logarithmic form as:

$$\ln\left(\rho_i(t) - \rho_{0_i}\right) = \ln\left(\alpha_{1_i}\right) + \alpha_{2_i} t, \tag{5.17}$$

then, it is discretized for the purpose of transforming it to a state-space model, so that the intended RZSM would be applied:

$$\ln\left(\rho_{i_k} - \rho_{0_i}\right) = \ln\left(\alpha_{1_{i_k}}\right) + \alpha_{2_{i_k}} kT_s. \tag{5.18}$$

Furthermore, given the fact that ρ_{i_k} is a varying parameter that is estimated as a zonotope at each iteration as explained in Section 5.3, and ρ_{0_i} is known as the rated value of each parameter. Thus, in order to differentiate between the ZSM for JESP and the RZSM for the degradation parameters estimation, the previously estimated parameter is denoted by $\hat{\rho}_{i_k}^{\text{ZSM}} \in \hat{\mathcal{X}}_{\rho_{i_k}}$, and is guaranteed by ZSM A.2.7.
Hence, the degradation model (5.18) is rewritten in a matrix multiplication form in order to reformulate it as a state-space:

$$\underbrace{\ln\left(\hat{\rho}_{i_k}^{\text{ZSM}} - \rho_{0_i}\right)}_{\mathbf{y}_{\rho_{i_k}}} = \underbrace{\begin{bmatrix}1 & kT_s\end{bmatrix}}_{\mathbf{C}_{\alpha_{i_k}}} \underbrace{\begin{bmatrix}\ln\left(\alpha_{1_{i_k}}\right) & \alpha_{2_{i_k}}\end{bmatrix}^{\intercal}}_{\mathbf{x}_{\alpha_{i_k}}^{\intercal}}, \tag{5.19}$$

where $\ln\left(\hat{\rho}_{i_k}^{\text{ZSM}} - \rho_{0_i}\right)$ is considered as the output measurement component $\mathbf{y}_{\rho_{i_k}}$ which is already estimated in our case. Thus, $\begin{bmatrix}\ln\left(\alpha_{1_{i_k}}\right) & \alpha_{2_{i_k}}\end{bmatrix}^{\intercal}$ is the vector containing the parameters $\mathbf{x}_{\alpha_{i_k}}^{\intercal}$ to be estimated using the RZSM. $\begin{bmatrix}1 & kT_s\end{bmatrix}$ is the output vector $\mathbf{C}_{\alpha_{i_k}}$ that varies in function of the time instant k.

Furthermore, there is no external input components affecting the degradation model as shown in (5.16) and in (5.19). Since the variations $\hat{\rho}_{i_{k+1}}^{\text{ZSM}} - \hat{\rho}_{i_k}^{\text{ZSM}}$ are very small, the variations of the degradation parameters are therefore small, and $\mathbf{x}_{\alpha_{i_{k+1}}} \approx \mathbf{x}_{\alpha_{i_k}}$. In consequence, $\mathbf{A}_\alpha = \mathbf{I}$, $\mathbf{u}_\alpha = 0$ and the state-space model of the degradation equation is obtained as shown in (5.14).

It is worth noting that the index i is introduced so that the degradation model (5.19) with its state-space model can be applied to more augmented critical parameters that describe the degradation of the components. □

Moreover, the parameters α_{1_i} and α_{2_i} of the model (5.14) are estimated using the ZSM technique as shown in (5.2) in the first step of the RZSM approach, with obvious adaptations. Finally, the estimated zonotopes of the parameters are obtained as:

$$\hat{\mathcal{X}}_{\alpha_{i_k}} = \langle \hat{\mathbf{x}}_{\alpha_{i_k}}, \hat{\mathbf{G}}_{\alpha_{i_k}} \rangle. \tag{5.20}$$

Remark 5.4.1. The RZSM for degradation parameters estimation do not require multiple-intersection process. Additionally, since the estimated parameters ρ by the previous ZSM for JESP are guaranteed and robust due to

the LMI-based optimization, we propose to tune the RZSM with the classical gain as follows:

$$\mathbf{L}_{\alpha_{i_k}} = \frac{(\hat{\mathbf{G}}_{\alpha_{i_k}} \hat{\mathbf{G}}^{\intercal}_{\alpha_{i_k}})\mathbf{C}_{\alpha_{i_k}}}{\mathbf{C}^{\intercal}_{\alpha_{i_k}}(\hat{\mathbf{G}}_{\alpha_{i_k}} \hat{\mathbf{G}}^{\intercal}_{\alpha_{i_k}})\mathbf{C}_{\alpha_{i_k}} + \mathbf{I}_{n^\alpha}}. \tag{5.21}$$

5.4.2 RUL forecasting based on the RZSM approach

The degradation prediction of the varying critical parameters ρ is recursively computed based on the previously-estimated degradation parameters in form of zonotopes $\hat{\mathcal{X}}_{\alpha_{i_k}}$. Therefore, the degradation profile of the proposed degradation model (5.16) will be predicted online starting from the k^{th} time instant that is assigned to the current measurement t_{current} as:

$$\tilde{\mathbf{x}}_{\rho_{i_{[k\to N]}}} = \rho_{0_i} + \hat{\alpha}_{1_i} e^{\hat{\alpha}_{2_i}[k+1\to N]}, \tag{5.22}$$

where $\tilde{\mathbf{x}}_{\rho_{i_{[k\to N]}}}$ is the predicted degradation starting from the current observation k which represents the t_{current} until N time units. Hence, $N \geq t_{\text{EoL}}$ is computed once an intersection between TH and the predicted degradation trajectory is detected. i refers to each varying parameter ρ_i.

Moreover, the bounds of the degradation parameters α are computed as follows:

$$[\underline{\hat{\alpha}}_{1_i},\ \overline{\hat{\alpha}}_{1_i}] = [\min\ (\hat{\mathbf{G}}_{\alpha_{i_k}}),\ \max\ (\hat{\mathbf{G}}_{\alpha_{i_k}})], \tag{5.23a}$$

$$[\underline{\hat{\alpha}}_{2_i},\ \overline{\hat{\alpha}}_{2_i}] = [\min\ (\hat{\mathbf{G}}_{\alpha_{i_k}}),\ \max\ (\hat{\mathbf{G}}_{\alpha_{i_k}})]. \tag{5.23b}$$

Next, the bounded degradation models are predicted by substituting (5.23) with (5.22) as:

$$\underline{\tilde{\mathbf{x}}}_{\rho_{i_{[k\to N]}}} = \rho_{0_i} + \underline{\hat{\alpha}}_{1_i} e^{\underline{\hat{\alpha}}_{2_i}[k+1\to N]}, \tag{5.24a}$$

$$\overline{\tilde{\mathbf{x}}}_{\rho_{i_{[k\to N]}}} = \rho_{0_i} + \overline{\hat{\alpha}}_{1_i} e^{\overline{\hat{\alpha}}_{2_i}[k+1\to N]}. \tag{5.24b}$$

Finally, the bounded EoL is computed by intersecting the bounded degradation models (5.24) with the TH_{ρ_i} of each degraded component as shown in Chapter 2 and Chapter 3:

$$\underline{\tilde{\text{EoL}}}_{i_k} \ :\ \underline{\tilde{\mathbf{x}}}_{\rho_{i_{[k\to N]}}} \ \cap\ \text{TH}_{\rho_i}, \quad k \leq \text{EoL}_{i_k} < N, \tag{5.25a}$$

$$\overline{\tilde{\text{EoL}}}_{i_k} \ :\ \overline{\tilde{\mathbf{x}}}_{\rho_{i_{[k\to N]}}} \ \cap\ \text{TH}_{\rho_i}, \quad k \leq \text{EoL}_{i_k} < N, \tag{5.25b}$$

where the predicted bounded EoL of each component are denoted by $\underline{\tilde{\text{EoL}}}_{i_k}$ and $\overline{\tilde{\text{EoL}}}_{i_k}$ for the lower and higher bounds respectively which are predicted

at time instant k for the varying parameter ρ_i. Therefore, the predicted EoL bounds are referred to the actual continuous time units (accelerated minutes in this case study), as $[\underline{\tilde{t}}_{\mathrm{EoL}_{i_k}}, \tilde{\bar{t}}_{\mathrm{EoL}_{i_k}}]$. Consequently, the bounded RUL are predicted as shown in Figure 5.3.

$$\underline{\tilde{t}}_{\mathrm{RUL}_{i_k}} = \underline{\tilde{t}}_{\mathrm{EoL}_{i_k}} - t_{\mathrm{current}}, \tag{5.26a}$$

$$\tilde{\bar{t}}_{\mathrm{RUL}_{i_k}} = \tilde{\bar{t}}_{\mathrm{EoL}_{i_k}} - t_{\mathrm{current}}. \tag{5.26b}$$

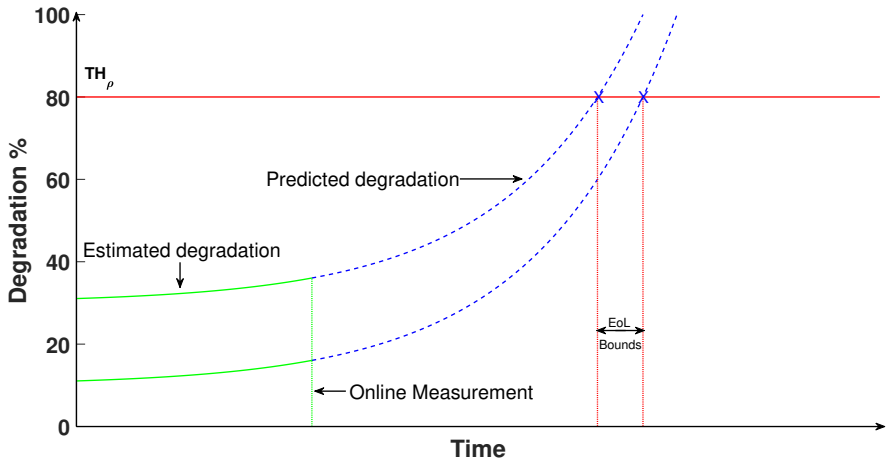

Figure 5.3: Bounded RUL demonstration

5.5 Homogeneous Algorithm of ZSM and RZSM

The full algorithm of the final proposed PHM approach in this thesis, is based on ZSM for JESP and RZSM for degradation and EoL prediction, and detailed in 4.

Algorithm 4: ZSM for JESP and RZSM for RUL Forecasting

Result: $[\underline{\tilde{t}}_{\text{RUL}}, \overline{\tilde{t}}_{\text{RUL}}]$
Initialization: $\tilde{\mathcal{X}}$, $\mathbf{E}_\omega$, $\mathbf{E}_v$, $\mathcal{W}$, $\mathcal{V}$, ρ, α;
Solve the LMI-based optimization problem offline and return $2^{n_\rho}\lambda$ (4.12c);
for $k = 1 : N$ **do**
  Compute $\mathbf{A}_k, \mathbf{B}_k, \mathbf{C}_k, \mathbf{D}_k$;
  Online bounding box approach to calculate $\lambda^\star_{i_k}$ (4.32);
  Prediction of the state vector center $\tilde{\mathbf{x}}_k$ (5.3a) and the generator matrix $\tilde{\mathbf{G}}_k$ (5.3b) of $\tilde{\mathcal{X}}_k$ (5.4);
  while $i \leq n_y$ **do**
    Computation of the strip $\mathcal{X}_{y_{i_k}}$ of measurement i (5.5);
    Intersection between $\tilde{\mathcal{X}}_k$ and $\mathcal{X}_{y_{i_k}}$ (5.6);
    Estimation of the state vector center $\hat{\mathbf{x}}_{i_k}$ (5.2a) and the generator matrix $\hat{\mathbf{G}}_{i_k}$ (5.2b) of $\hat{\mathcal{X}}_{i_k}$ (5.1);
    Application of the reduction operator $\downarrow_{q,W} \hat{\mathbf{G}}_{i_k}$;
    Repeat (5.12) until achieving the intersections with all the measurement outputs;
  end
  return $\hat{\mathcal{X}}_k$;
  Comment: *Based on the proposed degradation model, the RZSM runs with a single-time intersection*;
  Computation of the regressor vector $\mathbf{C}_{\alpha_k}$ and the output measurement $\mathbf{y}_{\alpha_k}$ (5.19);
  Prediction of the degradation coefficients center $\tilde{\mathbf{x}}_{\alpha_k}$ and their generator matrices $\tilde{\mathbf{G}}_{\alpha_k}$ of the zonotope $\tilde{\mathcal{X}}_{\alpha_k}$ of (5.15), by following the same structure of the ZSM in (5.3) for α parameters;
  Computation of the tuning matrix $\mathbf{L}_{\alpha_k}$ (5.21);
  Estimation of the degradation coefficients, the center $\hat{\mathbf{x}}_{\alpha_k}$, and their generator matrices $\hat{\mathbf{G}}_{\alpha_k}$ of the zonotope $\hat{\mathcal{X}}_{\alpha_k}$ in (5.20) by following the same structure of the ZSM in (5.2), for α parameters;
  Application of the reduction operator $\downarrow_q \hat{\mathbf{G}}_{\alpha_k}$;
  return $[\underline{\alpha}_i, \overline{\alpha}_i]$ (5.23);
  Prediction of the bounded degradation equations (5.24);
  Locate the intersection with TH and compute $[\underline{\tilde{t}}_{\text{EoL}_{i_k}}, \overline{\tilde{t}}_{\text{EoL}_{i_k}}]$ (5.25);
  return The forecasted bounded RUL $[\underline{\tilde{t}}_{\text{RUL}}, \overline{\tilde{t}}_{\text{RUL}}]$ (5.26);
  Update $\hat{\mathcal{X}}_{k+1}$, $\hat{\mathcal{X}}_{\alpha_{k+1}}$, $\mathbf{A}_{k+1}, \mathbf{B}_{k+1}, \mathbf{C}_{k+1}, \mathbf{D}_{k+1}$;
end

5.6 Case Study: Results and Analysis

The case study in this chapter follows the same problem set-up in Section 4.6 in a zonotopic LPV framework.

5.6.1 Scenario 1

Results of JESP using ZSM

The proposed ZSM approach for JESP of multi-output system has been applied in scenario 1. Both the classical online tuning approach (4.37) with $\lambda^{\star}_{\text{on}}$, and the LMI-based optimal tuning (4.12c) with $\lambda^{\star}$, have been compared in the same case study. The estimation results of the first three zonotopic states are illustrated in Figures 5.4a, 5.4b, and 5.4c. Accordingly featuring the propagated center and bounds of the generator matrices of each zonotopic state, compared to the stochastic EKF approach in Chapter 3, and the empirically-simulated degradation in Section 2.3.
A slight increment has affected the first state which describes $v_{C_{\text{in}}}$ as shown in Figure 5.4a. On the other hand, the degradation has decreased the second and the third states which represent I_L in Figure 5.4b and $v_{C_{\text{o}}}$ in Figure 5.4c respectively. The proposed LMI-tuned ZSM approach results perfect zonotopic estimation. In other words, the estimated centers $\hat{\mathbf{x}}_1$, $\hat{\mathbf{x}}_2$ and $\hat{\mathbf{x}}_3$, and their respective bounds $\hat{\mathbf{G}}_1$, $\hat{\mathbf{G}}_2$ and $\hat{\mathbf{G}}_3$, of the states follow the empirical states degradation with guaranteed bounding throughout the full simulation. Additionally, the classical-online-tuned ZSM approach has also been examined and show almost the same estimated zonotopes in the LMI-tuned approach. Furthermore, both approaches are also compared to the EKF in terms of centers estimation, and all approaches show very high accurate results and similarities in terms of centers estimation in the LPV framework.
Moreover, Figure 5.5 illustrates the estimation of the augmented critical parameter R_{ON} that shows an increment in the ON-resistance of the MOSFET with very high RA with respect to the empirical true degradation.
As illustrated in Figure 5.5, the $\lambda^{\star}_{c}$-tuned ZSM has provided a narrower and more conservative estimated bounds than the λ^{*}_{LMI}-tuned approach.
Table 5.1 shows the average RA of the estimated centers of the zonotopic states and the augmented parameter with both tuning approaches, compared to the stochastic EKF results.
Additionally, the bounds are perfectly adapted to each state, while a small difference was obtained in terms of zonotopic radii between the online and offline tuning techniques in the parameter estimation. Thus, the effect of cascading degradation is clearly propagating through the other components.

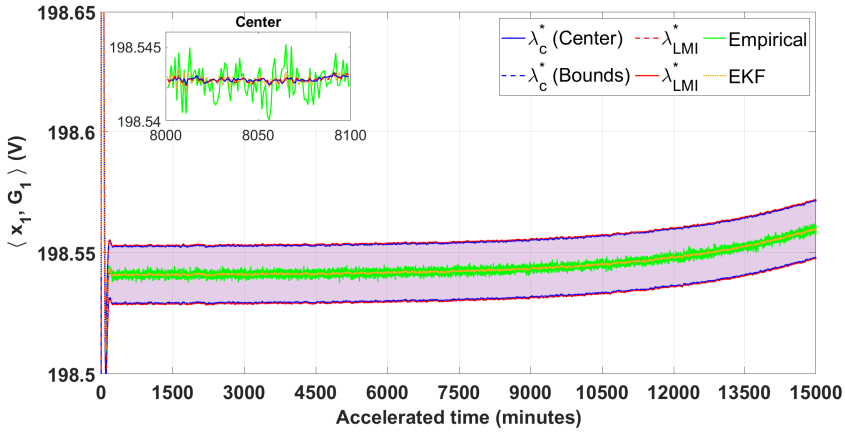

(a) $\hat{\mathcal{X}}_1$ with both tuning approaches versus the stochastic estimation and the empirical degradation in scenario 1

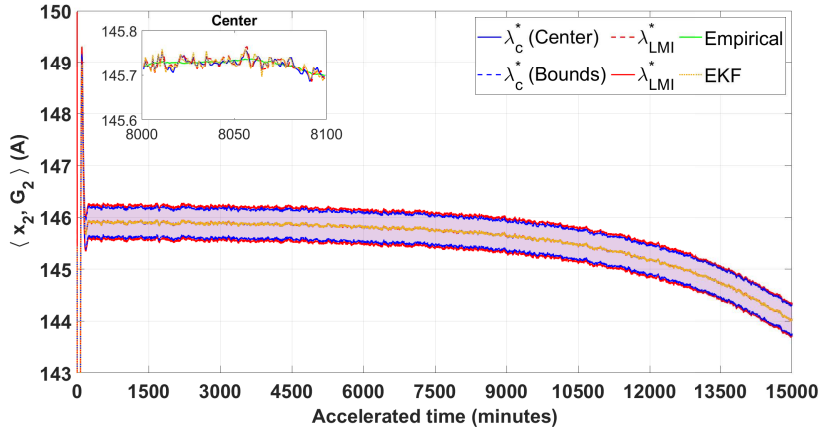

(b) $\hat{\mathcal{X}}_2$ with both tuning approaches versus the stochastic estimation and the empirical degradation in scenario 1

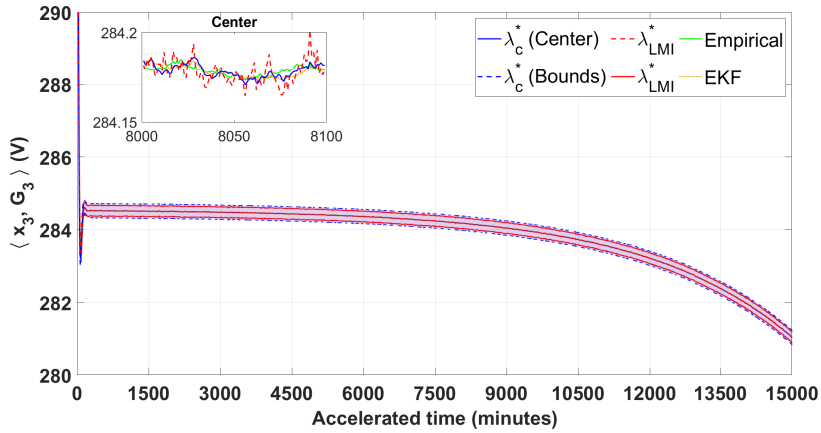

(c) $\hat{\mathcal{X}}_3$ with both tuning approaches versus the stochastic estimation and the empirical degradation in scenario 1

Figure 5.4: The estimated zonotopic states versus the corresponding stochastic estimation and the empirical degradation in scenario 1

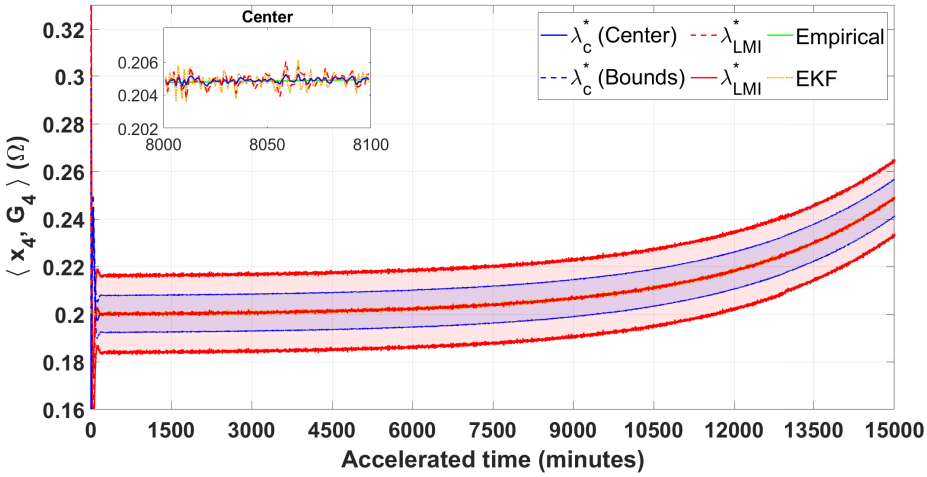

Figure 5.5: $\hat{\mathcal{X}}_4$ with both tuning approaches versus the stochastic estimation and the empirical degradation in scenario 1

Table 5.1: Average RA of the estimated centers of states and parameters by ZSM versus EKF in scenario 1

States and Parameters	RA^{S1} %		
	ZSM: λ^*_{LMI}	ZSM: λ^*_c	EKF
$\hat{\mathcal{X}}_1$	99.9999	99.9999	99.99999
$\hat{\mathcal{X}}_2$	99.9999	99.9998	99.99996
$\hat{\mathcal{X}}_3$	99.9998	99.9980	99.99995
$\hat{\mathcal{X}}_4$	99.9971	99.9573	99.99089

RZSM for RUL forecasting

As mentioned in Section 5.4, the proposed methodology consists of employing a second ZSM for parameters estimation of the proposed degradation model that has been linearized with two unknown parameters. The aim of this method is to predict the bounds of the degradation profiles recursively based on the critical parameters estimation.
Figures 5.6a and 5.6b illustrate the estimated parameters α_1 and α_2 of the proposed degradation model respectively.
After predicting the degradation model using the RZSM approach, the EoL

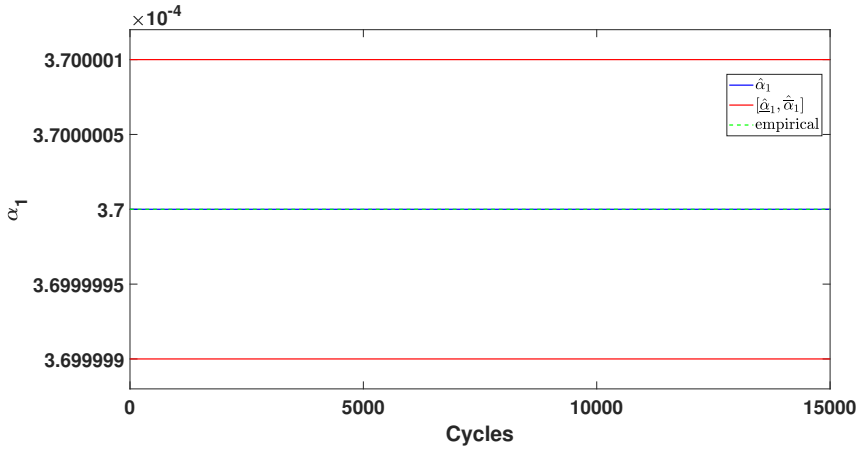

(a) $\hat{\alpha}_1$ of the predicted degradation model

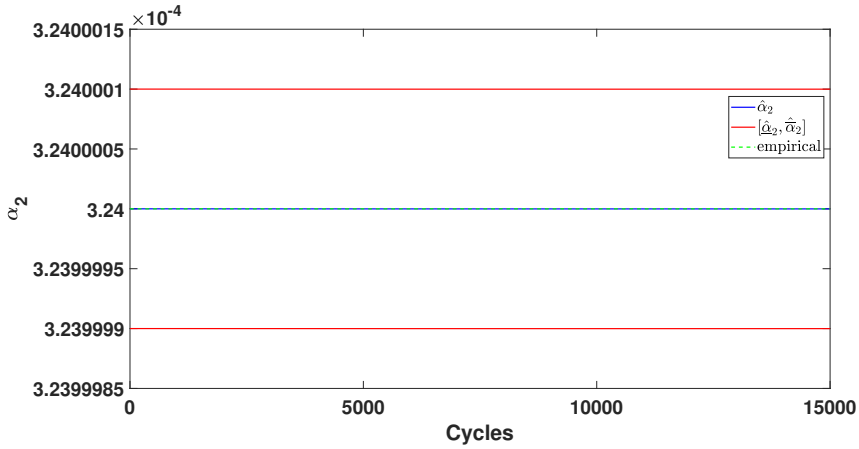

(b) $\hat{\alpha}_2$ of the predicted degradation model

Figure 5.6: The predicted parameters of the proposed degradation model

is first computed by intersecting the predicted degradation profile with the TH of R_{ON} in this scenario (10% increase) using (5.25), as shown in Section 2.3 in Chapter 2. Hence, the RUL bounds are predicted as in (5.26).
Figure 5.7 illustrates the zonotopic RUL prediction, where the x-axis denotes the online measurements that covers the period until after the true EoL of the concerned component. The y-axis shows the predicted RUL in minutes. The predicted zonotopic RUL is compared to the empirical true RUL.
Moreover, the predicted zonotopic RUL by the RZSM approach is assessed by its RA to the true empirical RUL. According to the estimated centers of the critical parameter as illustrated in Figure 5.5, the RA of RUL forecasting through both tuning approaches of ZSM for JESP is similar. Therefore, the

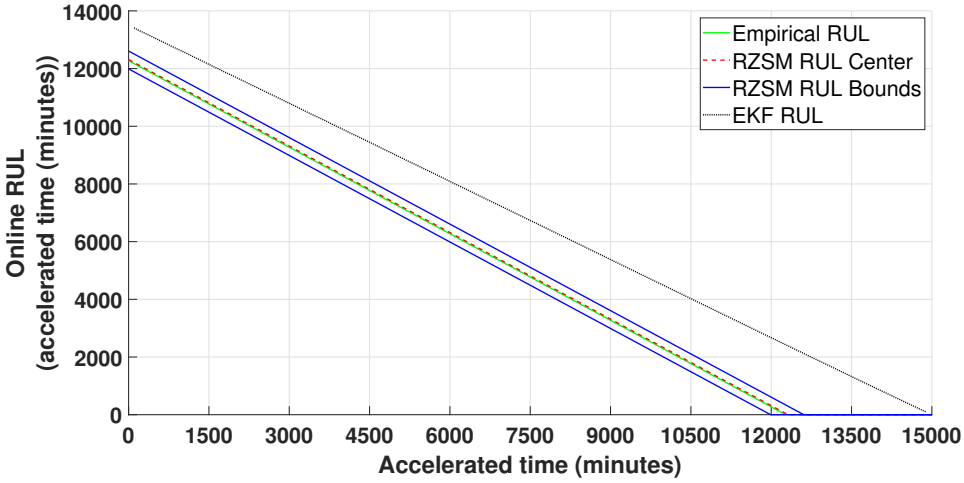

Figure 5.7: $[\underline{\tilde{\mathrm{RUL}}}, \overline{\tilde{\mathrm{RUL}}}]$ with the LMI-tuned RZSM approach versus the true empirical RUL in scenario 1

RA of the RUL forecasting in scenario 1 is 98.8664 %.

5.6.2 Comparative assessment: ZSM versus ZEKF for JESP

The ZSM and the ZEKF approaches were both used for JESP in this thesis. The main difference between the two deterministic methods is that the ZSM depends on the current time instant of output measurements, whereas the ZEKF depends on the previous time instant of the output measurements. Moreover, the ZSM approach considers each output of a multi-output system in order to perform simultaneous intersection between the predicted uncertain states and parameters and the outputs. On the other hand, the ZEKF follows the same structure of prediction and correction as in an EKF, in order to estimate the states and the parameters. Thus, the LMI-based optimization has been implemented to tune both observers as well as the classical online approach which performs as a typical KF gain. The estimated states and parameter of both estimation approaches that are tuned using two methods, are illustrated in Figures 5.8a, 5.8b, 5.8c, and 5.9.
Since the degradation analysis has been discussed in Chapter 2, the main differences between both estimation observers are briefly commented. It is clearly shown that the ZSM observer for JESP has shown tighter bounds than the ZEKF, given the same weighting of noises and uncertainties. This can be

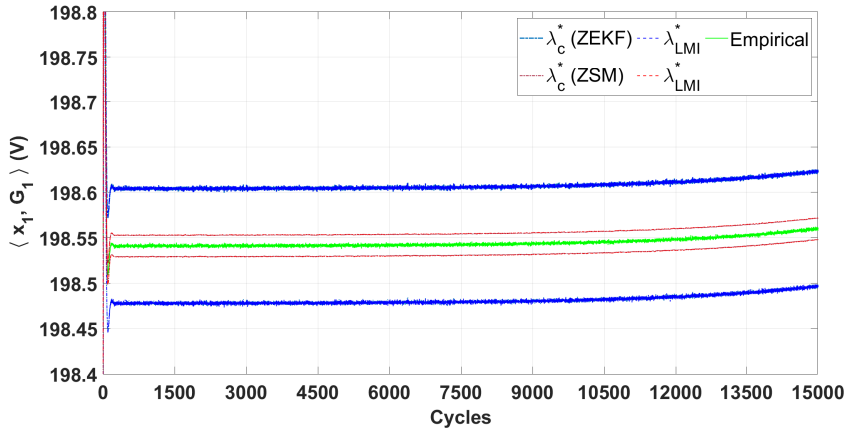

(a) $\hat{G}_1$ with both tuning approaches: ZSM versus ZEKF in scenario 1

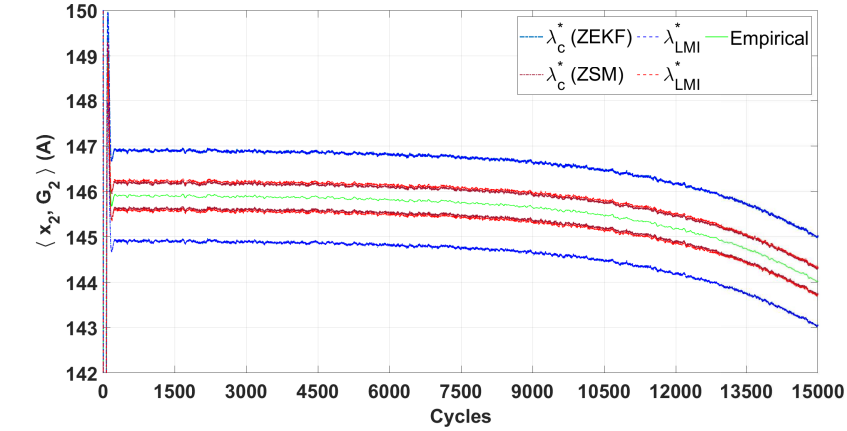

(b) $\hat{G}_2$ with both tuning approaches: ZSM versus ZEKF in scenario 1

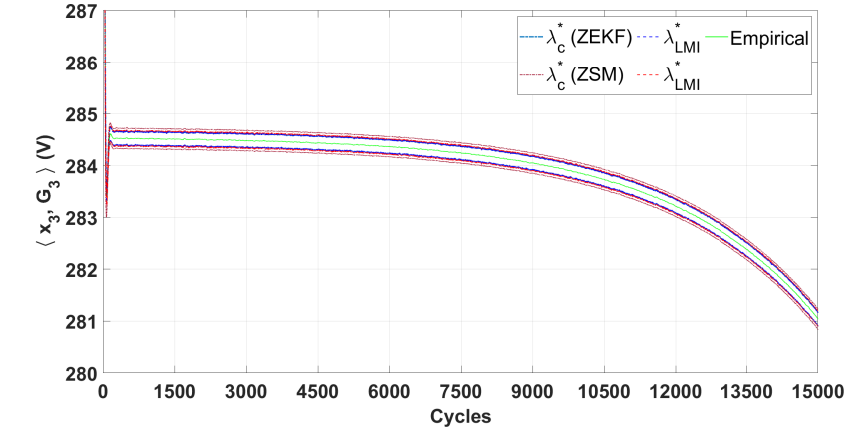

(c) $\hat{G}_3$ with both tuning approaches: ZSM versus ZEKF in scenario 1

Figure 5.8: The estimated zonotopic bounds of the states by ZSM versus ZEKF approaches in scenario 1

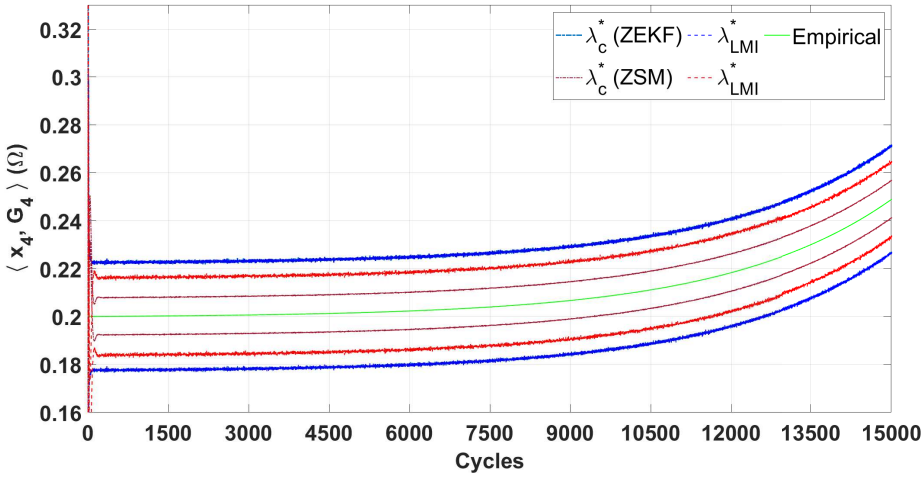

Figure 5.9: $\hat{G}_4$ with both tuning approaches: ZSM versus ZEKF in scenario 1

related to the multiple-intersection of the output measurements which provides more accurate estimation. Most importantly, the online classical tuning and the LMI-based optimization approaches have resulted similar bounds in each observer case, which proves the efficiency of the proposed LMI-based approach that is validated in different scenarios as shown in Chapter 4 and this chapter.

5.7 Conclusions

This chapter has been built upon the improvements of the previously-investigated PHM approaches. According to Chapter 4, the zonotopic observer performs for the benefits of the JESP with an indirect effect on the RUL, specifically when scenario 3 is compared to the stochastic approach. In addition to these reasons, the simple computation of zonotopes has motivated the employment of a ZSM observer in order to examine its performance with each output measurement. The differences of the structures of both zonotopic-based observers have not affected the estimation accuracy. However, considering each output measurement independently in the ZSM is recommended to guarantee the zonotopic inclusion of the propagated sets of states and parameters. Moreover, the polytopic LPV model representation has been utilized as explained in Chapter 4. Most importantly, the RUL forecasting has been accomplished with the same ZSM observer that recursively predicts the degradation tra-

jectories until the TH. In the proposed RUL forecasting approach, the degradation model is considered with an exponential trend that does not necessarily describes the same structure of the empirical degradation models. Whereas, the classical approach requires an exact knowledge of the polynomial degradation model with multiple unknown parameters which require more computations using an RLS filter for parameters estimation. Moreover, while the RLS-based prediction converges with more available observations, the RZSM-based prediction is guaranteed since the beginning until the EoL. Therefore, this approach has solved the intuitive EoL expectation issue using the linear EoL-RUL approach and exact knowledge of the high-degree degradation models. Additionally, the RZSM depends only on the estimated critical parameters and functions with unknown-but-bounded noises and uncertainties that did not affect the convergence of the RUL forecasting as seen in the previous approaches.

Conclusions and Perspectives

Conclusions

In this thesis, we investigated different model-based PHM approaches in order to fulfill the proposed objectives. Due to the lack of standardized PHM architectures for general-purpose applications, we decided to contribute to the whole structure towards the development of system-level prognostics. Throughout this research work, many challenges have arisen from the modeling of degraded system until the RUL forecasting process. Therefore, the contributions in each chapter along with the constructive development of the threefold PHM approaches are addressed below.

Chapter 1 is an essential starting phase of this work that addresses the existing PHM approaches. The literature review helps clarifying the main challenges that we can contribute to improve. Among many multidisciplinary prognostics approaches, it has been clear that the majority of the existing work focuses on the effort- and time-consuming knowledge of the PoF of the components. On the other hand, data-driven prognostics are employed for their simple application while they require huge amount of historical data for reliable prediction. Hence, the ideal PHM case is hypothetically proposed by featuring real applications which include various complex subsystems with degraded internal components, in addition to the lack of historical degradation data. Based on this proposition, some existing works proposed to deal with external observed effects of the degradation instead of localizing the main cause. However, to fulfill the main objective of the CBM strategy, we proposed to track and estimate the degradation of the critical components

in the system in order to optimize the lifecycle of the whole system. Therefore, we proposed a threefold PHM structure that deals with the modeling of a system with degraded components, degradation estimation of the critical components on a system-level, and online RUL forecasting with reduced computations.

Chapter 2 is dedicated to the modeling phase of the proposed PHM. The DC-DC converter case study has been chosen for many reasons that cope with the investigation of prognostics. Firstly, the power electronic systems suite best with model-based prognostics approach due to the advanced knowledge of their identification. Secondly, a power electronic converter describes subsystems with different operations and structures that form a complete system with multidisciplinary degraded parameters. Thirdly, such application can be generalized to all nonlinear dynamical systems to cope with the main objective of this thesis. For these purposes, we investigated this application under three degradation scenarios to analyze the most suitable and less complex failure precursors to adopt while estimating the SoH of the system. Hence, preparing the following PHM phase has necessitated a model representation that allows the estimation of the critical parameters in the system without knowledge of their degradation behaviors. Thus, among the investigated representation approaches, the average augmented system has been adopted for the benefits of decreasing the computations in addition to the global estimation of most states and parameters of the system. Consequently, a nonobservability issue was faced with such nonlinear model with varying parameter that requires to be fixed for the following phase.

Chapter 3 addresses the stochastic-based prognostics techniques applied to the proposed PHM structure. The investigation in this chapter has been carried out with EKF for JESP as most of the existing model-based approaches. The main reason behind this study is to assess the reliability of the existing approaches with such nonlinear application that allows us to point out the drawbacks that we can contribute to. Hence, the augmented model was linearized online using Jacobian method and has shown very accurate estimation results with scenarios of one degraded parameter. Whereas, the estimation error increases with the third scenario of multiple degraded parameters, which highlights a crucial issue since all real applications are subject to such degradation scenario and RUL forecasting is only based on the degradation estimation. Moreover, the classical RUL forecasting approach that depends on the knowledge of the degradation models of the failure precursors has been examined. It is worth noting that the PoF-based degradation models were eliminated for the sake of reducing the controversial issue

of time-consuming degradation modeling, and polynomial empirical degradation models of failure precursors have been employed for the prediction process. thus, the classical RUL forecasting is split into two steps, prediction of degradation profiles and intersection with the parameter TH for RUL forecasting. RLS filter for parameters estimation was adopted to estimate the parameters of the polynomial degradation models in addition to their regression until the TH. Hence, the predicted profile intersects with the TH and the EoL is then obtained. It was remarkable that the Gaussian uncertainties have affected the prediction process in addition to the elevated number of unknown parameters. For these reasons, we proposed to investigate a direct RUL prediction that eliminate the need of the degradation models, yet with intuitive EoL expectations. The overall results of these approaches have not proved a reliable condition for a generalized PHM application. Therefore, further propositions to improve these limitations are explained in the following chapter.

Chapter 4 has been conducted to overcome the majors issues due to the uncertain RUL forecasting and degradation estimation in multiple degradation scenario. Thus, the ZEKF is a suitable observer for JESP that merges the accuracy of the stochastic EKF in estimation and propagates bounded states and parameters by the simple implementation of the deterministic zonotopes. The main purpose that motivates this approach is that it bounds the estimated parameters which can solve the faced problem in scenario 3. Additionally, it indirectly bounds the predicted RUL which can increases its reliability. However, investigating the linear EoL-RUL approach using the ZEKF has shown improved but pessimistic results against the reliability constraint. Thus, we recall that the model representation has been transformed into a polytopic LPV framework to cope with the offline LMI-based tuning approach of the ZEKF observer for the sake of increasing the estimation robustness and decreasing the computational effort. Consequently, as the JESP issue has been validated for all degradation scenarios using zonotopes, the consisted cause of the low RUL forecasting reliability has been clarified. For these reasons, we propose to eliminate the linear EoL-RUL approach and investigate a generalized exponential trend with reduced number of parameters in a zonotopic framework.

The previously-experienced drawbacks and limitations have been solved in Chapter 5. A small difference between the ZSM observer and the ZEKF is related to the estimation of the measurements. However, we adopted the ZSM-based approach due to its ability to propagate guaranteed zonotopic states and parameters by considering each measurement alone that has

shown an improved accuracy. Moreover, similar to the ZEKF, the observer was tuned by the optimal LMI-based approach with an LPV representation. Furthermore, we proposed to follow a general exponential trend for degradation as remarked in most electronics applications. However, to avoid the 5-degree polynomial approximation or the implementation of stochastic observers, we proposed to recursively employ a ZSM for degradation predictions. Thus, in order to accomplish it with reduced computations, we created a regressor model with two unknown parameters and applied it for prediction using a RZSM which functions online and homogeneously with the ZSM for JESP. Consequently, the degradation profiles have been predicted with zonotopic bounds and the RUL has been forecasted with very high RA without using the exact degradation model and with reduced computations for real-time applications.

Perspectives

According to our observations throughout this work, we propose some potential applications for further investigations of the PHM.

- This case study has been investigated with constant load, however it is essential to investigate the effect of regulated application with variable load on the failure precursors. Since the estimation of failure precursors is crucial, the SoH assessment can be accomplished by monitoring the duty cycle of the switch. This case can be investigated in closed-loop system with variable resistive, inductive, etc. loads.

- According to the failure mechanisms of power semiconductors, high temperatures degraded the switches. Thus, as the temperature increases with the increase of the switching frequency, it is worth investigating the effect of the switching frequency on the age of the semiconductor module.

- Post-prognosis actions and decisions have not been addressed in this thesis. Hence, the CBM strategy could be extensively investigated in a cost optimization framework that studies the lifecyle of a system and optimizes the maintenance strategies for the degraded components in order to extend the life of the system and reduce the maintenance expenses.

- Further investigation on system-level prognostics will improve the reliability of such approaches with the objective of embedding enhanced

diagnostics with automatic control in a macro-system that is able to localize the degraded components and predict their RUL with an interrupted online diagnosis in a fault-tolerant control framework.

- It is also interesting to investigate the possibility of system-level RUL forecasting by direct degradation assessment without estimating the failure precursors.
- Uncertainties are the only link between simulation and real applications. Thus, it is crucial to consider the real effect of uncertainties on the whole prognostics process with validation on real systems.

This page is intentionally left blank

APPENDIX A

Mathematical Background: Definition and Properties

A.1 Matrices

Definition A.1.1 (Singular Matrix)**.** A *singular matrix* $\mathbf{M}$ is a square matrix that does not have an inverse. In other words, $\mathbf{M}$ is singular $\iff det(\mathbf{M}) = 0$.

Definition A.1.2 (Symmetric Positive Definite Matrix)**.** A *symmetric positive definite matrix* is a matrix whose eigen values are positive. In other terms, a square and symmetric matrix $\mathbf{M}$ is positive definite if:
$\lambda^\intercal \mathbf{M} \lambda > 0, \ \forall \ \lambda \in \ \mathbb{R}^{n_\lambda}$.

Definition A.1.3 (Strictly Positive Definite Matrix)**.** A matrix $\mathbf{M} = \mathbf{M}^\intercal \in \mathbb{R}^{n \times n}$ is called a *strictly positive definite matrix*, denoted by $\mathbf{M} \succ 0$, if:
$\mathbf{x}^\intercal \mathbf{M} \mathbf{x} > 0, \ \forall$ nonzero vectors $\mathbf{x}$ with real entries ($\mathbf{x} \in \mathbb{R}^n_{\neq 0}$).

Definition A.1.4 (Strictly Negative Definite Matrix)**.** A matrix $\mathbf{M} = \mathbf{M}^\intercal \in \mathbb{R}^{n \times n}$ is called a *strictly negative definite matrix*, denoted by $\mathbf{M} \prec 0$, if:
$\mathbf{x}^\intercal \mathbf{M} \mathbf{x} < 0, \ \forall$ nonzero vectors $\mathbf{x}$ with real entries ($\mathbf{x} \in \mathbb{R}^n_{\neq 0}$).

Definition A.1.5 (Positive Definite Matrix)**.** A matrix $\mathbf{M} = \mathbf{M}^\intercal \in \mathbb{R}^{n \times n}$ is called a *positive definite matrix*, denoted by $\mathbf{M} \succeq 0$, if:
$\mathbf{x}^\intercal \mathbf{M} \mathbf{x} \geq 0, \ \forall$ nonzero vectors $\mathbf{x}$ with real entries ($\mathbf{x} \in \mathbb{R}^n_{\neq 0}$).

Definition A.1.6 (Negative Definite Matrix)**.** A matrix $\mathbf{M} = \mathbf{M}^\intercal \in \mathbb{R}^{n \times n}$ is called a *negative definite matrix*, denoted by $\mathbf{M} \preceq 0$, if:
$\mathbf{x}^\intercal \mathbf{M} \mathbf{x} \leq 0, \ \forall$ nonzero vectors $\mathbf{x}$ with real entries ($\mathbf{x} \in \mathbb{R}^n_{\neq 0}$).

Definition A.1.7 (Euclidean Norm)**.** The *Euclidean norm* of a matrix $\mathbf{M} \in \mathbb{R}^{n\times n}$ is denoted by $\|\mathbf{x}\|^2_{\mathbf{M}}$ and defined by the quantity $\mathbf{x}^\intercal\mathbf{M}\mathbf{x} = \|\mathbf{x}\|^2_{\mathbf{M}}$, where $\mathbf{x} \in \mathbb{R}^n$, and $\mathbf{M} = \mathbf{M}^\intercal \succ 0$.

Definition A.1.8 (Trace)**.** The *trace* of a square matrix $\mathbf{M} \in \mathbb{R}^{n\times n}$ is denoted by $tr(M)$ and defined by the sum of the elements on its main diagonal (from upper left to lower right).

$$tr(\mathbf{M}) = \sum_{i=1}^{n} a_{ii} = a_{11} + a_{22} + \cdots + a_{nn}. \tag{A.1}$$

Moreover, for given square matrices $\mathbf{A}$ and $\mathbf{B}$, and a scalar a:

$$\begin{aligned} tr(\mathbf{A}) &= tr(\mathbf{A}^\intercal), \\ tr(\mathbf{A}+\mathbf{B}) &= tr(\mathbf{A}) + tr(\mathbf{B}), \\ tr(a\ \mathbf{A}) &= a\ tr(\mathbf{A}), \\ tr(\mathbf{B}\mathbf{A}\mathbf{B}^{-1}) &= tr(\mathbf{A}), \\ tr(\mathbf{A}\mathbf{B}) &= tr(\mathbf{B}\mathbf{A}). \end{aligned} \tag{A.2}$$

Definition A.1.9 (Frobenius Norm)**.** The *Frobenius norm* of a matrix $\mathbf{M} \in \mathbb{R}^{n\times m}$ is defined as the square root of the sum of the absolute squares of its elements:

$$\|M\|_F = \sqrt{tr(\mathbf{M}\mathbf{M}^\intercal)} = \sqrt{\sum_{i=1}^{n}\sum_{j=1}^{m} |a_{ij}|^2}, \tag{A.3}$$

where a_{ij} are the elements of $\mathbf{M}$.

Definition A.1.10 (Linear Matrix Inequality (LMI))**.** A *Linear Matrix Inequality* (LMI) is formulated in the following form:

$$\begin{aligned} \mathbf{F}(\mathbf{x}) &\triangleq \mathbf{F}_0 + \sum_{i=1}^{n} x_i\mathbf{F}_i \succ 0 \\ &= \mathbf{F}_0 + x_1\mathbf{F}_1 + x_2\mathbf{F}_1 + \cdots + x_n\mathbf{F}_n \succ 0, \end{aligned} \tag{A.4}$$

where the matrices $\mathbf{F}_i = \mathbf{F}_i^\intercal \in \mathbb{R}_{m\times m}$, $i = 0, \ldots, n$, and $\mathbf{x} = [x_1\ x_2\ \ldots\ x_n]^\intercal \in \mathbb{R}^n$ is the vector of the decision variables.

Remark A.1.1. The LMI in (A.4) is a convex constraint on $\mathbf{x}$ (i.e., the set $\{x \in \mathbb{R}^n \ : \ \mathbf{F}(x) \succ 0\}$ is convex). Moreover, the aforementioned LMI can represent a wide variety of convex constraints on x such as linear inequalities, convex quadratic inequalities, matrix norm inequalities, in addition

to constraints such as Lyapunov and convex quadratic matrix inequalities. Furthermore, the matrix decision variables can be used to formulate LMI problems (i.e., the Lyapunov inequality) as shown below:

$$\mathbf{A}^{\intercal}\mathbf{P} + \mathbf{P}\mathbf{A} \prec 0, \tag{A.5}$$

where the matrix $\mathbf{A} \in \mathbb{R}^{n\times n}$ is given, and $\mathbf{P} = \mathbf{P}^{\intercal} \in \mathbb{R}^{n\times n}$ denotes the decision variable.

Remark A.1.2. The LMI in (A.4) is equivalent to a set of n polynomial inequalities in x (i.e., the leading principal minors of $\mathbf{F}(x)$ must be positive).

Property A.1.1. Multiple LMIs $\mathbf{F}^{(1)}(x) > 0, \ldots, \mathbf{F}^{(p)}(x) > 0$ can be expressed as a single LMI $diag(\mathbf{F}^{(1)}(x), \ldots, \mathbf{F}^{(p)}(x) > 0)$.

Definition A.1.11 (Schur Complement (S. Boyd et al. 1994))**.** Considering the following LMI:

$$\begin{bmatrix} \mathbf{Q}(x) & \mathbf{S}(x) \\ \mathbf{S}^{\intercal}(x) & \mathbf{R}(x) \end{bmatrix} \succ 0, \tag{A.6}$$

where $\mathbf{Q}(x)$, $\mathbf{R}(x)$ are symmetric matrices and $\mathbf{Q}(x)$, $\mathbf{R}(x)$, and $\mathbf{S}(x)$ are affine in x. Thus, the LMI in (A.6) is equivalent to:

$$\begin{cases} \mathbf{Q}(x) \succ 0, \\ \mathbf{Q}(x) - \mathbf{S}(x)\mathbf{R}^{-1}(x)\mathbf{S}^{\intercal}(x) \succ 0, \end{cases} \tag{A.7}$$

or,

$$\begin{cases} \mathbf{R}(x) \succ 0, \\ \mathbf{R}(x) - \mathbf{S}^{\intercal}(x)\mathbf{Q}^{-1}(x)\mathbf{S}(x) \succ 0. \end{cases} \tag{A.8}$$

A.2 Sets

Definition A.2.1 (Convex Set)**.** A set $\mathcal{S} \subset \mathbb{R}^m$ is called a *convex set* if for any $x_1, x_2, \ldots, x_n \in \mathcal{S}$, and any $\alpha_1, \alpha_2, \ldots, \alpha_n \in \mathbb{R}_+$ such that $\sum_{i=1}^{n} \alpha_i = 1$, then the element $\sum_{i=1}^{n} \alpha_i x_i$ is in $\mathcal{S}$.

Definition A.2.2 (Convex Hull)**.** A *convex hull* of a set $\mathcal{S}$, denoted by $conv(\mathcal{S})$, is the smallest convex set that contains $\mathcal{S}$.

Definition A.2.3 (Inclusion Operator)**.** The *inclusion operator* between two sets is defined by $\mathcal{X} \subseteq \mathcal{Y}$, $\mathcal{X}$ is a subset of $\mathcal{Y}$, $\iff$ $\forall\, x \in \mathcal{X}$, then $x \in \mathcal{Y}$.

Definition A.2.4 (Intersection Operator)**.** The *intersection operator* of two sets $\mathcal{X}$ and $\mathcal{Y}$ is defined by $\mathcal{X} \cap \mathcal{Y} = \{x : x \in \mathcal{X} \text{ and } x \in \mathcal{Y}\}$.

Definition A.2.5 (Image of Sets)**.** The *image of a set* $\mathcal{S}$, projected under a map $\mathcal{M}$ is defined by a set $\mathcal{M}(\mathcal{S}) = \{y \ : \ y = \mathcal{M}(x), x \in \mathcal{S}\}$.

Definition A.2.6 (Minkowski Sum)**.** The *Minkowski sum* of two sets $\mathcal{X}$ and $\mathcal{Y}$ is defined by $\mathcal{X} \oplus \mathcal{Y} = \{x + y : x \in \mathcal{X} \text{ and } y \in \mathcal{Y}\}$.

A.2.1 Interval sets

Definition A.2.7 (Interval)**.** An interval $[a, b] \subset \mathbb{R}$ is defined by the set $\{x \in \mathbb{R} : a \leq x \leq b\}$.

Definition A.2.8 (Unitary Interval)**.** A *unitary interval* is defined as $\mathcal{B}^1 = [-1, 1]$.

Definition A.2.9 (Center and Radius)**.** The *center* of an interval $\mathcal{I} = [a, b]$ is defined by $mid(\mathcal{I}) = \frac{a+b}{2}$, and its *radius* is defined by $rad(\mathcal{I}) = \frac{b-a}{2}$.

Definition A.2.10 (Interval Vector: *box*)**.** An *interval vector* is a $box([a_1, b_1], \ldots, [a_n, b_n])^\intercal$, with $a_1 \leq b_i$ for $i = 1, \ldots, n$.

Definition A.2.11 (Unitary Box)**.** A *unitary box*, denoted by $\mathcal{B}^n \in \mathbb{R}$, is a *box* composed of n unitary intervals defined by $\{x \in ([a_1, b_1], \ldots, [a_n, b_n])^\intercal : a_i = -1, b_i = 1, i = 1, \ldots, n\} \subset \mathbb{R}^n$.

Definition A.2.12 (Interval Matrix)**.** An *interval matrix* $[\mathbf{M}]$ is a matrix whose elements are intervals. The center of $[\mathbf{M}]$ is denoted by $mid([\mathbf{M}])_{ij} = \frac{a_{ij}+b_{ij}}{2}$ and its radius is denoted by $rad([\mathbf{M}])_{ij} = \frac{a_{ij}-b_{ij}}{2}$, with $a_{ij} \leq m_{ij} \leq$

$b_{ij}, i = 1, \ldots, n$, and $j = 1, \ldots, m$.
The interval matrix $[\mathbf{M}]$ can be rewritten as:

$$[\mathbf{M} = mid([\mathbf{M}]) + \Delta\mathbf{M}], \tag{A.9}$$

with $\Delta\mathbf{M}$ is the uncertain part of the interval matrix $[\mathbf{M}]$. Thus, for ρ denoting the vector of the n_ρ uncertain parameters scalars, $\Delta\mathbf{M}$ is thus decomposed as:

$$\Delta\mathbf{M} = \sum_{i=1}^{n_\rho} \mathbf{M}_{\rho_i}\rho_i, \tag{A.10}$$

Remark A.2.1. The property of the interval matrix is applied for the presented system in this thesis, where the considered dynamical system is transformed into an LPV model containing interval parameters.

Property A.2.1 (Interval Operations)**.** The four basic operations with given interval matrices $[\mathbf{X}] = [\underline{x}, \overline{x}]$ and $[\mathbf{Y}] = [\underline{y}, \overline{y}]$ are shown below:

$$[\mathbf{X}] + [\mathbf{Y}] = [\underline{x}, \overline{x}] + [\underline{y}, \overline{y}] = [\underline{x} + \underline{y}, \overline{x} + \overline{y}], \tag{A.11a}$$

$$[\mathbf{X}] - [\mathbf{Y}] = [\underline{x}, \overline{x}] - [\underline{y}, \overline{y}] = [\underline{x} - \overline{y}, \overline{x} - \underline{y}], \tag{A.11b}$$

$$\begin{aligned}[\mathbf{X}][\mathbf{Y}] &= [\underline{x}, \overline{x}][\underline{y}, \overline{y}] \\ &= [min(\underline{x} \times \underline{y}, \underline{x} \times \overline{y}, \overline{x} \times \underline{y}, \overline{x} \times \overline{y}), max(\underline{x} \times \underline{y}, \underline{x} \times \overline{y}, \overline{x} \times \underline{y}, \overline{x} \times \overline{y})],\end{aligned} \tag{A.11c}$$

$$\frac{[\mathbf{X}]}{[\mathbf{Y}]} = \frac{[\underline{x}, \overline{x}]}{[\underline{y}, \overline{y}]} = [\underline{x}, \overline{x}][\frac{1}{\overline{y}}, \frac{1}{\underline{y}}], \quad \text{if } 0 \notin [\underline{y}, \overline{y}]. \tag{A.11d}$$

Definition A.2.13 (Strip)**.** A *strip* is defined as a set as shown below:

$$\mathcal{S}(y, \mathbf{d}, \sigma) = \{\mathbf{x} \in \mathbb{R}^n : |y - \mathbf{d}^\intercal \mathbf{x}| \leq \sigma\}, \tag{A.12}$$

where $y \in \mathbb{R}, \mathbf{d} \in \mathbb{R}^n$ and $\sigma \in \mathbb{R}_+$.

A.2.2 Zonotopic sets

Definition A.2.14 (Zonotope)**.** A *zonotope* $\mathcal{Z} = \langle \mathbf{c}, \mathbf{G} \rangle \subset \mathbb{R}^n$ with a center $c \in \mathbb{R}^n$ and a generator matrix $\mathbf{G} \in \mathbb{R}^{n \times m}$ is a polytopic set defined as a linear image of the unit hypercube $[-1, 1]^m$, as follows:

$$\langle \mathbf{c}, \mathbf{G} \rangle = \{\mathbf{c} + \mathbf{G}s, \|s\|_\infty \leq 1\}. \tag{A.13}$$

Definition A.2.15 (Generator Representation)**.** Given a vector $\mathbf{c} \in \mathbb{R}^n$ and a set of vectors $\mathcal{G} = \{\mathbf{g}_1, \mathbf{g}_2, \ldots, \mathbf{g}_m\} \subset \mathbb{R}^n, m \geq n$, a zonotope $\mathcal{Z}$ of order m is called an $m-$zonotope which means that this zonotope has m generators, and defined as follows:

$$\begin{aligned} \mathcal{Z} &= (\mathbf{c};\ \mathbf{g}_1, \mathbf{g}_2, \ldots, \mathbf{g}_m) \\ &= \{\mathbf{x} \in \mathbb{R}^n : \mathbf{x} = \mathbf{c} + \sum_{i=1}^{m} \alpha_i \mathbf{g}_i;\ -1 \leq \alpha_i \leq 1\}, \end{aligned} \tag{A.14}$$

Furthermore, this definition is equivalent to the definition of zonotopes obtained by the Minkowski sum of a finite number of line segments defined as follows:

$$\begin{aligned} \mathcal{Z} &= (\mathbf{c};\ \mathbf{g}_1, \mathbf{g}_2, \ldots, \mathbf{g}_m) \\ &= \mathbf{c} \oplus \mathbf{g}_1 \mathcal{B}^1 \oplus \cdots \oplus \mathbf{g}_m \mathcal{B}^1 \end{aligned} \tag{A.15}$$

Example A.2.1. Consider a 3-zonotope (third order) $\mathcal{Z}\langle \mathbf{c}, \mathbf{G} \rangle$ in $\mathbb{R}^2$ as illustrated in Figure A.1.

$$\mathbf{c} = \begin{bmatrix} 0 \\ 0 \end{bmatrix}, \quad \mathbf{G} = \begin{bmatrix} 1 & 2 & 3 \\ 3 & 2 & 1 \end{bmatrix}, \tag{A.16}$$

Each vertex of the zonotope $\mathbf{v}_{\mathcal{Z}_i} \in \mathcal{V}_{\mathcal{Z}}$, with $i = 1, \ldots, 2^3$ can be calculated by using the following equation:

$$\mathbf{v}_{\mathcal{Z}_i} = \mathbf{c} + \mathbf{G}\mathbf{v}_i, \tag{A.17}$$

where $\mathbf{v}_i \in \mathcal{V}_{\mathcal{B}^3}$.

Definition A.2.16 (Hypercube Affine Projection Representation)**.** An $m-$zonotope in $\mathbb{R}^n$, with $m \geq n$ is the translation by the center $\mathbf{p} \in \mathbb{R}^n$ of the image of an unitary hypercube of dimenstion $m \in \mathbb{R}^n$ under a *linear transformation*. Given a matrix $\mathbf{H} \in \mathbb{R}^{n \times m}$ representing the linear transformation, the zonotope $\mathcal{Z}$ is then defined by:

$$\mathcal{Z} = (\mathbf{p}; \mathbf{H}) = \mathbf{p} \oplus \mathbf{H}\mathcal{B}^m. \tag{A.18}$$

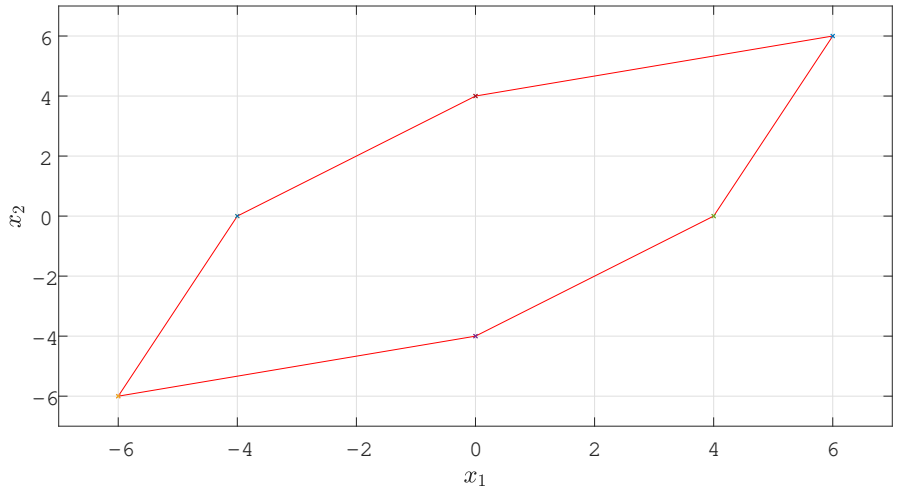

Figure A.1: 3-zonotope in $\mathbb{R}^2$

Remark A.2.2. The *hypercube affine projection* of a zonotope allows the representation of a zonotope using one vector and a matrix, or a matrix in the case of a centered zonotope (i.e. $\mathbf{c} = \mathbf{0}_{n\times 1}$).

Property A.2.2 (Particular Zonotope)**.** Given a centered zonotope $\mathcal{Z} = \mathbf{G}\mathcal{B}^m \in \mathbb{R}^n$.

- If $\mathbf{G}$ is an identity matrix, then $\mathcal{Z}$ is a unit box.
- If $\mathbf{G}$ is an diagonal matrix, then $\mathcal{Z}$ is a box.
- If $\mathbf{G}$ is an orthogonal matrix, then $\mathcal{Z}$ is a hypercube.
- If $\mathbf{G}$ is an invertible matrix, then $\mathcal{Z}$ is a parallelotope.

Property A.2.3 (Generator Permutation)**.** The permutation of the columns of the generator matrix $\mathbf{G}$ of a zonotope $\mathcal{Z}$ does not affect the zonotope.

Property A.2.4 (Sum of Zonotopes)**.** The Minkowski sum of two zonotopes results a zonotope. Given two zonotopes $\mathcal{Z}_1 = \mathbf{c}_1 \oplus \mathbf{G}_1\mathcal{B}^{m_1} \in \mathbb{R}^n$, and $\mathcal{Z}_2 = \mathbf{c}_2 \oplus \mathbf{G}_2\mathcal{B}^{m_2} \in \mathbb{R}^n$, their sum is defined as follows:

$$\mathcal{Z} = \mathcal{Z}_1 \oplus \mathcal{Z}_2 = (\mathbf{c}_1 + \mathbf{c}_2) \oplus [\mathbf{G}_1 \ \mathbf{G}_2]\mathcal{B}^{m_1+m_2}. \tag{A.19}$$

Proof. Based on the Definition A.2.6, the Minkowski sum of the two zonotopes can be obtained as follows:

$$\mathcal{Z}_1 \oplus \mathcal{Z}_2 = \{\mathbf{c}_1 + \mathbf{c}_2 + \mathbf{G}_1\mathbf{z}_1 + \mathbf{G}_1\mathbf{z}_1 : \mathbf{z}_1 \in \mathcal{B}^{m_1},\ \mathbf{z}_2 \in \mathcal{B}^{m_2}\}, \tag{A.20}$$

thus, it is rewritten in a matrix form as shown below:

$$\begin{aligned}\mathcal{Z}_1 \oplus \mathcal{Z}_2 &= \{\mathbf{c}_1 + \mathbf{c}_2 + [\mathbf{G}_1\mathbf{G}_1] \cdot \begin{bmatrix}\mathbf{z}_1\\ \mathbf{z}_2\end{bmatrix} : \begin{bmatrix}\mathbf{z}_1\\ \mathbf{z}_2\end{bmatrix} \in \mathcal{B}^{m_1+m_2}\} \\ &= (\mathbf{c}_1 + \mathbf{c}_2) \oplus [\mathbf{G}_1\ \mathbf{G}_2]\mathcal{B}^{m_1+m_2} = \mathcal{Z}.\end{aligned} \tag{A.21}$$

□

Property A.2.5 (Linear Image of a Zonotope)**.** The image of a zonotope $\mathcal{Z} = \mathbf{c} \oplus \mathbf{G}\mathcal{B}^m \in \mathbb{R}^n$ by a linear mapping $\mathbf{K}$ is computed by a standard matrix multiplication:

$$\mathbf{K} \odot \mathcal{Z} = (\mathbf{K} \cdot \mathbf{c}) \oplus (\mathbf{K} \cdot \mathbf{G})\mathcal{B}^m. \tag{A.22}$$

Proof. By applying the conventional matrix product: $\mathbf{K} \cdot \mathcal{Z} = \{\mathbf{K}(\mathbf{c} + \mathbf{G}\mathbf{z}) : \mathbf{z} \in \mathcal{B}^m\} = \{\mathbf{K}\mathbf{c} + \mathbf{K}\mathbf{G}\mathbf{z} : \mathbf{z} \in \mathcal{B}^m\} = (\mathbf{K}\mathbf{c}) \oplus (\mathbf{K}\mathbf{G})\mathcal{B}^m$. □

Definition A.2.17 (Covariance)**.** The *covariance* of a zonotope $\mathcal{Z} = \langle \mathbf{c}, \mathbf{G} \rangle$ is defined as $cov(\mathcal{Z}) = \mathbf{G}_{\mathcal{Z}}\mathbf{G}_{\mathcal{Z}}^{\intercal}$.

Definition A.2.18 ($F-$radius)**.** The $F-$radius of a given zonotope $\mathcal{Z} = \langle \mathbf{c}, \mathbf{G}_{\mathcal{Z}} \rangle \in \mathbb{R}^n$ is the Frobenius norm of the same zonotope:

$$\|\mathcal{Z}\|_F = \|\mathbf{G}\|_F. \tag{A.23}$$

Definition A.2.19 (F_W-radius)**.** The *weighted Frobenius radius* of a given zonotope $\mathcal{Z} = \langle \mathbf{c}, \mathbf{G}_{\mathcal{Z}} \rangle \in \mathbb{R}^n$ is the weighted Frobenius norm of the same zonotope:

$$\|\mathcal{Z}\|_{F,W} = \|\mathbf{G}\|_{F,W}. \tag{A.24}$$

Definition A.2.20 ($\mathbf{P}-$radius)**.** The $\mathbf{P}-$*radius* of a zonotope $\mathcal{Z} = \mathbf{p} \oplus \mathbf{G}\mathcal{B}^m$ is defined by:

$$r = \max_{z \in \mathcal{Z}}(\|\mathbf{z} - \mathbf{p}\|_{\mathbf{P}}^2), \tag{A.25}$$

where $\mathbf{P}$ is a strictly symmetric and positive definite matrix $\mathbf{P} = \mathbf{P}^{\intercal} \succ 0$.

Property A.2.6 (Interval hull (Kühn 1998))**.** The smallest interval box containing a given zonotope $\mathcal{Z} = \mathbf{c} \oplus \mathbf{G}\mathcal{B}^m \in \mathbb{R}^n$ is calculated as follows:

$$\blacksquare\mathcal{Z} = \mathbf{c} \oplus diag(\mathbf{G})\mathcal{B}^n, \tag{A.26}$$

where $diag(\mathbf{G})$ is a diagonal matrix such that $diag(\mathbf{G})_{ii} = \sum_{j=1}^{m} |\mathbf{G}_{ij}|, i = 1, \ldots, n$.

Property A.2.7 (Zonotope Inclusion (T. Alamo, Bravo, and Camacho 2005))**.** Given a zonotope $\mathcal{Z} = \mathbf{c} \oplus [\mathbf{G}]\mathcal{B}^m$, where $\mathbf{c} \in \mathbb{R}^n$, and $[\mathbf{G}]$ is an interval matrix of size $n \times m$, a zonotope inclusion is denoted by $\diamond\mathcal{Z}$, and defined by:

$$\diamond\,\mathcal{Z} = \mathbf{c} \oplus \begin{bmatrix} mid([\mathbf{G}]) & diag(\mathbf{M}) \end{bmatrix} \begin{bmatrix} \mathcal{B}^m \\ \mathcal{B}^n \end{bmatrix} = \mathbf{c} \oplus \mathbf{J}\mathcal{B}^{m+n}, \tag{A.27}$$

where $diag(\mathbf{M}) \in \mathbb{R}^{n\times n}$ is a diagonal matrix that satisfies:

$$diag(\mathbf{M})_{ii} = \sum_{j=1}^{m} \frac{rad(\mathbf{M}_{ij})}{2}, \quad i = 1, \ldots, n. \tag{A.28}$$

Therefore, $\mathcal{Z} \subseteq \diamond\mathcal{Z}$ under the aforementioned conditions.

Property A.2.8 (Reduction Operator $\downarrow_q$ (Combastel 2003; Combastel 2015))**.** A reduction operator $\downarrow_q$ is developed to achieve the numbers of vertices of the generator matrices of a zonotope $\langle \mathbf{c}, \mathbf{G} \rangle$ to a fixed number q while preserving the inclusion property $\langle \mathbf{c}, \mathbf{G} \rangle \cap \langle \mathbf{c}, \downarrow_q \{\mathbf{G}\} \rangle$. The author in (Combastel 2003) proposed a simple and efficient method to sorting the columns of $\mathbf{G}$ based on decreasing the Euclidean norm and enclosing the influence of the smaller columns, into an easily computable interval hull, so that the reduced generator matrix $\downarrow_q \{\mathbf{G}\}$ consists of only q columns.

Property A.2.9 (Criterion-based reduction (Combastel 2003; T. Alamo, Bravo, and Camacho 2005))**.** Given a zonotope $\mathcal{Z} = \langle \mathbf{c}, \mathbf{G} \rangle \in \mathbb{R}^n$ and an integer s, with $n < s < m$. The resulting matrix from the reordering of the columns of the generator matrix $\mathbf{G}$, by a criterion, is denoted by $\overline{\mathbf{G}}$. Thus the zonotope is rewritten as: $\mathcal{Z} = \mathbf{c} \oplus \overline{\mathbf{G}}_1\mathcal{B}^{s-n} \oplus \overline{\mathbf{G}}_2\mathcal{B}^{m-s+n}$, where $\overline{\mathbf{G}}_1$ is obtained from the first $s - n$ columns of the matrix $\overline{\mathbf{G}}$, and $\overline{\mathbf{G}}_2$ accounts for the remainder of $\overline{\mathbf{G}}$. Thus, the initial zonotope has been reduced by order s due to the over-approximation, i.e.$\mathcal{Z} \subseteq \mathbf{c} \oplus \overline{\mathbf{G}}_1\mathcal{B}^{s-n} \oplus Q\mathcal{B}^n$, where $Q\mathcal{B}^n$ is the over-approximation of the zonotope $\overline{\mathbf{G}}_2\mathcal{B}^{m-s+n}$.

This page is intentionally left blank

APPENDIX B

Additional Modeling Material

B.1 Numerical Models

B.1.1 Scenario 1: Augmented models

The augmented state-space matrices of subsystem 1 with $R_{\mathrm{ON}}(t)$ are:

$$\mathbf{A}_1^{\mathrm{S1}}(t) = \left[\begin{array}{ccc:c} \frac{-1}{C_{\mathrm{in}}(R_{\mathrm{in}}+\mathrm{ESR}_{\mathrm{in}})} & \frac{-R_{\mathrm{in}}}{C_{\mathrm{in}}(R_{\mathrm{in}}+\mathrm{ESR}_{\mathrm{in}})} & 0 & 0 \\ \frac{R_{\mathrm{in}}}{L(R_{\mathrm{in}}+\mathrm{ESR}_{\mathrm{in}})} & \frac{-(R_{\mathrm{in}}\mathrm{ESR}_{\mathrm{in}}+(R_L+\boxed{R_{\mathrm{ON}}(t)})(R_{\mathrm{in}}+\mathrm{ESR}_{\mathrm{in}}))}{L(R_{\mathrm{in}}+\mathrm{ESR}_{\mathrm{in}})} & 0 & 0 \\ 0 & 0 & 0 & 0 \\ \hdashline 0 & 0 & 0 & 1 \end{array}\right], \tag{B.1a}$$

$$\mathbf{B}_1^{\mathrm{S1}}(t) = \left[\begin{array}{cc} \frac{1}{C_{\mathrm{in}}(R_{\mathrm{in}}+\mathrm{ESR}_{\mathrm{in}})} & 0 \\ \frac{\mathrm{ESR}_{\mathrm{in}}}{L(R_{\mathrm{in}}+\mathrm{ESR}_{\mathrm{in}})} & 0 \\ 0 & \frac{-1}{C_o} \\ \hdashline 0 & 0 \end{array}\right], \tag{B.1b}$$

$$\mathbf{C}_1^{\mathrm{S1}}(t) = \left[\begin{array}{ccc:c} \frac{-1}{(R_{\mathrm{in}}+\mathrm{ESR}_{\mathrm{in}})} & \frac{\mathrm{ESR}_{\mathrm{in}}}{(R_{\mathrm{in}}+\mathrm{ESR}_{\mathrm{in}})} & 0 & 0 \\ 0 & 0 & 1 & 0 \end{array}\right], \tag{B.1c}$$

$$\mathbf{D}_1^{\mathrm{S1}}(t) = \begin{bmatrix} \frac{1}{(R_{\mathrm{in}}+\mathrm{ESR}_{\mathrm{in}})} & 0 \\ 0 & -\mathrm{ESR}_{\mathrm{o}} \end{bmatrix}, \tag{B.1d}$$

then, the augmented state-space matrices of subsystem 2 with $R_{\mathrm{ON}}(t)$ are:

$$\mathbf{A}_2^{\mathrm{S1}}(t) = \left[\begin{array}{ccc:c} \frac{-1}{C_{\mathrm{in}}(R_{\mathrm{in}}+\mathrm{ESR}_{\mathrm{in}})} & \frac{-R_{\mathrm{in}}}{C_{\mathrm{in}}(R_{\mathrm{in}}+\mathrm{ESR}_{\mathrm{in}})} & 0 & 0 \\ \frac{R_{\mathrm{in}}}{L(R_{\mathrm{in}}+\mathrm{ESR}_{\mathrm{in}})} & \frac{-(R_{\mathrm{in}}\mathrm{ESR}_{\mathrm{in}}+(R_L+\mathrm{ESR}_{\mathrm{o}})(R_{\mathrm{in}}+\mathrm{ESR}_{\mathrm{in}}))}{L(R_{\mathrm{in}}+\mathrm{ESR}_{\mathrm{in}})} & \frac{-1}{L} & 0 \\ 0 & \frac{1}{C_{\mathrm{o}}} & 0 & 0 \\ \hdashline 0 & 0 & 0 & 1 \end{array}\right], \tag{B.2a}$$

$$\mathbf{B}_2^{\mathrm{S1}}(t) = \left[\begin{array}{cc} \frac{1}{C_{\mathrm{in}}(R_{\mathrm{in}}+\mathrm{ESR}_{\mathrm{in}})} & 0 \\ \frac{\mathrm{ESR}_{\mathrm{in}}}{L(R_{\mathrm{in}}+\mathrm{ESR}_{\mathrm{in}})} & \frac{\mathrm{ESR}_{\mathrm{o}}}{L} \\ 0 & \frac{-1}{C_{\mathrm{o}}} \\ \hdashline 0 & 0 \end{array}\right], \tag{B.2b}$$

$$\mathbf{C}_2^{\mathrm{S1}}(t) = \left[\begin{array}{ccc:c} \frac{-1}{(R_{\mathrm{in}}+\mathrm{ESR}_{\mathrm{in}})} & \frac{\mathrm{ESR}_{\mathrm{in}}}{(R_{\mathrm{in}}+\mathrm{ESR}_{\mathrm{in}})} & 0 & 0 \\ 0 & \mathrm{ESR}_{\mathrm{o}} & 1 & 0 \end{array}\right], \tag{B.2c}$$

$$\mathbf{D}_2^{\mathrm{S1}}(t) = \begin{bmatrix} \frac{1}{(R_{\mathrm{in}}+\mathrm{ESR}_{\mathrm{in}})} & 0 \\ 0 & -\mathrm{ESR}_{\mathrm{o}} \end{bmatrix}. \tag{B.2d}$$

The numerical augmented state-space matrices of subsystem 1 with $R_{\mathrm{ON}}(t)$ are:

$$\mathbf{A}_1^{\mathrm{S1}}(t) = \left[\begin{array}{ccc:c} -113636 & -1136.36 & 0 & 0 \\ 622.665 & -6849.315\boxed{R_{\mathrm{ON}}(t)} - 96.513 & 0 & 0 \\ 0 & 0 & 0 & 0 \\ \hdashline 0 & 0 & 0 & 1 \end{array}\right], \tag{B.3a}$$

$$\mathbf{B}_1^{\mathrm{S1}}(t) = \left[\begin{array}{cc} 113636 & 0 \\ 6226.65 & 0 \\ 0 & -200 \\ \hdashline 0 & 0 \end{array}\right], \tag{B.3b}$$

$$\mathbf{C}_1^{\mathrm{S1}}(t) = \left[\begin{array}{ccc:c} -9.09 & 0.909 & 0 & 0 \\ 0 & 0 & 1 & 0 \end{array}\right], \tag{B.3c}$$

$$\mathbf{D}_1^{\mathrm{S1}}(t) = \begin{bmatrix} 9.09 & 0 \\ 0 & -0.08 \end{bmatrix}, \tag{B.3d}$$

then, the numerical augmented state-space matrices of subsystem 2 with $R_{\mathrm{ON}}(t)$ are:

$$\mathbf{A}_2^{R_{\mathrm{ON}}}(t) = \left[\begin{array}{ccc:c} -113636 & -1136.36 & 0 & 0 \\ 622.665 & -644.45 & -6849.315 & 0 \\ 0 & 200 & 0 & 0 \\ \hdashline 0 & 0 & 0 & 1 \end{array}\right], \tag{B.4a}$$

$$\mathbf{B}_2^{R_{\mathrm{ON}}}(t) = \left[\begin{array}{cc} 113636 & 0 \\ 6226.65 & 547.945 \\ 0 & -200 \\ \hdashline 0 & 0 \end{array}\right], \tag{B.4b}$$

$$\mathbf{C}_2^{R_{\mathrm{ON}}}(t) = \left[\begin{array}{ccc:c} -9.0909 & 0.90909 & 0 & 0 \\ 0 & 0.08 & 1 & 0 \end{array}\right], \tag{B.4c}$$

$$\mathbf{D}_2^{R_{\mathrm{ON}}}(t) = \begin{bmatrix} 9.0909 & 0 \\ 0 & -0.08 \end{bmatrix}. \tag{B.4d}$$

The Jacobian matrix of the scenario 1 is obtained as:

$$\mathbf{J}_{\mathbf{A}_1}^{\mathrm{S1}}(t) = \begin{bmatrix} -1.136.10^5 & -1.136.10^3 & 0 & 0 \\ 6.226.10^2 & -6.849.10^3\boxed{R_{ON}(t)} - 96.513 & 0 & -6.849.10^3\boxed{x_2(t)} \\ 0 & 0 & 0 & 0 \\ 0 & 0 & 0 & 1 \end{bmatrix}. \tag{B.5}$$

B.1.2 Scenario 2: Augmented models

The augmented state-space matrices of subsystem 1 with $\mathrm{ESR_o}(t)$ are:

$$\mathbf{A}_1^{\mathrm{S2}}(t) = \left[\begin{array}{ccc:c} \frac{-1}{C_{\mathrm{in}}(R_{\mathrm{in}}+\mathrm{ESR_{in}})} & \frac{-R_{\mathrm{in}}}{C_{\mathrm{in}}(R_{\mathrm{in}}+\mathrm{ESR_{in}})} & 0 & 0 \\ \frac{R_{\mathrm{in}}}{L(R_{\mathrm{in}}+\mathrm{ESR_{in}})} & \frac{-(R_{\mathrm{in}}\mathrm{ESR_{in}}+(R_L+R_{\mathrm{ON}})(R_{\mathrm{in}}+\mathrm{ESR_{in}}))}{L(R_{\mathrm{in}}+\mathrm{ESR_{in}})} & 0 & 0 \\ 0 & 0 & 0 & 0 \\ \hdashline 0 & 0 & 0 & 1 \end{array}\right], \quad \text{(B.6a)}$$

$$\mathbf{B}_1^{\mathrm{S2}}(t) = \left[\begin{array}{cc} \frac{1}{C_{\mathrm{in}}(R_{\mathrm{in}}+\mathrm{ESR_{in}})} & 0 \\ \frac{\mathrm{ESR_{in}}}{L(R_{\mathrm{in}}+\mathrm{ESR_{in}})} & 0 \\ 0 & \frac{-1}{C_o} \\ \hdashline 0 & 0 \end{array}\right] \quad \text{(B.6b)}$$

$$\mathbf{C}_1^{\mathrm{S2}}(t) = \left[\begin{array}{ccc:c} \frac{-1}{(R_{\mathrm{in}}+\mathrm{ESR_{in}})} & \frac{\mathrm{ESR_{in}}}{(R_{\mathrm{in}}+\mathrm{ESR_{in}})} & 0 & 0 \\ 0 & 0 & 1 & 0 \end{array}\right], \quad \text{(B.6c)}$$

$$\mathbf{D}_1^{\mathrm{S2}}(t) = \left[\begin{array}{cc} \frac{1}{(R_{\mathrm{in}}+\mathrm{ESR_{in}})} & 0 \\ 0 & -\boxed{\mathrm{ESR_o}(t)} \end{array}\right], \quad \text{(B.6d)}$$

then, the augmented state-space matrices of subsystem 2 with $\mathrm{ESR_o}(t)$ are:

$$\mathbf{A}_2^{\mathrm{S2}}(t) = \left[\begin{array}{ccc:c} \frac{-1}{C_{\mathrm{in}}(R_{\mathrm{in}}+\mathrm{ESR_{in}})} & \frac{-R_{\mathrm{in}}}{C_{\mathrm{in}}(R_{\mathrm{in}}+\mathrm{ESR_{in}})} & 0 & 0 \\ \frac{R_{\mathrm{in}}}{L(R_{\mathrm{in}}+\mathrm{ESR_{in}})} & \frac{-(R_{\mathrm{in}}\mathrm{ESR_{in}}+(R_L+\boxed{\mathrm{ESR_o}(t)})(R_{\mathrm{in}}+\mathrm{ESR_{in}}))}{L(R_{\mathrm{in}}+\mathrm{ESR_{in}})} & \frac{-1}{L} & 0 \\ 0 & \frac{1}{C_{\mathrm{o}}} & 0 & 0 \\ \hdashline 0 & 0 & 0 & 1 \end{array}\right], \quad \text{(B.7a)}$$

$$\mathbf{B}_2^{\mathrm{S2}}(t) = \left[\begin{array}{cc} \frac{1}{C_{\mathrm{in}}(R_{\mathrm{in}}+\mathrm{ESR_{in}})} & 0 \\ \frac{\mathrm{ESR_{in}}}{L(R_{\mathrm{in}}+\mathrm{ESR_{in}})} & \frac{\boxed{\mathrm{ESR_o}(t)}}{L} \\ 0 & \frac{-1}{C_{\mathrm{o}}} \\ \hdashline 0 & 0 \end{array}\right], \quad \text{(B.7b)}$$

$$\mathbf{C}_2^{\mathrm{S2}}(t) = \left[\begin{array}{ccc:c} \frac{-1}{(R_{\mathrm{in}}+\mathrm{ESR_{in}})} & \frac{\mathrm{ESR_{in}}}{(R_{\mathrm{in}}+\mathrm{ESR_{in}})} & 0 & 0 \\ 0 & \boxed{\mathrm{ESR_o}(t)} & 1 & 0 \end{array}\right], \quad \text{(B.7c)}$$

$$\mathbf{D}_2^{\mathrm{S2}}(t) = \begin{bmatrix} \frac{1}{(R_{\mathrm{in}}+\mathrm{ESR}_{\mathrm{in}})} & 0 \\ 0 & -\boxed{\mathrm{ESR}_{\mathrm{o}}(t)} \end{bmatrix}. \tag{B.7d}$$

The Jacobian matrices of Scenario 2 are obtained as:

$$\mathbf{J}_{\mathbf{A}_2^{\mathrm{S2}}}(t) = \begin{bmatrix} -1.136.10^5 & -1.136.10^3 & 0 & 0 \\ 6.226.10^2 & -6.849.10^3\boxed{\mathrm{ESR}_{\mathrm{o}}(t)} - 96.513 & -6.84910^3 & -6.849.10^3\boxed{x_2(t)} \\ 0 & 200 & 0 & 0 \\ 0 & 0 & 0 & 1 \end{bmatrix}, \tag{B.8}$$

$$\mathbf{J}_{\mathbf{C}_2^{\mathrm{S2}}}(t) = \begin{bmatrix} -9.09 & 0.909 & 0 & 0 \\ 0 & \boxed{\mathrm{ESR}_{\mathrm{o}}(t)} & 1 & \boxed{x_2(t)} \end{bmatrix}, \tag{B.9}$$

B.1.3 Scenario 3: Augmented models

The augmented matrices of subsystem 1 with $R_{\mathrm{ON}}(t)$ and $\mathrm{ESR_o}(t)$ are:

$$\mathbf{A}_1^{\mathrm{S3}}(t) = \left[\begin{array}{ccc:cc} \frac{-1}{C_{\mathrm{in}}(R_{\mathrm{in}}+\mathrm{ESR_{in}})} & \frac{-R_{\mathrm{in}}}{C_{\mathrm{in}}(R_{\mathrm{in}}+\mathrm{ESR_{in}})} & 0 & 0 & 0 \\ \frac{R_{\mathrm{in}}}{L(R_{\mathrm{in}}+\mathrm{ESR_{in}})} & \frac{-(R_{\mathrm{in}}\mathrm{ESR_{in}}+(R_L+\boxed{R_{\mathrm{ON}}(t)})(R_{\mathrm{in}}+\mathrm{ESR_{in}}))}{L(R_{\mathrm{in}}+\mathrm{ESR_{in}})} & 0 & 0 & 0 \\ 0 & 0 & 0 & 0 & 0 \\ \hdashline 0 & 0 & 0 & 1 & 0 \\ 0 & 0 & 0 & 0 & 1 \end{array}\right], \tag{B.10a}$$

$$\mathbf{B}_1^{\mathrm{S3}}(t) = \left[\begin{array}{cc} \frac{1}{C_{\mathrm{in}}R_{iC_{\mathrm{in}}}} & 0 \\ \frac{\mathrm{ESR_{in}}}{L(R_{\mathrm{in}}+\mathrm{ESR_{in}})} & 0 \\ 0 & \frac{-1}{C_o} \\ \hdashline 0 & 0 \\ 0 & 0 \end{array}\right], \tag{B.10b}$$

$$\mathbf{C}_1^{\mathrm{S3}}(t) = \left[\begin{array}{ccc:cc} \frac{-1}{(R_{\mathrm{in}}+\mathrm{ESR_{in}})} & \frac{\mathrm{ESR_{in}}}{(R_{\mathrm{in}}+\mathrm{ESR_{in}})} & 0 & 0 & 0 \\ 0 & 0 & 1 & 0 & 0 \end{array}\right], \tag{B.10c}$$

$$\mathbf{D}_1^{\mathrm{S3}}(t) = \left[\begin{array}{cc} \frac{1}{(R_{\mathrm{in}}+\mathrm{ESR_{in}})} & 0 \\ 0 & -\boxed{\mathrm{ESR_o}(t)} \end{array}\right], \tag{B.10d}$$

then, the augmented state-space matrices of subsystem 2 with $R_{\mathrm{ON}}(t)$ and $\mathrm{ESR_o}(t)$ are:

$$\mathbf{A}_2^{\mathrm{S3}}(t) = \left[\begin{array}{ccc:cc} \frac{-1}{C_{\mathrm{in}}(R_{\mathrm{in}}+\mathrm{ESR_{in}})} & \frac{-R_{\mathrm{in}}}{C_{\mathrm{in}}(R_{\mathrm{in}}+\mathrm{ESR_{in}})} & 0 & 0 & 0 \\ \frac{R_{\mathrm{in}}}{L(R_{\mathrm{in}}+\mathrm{ESR_{in}})} & \frac{-(R_{\mathrm{in}}\mathrm{ESR_{in}}+(R_L+\boxed{\mathrm{ESR_o}(t)})(R_{\mathrm{in}}+\mathrm{ESR_{in}}))}{L(R_{\mathrm{in}}+\mathrm{ESR_{in}})} & \frac{-1}{L} & 0 & 0 \\ 0 & \frac{1}{C_{\mathrm{o}}} & 0 & 0 & 0 \\ \hdashline 0 & 0 & 0 & 1 & 0 \\ 0 & 0 & 0 & 0 & 1 \end{array}\right], \tag{B.11a}$$

$$\mathbf{B}_2^{\mathrm{S3}}(t) = \left[\begin{array}{cc} \frac{1}{C_{\mathrm{in}}(R_{\mathrm{in}}+\mathrm{ESR}_{\mathrm{in}})} & 0 \\ \frac{\mathrm{ESR}_{\mathrm{in}}}{L(R_{\mathrm{in}}+\mathrm{ESR}_{\mathrm{in}})} & \frac{\boxed{\mathrm{ESR}_{\mathrm{o}}(t)}}{L} \\ 0 & \frac{-1}{C_{\mathrm{o}}} \\ \hdashline 0 & 0 \\ 0 & 0 \end{array}\right], \tag{B.11b}$$

$$\mathbf{C}_2^{\mathrm{S3}}(t) = \left[\begin{array}{ccc:cc} \frac{-1}{(R_{\mathrm{in}}+\mathrm{ESR}_{\mathrm{in}})} & \frac{\mathrm{ESR}_{\mathrm{in}}}{(R_{\mathrm{in}}+\mathrm{ESR}_{\mathrm{in}})} & 0 & 0 & 0 \\ 0 & \boxed{\mathrm{ESR}_{\mathrm{o}}(t)} & 1 & 0 & 0 \end{array}\right], \tag{B.11c}$$

$$\mathbf{D}_2^{\mathrm{S3}}(t) = \left[\begin{array}{cc} \frac{1}{(R_{\mathrm{in}}+\mathrm{ESR}_{\mathrm{in}})} & 0 \\ 0 & -\boxed{\mathrm{ESR}_{\mathrm{o}}(t)} \end{array}\right]. \tag{B.11d}$$

This page is intentionally left blank

Bibliography

A, Madhukar Rao and Umesh B Sand Sivakumar K (2013). "A Fault Tolerant Dual Inverter Configuration for Islanded Mode Photovoltaic Generation System". In: pp. 816–821.

Abu-Hanna, A. and Peter J. Lucas (Apr. 2001). "Prognostic Models in Medicine: AI and Statistical Approaches". In: *Methods of information in medicine* 40, pp. 1–5. DOI: 10.1055/s-0038-1634456.

Aeronautics, Office of and Space Technology (Oct. 1992). *Research and technology goals and objectives for integrated vehicle health management (IVHM).* Tech. rep. Report NASA-CR-192656. NASA.

Aggab, T. et al. (2018). "Model-based prognosis applied to a coupled four tank MIMO system". In: *IFAC-PapersOnLine* 51.24, pp. 655–661. ISSN: 24058963. DOI: 10.1016/j.ifacol.2018.09.645. URL: https://doi.org/10.1016/j.ifacol.2018.09.645%20https://linkinghub.elsevier.com/retrieve/pii/S2405896318323577.

Alamo, T et al. (2006). "Introducing linear matrix inequalities in a control course". In: *IFAC Proceedings Volumes* 39.6, pp. 205–210.

Alamo, T., J.M. Bravo, and E.F. Camacho (2005). "Guaranteed state estimation by zonotopes". In: *Automatica* 41.6, pp. 1035–1043. ISSN: 0005-1098. DOI: https://doi.org/10.1016/j.automatica.2004.12.008. URL: http://www.sciencedirect.com/science/article/pii/S0005109805000294.

Alamo, T., J.M. Bravo, M.J. Redondo, et al. (2008). "A set-membership state estimation algorithm based on DC programming". In: *Automatica* 44.1, pp. 216–224. ISSN: 0005-1098. DOI: https://doi.org/10.1016/j.automatica.2007.05.008. URL: http://www.sciencedirect.com/science/article/pii/S0005109807002518.

Alyakhni, A., A. Al-Mohamad, and G. Hoblos (Sept. 2019). "Joint Estimation of MOSFET Degradation in a DC-DC Converter Using Extended Kalman Filter". In: *2019 4th Conference on Control and Fault Tolerant Systems (SysTol)*, pp. 319–324. DOI: 10.1109/SYSTOL.2019.8864731.

An, D., N. H. Kim, and J. Choi (2015). "Practical options for selecting data-driven or physics-based prognostics algorithms with reviews". In: *Reliability Engineering & System Safety* 133, pp. 223–236. ISSN: 0951-8320. DOI: https://doi.org/10.1016/j.ress.2014.09.014. URL: https://www.sciencedirect.com/science/article/pii/S0951832014002245.

Anderson, J. M., R. W. Cox, and P. O'Connor (Aug. 2013). "Online algorithm for early stage fault detection in IGBT switches". In: *2013 9th IEEE International Symposium on Diagnostics for Electric Machines, Power Electronics and Drives (SDEMPED)*, pp. 1–8. DOI: 10.1109/DEMPED.2013.6645689.

Arulampalam, M.S. et al. (2002). "A tutorial on particle filters for online nonlinear/non-Gaussian Bayesian tracking". In: *IEEE Transactions on Signal Processing* 50.2, pp. 174–188. DOI: 10.1109/78.978374.

Åström, K. J. and B. Wittenmark (1898). *Adaptive control*. Addison-Wesley.

Azoui, T. et al. (Apr. 2012). "Numerical and experimental results correlation during power MOSFET ageing". In: *2012 13th International Thermal, Mechanical and Multi-Physics Simulation and Experiments in Microelectronics and Microsystems*, pp. 1/4–4/4. DOI: 10.1109/ESimE.2012.6191798.

Balaban, E., A. Saxena, S. Narasimhan, I. Roychoudhury, and K. Goebel (Mar. 2011). "Experimental Validation of a Prognostic Health Management System for Electro-Mechanical Actuators". In: *Infotech@Aerospace 2011*. DOI: 10.2514/6.2011-1518. eprint: https://arc.aiaa.org/doi/pdf/10.2514/6.2011-1518.

Balaban, E., A. Saxena, S. Narasimhan, I. Roychoudhury, M. Koopmans, et al. (2015). "Prognostic Health-Management System Development for Electromechanical Actuators". In: *Journal of Aerospace Information Systems* 12.3, pp. 329–344. DOI: 10.2514/1.I010171.

Bamieh, B. and L. Giarre (2002). "Identification of linear parameter varying models". In: *International Journal of Robust and Nonlinear Control: IFAC-Affiliated Journal* 12.9, pp. 841–853.

Baptista, M. et al. (2019). "Remaining useful life estimation in aeronautics: Combining data-driven and Kalman filtering". In: *Reliability Engineering & System Safety* 184. Impact of Prognostics and Health Management in Systems Reliability and Maintenance Planning, pp. 228–239. ISSN: 0951-8320. DOI: https://doi.org/10.1016/j.ress.2018.01.017. URL: https://www.sciencedirect.com/science/article/pii/S095183201731075X.

Becis-Aubry, Y. and N. Ramdani (2012). "State-bounding estimation for nonlinear models with multiple measurements". In: *2012 American Control Conference (ACC)*, pp. 1883–1888. DOI: 10.1109/ACC.2012.6315596.

Bertsekas, D. and I. Rhodes (1971). "Recursive state estimation for a set-membership description of uncertainty". In: *IEEE Transactions on Automatic Control* 16.2, pp. 117–128. DOI: 10.1109/TAC.1971.1099674.

Blanchard, E. D., A. Sandu, and C. Sandu (2007). "Parameter estimation method using an extended Kalman filter". In:

Bonissone, P. and K. Goebel (Dec. 2002). "When will it break? A hybrid soft computing model to predict time-to-break margins in paper machines". In: *Applications and Science of Neural Networks, Fuzzy Systems, and Evolutionary Computation V*. Ed. by B. Bosacchi, D. B. Fogel, and J. C. Bezdek. Vol. 4787. 1997, p. 53. DOI: 10.1117/12.455868. URL: http://proceedings.spiedigitallibrary.org/proceeding.aspx?doi=10.1117/12.455868.

Boyd, Donald W. (2001a). "CHAPTER 1 - Systems Analysis and Model Synthesis". In: *Systems Analysis and Modeling*. Ed. by D. W. Boyd. San Diego: Academic Press, pp. 3–33. ISBN: 978-0-12-121851-5. DOI: https://doi.org/10.1016/B978-012121851-5/50001-0. URL: https://www.sciencedirect.com/science/article/pii/B9780121218515500010.

Boyd, Donald W. (2001b). "CHAPTER 2 - Systems Modeling Principles". In: *Systems Analysis and Modeling*. Ed. by D. W. Boyd. San Diego: Academic Press, pp. 35–73. ISBN: 978-0-12-121851-5. DOI: https://doi.org/10.1016/B978-012121851-5/50002-2. URL: https://www.sciencedirect.com/science/article/pii/B9780121218515500022.

Boyd, Stephen et al. (1994). *Some Standard Problems Involving LMIs*, pp. 7–35. ISBN: 089871334X. DOI: 10.1137/1.9781611970777.ch2.

Brown, D. W. et al. (Feb. 2012). "Turn-Off Time as an Early Indicator of Insulated Gate Bipolar Transistor Latch-up". In: *IEEE Transactions on Power Electronics* 27.2, pp. 479–489. ISSN: 1941-0107. DOI: 10.1109/TPEL.2011.2159848.

C.D., Pettit et al. (Jan. 1999). "Reusable Rocket Engine Advanced Health Management System. Architecture and Technology Evaluation: Summary". In: *35th AIAA/ASME/SAR/ASEE joint propulsion conference and exhibit*.

CALCE (1986). *Center for Advanced Life Cycle Engineering*. http://www.calce.umd.edu.

Capelli-Schellpfeffer, M., M. Kang, and M. G. Pecht (2018). "PHM in Healthcare". In: *Prognostics and Health Management of Electronics*. John Wiley & Sons, Ltd. Chap. 15, pp. 431–449. ISBN: 9781119515326. DOI: https://doi.org/10.1002/9781119515326.ch15. eprint: https://onlinelibrary.wiley.com/doi/pdf/10.1002/9781119515326.ch15. URL: https://onlinelibrary.wiley.com/doi/abs/10.1002/9781119515326.ch15.

Celaya, J. et al. (2011). "A Model-based Prognostics Methodology for Electrolytic Capacitors Based on Electrical Overstress Accelerated Aging". In: *Annual Conference of the Prognostics and Health Management Society 2011*. Montreal QC, Canada: PHM, pp. 31–39. ISBN: 978-1-936263-03-5.

Celaya, J. R., A. Saxena, C. S. Kulkarni, et al. (Jan. 2012). "Prognostics approach for power MOSFET under thermal-stress aging". In: *2012 Proceedings Annual Reliability and Maintainability Symposium*, pp. 1–6. DOI: 10.1109/RAMS.2012.6175487.

Celaya, J. R., A. Saxena, S. Saha, and K. F. Goebel (2011). "Prognostics of Power MOSFETs under Thermal Stress Accelerated Aging using Data-

Driven and Model-Based Methodologies". In: *Annual Conference of the Prognostics and Health Management Society 2011*, pp. 443–452.

Celaya, J. R., A. Saxena, S. Saha, V. Vashchenko, et al. (May 2011a). "Prognostics of power MOSFET". In: *2011 IEEE 23rd International Symposium on Power Semiconductor Devices and ICs*, pp. 160–163. DOI: 10.1109/ISPSD.2011.5890815.

— (May 2011b). "Prognostics of power MOSFET". In: *2011 IEEE 23rd International Symposium on Power Semiconductor Devices and ICs*, pp. 160–163. DOI: 10.1109/ISPSD.2011.5890815.

Celaya, J. R., P. Wysocki, et al. (Sept. 2010). "Accelerated aging system for prognostics of power semiconductor devices". In: *2010 IEEE AUTOTESTCON*, pp. 1–6. DOI: 10.1109/AUTEST.2010.5613564.

Celaya, Jose R et al. (2010). "Towards Prognostics of Power MOSFETs: Accelerated Aging and Precursors of Failure". In: *Annual Conference of the Prognostics and Health Management Society 2010*. Portland, OR.

Celaya, J. R. and Saxena, A. and Saha, S. and Goebel, K. (2011). *MOSFET Thermal Overstress Aging Data Set*. NASA Ames Prognostics Data Repository (http://ti.arc.nasa.gov/project/prognostic-data-repository). NASA Ames Research Center, Moffett Field, CA.

Chang, M., J. Fan, et al. (2018). "PHM of Light-Emitting Diodes". In: *Prognostics and Health Management of Electronics*. John Wiley & Sons, Ltd. Chap. 14, pp. 377–430. ISBN: 9781119515326. DOI: https://doi.org/10.1002/9781119515326.ch14. eprint: https://onlinelibrary.wiley.com/doi/pdf/10.1002/9781119515326.ch14. URL: https://onlinelibrary.wiley.com/doi/abs/10.1002/9781119515326.ch14.

Chang, M., M. Kang, and M. Pecht (2017). "Prognostics-Based LED Qualification Using Similarity-Based Statistical Measure With RVM Regression Model". In: *IEEE Transactions on Industrial Electronics* 64.7, pp. 5667–5677. DOI: 10.1109/TIE.2017.2677301.

Chelidze, D., J. P. Cusumano, and Anindya Chatterjee (2001). "Procedure for tracking damage evolution and predicting remaining useful life with application to an electromechanical experiment system". In: *Component and Systems Diagnostics, Prognosis, and Health Management*. Ed. by P. K.

Willett and T. Kirubarajan. Vol. 4389. International Society for Optics and Photonics. SPIE, pp. 12–22. DOI: 10.1117/12.434238. URL: https://doi.org/10.1117/12.434238.

Chen, Y. et al. (2008). "Online Failure Prediction of the Electrolytic Capacitor for LC Filter of Switching-Mode Power Converters". In: 55.1, pp. 400–406.

Cheng, S., M. H. Azarian, and M. G. Pecht (2010). "Sensor Systems for Prognostics and Health Management". In: *Sensors* 10.6, pp. 5774–5797. ISSN: 1424-8220. DOI: 10.3390/s100605774. URL: https://www.mdpi.com/1424-8220/10/6/5774.

Cheng, S. and M. Pecht (Aug. 2009). "A fusion prognostics method for remaining useful life prediction of electronic products". In: *2009 IEEE International Conference on Automation Science and Engineering*, pp. 102–107. DOI: 10.1109/COASE.2009.5234098.

Choi, U., S. Jørgensen, and F. Blaabjerg (Dec. 2016). "Advanced Accelerated Power Cycling Test for Reliability Investigation of Power Device Modules". In: *IEEE Transactions on Power Electronics* 31.12, pp. 8371–8386. ISSN: 1941-0107. DOI: 10.1109/TPEL.2016.2521899.

Ciappa, Mauro (2002). "Selected failure mechanisms of modern power modules". In: *Microelectronics Reliability* 42.4, pp. 653–667. ISSN: 0026-2714. DOI: https://doi.org/10.1016/S0026-2714(02)00042-2.

Combastel, C. (2003). "A state bounding observer based on zonotopes". In: *2003 European Control Conference (ECC)*, pp. 2589–2594. DOI: 10.23919/ECC.2003.7085991.

— (2005). "A State Bounding Observer for Uncertain Non-linear Continuous-time Systems based on Zonotopes". In: *Proceedings of the 44th IEEE Conference on Decision and Control*, pp. 7228–7234. DOI: 10.1109/CDC.2005.1583327.

— (2015). "Zonotopes and Kalman observers: Gain optimality under distinct uncertainty paradigms and robust convergence". In: *Automatica* 55, pp. 265–273. ISSN: 0005-1098. DOI: https://doi.org/10.1016/j.automatica.2015.03.008.

Daigle, M. J. and K. Goebel (May 2013). "Model-Based Prognostics With Concurrent Damage Progression Processes". In: *IEEE Transactions on Systems, Man, and Cybernetics: Systems* 43.3, pp. 535–546. ISSN: 2168-2216. DOI: 10.1109/TSMCA.2012.2207109. URL: http://ieeexplore.ieee.org/document/6301756/.

Daroogheh, N. et al. (2015). "A hybrid prognosis and health monitoring strategy by integrating particle filters and neural networks for gas turbine engines". In: *2015 IEEE Conference on Prognostics and Health Management (PHM)*, pp. 1–8. DOI: 10.1109/ICPHM.2015.7245020.

Darouach, M., M. Zasadzinski, and S.J. Xu (1994). "Full-order observers for linear systems with unknown inputs". In: *IEEE Transactions on Automatic Control* 39.3, pp. 606–609. DOI: 10.1109/9.280770.

Dat, M A I Tuan et al. (2012). "Fault-Tolerant Topology of a Grid-Connected PV Inverter Coupled by a Scott Transformer". In: pp. 428–433.

defense, Office of the secretary of (Apr. 2002). *Mandatory Procedures for Major Defense Acquisition Programs (MDAPS) and Major Automated Information Systems (MAIS) acquisition programs*. en. Standard DoD 5000.2-R. USA: Office of the secretary of defense.

Denson, W. (Sept. 1998). "The history of reliability prediction". In: *IEEE Transactions on Reliability* 47.3, SP321–SP328. ISSN: 1558-1721. DOI: 10.1109/24.740547.

Denson, W.A. (1999). "A tutorial: PRISM". In: *RAC Journal*, pp. 1–6.

Djeziri, M. A., S. Benmoussa, and R. Sanchez (2018). "Hybrid method for remaining useful life prediction in wind turbine systems". In: *Renewable Energy* 116, pp. 173–187. ISSN: 18790682. DOI: 10.1016/j.renene.2017.05.020. URL: https://doi.org/10.1016/j.renene.2017.05.020.

Djeziri, M.A., S. Benmoussa, and M.EH. Benbouzid (2019). "Data-driven approach augmented in simulation for robust fault prognosis". In: *Engineering Applications of Artificial Intelligence* 86, pp. 154–164. ISSN: 0952-1976. DOI: https://doi.org/10.1016/j.engappai.2019.09.002. URL: https://www.sciencedirect.com/science/article/pii/S0952197619302180.

Dupont, L. et al. (Sept. 2007). "Ageing Test Results of low voltage MOSFET Modules for electrical vehicles". In: *2007 European Conference on Power Electronics and Applications*, pp. 1–10. DOI: 10.1109/EPE.2007.4417433.

Durieu, C., É. Walter, and B. Polyak (Nov. 2001). "Multi-Input Multi-Output Ellipsoidal State Bounding". In: *Journal of Optimization Theory and Applications* 111.2, pp. 273–303. ISSN: 0022-3239. DOI: 10.1023/A:1011978200643. URL: http://link.springer.com/10.1023/A:1011978200643.

Dusmez, S. and B. Akin (May 2015a). "An accelerated thermal aging platform to monitor fault precursor on-state resistance". In: *2015 IEEE International Electric Machines Drives Conference (IEMDC)*, pp. 1352–1358. DOI: 10.1109/IEMDC.2015.7409238.

— (2015b). "Remaining useful lifetime estimation for degraded power MOSFETs under cyclic thermal stress". In: *2015 IEEE Energy Conversion Congress and Exposition (ECCE)*, pp. 3846–3851. DOI: 10.1109/ECCE.2015.7310203.

Dusmez, S., S. H. Ali, et al. (2017). "Aging Precursor Identification and Lifetime Estimation for Thermally Aged Discrete Package Silicon Power Switches". In: *IEEE Transactions on Industry Applications* 53.1, pp. 251–260.

Dusmez, S., H. Duran, and B. Akin (May 2016). "Remaining Useful Lifetime Estimation for Thermally Stressed Power MOSFETs Based on on-State Resistance Variation". In: *IEEE Transactions on Industry Applications* 52.3, pp. 2554–2563. ISSN: 1939-9367. DOI: 10.1109/TIA.2016.2518127.

Ekanayake, T. et al. (2019). "Model-based fault diagnosis and prognosis of dynamic systems: a review". In: *Procedia Manufacturing* 30. Digital Manufacturing Transforming Industry Towards Sustainable Growth, pp. 435–442. ISSN: 2351-9789. DOI: https://doi.org/10.1016/j.promfg.2019.02.060. URL: https://www.sciencedirect.com/science/article/pii/S2351978919300903.

Elattar, Hatem M., Hamdy K. Elminir, and A. M. Riad (2016). "Prognostics: a literature review". In: *Complex & Intelligent Systems* 2.2, pp. 125–154. ISSN: 2199-4536. DOI: 10.1007/s40747-016-0019-3.

Eleffendi, M. A. and C. M. Johnson (Sept. 2015). "Evaluation of on-state voltage VCE(ON) and threshold voltage Vth for real-time health monitoring of IGBT power modules". In: *2015 17th European Conference on Power Electronics and Applications (EPE'15 ECCE-Europe)*, pp. 1–10. DOI: 10.1109/EPE.2015.7309265.

Evans, PC and M Annunziata (2012). *Industrial internet: pushing the boundaries of minds and machines*. en. Standard 11.26.2012. General Electric. URL: http://www.ge.com/docs/chapters/Industrial_Internet.pdf.

Feather, M. S. et al. (Sept. 2008). "Guiding Technology Deployment Decisions using a Quantitative Requirements Analysis Technique". In: *2008 16th IEEE International Requirements Engineering Conference*, pp. 271–276. DOI: 10.1109/RE.2008.37.

Ferhat, T. (Sept. 2020). "Towards system-level prognostics : Modeling, uncertainty propagation and system remaining useful life prediction". PhD thesis. DOI: 10.13140/RG.2.2.32479.48801.

FIDES Group (2004) (2004). *FIDES Guide–Reliability Methodology for Electronic Systems*. en. Tech. rep. FIDES Group.

Flynn, D. et al. (2018). "PHM of Subsea Cables". In: *Prognostics and Health Management of Electronics*. John Wiley & Sons, Ltd. Chap. 16, pp. 451–478. ISBN: 9781119515326. DOI: https://doi.org/10.1002/9781119515326.ch16. eprint: https://onlinelibrary.wiley.com/doi/pdf/10.1002/9781119515326.ch16. URL: https://onlinelibrary.wiley.com/doi/abs/10.1002/9781119515326.ch16.

Gaspar, P., Z. Szabo, and J. Bokor (2005). "Gray-Box Continuous-Time Parameter Identification for Lpv Models with Vehicle Dynamics Applications". In: *Proceedings of the 2005 IEEE International Symposium on, Mediterrean Conference on Control and Automation Intelligent Control, 2005.* Pp. 393–398. DOI: 10.1109/.2005.1467047.

— (2007). "A grey-box identification of an LPV vehicle model for observer-based side slip angle estimation". In: *2007 American Control Conference*, pp. 2961–2966. DOI: 10.1109/ACC.2007.4282629.

Gavin, H. P. (2020). *The Levenburg-Marqurdt Algorithm For Nonlinear Least Squares Curve-Fitting Problems*. Tech. rep., pp. 1–19. URL: http://people.duke.edu/%7B~%7Dhpgavin/ce281/lm.pdf.

Goebel, K., N. Eklund, and P. Bonanni (Mar. 2006). "Fusing competing prediction algorithms for prognostics". In: *2006 IEEE Aerospace Conference*. DOI: 10.1109/AERO.2006.1656116.

Goebel, K., B. Saha, et al. (Aug. 2008). "Prognostics in Battery Health Management". In: *IEEE Instrumentation Measurement Magazine* 11.4, pp. 33–40. ISSN: 1941-0123. DOI: 10.1109/MIM.2008.4579269.

Goebel, K., A. Saxena, et al. (2012). "Introduction to Prognostics". In: *First European Conference of the Prognostics and Health Management Society 2012*. URL: https://phmsociety.org/wp-content/uploads/2011/08/Tutorial%7B%5C_%7DPrognostics.pdf.

Goodman, D., J. Hofmeister, and J. Judkins (2007). "Electronic prognostics for switched mode power supplies". In: *Microelectronics Reliability* 47.12. Electronic system prognostics and health management, pp. 1902–1906. ISSN: 0026-2714. DOI: https://doi.org/10.1016/j.microrel.2007.02.021. URL: https://www.sciencedirect.com/science/article/pii/S0026271407001370.

Groot Wassink, M. et al. (2005). "LPV control for a wafer stage: beyond the theoretical solution". In: *Control Engineering Practice* 13.2, pp. 231–245. ISSN: 0967-0661. DOI: https://doi.org/10.1016/j.conengprac.2004.03.008. URL: https://www.sciencedirect.com/science/article/pii/S0967066104000565.

Hanif, A. et al. (2019). "A Comprehensive Review Toward the State-of-the-Art in Failure and Lifetime Predictions of Power Electronic Devices". In: *IEEE Transactions on Power Electronics* 34.5, pp. 4729–4746. DOI: 10.1109/TPEL.2018.2860587.

Hart, D. W. (2010). *Power Electronics*. McGraw-Hill. ISBN: 978-0-07-338067-4.

He, Y. et al. (2018). "Kalman Filtering Algorithm for Systems with Stochastic Nonlinearity Functions, Finite-Step Correlated Noises, and Missing Measurements". In: *Discrete Dynamics in Nature and Society* 2018, pp. 1–

12. ISSN: 1026-0226. DOI: 10.1155/2018/1516028. URL: https://www.hindawi.com/journals/ddns/2018/1516028/.

Hu, C., G. Jain, P. Tamirisa, et al. (2014). "Method for estimating capacity and predicting remaining useful life of lithium-ion battery". In: *Applied Energy* 126.C, pp. 182–189. DOI: 10.1016/j.apenergy.2014.0. URL: https://ideas.repec.org/a/eee/appene/v126y2014icp182-189.html.

Hu, C., G. Jain, P. Zhang, et al. (2014). "Data-driven method based on particle swarm optimization and k-nearest neighbor regression for estimating capacity of lithium-ion battery". In: *Applied Energy* 129.C, pp. 49–55. DOI: 10.1016/j.apenergy.2014.0. URL: https://ideas.repec.org/a/eee/appene/v129y2014icp49-55.html.

Hu, C., B. D. Youn, and J. Chung (2012). "A multiscale framework with extended Kalman filter for lithium-ion battery SOC and capacity estimation". In: *Applied Energy* 92.C, pp. 694–704. DOI: 10.1016/j.apenergy.2011.0. URL: https://ideas.repec.org/a/eee/appene/v92y2012icp694-704.html.

Hyde, R. A. and K. Glover (July 1993). "The application of scheduled H/sub infinity / controllers to a VSTOL aircraft". In: *IEEE Transactions on Automatic Control* 38.7, pp. 1021–1039. ISSN: 1558-2523. DOI: 10.1109/9.231458.

ISO Central Secretary (Sept. 2015). *ISO 13381-1:2015 Condition monitoring and diagnostics of machines — Prognostics — Part 1: General guidelines*. en. Standard ISO 13381-1:2015. Geneva, CH: International Organization for Standardization. URL: https://www.iso.org/standard/51436.html.

Julier, S.J. and J.K. Uhlmann (Mar. 2004). "Unscented Filtering and Nonlinear Estimation". In: *Proceedings of the IEEE* 92.3, pp. 401–422. ISSN: 0018-9219. DOI: 10.1109/JPROC.2003.823141. URL: http://ieeexplore.ieee.org/document/1271397/.

Kalman, R. E. (Mar. 1960). "A New Approach to Linear Filtering and Prediction Problems". In: *Journal of Basic Engineering* 82.1, pp. 35–45. ISSN: 0021-9223. DOI: 10.1115/1.3662552. eprint: https://asmedigitalcollection.

asme.org/fluidsengineering/article-pdf/82/1/35/5518977/35_1.pdf. URL: https://doi.org/10.1115/1.3662552.

Katsis, D. C. and J. D. van Wyk (Sept. 2001). "Void induced thermal impedance in power semiconductor modules: some transient temperature effects". In: *Conference Record of the 2001 IEEE Industry Applications Conference. 36th IAS Annual Meeting (Cat. No.01CH37248)*. Vol. 3, 1905–1911 vol.3. DOI: 10.1109/IAS.2001.955790.

Khorshed Alam, Mohammed and Faisal H. Khan (2013). "Reliability Analysis and Performance Degradation of a Boost Converter". In: *IEEE Energy Conversion Congress and Exposition (ECCE)*.

Kim, N., D. An, and J. Choi (2017a). "Applications of Prognostics". In: *Prognostics and Health Management of Engineering Systems: An Introduction*. Cham: Springer International Publishing, pp. 281–344. ISBN: 978-3-319-44742-1. DOI: 10.1007/978-3-319-44742-1_7. URL: https://doi.org/10.1007/978-3-319-44742-1_7.

— (2017b). "Introduction". In: *Prognostics and Health Management of Engineering Systems: An Introduction*. Cham: Springer International Publishing, pp. 1–24. ISBN: 978-3-319-44742-1. DOI: 10.1007/978-3-319-44742-1_1. URL: https://doi.org/10.1007/978-3-319-44742-1_1.

— (2017c). "Physics-Based Prognostics". In: *Prognostics and Health Management of Engineering Systems: An Introduction*. Cham: Springer International Publishing, pp. 127–178. ISBN: 978-3-319-44742-1. DOI: 10.1007/978-3-319-44742-1_4. URL: https://doi.org/10.1007/978-3-319-44742-1_4.

— (2017d). "Tutorials for Prognostics". In: *Prognostics and Health Management of Engineering Systems: An Introduction*. Cham: Springer International Publishing, pp. 25–71. ISBN: 978-3-319-44742-1. DOI: 10.1007/978-3-319-44742-1_2. URL: https://doi.org/10.1007/978-3-319-44742-1_2.

Kothamasu, R., S. H. Huang, and W. H. VerDuin (2005). "System health monitoring and prognostics - a review of current paradigms and practices". In:

Krebs, T. et al. (2013). "A Breakthrough in Power Electronics Reliability – New Die Attach and Wire Bonding Materials". In: pp. 1746–1752.

Kühn, W. (1998). "Rigorously Computed Orbits of Dynamical Systems without the Wrapping Effect". In: *Computing (Vienna/New York)* 61.1, pp. 47–67. ISSN: 0010485X. DOI: 10.1007/BF02684450.

Kulkarni, C., J. Celaya, G. Biswas, et al. (2011). "Prognostic Modeling and Experimental Techniques for Electrolytic Capacitor Health Monitoring". In: *Structural Health Monitoring 2011: Condition-Based Maintenance and Intelligent Structures - Proceedings of the 8th International Workshop on Structural Health Monitoring*. National Aeronautics and Space Administration MOFFETT Field CA AMES Research Center, pp. 1225–1232. ISBN: 9781605950532 (ISBN).

Kulkarni, C., J. Celaya, K. Goebel, et al. (Sept. 2012). "Bayesian Framework Approach for Prognostic Studies in Electrolytic Capacitor under Thermal Overstress Conditions". In: *Annual Conference of the PHM Society, 4(1)*. DOI: 10.36001/phmconf.2012.v4i1.2138.

Kulkarni, C. S. et al. (Sept. 2012). "Prognostics of Power Electronics, methods and validation experiments". In: *2012 IEEE AUTOTESTCON Proceedings*, pp. 194–199. DOI: 10.1109/AUTEST.2012.6334578.

Kulkarni, Chetan, Gautam Biswas, Jose Celaya, et al. (Feb. 2011). "Prognostic Techniques for Capacitor Degradation and Health Monitoring". In:

Kulkarni, Chetan, Gautam Biswas, X. Koutsoukos, et al. (Feb. 2010). "Physics of Failure Models for Capacitor Degradation in DC-DC Converters". In:

Kulkarni, Chetan S., Gautam Biswas, José R. Celaya, et al. (2012). "Physics Based Electrolytic Capacitor Degradation Models for Prognostic Studies under Thermal Overstress". In: *European Conference of the Prognostics and Health Management Society* 4.1, pp. 1–9. ISSN: 21532648. URL: http://www.phmsociety.org/node/936.

Kulkarni, Chetan S., Gautam Biswas, and Xenofon Koutsoukos (2009). "A prognosis case study for electrolytic capacitor degradation in DC-DC converters". In: *Annual Conference of the Prognostics and Health Management Society, PHM 2009*, pp. 1–10.

Kwon, D., M. H. Azarian, and M. Pecht (Nov. 2015). "Remaining-Life Prediction of Solder Joints Using RF Impedance Analysis and Gaussian Process Regression". In: *IEEE Transactions on Components, Packaging and Manufacturing Technology* 5.11, pp. 1602–1609. ISSN: 2156-3985. DOI: 10.1109/TCPMT.2015.2477098.

Kwon, D. and J. Yoon (Oct. 2016). "A model-based prognostic approach to predict interconnect failure using impedance analysis". In: *Journal of Mechanical Science and Technology* 30, pp. 4447–4452. DOI: 10.1007/s12206-016-0910-2.

L.H., Chiang, Russel E.L., and Braatz R.D. (2001). *Fault Detection and Diagnosis in Industrial Systems*. London: Springer-Verlag.

Le, Susana Estefany De et al. (2013). "Effect of the Mission Profile on the Reliability of a Power Converter Aimed at Photovoltaic Applications — A Case Study". In: 28.6, pp. 2998–3007.

Le, V. T. H. et al. (2013). "Zonotope-based set-membership estimation for Multi-Output uncertain systems". In: *2013 IEEE International Symposium on Intelligent Control (ISIC)*, pp. 212–217. DOI: 10.1109/ISIC.2013.6658619.

— (2013a). "Several Approaches on Zonotopic Guaranteed Set-Membership Estimation". In: *Zonotopes*. John Wiley & Sons, Ltd. Chap. 2, pp. 27–47. ISBN: 9781118761588. DOI: https://doi.org/10.1002/9781118761588.ch2. eprint: https://onlinelibrary.wiley.com/doi/pdf/10.1002/9781118761588.ch2. URL: https://onlinelibrary.wiley.com/doi/abs/10.1002/9781118761588.ch2.

— (2013b). "Zonotopic Guaranteed State Estimation Based on P-Radius Minimization". In: *Zonotopes*. John Wiley & Sons, Ltd. Chap. 3, pp. 49–93. ISBN: 9781118761588. DOI: https://doi.org/10.1002/9781118761588.ch3. eprint: https://onlinelibrary.wiley.com/doi/pdf/10.1002/9781118761588.ch3. URL: https://onlinelibrary.wiley.com/doi/abs/10.1002/9781118761588.ch3.

Le, Vu Tuan Hieu et al. (Nov. 2013). "Zonotopic Guaranteed State Estimation for Uncertain Systems". In: *Automatica* 49.11, pp. 3418–3424. ISSN: 0005-1098. DOI: 10.1016/j.automatica.2013.08.014. URL: https://doi.org/10.1016/j.automatica.2013.08.014.

Leao, B. P. et al. (2008). "Prognostics performance metrics and their relation to requirements, design, verification and cost-benefit". In: *2008 International Conference on Prognostics and Health Management*, pp. 1–8. DOI: 10.1109/PHM.2008.4711429.

Lee, L. H. and K. Poolla (1996). "Identification of linear parameter-varying systems via LFTs". In: *Proceedings of 35th IEEE Conference on Decision and Control*. Vol. 2, 1545–1550 vol.2. DOI: 10.1109/CDC.1996.572742.

Li, M. et al. (Aug. 2013). "Prognostics of Analog Filters Based on Particle Filters Using Frequency Features". In: *Journal of Electronic Testing* 29.4, pp. 567–584. ISSN: 0923-8174. DOI: 10.1007/s10836-013-5383-y. URL: http://link.springer.com/10.1007/s10836-013-5383-y.

Li, Z., Z. Zheng, and R. Outbib (2018). "A prognostic methodology for power MOSFETs under thermal stress using echo state network and particle filter". In: *Microelectronics Reliability* 88-90. 29th European Symposium on Reliability of Electron Devices, Failure Physics and Analysis (ESREF 2018), pp. 350–354. ISSN: 0026-2714. DOI: https://doi.org/10.1016/j.microrel.2018.07.137.

Liu, D. et al. (2013). "Prognostics for state of health estimation of lithium-ion batteries based on combination Gaussian process functional regression". In: *Microelectronics Reliability* 53.6, pp. 832–839. ISSN: 0026-2714. DOI: https://doi.org/10.1016/j.microrel.2013.03.010. URL: https://www.sciencedirect.com/science/article/pii/S0026271413000747.

Lombardo, Salvatore et al. (2005). "Dielectric breakdown mechanisms in gate oxides". In: *Journal of Applied Physics* 98.12, p. 121301. DOI: 10.1063/1.2147714.

Lovera, M., M. Bergamasco, and F. Casella (2013). "LPV Modelling and Identification: An Overview". In: *Robust Control and Linear Parameter Varying Approaches: Application to Vehicle Dynamics*. Ed. by O. Sename, P. Gaspar, and J. Bokor. Berlin, Heidelberg: Springer Berlin Heidelberg, pp. 3–24. ISBN: 978-3-642-36110-4. DOI: 10.1007/978-3-642-36110-4_1. URL: https://doi.org/10.1007/978-3-642-36110-4_1.

Luo, J., M. Namburu, and K. Pattipati (2003). "Model-based Prognostic Techniques". In: *IEEE*.

Ma, H. et al. (2020). *Kalman Filtering and Information Fusion*. Singapore: Springer Singapore. DOI: 10.1007/978-981-15-0806-6. URL: http://link.springer.com/10.1007/978-981-15-0806-6.

Mazzaro, M. C., E. A. Movsichoff, and R. S. S. Pena (June 1999). "Robust identification of linear parameter varying systems". In: *Proceedings of the 1999 American Control Conference (Cat. No. 99CH36251)*. Vol. 4, 2282–2284 vol.4. DOI: 10.1109/ACC.1999.786419.

Medjaher, K. and N. Zerhouni (2009). "Residual-based failure prognostic in dynamic systems". In: *IFAC Proceedings Volumes* 42.8. 7th IFAC Symposium on Fault Detection, Supervision and Safety of Technical Processes, pp. 716–721. ISSN: 1474-6670. DOI: https://doi.org/10.3182/20090630-4-ES-2003.00119. URL: https://www.sciencedirect.com/science/article/pii/S1474667016358621.

Merhy, D. (Oct. 2019). "Contribution to ellipsoidal and zonotopic set-membership state estimation". PhD thesis.

MIL-HDBK 217 (1965) (1965). *Military Handbook for Reliability Prediction of Electronic Equipment*. en. Tech. rep. United States of America: US Department of Defense.

Mohagheghi, S., R. G. Harley, and T. G. Habetler (2009). "Condition Monitoring of Power Electronic Circuits Using Artificial Neural Networks". In: 24.10, pp. 2363–2367.

Al-Mohamad, A., G. Hoblos, and V. Puig (Sept. 2019). "A Model-Based Prognostics Approach for RUL Forecasting of a Degraded DC-DC Converter". In: *2019 4th Conference on Control and Fault Tolerant Systems (SysTol)*, pp. 312–318. DOI: 10.1109/SYSTOL.2019.8864778.

— (2020). "A hybrid system-level prognostics approach with online RUL forecasting for electronics-rich systems with unknown degradation behaviors". In: *Microelectronics Reliability* 111, p. 113676. ISSN: 0026-2714. DOI: https://doi.org/10.1016/j.microrel.2020.113676.

Al-Mohamad, A., V. Puig, and G. Hoblos (Sept. 2020). "Zonotopic Extended Kalman Filter For RUL Forecasting With Unknown Degradation Behaviors". In: *2020 28th Mediterranean Conference on Control and Automation (MED)*, pp. 574–579. DOI: 10.1109/MED48518.2020.9182829.

— (July 2021a). "Prognosis Based on the Joint Parameter/State Estimation Using Zonotopic LPV Set-Membership Approach". In: *2021 19th IFAC Symposium on System Identification (SYSID)*.

— (Oct. 2021b). "Robust Zonotopic Prognostics Approaches for LPV Systems Based on Set-Membership and Extended Kalman Filter". In: *2021 5th International Conference on Control, Automation and Diagnosis (ICCAD)*.

— (June 2021c). "Robust Zonotopic Set-Membership Approach for Model-Based Prognosis: Application on Linear Parameter-Varying Systems". In: *2021 19th European Control Conference (ECC)*.

Nasrin, M. S., F. H. Khan, and M. K. Alam (June 2014). "Quantifying Device Degradation in Live Power Converters Using SSTDR Assisted Impedance Matrix". In: *IEEE Transactions on Power Electronics* 29.6, pp. 3116–3131. ISSN: 1941-0107. DOI: 10.1109/TPEL.2013.2273556.

Nemani, M., R. Ravikanth, and B. A. Bamieh (Dec. 1995). "Identification of linear parametrically varying systems". In: *Proceedings of 1995 34th IEEE Conference on Decision and Control*. Vol. 3, 2990–2995 vol.3. DOI: 10.1109/CDC.1995.478600.

Packard, A. (1994). "Gain scheduling via linear fractional transformations". In: *Systems & Control Letters* 22.2, pp. 79–92. ISSN: 0167-6911. DOI: https://doi.org/10.1016/0167-6911(94)90102-3. URL: https://www.sciencedirect.com/science/article/pii/0167691194901023.

Paijmans, B. et al. (2008). "Identification of Interpolating Affine LPV Models for Mechatronic Systems with one Varying Parameter". In: *European Journal of Control* 14.1, pp. 16–29. ISSN: 0947-3580. DOI: https://doi.org/10.3166/ejc.14.16-29. URL: https://www.sciencedirect.com/science/article/pii/S0947358008707453.

Patil, M. A. et al. (2015). "A novel multistage Support Vector Machine based approach for Li ion battery remaining useful life estimation". In: *Applied Energy* 159, pp. 285–297. ISSN: 0306-2619. DOI: https://doi.org/10.1016/j.apenergy.2015.08.119. URL: https://www.sciencedirect.com/science/article/pii/S0306261915010557.

Patil, N. et al. (June 2009). "Precursor Parameter Identification for Insulated Gate Bipolar Transistor (IGBT) Prognostics". In: *IEEE Transactions on Reliability* 58.2, pp. 271–276. ISSN: 1558-1721. DOI: 10.1109/TR.2009.2020134.

Patil, Nishad, Diganta Das, and Michael Pecht (2012). "A prognostic approach for non-punch through and field stop IGBTs". In: *Microelectronics Reliability* 52.3. Special section on International Seminar on Power Semiconductors 2010, pp. 482–488. ISSN: 0026-2714. DOI: https://doi.org/10.1016/j.microrel.2011.10.017.

PCoE (1986). *Prognostics Center of Excellence*. http://ti.arc.nasa.gov/tech/dash/pcoe.

Pecht, M. (2006). "Prognostics and Health Monitoring of Electronics". In: *2006 International Conference on Electronic Materials and Packaging*, pp. 1–10.

— (2011). "A Prognostics and Health Management for Information and Electronics-Rich Systems". In: pp. 19–30. DOI: 10.1007/978-0-85729-493-7.

Pecht, M. G. (2018). "A PHM Roadmap for Electronics-Rich Systems". In: *Prognostics and Health Management of Electronics*. John Wiley & Sons, Ltd. Chap. 23, pp. 649–689. ISBN: 9781119515326. DOI: https://doi.org/10.1002/9781119515326.ch23. eprint: https://onlinelibrary.wiley.com/doi/pdf/10.1002/9781119515326.ch23. URL: https://onlinelibrary.wiley.com/doi/abs/10.1002/9781119515326.ch23.

Pecht, M. G. and M. Kang (2018). "Introduction to PHM". In: *Prognostics and Health Management of Electronics*. John Wiley & Sons, Ltd. Chap. 1, pp. 1–37. ISBN: 9781119515326. DOI: https://doi.org/10.1002/9781119515326.ch1. eprint: https://onlinelibrary.wiley.com/doi/pdf/10.1002/9781119515326.ch1. URL: https://onlinelibrary.wiley.com/doi/abs/10.1002/9781119515326.ch1.

Pippola, J. et al. (May 2015). "Product Level Accelerated Reliability Testing of Motor Drives With Input Power Interruptions". In: *IEEE Transactions on Power Electronics* 30.5, pp. 2614–2622. ISSN: 1941-0107. DOI: 10.1109/TPEL.2014.2359734.

Pourasghar, M., V. Puig, and C. Ocampo-Martinez (2016). "Comparison of set-membership and interval observer approaches for state estimation of uncertain systems". In: *2016 European Control Conference (ECC)*, pp. 1111–1116. DOI: 10.1109/ECC.2016.7810438.

— (2019). "Robust Zonotopic Observer Design: Interval Observer versus Set-membership Approaches". In: *2019 4th Conference on Control and Fault Tolerant Systems (SysTol)*, pp. 189–194. DOI: 10.1109/SYSTOL.2019.8864760.

Pourasghar, Masoud et al. (2019). "FD-ZKF: A Zonotopic Kalman Filter optimizing fault detection rather than state estimation". In: *Journal of Process Control* 73, pp. 89–102. ISSN: 0959-1524. DOI: https://doi.org/10.1016/j.jprocont.2018.12.003.

Puig, V., P. Cugueró, and J. Quevedo (2001). "Worst-case state estimation and simulation of uncertain discrete-time systems using zonotopes". In: *2001 European Control Conference (ECC)*, pp. 1691–1697. DOI: 10.23919/ECC.2001.7076164.

Puig, Vicenç, Jordi Saludes, and Joseba Quevedo (2003). "Worst-case simulation of discrete linear time-invariant interval dynamic systems". In: *Reliable Computing* 9.4, pp. 251–290. ISSN: 13853139. DOI: 10.1023/A:1024666428387.

Qingchuan, H. et al. (2017). "A prognostic method for predicting failure of dc/dc converter". In: *Microelectronics Reliability* 74, pp. 27–33. ISSN: 00262714. DOI: 10.1016/j.microrel.2017.05.014.

Renwick, J. and Kulkarni, C. and Celaya, J. (2015). *Capacitor Electrical Stress Data Set*. NASA Ames Prognostics Data Repository (http://ti.arc.nasa.gov/project/prognostic-data-repository). NASA Ames Research Center, Moffett Field, CA.

Richardson, R. R., M. A. Osborne, and D. A. Howey (2017). "Gaussian process regression for forecasting battery state of health". In: *Journal of Power Sources* 357, pp. 209–219. ISSN: 0378-7753. DOI: https://doi.org/10.1016/j.jpowsour.2017.05.004. URL: https://www.sciencedirect.com/science/article/pii/S0378775317306250.

Rigamonti, M., P. Baraldi, and E. Zio (2018). "Echo State Network for the Remaining Useful Life Prediction of a Turbofan Engine". In:

Ristic, B., S. Arulampalm, and N. Gordon (2004). *Beyond the Kalman filter : particle filters for tracking applications*. English. Artech House Boston, Ma. ; London.

Ristow, A. and M. Begovi (2008). "Development of a Methodology for Improving Photovoltaic Inverter Reliability". In: 55.7, pp. 2581–2592.

Robinson, E. (Oct. 2018). "Filtering and uncertainty propagation methods for model-based prognosis". PhD thesis.

Rugh, W. J. (1991). "Analytical framework for gain scheduling". In: *IEEE Control Systems Magazine* 11.1, pp. 79–84. DOI: 10.1109/37.103361.

Rugh, W. J. and J. S. Shamma (2000). "Research on gain scheduling". In: *Automatica* 36.10, pp. 1401–1425. ISSN: 0005-1098. DOI: https://doi.org/10.1016/S0005-1098(00)00058-3. URL: https://www.sciencedirect.com/science/article/pii/S0005109800000583.

Saha, B. et al. (2009). "Towards prognostics for electronics components". In: *2009 IEEE Aerospace conference*, pp. 1–7.

Saha, S. et al. (May 2011). "Accelerated aging with electrical overstress and prognostics for power MOSFETs". In: *IEEE 2011 EnergyTech*, pp. 1–6. DOI: 10.1109/EnergyTech.2011.5948532.

Sai Sarathi Vasan, A., B. Long, and M. Pecht (Nov. 2013). "Diagnostics and Prognostics Method for Analog Electronic Circuits". In: *IEEE Transactions on Industrial Electronics* 60.11, pp. 5277–5291. ISSN: 1557-9948. DOI: 10.1109/TIE.2012.2224074.

Samavatian, V., Y. Avenas, and H. Iman-Eini (2018). "Mutual and self-aging effects of power semiconductors on the thermal behaviour of DC-DC boost power converter". In: *Microelectronics Reliability* 88-90. 29th European Symposium on Reliability of Electron Devices, Failure Physics and Analysis (ESREF 2018), pp. 493–499. ISSN: 0026-2714. DOI: https://doi.org/10.1016/j.microrel.2018.06.022. URL: https://www.sciencedirect.com/science/article/pii/S0026271418304396.

Sankararaman, S. (2018). "Uncertainty Representation, Quantification, and Management in Prognostics". In: *Prognostics and Health Management of Electronics*. John Wiley & Sons, Ltd. Chap. 8, pp. 193–220. ISBN: 9781119515326. DOI: https://doi.org/10.1002/9781119515326.ch8. eprint: https://onlinelibrary.wiley.com/doi/pdf/10.1002/9781119515326.ch8. URL: https://onlinelibrary.wiley.com/doi/abs/10.1002/9781119515326.ch8.

Saxena, A. et al. (2010a). "Evaluating prognostics performance for algorithms incorporating uncertainty estimates". In: *2010 IEEE Aerospace Conference*, pp. 1–11. DOI: 10.1109/AERO.2010.5446828.

— (2010b). "Metrics for Offline Evaluation of Prognostic Performance". In: *International Journal of Prognostics and Health Management* 1.1.

Saxena, S., Y. Xing, and M. G. Pecht (2018). "PHM of Li-ion Batteries". In: *Prognostics and Health Management of Electronics*. John Wiley & Sons, Ltd. Chap. 13, pp. 349–375. ISBN: 9781119515326. DOI: https://doi.org/10.1002/9781119515326.ch13. eprint: https://onlinelibrary.wiley.com/doi/pdf/10.1002/9781119515326.ch13. URL: https://onlinelibrary.wiley.com/doi/abs/10.1002/9781119515326.ch13.

Schmidt, R., C. König, and P. Prenosil (2012). "Novel wire bond material for advanced power module packages". English. In: *Microelectronics Reliability* 52.9-10, pp. 2283–2288. DOI: 10.1016/j.microrel.2012.06.139.

Schwabacher, M. and K. Goebel (Jan. 2007). "A survey of artificial intelligence for prognostics". In: *AAAI Fall Symposium - Technical Report*.

Schweppe, F. (1968). "Recursive state estimation: Unknown but bounded errors and system inputs". In: *IEEE Transactions on Automatic Control* 13.1, pp. 22–28. DOI: 10.1109/TAC.1968.1098790.

Sename, O., J. Tudon-Martinez, and S. Fergani (2013). "LPV methods for fault-tolerant vehicle dynamic control". In: *2013 Conference on Control and Fault-Tolerant Systems (SysTol)*, pp. 116–130. DOI: 10.1109/SysTol.2013.6693821.

Sename, Olivier and Soheib Fergani (2017). "Linear Parameter Varying systems: from modelling to control". In: *Intelligent Vehicles International Summer School (IVSS)*.

Shamma, J. S. and M. Athans (Aug. 1990). "Analysis of gain scheduled control for nonlinear plants". In: *IEEE Transactions on Automatic Control* 35.8, pp. 898–907. ISSN: 1558-2523. DOI: 10.1109/9.58498.

— (1992). "Gain scheduling: potential hazards and possible remedies". In: *IEEE Control Systems Magazine* 12.3, pp. 101–107. DOI: 10.1109/37.165527.

Al-Sheikh, H., O. Bennouna, and G. Hoblos (2014). "Power Electronics Interface Configurations for Hybrid Energy Storage in Hybrid Electric Vehicles". In: April, pp. 13–16.

Al-Sheikh, H., O. Bennouna, G. Hoblos, and N. Moubayed (June 2014). "Modeling, design and fault analysis of bidirectional DC-DC converter for hybrid electric vehicles". In: *2014 IEEE 23rd International Symposium on Industrial Electronics (ISIE)*, pp. 1689–1695. DOI: 10.1109/ISIE.2014.6864869.

Smet, V. et al. (July 2013). "Evaluation of V_{ce} Monitoring as a Real-Time Method to Estimate Aging of Bond Wire-IGBT Modules Stressed by Power Cycling". In: *IEEE Transactions on Industrial Electronics* 60.7, pp. 2760–2770. ISSN: 1557-9948. DOI: 10.1109/TIE.2012.2196894.

Smith, B. J. (Feb. 2011). *Satellite Enabled Vehicle Prognostic and Diagnostic System*. Pat. Colorado Springs, US.

Telcordia Technologies (2001) (2001). *Special Report SR-332 of Reliability Prediction Procedure for Electronic Equipment*. en. Tech. rep. Piscataway, NJ, USA: Telcordia Technologies.

Steinbuch, M., R. van de Molengraft, and A. van der Voort (2003). "Experimental modelling and LPV control of a motion system". In: *Proceedings of the 2003 American Control Conference, 2003.* Vol. 2, pp. 1374–1379. DOI: 10.1109/ACC.2003.1239782.

Sun, B. et al. (2012). "Benefits and Challenges of System Prognostics". In: *IEEE Transactions on Reliability* 61.2, pp. 323–335. DOI: 10.1109/TR.2012.2194173.

Swanson, D. (2001). "A general prognostic tracking algorithm for predictive maintenance". In: *Proc. IEEE International Conference on Aerospace* 6, pp. 2971–2977.

Sznaier, M., C. Mazzaro, and T. Inanc (2000). "An LMI approach to control oriented identification of LPV systems". In: *Proceedings of the 2000 American Control Conference. ACC (IEEE Cat. No.00CH36334)*. Vol. 5, 3682–3686 vol.5. DOI: 10.1109/ACC.2000.879257.

Tajfar, Alireza and Sudip K. Mazumder (2012). "A Fault-Tolerant Switching Scheme for a photovoltaic high-frequency-link inverter". In: pp. 2087–2094.

Tidriri, Khaoula et al. (2019). "A Decision Fusion Based Methodology for fault Prognostic and Health Management of Complex Systems". In: *Applied Soft Computing Journal*, p. 105622. ISSN: 1568-4946. DOI: 10.1016/j.asoc.2019.105622.

Tóth, R. (Jan. 2010). *Modeling and Identification of Linear Parameter-Varying Systems*. Vol. 403. Springer-Verlag Berlin Heidelberg. DOI: 10.1007/978-3-642-13812-6.

Tudón-Martínez, J. C. et al. (2013). "Fault tolerant strategy for semi-active suspensions with LPV accommodation?" In: *2013 Conference on Control and Fault-Tolerant Systems (SysTol)*, pp. 631–636. DOI: 10.1109/SysTol.2013.6693942.

Uckun, S., K. Goebel, and P. J.F. Lucas (2008). "Standardizing research methods for prognostics". In: *2008 International Conference on Prognostics and Health Management*, pp. 1–10. DOI: 10.1109/PHM.2008.4711437.

UK Offshore Commercial Air Transport Helicopter Safety Record (1981 – 2010) (2011). en. Standard. United Kingdom: John Burt Associates Limited. URL: https://www.skybrary.aero/bookshelf/books/2657.pdf.

Vachtsevanos, G., F. Lewis, Roemer M., et al. (2006). "Introduction". In: *Intelligent Fault Diagnosis and Prognosis for Engineering Systems*. John Wiley & Sons, Ltd. Chap. 1, pp. 1–12. ISBN: 9780470117842. DOI: https://doi.org/10.1002/9780470117842.ch1. eprint: https://onlinelibrary.

wiley.com/doi/pdf/10.1002/9780470117842.ch1. URL: https://onlinelibrary.wiley.com/doi/abs/10.1002/9780470117842.ch1.

Vachtsevanos, G., F. Lewis, M. Roemer, et al. (2006a). John Wiley & Sons, Ltd. ISBN: 9780470117842. DOI: https://doi.org/10.1002/9780470117842. URL: https://onlinelibrary.wiley.com/doi/book/10.1002/9780470117842.

— (2006b). "Fault Diagnosis and Prognosis Performance Metrics". In: *Intelligent Fault Diagnosis and Prognosis for Engineering Systems*. John Wiley & Sons, Ltd. Chap. 7, pp. 355–399. ISBN: 9780470117842. DOI: https://doi.org/10.1002/9780470117842.ch7. eprint: https://onlinelibrary.wiley.com/doi/pdf/10.1002/9780470117842.ch7. URL: https://onlinelibrary.wiley.com/doi/abs/10.1002/9780470117842.ch7.

Valentine, Nathan, Diganta Das, and Prof Michael Pecht (2015). "Failure Mechanisms of Insulated Gate Bipolar Transistors (IGBTs)". In: *2015 NREL Photovoltaic Reliability Workshop*.

Vasan, A. S. S. and M. G. Pecht (2018). "Health and Remaining Useful Life Estimation of Electronic Circuits". In: *Prognostics and Health Management of Electronics*. John Wiley & Sons, Ltd. Chap. 11, pp. 279–327. ISBN: 9781119515326. DOI: https://doi.org/10.1002/9781119515326.ch11. eprint: https://onlinelibrary.wiley.com/doi/pdf/10.1002/9781119515326.ch11. URL: https://onlinelibrary.wiley.com/doi/abs/10.1002/9781119515326.ch11.

Health Monitoring and Degradation Prognostics in Gas Turbine Engines Using Dynamic Neural Networks (June 2015). Vol. Volume 6: Ceramics; Controls, Diagnostics and Instrumentation; Education; Manufacturing Materials and Metallurgy; Honors and Awards. Turbo Expo: Power for Land, Sea, and Air. V006T05A030. DOI: 10.1115/GT2015-44101. eprint: https://asmedigitalcollection.asme.org/GT/proceedings-pdf/GT2015/56758/V006T05A030/4238171/v006t05a030-gt2015-44101.pdf. URL: https://doi.org/10.1115/GT2015-44101.

Verdult, V., L. Ljung, and M. Verhaegen (2002). "Identification of composite local linear state-space models using a projected gradient search". In: *International Journal of Control* 75.16-17, pp. 1385–1398. DOI: 10.1080/00207170210001023807.

Verhaegen, M. (1994). "Identification of the deterministic part of MIMO state space models given in innovations form from input-output data". In: *Automatica* 30.1. Special issue on statistical signal processing and control, pp. 61–74. ISSN: 0005-1098. DOI: https://doi.org/10.1016/0005-1098(94)90229-1. URL: https://www.sciencedirect.com/science/article/pii/0005109894902291.

Vicino, A. and G. Zappa (1996). "Sequential approximation of feasible parameter sets for identification with set membership uncertainty". In: *IEEE Transactions on Automatic Control* 41.6, pp. 774–785. DOI: 10.1109/9.506230.

Walter, E. and H. Piet-Lahanier (1989). "Exact recursive polyhedral description of the feasible parameter set for bounded-error models". In: *IEEE Transactions on Automatic Control* 34.8, pp. 911–915. DOI: 10.1109/9.29443.

Walthall, R. and R. Rajamani (2018). "The Role of PHM at Commercial Airlines". In: *Prognostics and Health Management of Electronics*. John Wiley & Sons, Ltd. Chap. 18, pp. 503–534. ISBN: 9781119515326. DOI: https://doi.org/10.1002/9781119515326.ch18. eprint: https://onlinelibrary.wiley.com/doi/pdf/10.1002/9781119515326.ch18. URL: https://onlinelibrary.wiley.com/doi/abs/10.1002/9781119515326.ch18.

Wan, E.A. and R. Van Der Merwe (2000). "The Unscented Kalman Filter for Nonlinear Estimation". In: pp. 153–158. DOI: 10.1109/ASSPCC.2000.882463.

Wang, D., Q. Miao, and M. Pecht (Oct. 2013). "Prognostics of lithium-ion batteries based on relevance vectors and a conditional three-parameter capacity degradation model". English. In: *Journal of Power Sources* 239, pp. 253–264. ISSN: 0378-7753. DOI: 10.1016/j.jpowsour.2013.03.129.

Wang, P. and G. Vachtsevanos (1999). "Fault prognosis using dynamic wavelet neural networks". In: *Maintenance and Reliability Conference* MARCON 99.

Wang, W. and A. Wong (2002). "Autoregressive model based gear fault diagnosis". In: *Journal of Vibration and Acoustics* 124, pp. 172–179.

Wang, Ye, Vicenç Puig, and Gabriela Cembrano (Aug. 2018). "Set-membership approach and Kalman observer based on zonotopes for discrete-time descriptor systems". In: *Automatica* 93. DOI: 10.1016/j.automatica.2018.03.082.

Wang, Z. et al. (2017). "Voltage fault diagnosis and prognosis of battery systems based on entropy and Z-score for electric vehicles". In: *Applied Energy* 196, pp. 289–302. ISSN: 0306-2619. DOI: https://doi.org/10.1016/j.apenergy.2016.12.143. URL: https://www.sciencedirect.com/science/article/pii/S0306261916319262.

Wheeler, K. R., T. Kurtoglu, and S. D. Poll (2010). "A Survey of Health Management User Objectives in Aerospace Systems Related to Diagnostic and Prognostic Metrics". In: *International Journal of Prognostics and Health Management* 1.1. DOI: 10.36001/ijphm.2010.v1i1.1345. URL: https://papers.phmsociety.org/index.php/ijphm/article/view/1345.

Witsenhausen, H. (1968). "Sets of possible states of linear systems given perturbed observations". In: *IEEE Transactions on Automatic Control* 13.5, pp. 556–558. DOI: 10.1109/TAC.1968.1098995.

Wolfgang, E. (2007). "Examples for failures in power electronics systems". In: *ECPE tutorial on reliability of power electronic systems, Nuremberg, Germany*, pp. 19–20.

Xiang, D., L. Ran, P. Tavner, A. Bryant, et al. (2011). "Monitoring Solder Fatigue in a Power Module Using Case-Above-Ambient Temperature Rise". In: 47.6, pp. 2578–2591.

Xiang, D., L. Ran, P. Tavner, S. Yang, et al. (2012). "Condition Monitoring Power Module Solder Fatigue Using Inverter Harmonic Identification". In: 27.1, pp. 235–247.

Xiong, Y. et al. (June 2008). "Prognostic and Warning System for Power-Electronic Modules in Electric, Hybrid Electric, and Fuel-Cell Vehicles". In: *IEEE Transactions on Industrial Electronics* 55.6, pp. 2268–2276. ISSN: 1557-9948. DOI: 10.1109/TIE.2008.918399.

Yan, J., M. Koç, and J. Lee (Dec. 2004). "A prognostic algorithm for machine performance assessment and its application". In: *Production Planning &*

Control - PRODUCTION PLANNING CONTROL 15, pp. 796–801. DOI: 10.1080/09537280412331309208.

Yan, R. et al. (2019). "Deep learning for fault diagnosis and prognosis in manufacturing systems". In: *Computers in Industry* 110, pp. 1–2. ISSN: 0166-3615. DOI: https://doi.org/10.1016/j.compind.2019.05.002. URL: https://www.sciencedirect.com/science/article/pii/S0166361519303483.

Yang, B., R. Liu, and E. Zio (Dec. 2019). "Remaining Useful Life Prediction Based on a Double-Convolutional Neural Network Architecture". In: *IEEE Transactions on Industrial Electronics* 66.12, pp. 9521–9530. ISSN: 1557-9948. DOI: 10.1109/TIE.2019.2924605.

Yang, S. et al. (Nov. 2010). "Condition Monitoring for Device Reliability in Power Electronic Converters: A Review". In: *IEEE Transactions on Power Electronics* 25.11, pp. 2734–2752. ISSN: 1941-0107. DOI: 10.1109/TPEL.2010.2049377.

Yang, W. (2001). "Towards dynamic model-baed prognostics for transmossopn gears". In: *SPIE Conference Proceedings* 4733, pp. 157–167.

Yung, J H (2001). "Gain scheduling for geometrically nonlinear flexible space structures". In: *Nonlinearity*. URL: http://mit.dspace.org/bitstream/handle/1721.1/16838/51283889.pdf?sequence=1.

Zhang, C. et al. (June 2014). "A Novel Approach for Analog Circuit Fault Prognostics Based on Improved RVM". In: *Journal of Electronic Testing* 30.3, pp. 343–356. ISSN: 0923-8174. DOI: 10.1007/s10836-014-5454-8. URL: http://link.springer.com/10.1007/s10836-014-5454-8.

Zhang, D. (Jan. 2018). "Contribution to prognostics of proton exchange membrane fuel cells : approaches based on degradation information at multiple levels". Theses. Université Grenoble Alpes. URL: https://tel.archives-ouvertes.fr/tel-01725849.

Zhang, Q., M. Basseville, and A. Benveniste (1994). "Early warning of slight changes in systems". In: *Automatica* 30, pp. 95–114.

Zhang, Y. et al. (2020). "Remaining Useful Life Estimation Using Long Short-Term Memory Neural Networks and Deep Fusion". In: *IEEE Access* 8,

pp. 19033–19045. ISSN: 2169-3536. DOI: 10.1109/ACCESS.2020.2966827. URL: https://ieeexplore.ieee.org/document/8960368/.

Zhang, Z., F. Dong, and L. Xie (2018). "Data-Driven Fault Prognosis Based on Incomplete Time Slice Dynamic Bayesian Network". In: *IFAC-PapersOnLine* 51.18. 10th IFAC Symposium on Advanced Control of Chemical Processes ADCHEM 2018, pp. 239–244. ISSN: 2405-8963. DOI: https://doi.org/10.1016/j.ifacol.2018.09.306. URL: https://www.sciencedirect.com/science/article/pii/S2405896318319876.

Zhou, D. et al. (2018). "Prognostics for State of Health of Lithium-Ion Batteries Based on Gaussian Process Regression". In: *Mathematical Problems in Engineering* 2018, pp. 1–11. ISSN: 1024-123X. DOI: 10.1155/2018/8358025. URL: https://www.hindawi.com/journals/mpe/2018/8358025/.

Zhou, J., S. Tian, and C. Yang (2014). "A Novel Prediction Method about Single Components of Analog Circuits Based on Complex Field Modeling". In: *The Scientific World Journal* 2014, pp. 1–14. ISSN: 2356-6140. DOI: 10.1155/2014/530942. URL: https://www.hindawi.com/journals/tswj/2014/530942/.

Zhou, S., L. Zhou, and P. Sun (2013). "Monitoring Potential Defects in an IGBT Module Based on Dynamic Changes of the Gate Current". In: 28.3, pp. 1479–1487.

Zio, E. and F. Di Maio (2012). "Fatigue crack growth estimation by relevance vector machine". In: *Expert Systems with Applications* 39.12, pp. 10681–10692. ISSN: 0957-4174. DOI: https://doi.org/10.1016/j.eswa.2012.02.199. URL: https://www.sciencedirect.com/science/article/pii/S0957417412005295.